

Dissertation zur Erlangung des Doktorgrades  
der Fakultät für Chemie und Pharmazie  
der Ludwig-Maximilians-Universität München

# Interferon induction inhibition by the measles virus C protein



**Konstantin Maria Johannes Sparrer**

aus

München, Deutschland

2013

**Erklärung:**

Diese Dissertation wurde im Sinne von §7 der Promotionsordnung vom 28. November 2011 von Herrn Prof. Conzelmann betreut und von Herrn Prof. Hopfner vor der Fakultät für Chemie und Pharmazie vertreten.

**Eidesstattliche Versicherung:**

Diese Dissertation wurde eigenständig und ohne unerlaubte Hilfe erarbeitet.

München, den

.....

(Unterschrift des Autors)

Dissertation eingereicht am: 14.10.2013

Erstgutachter: Prof. Dr. Karl-Peter Hopfner

Zweitgutachter: Prof. Dr. Karl-Klaus Conzelmann

Tag der mündlichen Prüfung: 9.12.2013

This thesis has been prepared in the laboratory of Prof. Karl-Klaus Conzelmann at the Max von Pettenkofer-Institute and Gene Center of the Ludwig-Maximilians-University Munich.

Parts of this thesis were published in Journal of Virology in 2012:

[Measles virus C protein interferes with Beta interferon transcription in the nucleus.](#) Sparrer KM, Pfaller CK, Conzelmann KK. J Virol. 2012 Jan;86(2):796-805. doi: 10.1128/JVI.05899-11. Epub 2011 Nov 9.

# TABLE OF CONTENTS

<b>ACKNOWLEDGEMENTS</b>	<b>VII</b>
<b>SUMMARY</b>	<b>IX</b>
<b>INTRODUCTION</b>	<b>1</b>
<b>1. Measles Virus</b>	<b>1</b>
1.1. A general overview - classification and pathogenesis	1
1.2. Vaccines and circulating wildtype strains	3
1.3. Structure and molecular biology of measles virus	5
1.4. The P gene products and their functions	8
<b>2. Defense of a host against viruses and viral counter-measures</b>	<b>10</b>
2.1. Adaptive immunity	10
2.2. Adaptive immunity during MV infection	11
2.3. Innate immunity	11
2.4. Viral innate immune evasion strategies	15
<b>3. Generating recombinant viruses</b>	<b>17</b>
<b>4. Aim of this thesis</b>	<b>19</b>
<b>MATERIALS AND METHODS</b>	<b>21</b>
<b>1. Materials</b>	<b>21</b>
1.1. Chemicals	21
1.2. Kits	22
1.3. Enzymes and buffers	22
1.4. Antibodies	22
1.5. Oligonucleotides	23
1.6. Miscellaneous	27
1.7. Cell lines and media	27
1.8. Plasmids and bacteria	28
1.9. Viruses	35
1.10. Buffers and solutions	36

---

<b>2. Methods</b>	<b>40</b>
2.1. Working with DNA	40
2.2. Working with proteins	44
2.3. Working with cells	47
2.4. Working with RNA	51
2.5. Working in silico	53
2.6. Working with viruses	55
<b>RESULTS</b>	<b>57</b>
<b>1. Interferon inhibition of MV C depends on its intracellular localisation</b>	<b>57</b>
1.1. Measles virus C protein is able to inhibit interferon induction	58
1.2. MV C proteins of vaccine strains show a decreased inhibition	60
1.3. In silico characterisation of MV C	62
1.4. Nuclear localization of MV C correlates with interferon inhibition	67
1.5. MV C does not interfere with activation of IRF3	70
<b>2. Identification of cellular interaction partners of MV C</b>	<b>73</b>
2.1. Interaction partners in the interferon pathway	73
2.2. Known binding partners of MV C	75
2.3. Screening for cellular interaction partners of MV C	76
<b>3. Analysis of MV C in the viral context</b>	<b>87</b>
3.1. Host transcription regulation induced by rMV vac2 infection	89
3.2. MV C <sup>ko</sup> viruses are heavily attenuated	93
3.3. The localisation of C during infection	98
3.4. Characterisation of C and its NLS in the viral context	102
<b>DISCUSSION</b>	<b>105</b>
<b>1. The impact of MV infection on host transcription</b>	<b>105</b>
<b>2. MV C is a nuclear inhibitor of innate immunity – alone and during infection</b>	<b>106</b>
2.1. Nuclear localisation of C as a hallmark of wildtype strains	107
2.2. Comparison of overexpression experiments and infection	108
2.3. Infections in vivo vs cell culture	109
2.4. Comparison to related C proteins	110
2.5. The attenuation of C <sup>ko</sup> viruses	111
2.6. Mechanistic proposals	112

<b>3. Model of C in the context of infection</b>	<b>118</b>
<b>4. Outlook and future perspectives</b>	<b>121</b>
<b>REFERENCES</b>	<b>123</b>
<b>APPENDIX</b>	<b>136</b>
<b>List of abbreviations</b>	<b>136</b>
<b>List of figures</b>	<b>140</b>
<b>Supplementary Data:</b>	<b>142</b>
App. 1: Consurf Settings:	142
App. 2: I-Tasser settings:	142
App. 3: Full Clustering:	145
App. 4: Full Annotations:	147
App. 5: Individual Massspectrometry data:	153
<b>Publications and Presentations</b>	<b>158</b>

## ACKNOWLEDGEMENTS

Mein Dank gilt allen, die mich in den Jahren der Doktorarbeit und des Studiums unterstützt haben, auch wenn es manchmal deutliche Höhen und Tiefen gab. Vielen Dank !

In erster Linie möchte ich mich bei Prof. Karl-Klaus Conzelmann bedanken, der es mir ermöglicht hat an diesem Projekt zu arbeiten und mich während der Doktorarbeit betreut hat. Insbesondere danke ich dafür, dass er immer Zeit für Diskussion hatte und mir auch immer genug Freiheit ließ, eigene Idee und experimentelle Ansätze umzusetzen und diese danach konstruktiv kritisch zu beurteilen.

Bei Prof. Karl-Peter Hopfner, der sich bereit erklärt hat meine Doktorarbeit für die Fakultät für Chemie und Pharmazie zu vertreten möchte ich mich auch noch insbesondere bedanken. Darüber hinaus war die Zusammenarbeit mit seiner Arbeitsgruppe immer abwechslungsreich und spannend. Den Mitgliedern der Prüfungskommission für diese Dissertation möchte ich auch meinen Dank aussprechen, namentlich sind dies Dr. Dietmar Martin, Prof. Roland Beckmann, Prof. Klaus Förstemann und Prof. Ulrike Gaul. Vielen Dank für ihre Mühen !

Einen weiteren wichtigen und nicht zu unterschätzenden Beitrag zum Gelingen dieser Arbeit und insbesondere zum Schaffen eines angenehmen und produktiven Arbeitsklimas haben natürlich alle im folgenden genannten Mitglieder der Arbeitsgruppe sowie viele direkte Kollaborationspartner geleistet. Allen voran Christian Pfaller, der mich sowohl als Bachelorstudent und später dann als Masterstudent betreut und die ersten Schritte im Labor beigebracht hat. Super vielen Dank dafür, und auch für die vielen privaten Gespräche und DSA Runden! Vielen, vielen Dank auch an die gute Seele des Labors, Nadin Zapf für alle Hilfe und Ratschläge ! Dann selbstverständlich Kerstin Schuhmann (Subber Measles Girl), Alex Ghanem (Klonierungskrieger) die mich am längsten im Labor während der Doktorarbeit auch immer mit Hilfe und Konversation unterstützt haben. Weiterhin ein Dankeschön an die ‚Neulinge‘ Max Eizinger, Tobias Halbach und Marco Wachowius und die Alumnis die ich noch gekannt habe: Martina, Anika, Lisa, Adriane und Laetitia. Der Zusammenhalt der Gruppe und die gegenseitige produktive Unterstützung war/ist einfach super! Zusätzlich dazu war es immer toll in Kooperationen zu arbeiten, allen voran sei hier den ‚Hopfnern‘: Simon Runge und Charlotte Lässig gedankt, aber auch Johannes Harder von der AG Carell. Alle hier genannten tragen zusammen mit Prof. Klaus Conzelmann schließlich einen Hauptteil der ‚Schuld‘, dass ich in der Virologie meine Doktorarbeit machen wollte und meine Entscheidung nicht bereut und die Faszination an diesem Themengebiet (noch) nicht verloren habe.

Meinen Dank gilt natürlich auch denjenigen die mir privat während dieser Zeit immer Abwechslung und Motivation gebracht haben: Die DSA Runde(n) mit Phips, Qi, Felix, Sven, Björn, Roman, Stephan und Oliver. Hin und wieder mal in eine andere (heilere?) Welt abtauchen hat einiges für sich! Die ‚Puchheimer‘ (ein paar Überschneidungen mit der DSA

Runde): Iris, Claudia & Christian, Lisa & die Heinzels. Des Weiteren noch die ‚Unileute‘ und inzwischen teilweise sogar Nachbarn: Amelie, Lydia, Claudia, Francisco, Anna und Jens.

Nicht zu vergessen sind auch die Eltern & Geschwister von meinem Freund: Josef, Gudrun, Katharina, Georg und Johannes. Danke für die Zeit, die ich bei euch verbringen durfte, das war immer super schön und entspannend (warmer Kachelofen im Wohnzimmer & super leckeres Essen).

Desweiteren gilt natürlich ein Dank meiner tollen Verwandtschaft (das kann ja nicht jeder behaupten zu haben): Dominik & Familie, Berthold & Barbara, Irmgard & Helmut, Claudia, Aurelia und Madita und Niels sowie meiner Oma und meinem Opa!

Ganz besonders möchte ich noch meinen Eltern Georg und Mariele, sowie meiner Schwester Elena danken!!! Vielen Dank einfach für eure Unterstützung und dass ihr zu mir steht, das bedeutet mir echt viel!

Vielen, vielen, vielen, vielen Dank auch an meinen Freund Josef, der immer Geduld bewiesen hatte, wemals mal nicht so gut lief. Er schaffte es immer mich aufzumuntern und zu motivieren mich weiter durchzubeißen, auch wenn ich hin und wieder mal die Wände hochgelaufen bin und vermutlich stundenlang dabei nicht aufgehört habe zu schimpfen. Einen besseren Freund kann man sich nicht vorstellen und ohne ihn hätte ich diese Arbeit nicht geschafft!

## SUMMARY

Effective vaccination relies on the rapid and efficient activation of the human innate immune system. Measles virus (MV, Genus *Morbillivirus*), a member of the paramyxovirus family, is known to induce life-long immunity against reinfection. However, the acute infection is associated with a dramatic immunosuppression, potentially accompanied by secondary infections, which can eventually kill a host. The pathogenesis of established MV vaccine strains is less severe and the typical immunosuppression is less pronounced, while life-long protection against MV is induced as well, indicating efficient stimulation of the immune system. Infection of cells by MV is sensed predominantly by RIG-I recognizing viral 5'-triphosphate RNAs, and MDA-5 using as yet unknown ligands. The 186 amino acid MV C protein, which shuttles between the nucleus and cytoplasm, is identified in this thesis as a major viral inhibitor of IFN- $\beta$  transcription in human cells. Notably, C proteins of wildtype MV isolates, known as poor IFN- $\beta$  inducers, were found to comprise a canonical nuclear localization signal (NLS), whereas the respective sequence of all vaccine strains, irrespective of their origin, was mutated. Site-directed mutagenesis of the C proteins from a MV wildtype isolate and from a vaccine virus confirmed a correlation of nuclear localization and inhibition of IFN- $\beta$  transcription. A functional NLS and efficient nuclear accumulation is therefore critical for MV C to retain full potential to downregulate IFN- $\beta$  induction. The activation of the crucial transcription factor IRF3 by phosphorylation, dimerization and nuclear translocation was not altered by both vaccine and wildtype MV C. Several protein-protein interactions of MV C could be identified during this study and validated by different assays including mass spectrometry, co-immunoprecipitation and immunofluorescence. Most prominent targets were IPS-1/MAVS and 19S proteasomal components. Knockout of the C protein in recombinant viruses caused a severe growth defect in interferon competent cells and strong interferon induction. Recombinant MV expressing fluorescently tagged C NLS variants confirmed the nuclear localisation of C during infection. In addition a considerable fraction of C accumulated in peri-nuclear inclusion bodies during infection, which were previously described as viral replication factories or stress granules. The MV P protein was shown to be sufficient for the formation and recruitment of C to these cytosolic inclusion bodies. To study the interferon induction caused by an infection, recombinant viruses were generated, differing only in their C NLS localisation signal. Interferon induction caused by rMV without a functional C NLS was stronger and the virus grew slower on interferon

competent cells than with a wildtype C NLS. Taken together, a defect in efficient nuclear import of C protein is suggested to contribute to the attenuation of MV vaccine strains and indicates an important difference between vaccine and wildtype virus strains. Additionally, possible molecular mechanisms supported by experimental data are discussed and evaluated.

# INTRODUCTION

## 1. Measles Virus

Viruses know us humans inside out. We share thousands of years of co-evolution and co-habitation. The human immune system evolved to fight invading pathogens, and viral infections contributed a considerable part. Retroviral transposons and other genomic modifications caused by viruses are importantly contributing to the genome we have now. Hosts challenged by viral infection they want to get rid of, evolve and change according to the circumstances. However, viruses also evolve and come up with perfidious strategies to overcome the hosts defence emerged. And those viruses still existing today are the winners of a constant battle between the defence system of the host and the viral countermeasures. Even modern medicine could not provide cures for every viral disease; no antibiotic analogue against viruses has been identified so far. Millions of years of evolution created viruses as organisms on the verge of life and death in before unseen diversity. Some viruses are able to infect broad host ranges; they represent typical zoonotic viruses like influenza. They can infect animals and humans alike, though certain measures have to be considered when crossing the species barrier. Other viruses evolved to a small host range, for example the measles virus, which has only one natural host, the human being.

### 1.1. A general overview - classification and pathogenesis

The negative-sense single-stranded helically packed RNA genome of measles virus (MV) is non-segmented and approximately 16k nucleotides long. Therefore, MV belongs to the order of *Mononegavirales* and the family of *Paramyxoviridae*, which is further divided into two subfamilies. Measles virus belongs to the subfamily of *Paramyxovirinae* and the genus *Morbillivirus* along with the Rinderpest virus (RPV) or the canine distemper virus (CDV). Other genera of the *Paramyxovirinae* subfamily include the *Avulavirus* genus (e.g. Newcastle disease virus, NDV), the *Henipaviruses* (e.g. Hendra virus, HeV), *Respiroviruses* (e.g. Sendai virus, SeV) and *Rubulaviruses* (e.g. mumps virus, MuV). The second subfamily, *Pneumovirinae*, comprises two genera: *Respirovirus* (e.g. respiratory syncytial virus, RSV) and *Metapneumovirus* (e.g. human metapneumovirus, hMPV). Altogether all these viruses are

responsible for causing a number of different diseases in humans or animals (Fields et al., 2007).

The primary host species of MV are humans, but also other primates can be infected, although the infection appears to be attenuated (de Swart et al., 2007; van Binnendijk et al., 1990). Wildtype MV infections of other species than primates and humans have not been reported. *In vivo* model systems for MV infection using cotton rats, macaques and mice still remains highly controversial (de Swart, 2009; Niewiesk et al., 1997; Ohno et al., 2007). The highly virulent MV caused more than 20 million infections and approximately 158,000 deaths worldwide in 2011 (WHO, 2013b). Though effective vaccines exist (e.g. the Schwarz strain of the Edmonston lineage (ENDERS et al., 1962; Schwarz, 1964)), which lead to life-long immunity, MV is still a major cause of childhood morbidity and mortality, especially in countries of the Third World. Elimination of MV by the WHO worldwide is currently in progress. The first goal set by the WHO to eliminate measles in 2010 could not be reached. This was attributed to lowering vaccine coverage in Europe and North America, mainly due to vaccine scepticism, as well as the need for higher vaccination coverage in developing countries to achieve to goal of herd immunity. Eventually a new strategy was devised. Until the end of 2015, global measles deaths shall be reduced by at least 95% compared with 2000 levels. By the end of 2020 measles elimination shall be achieved in at least five WHO regions (WHO, 2013a). A close relative of MV, the Rinderpest virus (RPV) was formally declared eradicated in June 2011, with the last case of a wildtype infection being reported in 2001 (Normile, 2008).

The virus enters the organism via the respiratory route, infecting lung tissue via aerosol inhalation, followed by a primary viremia targeting blood and lymphoid cells (de Swart et al., 2007; de Vries et al., 2010; Ludlow et al., 2010). First clinical signs of a measles virus infection show up 10 days post infection and are fever and Koplik's spots, followed by a characteristic macropapular rash that lasts for 3-5 days. At later stages of the infection, other tissues like the skin are also affected, causing the typical rash (Fields et al., 2007; Griffin, 2010; Yanagi et al., 2006) due to invading T cells (Griffin, 2010; Hirsch et al., 1984). Clearance of infectious virus begins with onset of this rash and is completed approximately 20 days after the infection (Griffin, 2010; Griffin and Oldstone, 2009). However, viral RNA still is detectable in peripheral blood mononuclear cells (PBMCs) and respiratory secretions several weeks after recovery, indicating ongoing expression of viral antigens (Riddell et al., 2007). This may be one cause of the induction of a robust, lifelong immunity. In rare cases the

virus can persist in the human organism leading to a mortal disease, SSPE (subacute sclerosing panencephalitis) (Johnson et al., 1984).

Associated with an infection with MV is a severe immunosuppression causing a high and dangerous susceptibility to other infections (Slifka et al., 2003), responsible for most of the fatal cases in developing countries. Several weeks after infection T cells still show a decreased *in vitro* proliferation in response to mitogens (Ward et al., 1991). The infection is also characterised by lymphopenia, a depletion of T and B cell numbers in circulation during the rash (Arneborn and Biberfeld, 1983; Ryon et al., 2002), and suppression of lymphocyte proliferation (Auwaerter et al., 1999; Hirsch et al., 1984). Also dendritic cells were observed to be infected *in vivo* in macaques (de Swart et al., 2007) and inhibition caused by viral gene expression on signalling pathways related to the innate immune system was identified (Pfaller and Conzelmann, 2008; Schuhmann et al., 2011). This very effective blockage of the immune system of the host on the one hand and the induction of lifelong immunity upon clearance of the infection on the other hand is called the “measles paradoxon”. Interestingly, only one serotype of MV exists worldwide and the MV encoded antigens are remarkably stable (Fine, 1993; WHO, 2013b). A survived wildtype infection or a successful vaccination using the established vaccine strains fully protects against any wildtype infection known so far.

## 1.2. Vaccines and circulating wildtype strains

Although only one serotype of MV exists, the viruses can be classified according to their N gene sequence (sometimes also the H sequence is additionally used). The WHO currently officially recognizes 8 clades called A, B, C, D, E, F, G, and H. These clades are further divided into 23 genotypes, designated A, B1, B2, B3, C1, C2, D1, D2, D3, D4, D5, D6, D7, D8, D9, D10, E, F, G1, G2, G3, H1, and H2 (WHO, 2001). The circulating wildtype strains of 2012 were predominantly B3, D4, D8, D9, G3 and H1. In America the D and B genotypes were dominant, whereas in Africa almost exclusively the B genotype circulated. In Europe, Asia and Australia, the main MV genotypes found were D4, D8 and D9, with D9 being more prominent in southern Asia (WHO, 2013c) (Fig. 1).

The current epidemic MV strains evolved probably at the beginning until the midst of the 20<sup>th</sup> century (Pomeroy et al., 2008). The ancestor of MV is the now extinct Rinderpest virus (RPV), which infected only cattle. The exact time point of the divergence of both viruses is debated. Sequence analysis studies suggest the 11<sup>th</sup> and 12<sup>th</sup> century (Furuse et al., 2010). It is however also stated in the study that the linguistic evidence (Fields et al., 2007), which

suggests measles infections as early as the 5<sup>th</sup> to 7<sup>th</sup> century is well within the 95% confidence interval (Furuse et al., 2010).

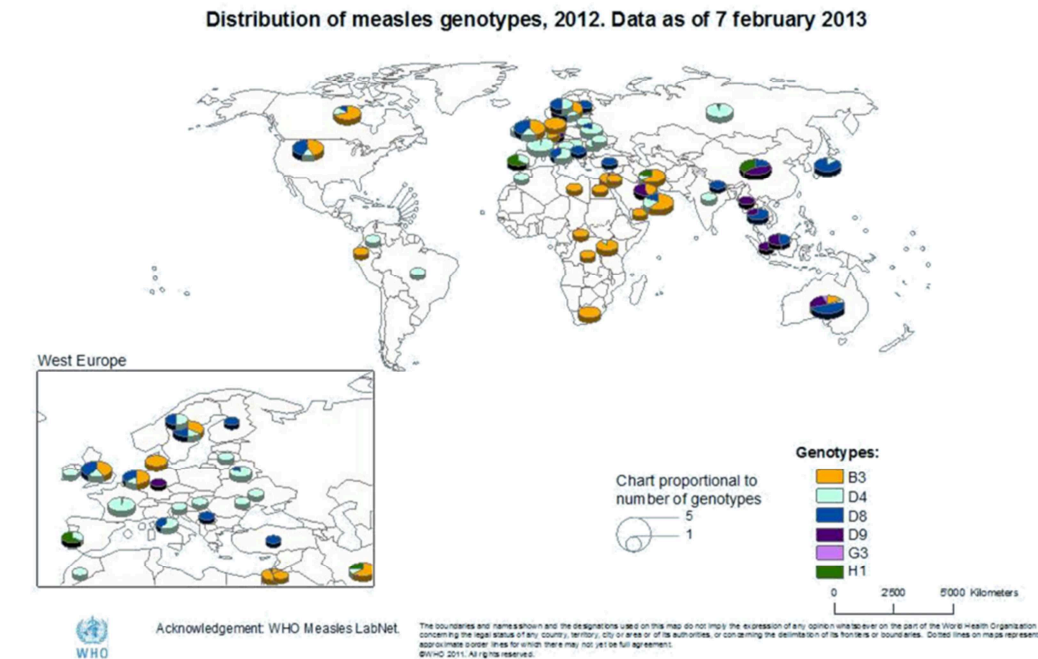


**Figure 1: Measles wildtype genotype distribution worldwide in 2012.**

Adapted from the measles surveillance data of the WHO (WHO, 2013c). The colour codes of the individual genotypes are indicated in the figure.

Worldwide, wildtype outbreaks occur mainly in developing countries, however the number of MV cases in Europe and North America is increasing in the last few years (Sleeman et al., 2008). This can be partially attributed to lower vaccine coverage especially in Europe, following vaccine scares and fraud MV vaccine publications linking it to autism (Murch et al., 2004) as well as the increasing global trafficking (Edelson, 2012). Recent outbreaks of measles virus in Germany were reported to be in Berlin in 2011 (Lassen et al., 2013), and in Berlin and Munich 2013 (unpublished data).

Vaccination protects effectively against infection by any wildtype virus known so far and the first vaccine to be licensed was Rubeovax in 1963 (Hilleman et al., 1968). The basis for the generation was the isolate of measles virus from human kidney cells of an infected child. All vaccine strains available are of the genotype A, curiously, no wildtype strain of genotype A was ever sequenced or isolated recently. It was reported that only 4 vaccine strains were generated from different wildtype isolates (Bankamp et al., 2011), namely the Edmonston lineage of vaccine strains (ENDERS et al., 1962; Schwarz, 1964), Leningrad-4 (Smorodintsev

et al., 1960), CAM-70 (Athman and Philpott, 2004) and Shanghai-191. The Schwarz strain (Schwarz, 1964), which is widely used in Germany for vaccinations, is based on the Edmonston isolate, thus belonging to the same lineage. It was generated by additional passaging of the Edmonston strain in chicken embryo fibroblasts.

Hallmarks of all vaccine strains are a generally higher induction of the innate immune system (Haralambieva et al., 2010; Kessler et al., 2011) and the usage of CD46 (Dörig et al., 1993; Naniche et al., 1993) as an additional cell entry receptor besides the wildtype receptors signalling lymphoid activating molecule (SLAM) (Tatsuo et al., 2000) and nectin-4 (Muhlebach et al., 2011; Noyce et al., 2011).

### 1.3. Structure and molecular biology of measles virus

The measles virus is a membrane-bound particle of variable size (Fig. 2 A) ranging from approximately 350-400nm (Fields et al., 2007). These particles are pleomorphic and occasionally polyploid with a lipid bilayer envelope (Fig. 2 A and C). The (-)-ssRNA ca. 16 kb genome comprises six genes, flanked by short terminal leader (3' end) and trailer sequences (5' end). From these genes, a total of six essential structural proteins (N, P, M, F, H and L) and two non-structural and non-essential proteins are expressed (V and C) (Fig. 2 B).

The RNA genome is protected against degradation by the nucleocapsid protein (N), which is responsible for packaging it into the ribonucleoprotein complex (RNP). One N protein is able to bind to and protect exactly six nucleotides, resulting in the fact that the genome length has to be a multiple of six to ensure proper encapsidation ("rule of six") (Calain and Roux, 1993). Associated with the nucleoprotein and the RNA are the phosphoprotein (P) and large protein (L). Both L and P form the viral RNA-dependent RNA polymerase with L as the catalytic subunit and P as an essential co-factor. The P protein links both N and L, thus enabling efficient viral transcription and replication (Liston et al., 1995). Only RNPs can serve as templates for the polymerase for both transcription and replication. The RNA dependent RNA polymerase has to be present in the virion to ensure infectivity (Rima and Duprex, 2009). Transcription and replication of the viral genomic RNA (vRNA) occur mainly in perinuclear compartments (Wileman, 2007) resembling intracellular inclusion bodies.

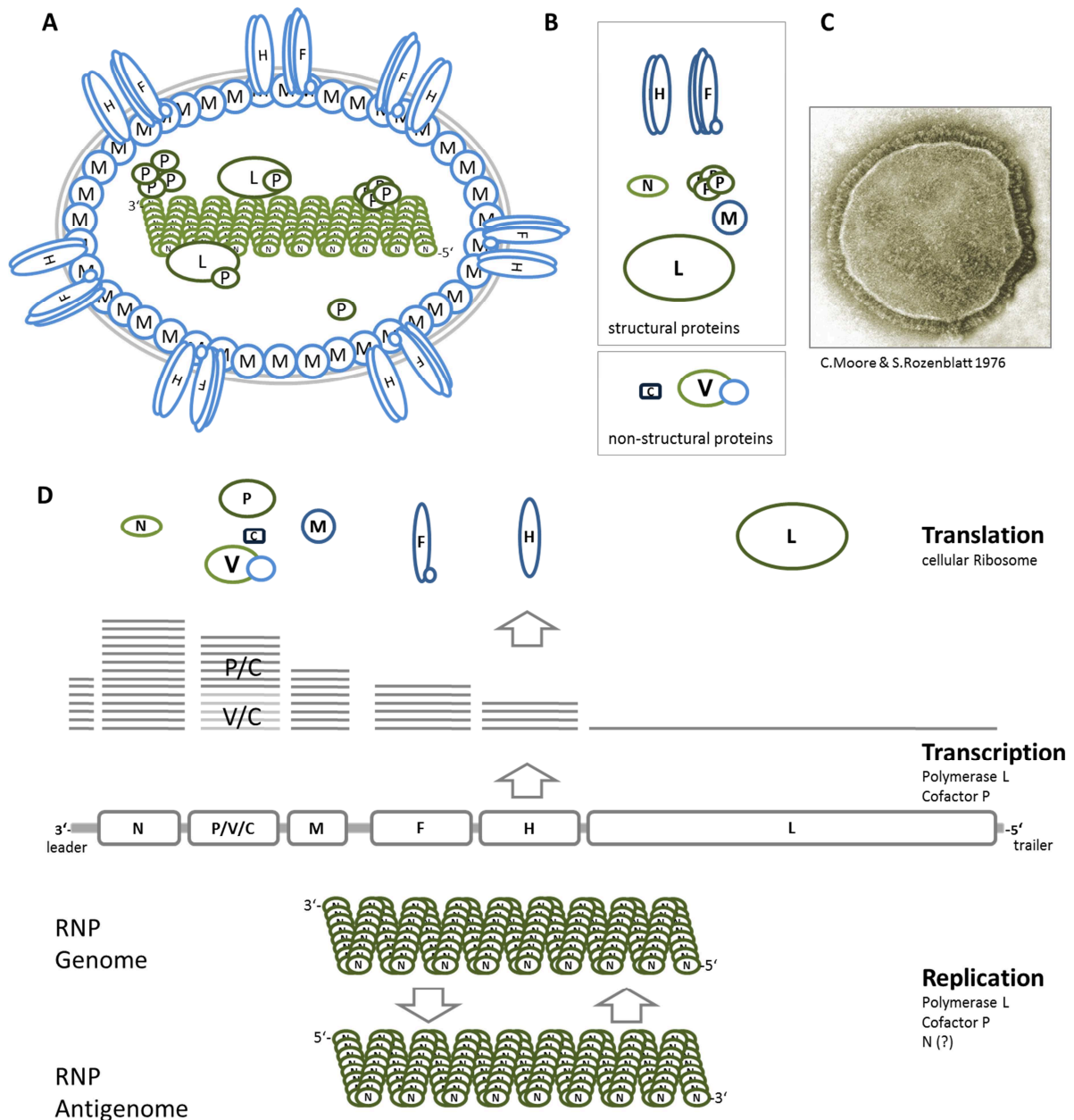


**Figure 2: Measles virus morphology, replication and transcription**

(A) Scheme of the measles virus particle composed of the structural proteins in (B). RNP components are depicted in green, other MV proteins in blue. N encapsidates the genomic RNA to form the RNP, L and P associate with it. M surrounds the viral RNP lining it to the lipid bilayer membrane, depicted in grey here. The two membrane spanning proteins are F, a trimer and H a dimer. The F protein consists of two fragments held together by disulfide bonds. The non-structural proteins C and V (B) are not part of the virion, and are only expressed in infected cells. (C) Electron microscopy picture of a typical measles virus. The surface proteins are visible as spikes around the membrane, whereas the RNP with the genomic RNA can be seen inside the membranous structure. (D) Overview on transcription from the MV genome, as well as replication and translation from the subgenomic RNAs.

Leader RNA and the mRNAs are transcribed from the genome in a stepwise manner, mRNAs are posttranscriptionally modified by 5' capping and 3' polyadenylation. The polymerase complex is able to dissociate from the RNP at the gene borders, however transcription always starts at the leader sequence. This results in the appearance of a gradient of mRNAs (Barrett and Underwood, 1985), although the slope can vary (Cattaneo et al., 1987). The mRNAs transcribed by the viral RNA dependent RNA polymerase do not differ from cellular mRNAs in that they contain a 5' cap and a 3' poly(A) tail. Therefore, they can be translated by the cellular ribosomes (Gerlier and Valentin, 2009). The polymerase is also capable of replicating the whole genome, resulting in the production of an antigenomic positive sense RNA strand (cRNA) which is concurrently encapsidated by N proteins. This RNP is then replicated into vRNAs again and immediately complex with N proteins to form genomic RNPs (Kingsbury, 1974; Rima and Duprex, 2009) (Fig. 2 D).

The M (matrix) protein co-localises with the RNPs and is required for virus budding (Rima and Duprex, 2009). It is also part of the virion. Responsible for the attachment to target cells is the viral transmembrane hemagglutinin protein (H). It forms dimers of dimers (tetramers) (Gerlier and Valentin, 2009) and mediates the binding to the cellular entry receptors (Santiago et al., 2002). Wildtype MV use the human signalling lymphocyte activation molecule (hSLAM; or CD150) (Tatsuo et al., 2001) and nectin-4 (Muhlebach et al., 2011; Noyce et al., 2011), whereas attenuated strains also can additionally utilize the CD46 receptor (Dorig et al., 1993; Naniche et al., 1993) for their entry. Wildtype H, however can be artificially adapted to recognize CD46 (Nielsen et al., 2001) reproducing the adaptation process during vaccine production. Once the H protein recognizes the receptor, the fusion between viral membrane and cellular membrane is accomplished by the fusion protein (F), a membrane-spanning trimer (Ader et al., 2013; Brindley et al., 2012). F is a class I fusion protein, consisting of two processed peptides F1 and F2 which are derived from the F0 precursor protein and linked by a disulphide bridge (Smith et al., 2009). Both F and H are responsible for the fusion of neighbouring cells, generating the so-called syncytia, giant fused cells (BLACK et al., 1956; Gerlier, 2006). This syncytia formation is a hallmark of infection in most cell lines, as well as in vivo (Nozawa et al., 1994; Wild et al., 1991).

Although MV possesses only 6 genes, 8 proteins are translated. The two additional, but non-structural proteins (C and V) are encoded in the genome, namely in the P gene (Bellini et al., 1985; Cattaneo et al., 1989); they have important functions as virulence factors and

antagonists of cellular immune responses (Conzelmann, 2005; Gerlier and Valentin, 2009; Goodbourn and Randall, 2009; Pfaller and Conzelmann, 2008; Rima and Duprex, 2009).

#### 1.4. The P gene products and their functions

The P gene is unique among the genes of multiple Mononegavirales, due to its ability to be able to encode 3 different proteins: P, V and C.

The exact transcript of the P gene generated by the viral polymerase complex during infection is the P mRNA. The first translation product of the P mRNA is the P protein, the essential co-factor of the viral polymerase complex. Both the V and the C protein are non-essential for the viability of the viruses (Radecke and Billeter, 1996; Schneider et al., 1997).

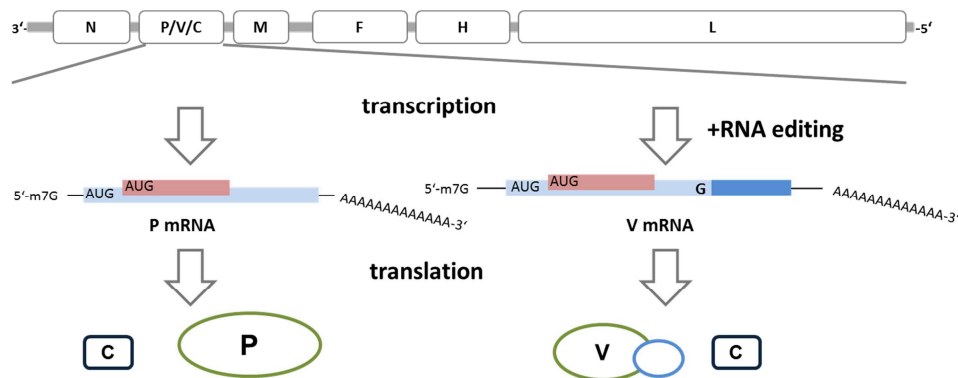


**Figure 3: Schematic view on the transcription and translation from the MV P gene.**

The P gene is transcribed from the MV genome during infection by the viral polymerase complex L and P, including capping and polyadenylation. The exact transcript of the P gene is the P mRNA, whereas the V mRNA has a non-templated G residue inserted at a defined position (editing site). The translational product of the first AUG of the P mRNA is the P protein; the translation product of the first AUG of the V mRNA is the V protein, thus having the same N-terminus as the P protein but distinct C-terminal domain due to the frameshift induced by the inserted G residue into the mRNA. From both mRNAs the C protein is translated from a second AUG start codon downstream of the first by ribosomal leaky scanning.

The V protein is expressed from the V mRNA which is a result of RNA editing of the P mRNA by the viral polymerase complex. A non-templated G is inserted at a defined position in the mRNA eventually resulting in the translation of the V protein, which shares the N-terminal domain with P but has a distinct C-terminus (Cattaneo et al., 1989). This small zinc-finger domain (Liston and Briedis, 1994) turned out to represent a hub module for binding and inhibiting the function of a variety of cellular molecules (Andrejeva et al., 2004;

Cruz et al., 2006; Palosaari et al., 2003; Pfaller and Conzelmann, 2008; Ramachandran and Horvath, 2010; Schuhmann et al., 2011). From both mRNAs of the P gene the C protein is expressed via an alternative start codon, recognized by the cellular ribosome via leaky scanning (Bellini et al., 1985) (Fig. 3).

The main function of the P protein is to serve as the co-factor of the viral polymerase L (Horikami et al., 1994). It is able to bind to the N protein, linking the polymerase complex with the RNP. Additionally it is proposed to position incoming N proteins on the nascent RNA (Devaux and Cattaneo, 2004).

In contrast to the cytoplasmic P and V proteins, C shuttles between the cytoplasm and nucleus (Nishie et al., 2007). MV C protein has been reported to down-regulate viral transcription and replication (Bankamp et al., 2005; Reutter et al., 2001) and to act as a viral release and infectivity factor (Devaux and Cattaneo, 2004), by modulating the polymerase activity by binding together with P to the cellular molecule SHCBP1 (Ito et al., 2013).

The MV P gene products -P, V and C- are long known as viral virulence factors (Escoffier et al., 1999; Goodbourn and Randall, 2009; Mrkic et al., 2000; Patterson et al., 2000; Radecke and Billeter, 1996; Randall and Goodbourn, 2008; Valsamakis et al., 1998) being able to counteract both adaptive and innate immune responses, but only recently more detailed knowledge on the multiplicity of their individual and cooperative roles in modulating innate immune responses is emerging.

## 2. Defense of a host against viruses and viral counter-measures

During evolution the hosts of viruses evolved strategies to counteract the invading pathogen and facilitate clearance of infections. These strategies can be summed up as the immune system. The human immune system uses elaborate mechanisms ranging from pattern recognitions to specific non-self structure recognition to identify potential threats. The response generated is mostly protein based (Chaplin, 2006; Litman et al., 2010), although in invertebrates and plants siRNA strategies against viruses are also common (Stram and Kuzntzova, 2006).

The human immune system can be subdivided into the innate immune system and the adaptive immune system. While the former is non-adaptive and reacts only to specific pathogen associated molecular patterns (PAMP), the latter is a highly diverse and specific system to recognise non-self peptides, proteins, structures and modifications.

### 2.1. Adaptive immunity

The diversity and adaptability of the adaptive immune system heavily relies on immunoglobulins which are encoded by rearrangeable gene segments. These immunoglobulins encoded by T and B cells, are able to recognise a multitude of epitopes, not all of them foreign (Pancer and Cooper, 2006). Therefore it is crucial for the host to distinguish between self and non-self antigens from e.g. pathogens. To this end, T-cells undergo a selection process leaving only those clones alive, which recognize non self antigens. T cells can recognize antigens presented by antigen presenting cells (APC). All cells with the exception of non-nucleated cells are able to present antigens on major histocompatibility complex (MHC) molecules. Two different isoforms of the protein MHC exist: MHC classes I and II. While MHC class I proteins are loaded with peptides derived from a special proteasomal degradation process, thus presenting intracellular pathogens, the endosomal pathway is mainly responsible for providing the peptides for MHC class II molecules. Therefore they represent fragments of foreign pathogens from the extracellular space. Recognition of a foreign antigen by T cells leads to activation and proliferation of a subset of B cells in the case of MHC-II antigen presenting or killing of the non-self antigen presenting cell by T Killer cells for MHC-I antigen presenting cells.

The B cells in turn are the main antibody producing cells, and release neutralizing antibodies into the bloodstream, which then can bind and inactivate pathogens. The B cells

can also evolve in memory B cells, providing a long-term memory of the pathogen for eventual rapid re-release of antibody upon a reinfection. This mechanism is the base for a successful vaccination, eventually leading to life-long immunity against the vaccinated pathogen (Charles A Janeway, 2001; Litman et al., 2010).

## **2.2. Adaptive immunity during MV infection**

Measles virus activates a T cell response 10-14 days after infection, and the rash is caused by infiltrating by CD4+ and CD8+ T cells. Viremia is cleared within a few days after. MV can no longer be isolated from PBMCs thereafter. The mechanism how this clearance occurs is however not fully understood. Interestingly, MV induces lymphopenia, a decrease in numbers of circulating B and T cells (Ryon et al., 2002) as well as a suppression of lymphocyte proliferation *in vivo*. Lymphopenia is probably caused by altered trafficking and increased cell death. The status is however returned to normal after the rash disappears (Auwaerter et al., 1999). In the case of lymphocyte proliferation it is speculated that a lack of IL-2 is responsible for part of the defect (Griffin et al., 1987) and the interaction of MV virions with hSLAM may contribute to the phenotype (Schlender et al., 1996). Additionally the cell cycle of these cells is arrested in G1 (McChesney et al., 1988; McChesney et al., 1987). In immunocompromised patients MV infection may lead to fatal giant cell pneumonia or inclusion body encephalitis, underlining the importance of the adaptive immunity response during MV infection (Griffin, 2010).

## **2.3. Innate immunity**

The innate immune system is the first line of defence against invading pathogen. It responds to stimulation with patterns associated with pathogens (PAMPs) and danger-associated molecular patterns (DAMPs). In contrast to PAMPs, DAMPs are molecules that initiate a response, although not being part of invading pathogens. Typically these cytosolic and nuclear molecules are released upon tissue damages or cell necrosis. Invading pathogens are detected via patterns associated with pathogens (PAMPs), such as LPS (Athman and Philpott, 2004; Philpott and Girardin, 2004) from bacteria or dsRNA and triphosphorylated RNA (Cui et al., 2008; Hornung et al., 2006; Pichlmair et al., 2006; Pichlmair and Sousa, 2007) from viruses. It is not as flexible as the adaptive immune system and it does not possess any memory of previous infections. The response evoked by PAMP recognition is not subject to any variation fitting to the invading pathogen, it is more a general defence initiated with a huge variety of mechanisms used, though. Upon PAMP recognition by various cellular and extra-cellular pattern recognition receptors (PRRs), the immediate response is the induction of

interferon (IFN) and cytokines and the secretion of these cytokines, which in turn signal on neighbouring cells to set up an antiviral state (Fig. 4).

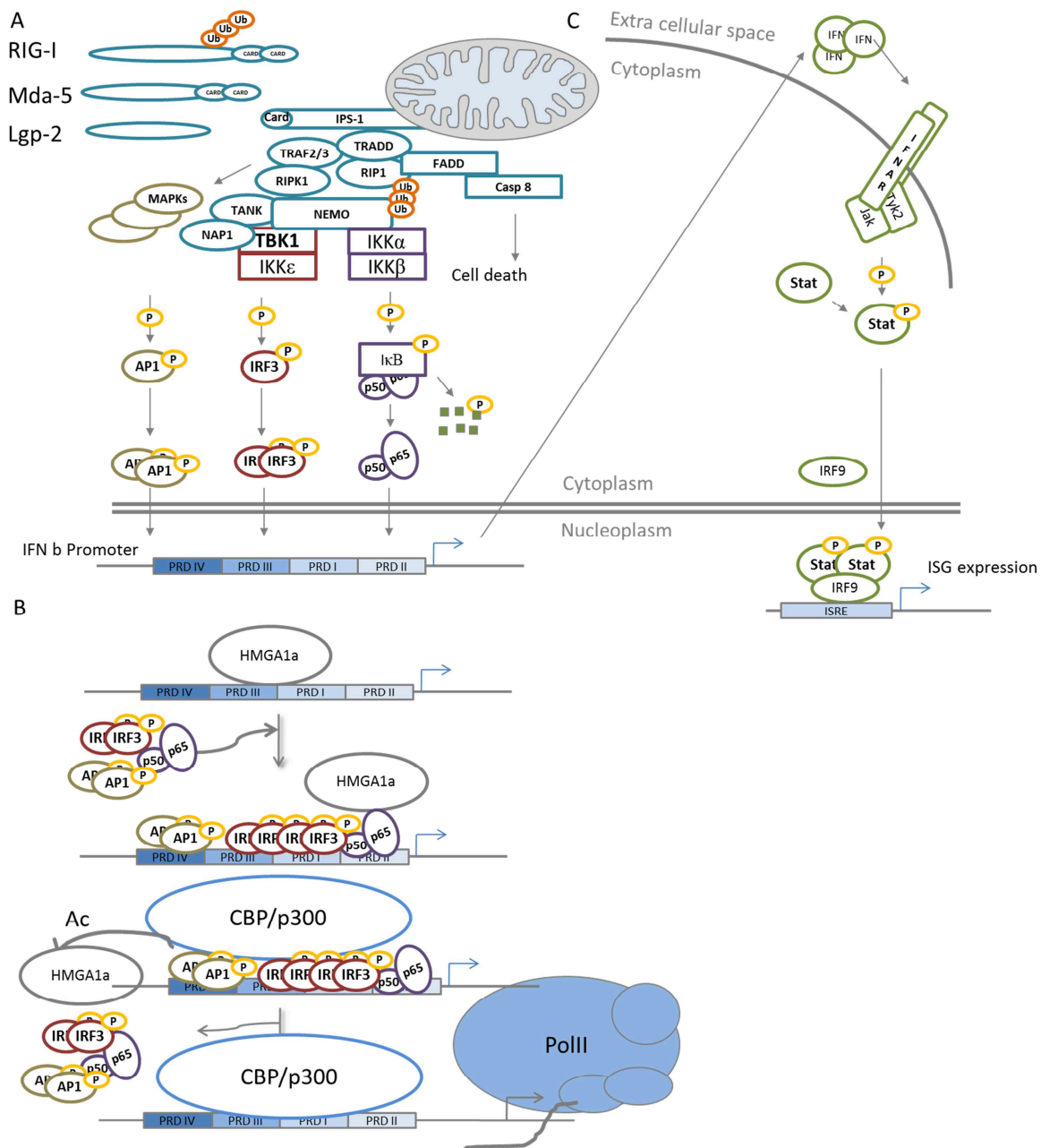


**Figure 4: Schematic depiction of the intracellular signalling pathway leading to interferon beta induction and the interferon signalling pathway.**

(A) Induction of interferon beta. Foreign intracellular RNA is sensed by the RIG-like-helicases which in turn are activated and bind to IPS-1. IPS-1 serves as an assembly platform for diverse effector molecules, most prominent among them the IKK kinases, TBK1 and the MAP kinases. They lead to the activation and nuclear accumulation of the transcription factors NF-κB, IRF3 and AP1 respectively (Randall and Goodbourn, 2008). Common signalling proteins are depicted in blue, the AP1 pathway in brown, the IRF3 pathway in red and the NF-κB pathway in purple.

Modifications by phosphorylation are depicted in yellow, ubiquitination in orange. (B) Model of enhanceosome assembly and disassembly: The interferon  $\beta$  enhancer is a 57bp element and can be separated into different transcription factor binding domains (positive regulatory domains, PRDs). In an unstimulated cell, HMGA1a binds to the enhancer DNA element. HMGA1a is thought to orchestrate the binding of transcription factors such as Fos/Jun (AP1), dimers of phosphorylated IRF3 and IRF7 and NF- $\kappa$ B to the enhancer element of the interferon  $\beta$  promoter upon receiving a stimulus. After acetylation of HMGA1a by the recruited p300/CBP the enhanceosome disassembles and RNA polymerase II is recruited and transcription starts. (Panne et al., 2007; Thanos et al., 1993; Yie et al., 1999) (C) Interferon signalling cascades and induction of ISGs. Secreted interferon  $\beta$  binds to the IFNAR receptor on neighbouring cells, activating JAK kinases, which phosphorylates STAT1. Active STAT1 dimerises, binds IRF9 and activates transcription of interferon stimulated genes (ISGs) in the nucleus. The proteins involved are depicted in green, modification by phosphorylation in yellow.

PRRs can be grouped with respect to their cellular localization. Toll-like receptors (TLRs) are located on the extracellular surface or on the inner membrane of endosomes, thus responding to extracellular PAMPs. They recognize various ligands, ranging from viral and bacterial nucleic acids to specific components of the membrane of pathogens. (Kawai and Akira, 2008; Kawai and Akira, 2011; Kumar et al., 2009; Kumar et al., 2011; Randall and Goodbourn, 2008).

### ***Interferon induction by RLRs***

The main intracellular PRRs are RIG-like-helicases (RLRs), among them retinoic acid inducible gene I (RIG-I), melanoma-differentiation-associated gene 5 (MDA-5) and Laboratory of Genetics and Physiology 2 (LGP2). RIG-I is known to bind to 5'-triphosphorylated RNA (Cui et al., 2008; Hornung et al., 2006; Pichlmair et al., 2006), and the search for an MDA-5 ligand is ongoing, though polyI:C and long dsRNA have been identified as activators of MDA-5 (Wu et al., 2013). It was also speculated that viral RNA lacking 2'-O methylation is an inducer of MDA-5 (Zust et al., 2011). During MV infection, leader RNA and the genomic/antigenomic RNA can induce activation of RIG-I (Rima and Duprex, 2009). Upon binding of its ligand the receptor is activated by dimerization and exposure of its CARD domains (Zeng et al., 2010), leading to the activation of a subsequent signalling cascade. The exact nature of the MV ligand of MDA-5 is not known, but it is activated during viral infection (Ikegame et al., 2010). Importantly, defective interfering particle production by

measles virus could lead to a robust interferon induction, as seen for the closely related parainfluenza 5 virus (Killip et al., 2011), probably via both RIG-I and MDA-5.

Both activated RIG-like helicases recruit and activate the mitochondrial membrane-bound IPS-1/MAVS/Cardif/VISA protein (Kawai et al., 2005; Randall and Goodbourn, 2008), which then forms clusters at the mitochondrial surface upon activation (Onoguchi et al., 2010b; Takamatsu et al., 2013). This adaptor is essential for the three main signalling cascades leading eventually to the activation of the cellular transcription factors ATF2/Jun, NF- $\kappa$ B and IRF3 (Kumar et al., 2006; Xu et al., 2005). IPS-1 leads to activation of FADD/TRAF6 in the NF- $\kappa$ B branch, which subsequently activates the IKK complex. The IKK complex phosphorylates I $\kappa$ B, which is then degraded (Alkalay et al., 1995) and the transcription factor NF- $\kappa$ B is released and can enter the nucleus to stimulate transcription. IPS-1 also activates the TBK1/TANK complex via direct interaction with TRAF3 (Xu et al., 2005) (Fig. 4 A).

IRF3 is a transcription factor activated by phosphorylation via the kinases TBK1/IKKi at its C-terminal domain (Panne et al., 2007b). It was suggested that expression of the MV N protein can in addition to the classical induction cascade enhance IRF3 phosphorylation (tenOever et al., 2002). Phosphorylated IRF3 then forms dimers and accumulates in the nucleus where it binds to the IFN- $\beta$  promoter region together with NF- $\kappa$ B and ATF2/c-Jun to effectively activate IFN- $\beta$  transcription (Ohno and Taniguchi, 1983). Regulation of IRF3 activity is further ensured by association with beta-catenin, which has to be deacetylated by histone deacetylases, bridging IRF3 to CBP (Chattopadhyay et al., 2013). If IRF7 is present in the cells (e.g. dendritic cells) it can additionally bind in its activated form to the promoter region to further stimulate IFN $\beta$  expression. The assembly is thought to be orchestrated by high mobility group AT-hook 1 proteins HMGA1, although they cannot be part of the final IFN- $\beta$  enhanceosome, due to overlapping binding sites (Panne et al., 2007a; Panne et al., 2007b; Thanos et al., 1993; Yie et al., 1999). This enhanceosome binds CREB Binding Protein (CBP) or p300, which in turn acetylates HMGA1a, eventually causing the disruption of the assembly (Yie et al., 1999). CBP/p300 can recruit the RNA polymerase II complex and enables efficient transcription by histone remodelling (Vo and Goodman, 2001) (Fig. 4 B).

To terminate the IRF3 signal, the activated protein binds to Pin1 (Saitoh et al., 2006), which causes ubiquitinylation of IRF3 by RBCK1 and degradation via the proteasomal pathway (Zhang et al., 2008). The activation of IRF3 is also thought to eventually induce apoptosis directly (Chattopadhyay et al., 2010), if not properly terminated. Therefore a fully

functional proteasome is critical for this cellular signalling cascade as well, terminating the signal, as well as facilitating induction by degrading the inhibitor of p65 and p55.

Interferon beta is the main cytokine induced by the above explained cascade. In addition to that, other proinflammatory cytokines, PRRs itself and other interferon are upregulated as well. The induced interferons can be further divided in three major groups, based on their cellular surface receptor. Type I interferons use the IFNAR receptor and include IFN $\alpha$ , IFN $\beta$  and IFN $\omega$ . Especially IFN $\alpha$  can be further classified into subgroups according to the gene responsible for expression (de Weerd et al., 2007). In contrast to that, only one gene is responsible for the expression of IFN $\beta$ , consequently only one subgroup exists. Type II interferons use the IFNGR and include the single IFN $\gamma$ . This response is differently stimulated than the Type I response. Another group are type III interferons which bind the IL10R2 and IFNLR1 and include IFN $\lambda$  (Fensterl and Sen, 2009).

### ***Interferon type I induced signalling***

Neighbouring cells have the outlined specific interferon receptors, which subsequently induce signalling cascades leading to the expression of interferon stimulated genes and also provide feedback to interferon release. These transcribed genes set the cells in an anti-viral state and can eventually induce apoptosis in infected cells to clear the organism from the pathogen (Randall and Goodbourn, 2008). Secreted interferon beta and alpha activates the JAK/STAT-signalling cascade by binding to the type-I interferon receptor (IFNAR), leading to the phosphorylation of the transcription factor STAT1. STAT1 dimerizes, binds to IRF9 and accumulates in the nucleus, where it stimulates the expression of interferon stimulated genes (ISGs). Among these are antiviral proteins (e.g. RNase L, oligoadenylate synthetase (OAS) or Mx) and components of the IFN-induction pathways (e.g. the transcription factor IRF7), thus creating a positive feedback signal for the enhancement of IFN production (Levy et al., 2002; Randall and Goodbourn, 2008). IRF7 can also be activated directly via Toll-like-receptor signalling in dendritic cells, where it is constitutively expressed (Randall and Goodbourn, 2008) (Fig. 4 C).

## **2.4. Viral innate immune evasion strategies**

Different viruses have developed different strategies to evade the antiviral innate immune response. In the case of measles the main virulence factors antagonizing innate immune responses have been identified to be encoded in the P gene: P, V and C. Additionally, the N protein of N was also implicated to play a role by blocking nuclear import of activated Stat1

(Takayama et al., 2012). A stimulating effect on IFN induction, however, was also reported (tenOever et al., 2002).

The V and P proteins of MV were long identified as potent antagonists of both interferon signalling and interferon production. The shared N-terminal domain of P and V for example can block STAT1 phosphorylation (Caignard et al., 2009; Devaux et al., 2007). V, in addition, binds to STAT2 and JAK1 via the V<sub>CTD</sub> (Caignard et al., 2007; Ohno et al., 2004; Palosaari et al., 2003; Ramachandran et al., 2008; Yokota et al., 2003). Moreover the V protein C-terminal domain is capable of binding to IKK $\alpha$  and IRF7, acting as a decoy substrate for phosphorylation (Pfaller and Conzelmann, 2008). Additionally it is able to bind and block MDA-5 (Childs et al., 2007; Motz et al., 2013), but not RIG-I. Furthermore, this hub-domain associates with p65, thus blocking its nuclear import and the proper activation of the Nf- $\kappa$ B response (Schuhmann et al., 2011). The MV P protein, in addition, was shown to induce transcription of the TLR inhibitor A20 in macrophage cell lines (Yokota et al., 2008) which might enhance negative feedback to proinflammatory responses in these cells.

A contribution of the C protein to the regulation of IFN induction was suggested recently. Specifically, MV mutants deficient for C protein production (C<sup>ko</sup>) viruses were better inducers of IFN- $\beta$  compared to parental or V<sup>ko</sup> viruses (McAllister and Samuel, 2009; Nakatsu et al., 2006). The observed activation of PKR (Toth et al., 2009), which leads to enhancement of IFN induction via activation of ATF-2 and NF- $\kappa$ B (McAllister and Samuel, 2009), suggested that in the presence of C the accumulation of viral dsRNA serving as a molecular pattern for RLR is down regulated (McAllister et al., 2010). Additionally, it was suggested, that the MV C protein either shelters viral RNA or decreasing the overall viral RNA load in the cell (Nakatsu et al., 2006; Nakatsu et al., 2008; Sleeman et al., 2008) thus interfering with the recognition of the viral RNA by RIG-I or PKR. C protein was also implicated in preventing type I IFN-mediated expression of ISG, though less efficiently than V (Fontana et al., 2008; Shaffer et al., 2003; Yokota et al., 2011b).

Among the *Morbilliviruses* MV is most closely related to Rinderpest virus (RPV) (Furuse et al., 2010), which also encodes for a C protein, in a different ORF of the P gene mRNAs. It was reported that the RPV C protein blocks interferon  $\beta$  induction presumably in the nucleus, although the exact mechanism remains unclear (Boxer et al., 2009). Another close relative of MV is the parainfluenza 5 virus. It lacks the expression of a C protein, but the V protein is an important virulence factor. Similar to MV V it binds STAT1 and MDA-5 (Childs et al., 2007;

Motz et al., 2013), but in addition is able to modulate DDB1 (Li et al., 2006) to induce Stat2 degradation.

The Sendai virus C protein is able to restrict production of dsRNA during infection, thereby inhibiting the recognition of the virus by the intracellular Rig-like helicases and PKR (Takeuchi et al., 2008). The same effect was also reported for yet another Paramyxovirus, the human parainfluenza virus 1 (HPIV1) (Boonyaratanakornkit et al., 2011).

The phosphoprotein (P) of the rhabdovirus rabies virus is able to bind to the TBK1 complex, thereby inhibiting phosphorylation of IRF3 including its dimerization and nuclear translocation (Brzozka et al., 2005; Rieder et al., 2011; Rieder and Conzelmann, 2009). Moreover it is also able to inhibit the signalling pathway, which is activated after stimulation of the cells with interferon type I (Interferon  $\alpha/\beta$ ), by binding to phosphorylated STAT1 and STAT2 (Brzozka et al., 2006). Rabies virus does not encode any V or C accessory proteins, VSV however has a conserved C ORF with yet unknown function.

### 3. Generating recombinant viruses

To study changes of viral proteins in the viral context, recombinant viruses with distinct sequences and properties have to be generated. In contrast to DNA or positive strand RNA viruses, the viral genome of negative strand RNA viruses per se is not infectious. The negative sense orientation of the genomes is responsible for its inability to directly use the cellular machinery for transcription and eventually the translation of proteins. The viral polymerase complex has to generate subgenomic positive-orientation mRNAs first, and is therefore also present in infectious virions. To this end, a rescue of negative strand RNA viruses was developed using reverse genetics, relying on the co-transfection of the viral cDNA together with helper proteins encoding N, P and L into cells (Conzelmann, 2004; Conzelmann et al., 1990; Schnell et al., 1994).

Once viral antigenomic RNA is generated from a cDNA plasmid using T7 polymerase dependent transcription it is loosely encapsidated by the viral N protein which is provided either by plasmid transfection or stable cell lines. This loosely packed RNP is then recognized by the viral polymerase complex and the transcription of the genome starts. This nascent RNA is co-transcriptionally encapsidated by N and in turn used to transcribe viral subgenomic mRNAs and to replicate. Upon translation of the viral proteins by the cellular ribosome from the subgenomic RNA, the life cycle of the virus starts and infectious particles are released

from the cells to spread the infection (Fig 5 A) (Radecke et al., 1995; Schnell et al., 1994; Takeda et al., 2000).

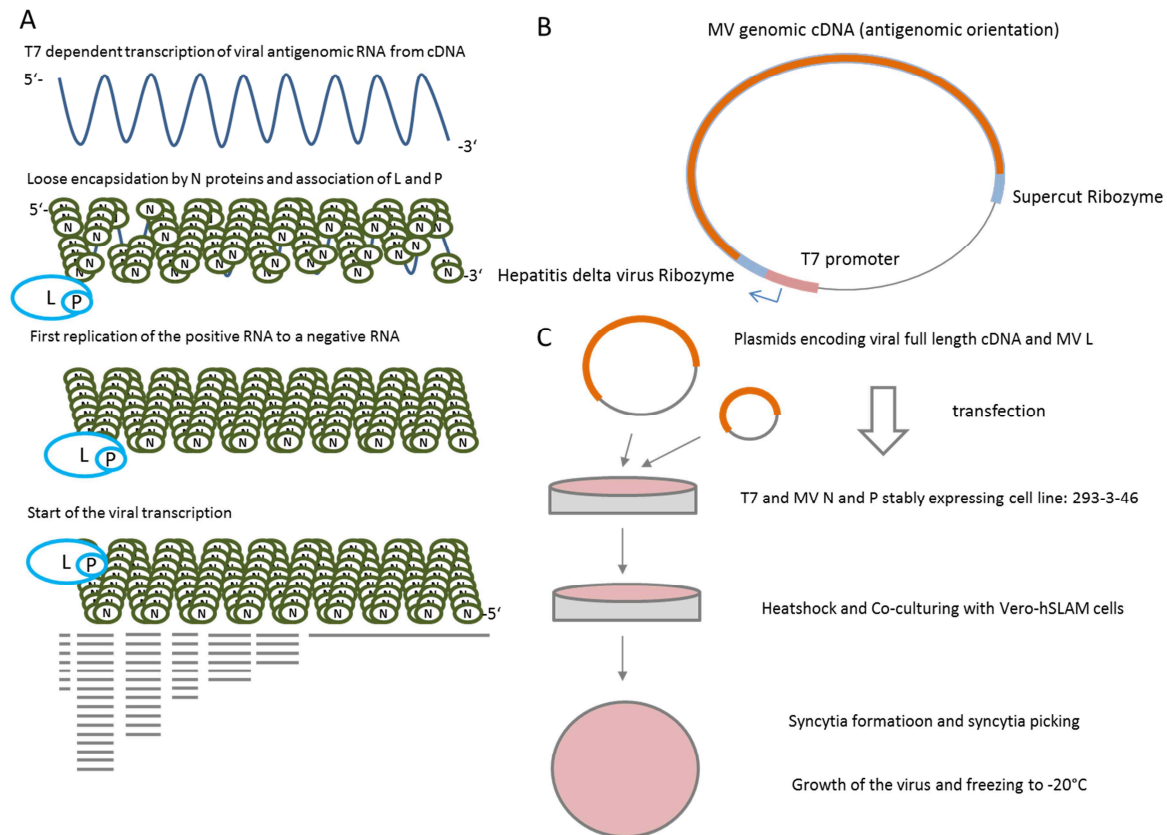


**Figure 5: Schematic depiction of MV rescue and the plasmids used.**

(A) The processes inside the cell: The viral antigenomic full length RNA (in dark blue) is transcribed from cDNA by the T7 polymerase and the 3' and 5' ends processed by ribozymes. N protein (green) loosely encapsidates the viral RNA. The viral polymerase complex (L and P, light blue), which are co-expressed as well, form the viral replication polymerase complex and replicate the antigenomic RNA to form genomic RNA. From the genomic RNA, the normal viral transcription takes place and the viral proteins are expressed by the host machinery. From these cells, infectious viral particles are released completing the rescue of recombinant virus. (B) Scheme of the plasmid used for viral cDNA transfection. The antigenomic RNA is transcribed T7 polymerase dependent and the ends of the RNA cropped by the indicated ribozymes to ensure the proper length and termini. (C) Scheme of the method for rescuing measles virus. Plasmids encoding viral full-length RNA and MV L are transfected into 293-3-46 cells, which express stably MV N, P and the T7 Polymerase. After heat shocking the cells at 42°C they are co-cultured with Vero-hSLAM cells to provide easily infected cells for emerging rescued virus. A successful rescue is detected by syncytia formation of Vero-hSLAM cells and these syncytia are picked and the rescue virus multiplied on Vero cells.

This basic system works in principle for every negative strand RNA virus. In the case of MV, the T7 polymerase and the viral proteins N and P are stably expressed by the 293-3-46 cell line (Radecke et al., 1995). Only transfection of the viral genome in cDNA and a plasmid encoding the MV L protein is necessary. In this study the cDNA was based on the vac2 plasmid, encoding a Schwarz strain identical viral cDNA (del Valle et al., 2007). This sequence was subcloned into the pBluescript vector and flanked with ribozymes (Ghanem et al., 2012; Pfaller, 2010) (Fig. 5 B). The ribozymes ensure proper processing of the genomic ends dramatically increasing the efficiency of the rescue. Heat shocking the transfected cells after 2 days increases the efficiency of the viral rescue, as well, (Parks et al., 1999) by inducing cellular heat shock proteins and increasing MV transcription rates. Co-cultivating these rescue cells with Vero cells stably expressing the MV high affinity receptor hSLAM (Vero-hSLAM, (Ohno et al., 2007)), leads to spread of the virus on these easily infected, interferon-negative cells upon successful rescue (Fig. 5 C). Once syncytia formation is visible, these plaques can be picked to isolate clones of rescued virus, which are subsequently propagated on Vero and Vero-hSLAM cells (Radecke et al., 1995) for stock production.

#### 4. Aim of this thesis

The aim of this thesis is to characterise the interplay between the innate immune system and the measles virus C protein in more detail, especially focusing on revealing differences between wildtype and vaccine MV strains. Although a primary target of the C protein is the viral replication and transcription machinery, as established by previous publications, the impact of C on the host cell signalling pathway cannot be disregarded. Modulation of the host cell and especially the innate immune response greatly influences the infectivity and growth of the virus in general. Especially in vivo the innate immune system significantly contributes to the clearance of pathogens from the host, activating and stimulating the adaptive immune response (Le Bon and Tough, 2002). Therefore viruses strive to modulate mechanisms involved, targeting cellular signalling pathways and altering their functions to their own extend. To this end the impact of C on the host cell innate immune system shall be studied at first while overexpressed in cell culture. Additional mechanistic studies are to be done, such as screening for protein interaction partners. The insights gained by these experiments are used to create recombinant measles virus, which harbours specific alterations in the C protein encoding P gene. These viruses are to be used for characterisation of C in the viral context, establishing a system, which monitors the cellular response. Moreover, the effects these

Aim of this thesis

mutations show in overexpression systems on the hosts signalling cascades shall be confirmed during infection.

# MATERIALS AND METHODS

## 1. Materials

### 1.1. Chemicals

Acetone p.a.	Roth
Acridine orange	Roth
Acrylamide/Bisacrylamide 29:1 Rotiphorese Gel 40	Roth
Agarose	Invitrogen
Ampicillin	Roth
APS (Ammonium persulfate)	Amresco
Bactotrypton	BD
Bacto Yeast-extract	BD
$\beta$ -Mercaptoethanol	Sigma
Bromphenolblue	Sigma
DMSO (Dimethylsulfoxide)	J.T.Baker
EDTA (Ethylendiamin-tetraacetat)	Sigma
Ethanol abs. p.a.	Roth
Ethidumbromide solution 1 %	Roth
Formaldehyde 37% solution	Sigma
Glycerol p.a.	Roth
Glycine p.a.	Roth
Glyoxal	Roth
Isopropanol p.a.	Merck
HOAc abs. p.a.	Roth
KOAc (potassium acetate)	Merck
Milk powder	Merck
Methanol abs. p.a.	Roth
MgSO <sub>4</sub> ·7H <sub>2</sub> O (Magnesiumsulfate-heptahydrate)	Merck
Na <sub>2</sub> HPO <sub>4</sub> ·2H <sub>2</sub> O (Disodiumhydrogenphosphate-dihydrate)	Merck
NaCl (Sodium chloride)	Merck
NaOH (Sodium hydroxide)	Merck
NH <sub>4</sub> Cl (Ammonium chloride)	Merck
Orange G	Sigma / Fluka
Phenolred	Merck
SDS (Sodium dodecylsulfate)	Merck
TEMED p.a. (N,N,N',N'-Tetramethyl-ethylen-1,2-diamine)	Roth
Tricine PUFFERAN	Roth
Tris PUFFERAN p.a.	Roth
Triton-X100	Merck / Roth

**Materials**

Tween20	Roth
Complete Protease Inhibitor Cocktail	Roche
Na <sub>3</sub> VO <sub>4</sub> (sodium orthovanadate)	Sigma
NP40 (Nonidet P40)	Fluka
Polyethyleneimine (PEI)	Sigma Aldrich
Precision Plus Protein Standarts All Blue	Biorad
Vectashield Hard Set	Vector Laboratories

**1.2. Kits**

Dual Luciferase Reporter Assay System	Promega
Lipofectamine 2000	Invitrogen
Nucleobond Plasmid DNA Purification AX-100	Macherey&Nagel
QIAquick Gel Extraction Kit	QIAGEN
QIAquick PCR Purification Kit	QIAGEN
Western Lightning Chemiluminescence Reagent Plus	Perkin-Elmer
Calciumphosphate Transfection Kit	Promega
BCA Assay Kit	Pierce
QIAEx II	QIAGEN
QIAGEN RNA purification	QIAGEN
SilverQuest Silver Staining	Invitrogen

**1.3. Enzymes and buffers**

Pfu DNA polymerase	Fermentas
Restriction enzymes	New England Biolabs
T4 DNA ligase	New England Biolabs
100x BSA	New England Biolabs
10x Pfu DNA polymerase buffer	Fermentas
NE buffer 1, 2, 3, 4, EcoRI buffer	New England Biolabs
10x T4 DNA ligase buffer	New England Biolabs
Phusion DNA Polymerase	Finnzyme
5xPhusion Buffer HF	Finnzyme

**1.4. Antibodies****1.4.1. Primary**

<b>Name</b>	<b>Source</b>	<b>Supplier</b>
α-actin	rabbit	Sigma-Aldrich
α-flag	rabbit	Sigma-Aldrich
α-HA	rat	Sigma-Aldrich
α-MV C 1240	rabbit	R. Cattaneo
α-MV C 1242	rabbit	R. Cattaneo

## Materials

$\alpha$ -MV C	rabbit	Peptidserum: C. Pfaller
$\alpha$ -MV V/P	rabbit	Peptidserum: C. Pfaller
$\alpha$ -RV P (FCA)	rabbit	Metabion
$\alpha$ -flag	mouse	Sigma-Aldrich
$\alpha$ -IRF3	rabbit	Santa Cruz
$\alpha$ -IRF3 p386	rabbit	
$\alpha$ -IRF3 p396	rabbit	
$\alpha$ -MV N (unconj. or FITC-conj.)	mouse	Millipore

**1.4.2. Secondary**

Antibody	Supplier
$\alpha$ -rabbit-PO	Dianova
$\alpha$ -mouse-PO	Dianova
$\alpha$ -rabbit Alexa 488	Invitrogen (Molecular Probes)
$\alpha$ -mouse Alexa 555	Invitrogen (Molecular Probes)
$\alpha$ -mouse TMR	Invitrogen (Molecular Probes)
$\alpha$ -rabbit Alexa 633	Invitrogen (Molecular Probes)

**1.5. Oligonucleotides****1.5.1. For cloning and sequencing:**

No.	Name	Sequence
1	MVNfwdSnaBI	ATA TAC GTA ATG GCC ACA CTT TTA AGG
2	MVFfwdSnaBI	ATA TAC GTA ATG CCC GAA ACG ACC CCC
3	MVHfwdSnaBI	ATA TAC GTA ATG TCA CCA CAA CGA GAC
4	MVMfwdSnaBI	ATA TAC GTA ATG ACA GAG ACC TAC GAC
5	MVNrevXhoI	ATA CTC GAG CTA GTC TAG AAG ATT
6	MVCNLS_AAfwd	ACA GGA CCG AGC CAC CTG CAG CGG CGA GAA GGC AGG CAG TTC GGG T
7	MVCNLS_AArev	ACC CGA ACT GCC TGC CTT CTC GCC GCT GCA GGT GGC TCG GTC CTG T
8	EcoRI-MVCwt-woATG-fwd	ATA GAA TTC AAA AAC GGA CTG GAA T
9	NotI-MVCwt-rev	TAT GCG GCC GCT ATC AAG AGC TCG TGG ATC T
10	MVCsG44R_fwd	GGA CAG GAG CGA GCC ACC TGC ACG GAA GAG AAG GCA GGC AGT TCG GG
11	MVCsG44R_rev	CCC GAA CTG CCT GCC TTC TCT TCC GTG CAG GTG GCT CGC TCC TGT CC
12	MVCsNotI_rev	CAC GCG GCC GCT ATC AGG AGC TCG TGG ATC TCC CCT CCT TC
13	MVCsSnaBI_fwd	GTG TAC GTA GCC ACC ATG TCA AAA ACG GAC TGG AAT GCA TCC G

## Materials

14	MVCs/wtBamHISnaBIHA	GTG GGA TCC TAC GTA GCC ACC ATG TAT CCT TAT GAC GTG CCT GAC TAT GCC AGC CTG GGA GGA CCT TCA AAA ACG GAC TGG AAT
15	MV-Cwt-SnaBI-fwd	GTG TAC GTA GCC ACC ATG TCA AAA ACG GAC TGG AAT GTA TCC G
16	MVCwtBamHI_fwd	GTG GGA TCC GCC ACC ATG TCA AAA ACG GAC TGG AAT GTA TCC G
17	MVLeader-qRT-fwd	ACC AAA CAA AGT TGG GTA AG
18	MVLeader-qRT-rev	AAG TGC ACT AGA AGA TGA TC
19	MVvac2CstoCwtNLS_fwd	AGG ACA GGA GCG AGC CAC CTG CAA GGA AGA GAA GGC AGG CAG TTC GGG T
20	MVvac2CstoCwtNLS_rev	ACC CGA ACT GCC TGC CTT CTC TTC CTT GCA GGT GGC TCG CTC CTG TCC T
21	TagRFPfwdBamHISnaBI	GTG GGA TCC TAC GTA CCG CCA TGG TGT CTA AGG GCG AAG AGC TG
22	TagRFPNotI_rev	CAC GCG GCC GCT TAA TTA AGT TTG TGC CCC A
23	TagRFPfusionNsiI_rev	CAC ATG CAT TAA GTT TGT GCC CCA GTT TGC TAG GGA
24	CwtNotIwoTA_rev	CAC GCG GCC GCT CAA GAG CTC GTG GAT CTC CCC TCC TTC TGC A
25	CsNotIwoTA_rev	CAC GCG GCC GCT CAG GAG CTC GTG GAT CTC CCC TCC TTC TGC A
26	Cs/wtlinkerwoATG_fwd	GTG ATG CAT CCG GCG GCG GCT CAA AAA CGG ACT GGA AT
27	MVC-SV40NLS	GAG GGA TCC GCC ACC ATG ACT GCT CCA AAG AAG AAG CGT AAG TCA AAA ACG GAC TGG AAT
28	MV-M(4336)-rev	CCT CAA CAA CCC CCA GCA GA
29	MV-Cwt-XhoI-rev	CGC CTC GAG TCA AGA GCT CGT GGA TCT CCC CTC
30	MV-Cwt/s-Acc65I-fwd	GCG GGT ACC GCC ACC ATG TCA AAA ACG GAC TGG AAT G
31	MVCko-rev	GGA TGC ATT CTA GTC CGT TTT TCA CGT GGC GTG CCT GCT CT
32	TagRFPfusionAscI-rev	GCC GCC CGG CGC GCC ATT AAG TTT GTG CCC CAG TTT
33	MVClinkerwoATG-AscI-fwd	GTG GGC GCG CCG GGC GGC TCA AAA ACG GAC TGG AAT
34	MVCHA-fwd-BamHI/SnaBI-corr	ATA GGA TCC TAC GTA GCC ACC ATG TAC CCA TAC GAT GTT CCA GAT TAC GCT GGC TCA AAA ACG GAC TGG AAT
35	GFP-woATG-AscI-fwd	GCG GGC GCG CCG GTG AGC AAG GGC GAG GAG CTG

## Materials

36	GFP-XhoI-rev	CGC CTC GAG TTA CTT GTA CAG CTC GTC CAT
37	p125-EcoRI-fwd	GCG GAA TTC GTT TTA GAA ACT ACT AAA A
38	p125-BamHI-rev	CGC GGA TCC AAG GTT GCA GTT AGA AT
39	MVCs/wt-EcoRI-fwd	GCG GAA TTC GCC ACC ATG TCA AAA ACG GAC TGG AAT G
40	MVCs-XhoI-rev	GCC TCG AGT CAG GAG CTC GTG GAT CTC CCC TC
41	NotI-flag-MAP1B-fwd	ATA GCG GCC GCG CCA CCA TGG ACT ACA AAG ACG ATG ACG ATA AAG GAG CGA CCG TGG TGG TGG AAG CCA
42	NotI-MAP1B-fwd	ATA GCG GCC GCG CCA CCA TGG CGA CCG TGG TGG TGG AAG CCA
43	flag-ApaI-MAP1B-rev	TAT GGG CCC TTA TCC TTT ATC GTC ATC GTC TTT GTA GTC CAG TTC AAT CTT GCA TGC AGG GAA
44	ApaI-MAP1B-rev	TAT GGG CCC TTA CAG TTC AAT CTT GCA TGC AGG GAA
45	IPO8-BamHI-Ha-fwd	GCG GGA TCC ACC GCC ATG TAT CCT TAT GAC GTG CCT GAC TAT GCC AGC CTG GGA GGA CCT GAC CTC AAC CGG ATC ATC CAG GCG CTG
46	IPO8-NotI-rev	TAT GCG GCC GCT CAG TTG TTG CTG GGC ACA GTC CC
47	IPO7-BamHI-Ha-fwd	GCG GGA TCC ACC GCC ATG TAT CCT TAT GAC GTG CCT GAC TAT GCC AGC CTG GGA GGA CCT GAG ACC ATG GCG AGC CCA GGG AAA GAC
48	IPO7-NotI-rev	TAT GCG GCC GCT TAT AGC TGG AAG CCC TCC ATG GGG GCC TCA
49	IPO9-Acc65I-Ha-fwd	GCG GGT ACC ACC GCC ATG TAT CCT TAT GAC GTG CCT GAC TAT GCC AGC CTG GGA GGA CCT GCG GCG GCG GCG GCA GCT GGT GCG GCC
50	IPO9-NotI-rev	TAT GCG GCC GCT TAG ATG CCG ATG GTC TGT AGA ACT C
51	MVCwt/s-flag-SnaBI-fwd	GTG TAC GTA GCC ACC ATG GAC TAC AAA GAC GAT GAC GAT AAA GGA GCG TCA AAA ACG GAC TGG AAT G
52	MCSseq-fwd	GGA GCC ATT CGA AGG CCG GCC G
53	qPCR-MVNfwd-60	TCA AGA GAA CAC CCG GAA AC
54	qPCR-MVNrev-60	TTC ATG CAG TCC AAG AGC AG
55	qPCR-GAPDHfwd-60	AGC CAC ATC GCT CAG ACA C
56	qPCR-GAPDHrev-60	GCC CAA TAC GAC CAA ATC C
57	qPCR-IFNbfwd-60	AGG GGA AAA CTC ATG AGC AG
58	qPCR-IFNbrev-60	TCC TTG GCC TTC AGG TAA TG

## Materials

59	flag-MVN-NotI-fwd	ATA GCG GCC GCG CCA CCA TGG ACT ACA AAG ACG ATG ACG ATA AAG GAG CCA CAC TTT TAA GGA GCT TAG
60	flag-MVM-NotI-fwd	ATA GCG GCC GCG CCA CCA TGG ACT ACA AAG ACG ATG ACG ATA AAG GAA CAG AGA CCT ACG ACT TCG ACA AGT CG
61	MVF-fwd-NotI	ATA GCG GCC GCG CCA CCA TGT CCA TCA TGG GTC TCA AGG TGA AC
62	MVF-flag-rev-XhoI	CGC CTC GAG TCA TCC TTT ATC GTC ATC GTC TTT GTA GTC GAG CGA CCT TAC ATA GGA TTT TGA T
63	flag-MVH-fwd-NotI	ATA GCG GCC GCG CCA CCA TGG ACT ACA AAG ACG ATG ACG ATA AAG GAT CAC CAC AAC GAG ACC GGA TAA ATG CCT TC
64	BamHI-flag-IRGM-fwd	GCG GGA TCC GCC ACC ATG GAC TAC AAA GAC GAT GAC GAT AAA GGA GAA GCC ATG AAT GTT GAG AAA GCC TC
65	IRGM-NotI-rev	TAT GCG GCC GCT TAG TAT TCA CAT ACC CGC TCC TTC T
66	flagPSMD2-XhoI-fwd-longer	GCG GGA TCC GCC ACC ATG GAC TAC AAA GAC GAT GAC GAT AAA GGA GAG GAG GGA GGC CGG GAC AAG GCG CCG GTG CAG CC
67	Map1b-first571-apa1-rev	AAA CCC CTG AGG TCA CAA AAG TGA ATT AAG GGC CCA TA
68	NotI-PSMD2-rev	TAT GCG GCC GCT TAG AGA TCA TAA TTG GGG TTC TTC
69	flag-PSMC3-XhoI-fwd	GCG GGA TCC GCC ACC ATG GAC TAC AAA GAC GAT GAC GAT AAA GGA AAT CTG CTG CCG AAT ATT GAG AGT CCA GTG
70	PSMC3-NotI-rev	TAT GCG GCC GCC TAG GCG TAG TAT TGT AGG TTG GC
71	flag-BamHI-CTNNB-fwd	GCG GGA TCC GCC ACC ATG GAC TAC AAA GAC GAT GAC GAT AAA GGA GCT ACT CAA GCT GAT TTG ATG GA
72	NotI-CTNNB-rev	TAT GCG GCC GCT TAC AGG TCA GTA TCA AAC CAG GC

**1.5.2. Primer used for qRT PCRs**

#	Name:	Sequence:
1	qRTMVL-fwd	ATC AGG GAA ATA TCA GAT GG
2	qRTMVL-rev	AGT TGT GTG CAA GTT TTG AG

**Materials**

3	qPCR-MVNfwd	TCA AGA GAA CAC CCG GAA AC
4	qPCR-MVNrev	TTC ATG CAG TCC AAG AGC AG
5	qPCR-GAPDHfwd	AGC CAC ATC GCT CAG ACA C
6	qPCR-GAPDHrev	GCC CAA TAC GAC CAA ATC C
7	qPCR-IFNbfwd	AGG GGA AAA CTC ATG AGC AG
8	qPCR-IFNrev	TCC TTG GCC TTC AGG TAA TG

**1.6. Miscellaneous**

Eppendorf-Cups 1.5 mL, 2.0 mL	Eppendorf
Falcon flasks 15 mL, 50 mL	BD
Hyperfilm ECL	Amersham
Multiwell-dishes 24 wells, 12 wells, 6 wells, 96 wells	BD
PVDF Membrane	Millipore
PCR Cups 200 µL	biozym
Pipettetips 1000 µL, 200 µL, 10 µL	Peske, HTL
Gel-Blotting paper	Roth
Cell culture flasks T25, T75	BD

**1.7. Cell lines and media**

D-MEM (Dulbecco's Modified Eagle Medium)	Invitrogen Gibco
Trypsin-EDTA	Invitrogen Gibco
Penicillin-Streptomycin (PenStrep)	Invitrogen Gibco
L-Glutamine	Invitrogen Gibco
Fetal Bovine Serum (FBS)	Invitrogen Gibco
Optimem	Invitrogen Gibco/ Life Technologies
RPMI 1640	Invitrogen Gibco
G418	

Medium for the cell lines: D-MEM

+ 10 % FBS  
+ 2 % L-Glutamine  
+ 0.2 % PenStrep.  
= D-MEM +3

RPMI 1640  
+19% FCS  
+0.2% PenStrep  
= RPMI+2

**Materials**

HEK-293T	Human embryonic kidney cells, expressing the T antigen of SV40
Vero	African green monkey cells
Vero-hSLAM	Vero cells stably expressing the human SLAM receptor
293-3-46	HEK293 cells stably expressing MV N and P & T7 polymerase
Hep2	human larynx carcinoma cell line
HeLa	human cervix carcinoma cell line
293T-STAT-/-	human embryonic kidney cell line 293T with a knockout of the STAT1 gene
A549	human lung epithelial cell line
DG75 wt	human B cell line

**1.8. Plasmids and bacteria**

*E. coli* XL1 (blue; Stratagene) was used for plasmid preparations.

#	Name:	Description:	Cloning:	Source:
1	pCR3	empty vector		empty vector
2	pBluescript SK II (-)	empty vector		empty vector
3	pCR3-fl-MVC(wt)	expressing a flag tagged version of C wildtype	EcoRI-flag-Cwt-XhoI	
4	pCR3-MVC(wt)	expression vector for Cwt	EcoRI-Cwt-XhoI	
5	pCR3-fl-MVc(schw)	expression vector for flag tagged C Schwarz	EcoRI-fl-Cs-XhoI	by Christian Pfaller
6	pCR3-MVC(schw)	expression vector for Cs	EcoRI-Cs-XhoI	by Christian Pfaller
7	pBS-HHRz-MVvac2-HdRz(sc)	Antigenomic cDNA vector for MV vac2 flanked by a Hammerhead Ribozyme and a SuperCut Ribozyme		from R. Cattaneo/ Christian Pfaller
8	pEMC-MV L	Expression vector for MV L, EMCV IRES driven		by R. Cattaneo
9	p55c1b-Luc	Reporter plasmid for the IRF3 recognition site, expresses Firefly luciferase		by T. Fujita
10	pCMV-RL	Renilla luciferase controlled by the CMV promoter		ordered from Promega
11	fl-IRF3	Expression plasmid for flag tagged IRF3		by K. Brzozka
13	p125-Luc	Reporter plasmid for the whole IFN $\beta$ promoter, drives expression of Firefly Luciferase		by T. Fujita

## Materials

14	pEGFP	Expression vector for eGFP	ordered from Promega
15	pTIT-GFP	Expression vector for eGFP, T7 promoter	by N. Zapf
16	pFLAG--IKKa	Expression vector for flag-tagged IKKa	by K. Ruckdeschl
17	pCR3-flag-TBK1	Expression vector for flag-tagged TBK1	by K. Brzozka
18	RV P	Expression vector for rabies virus P protein	by K. Brzozka
19	MV V	Expression vector for MV V protein	by Christian Pfaller
20	pCR3- fl MV L	Expression vector for flag-tagged MV L protein	by Kerstin Schuhmann
21	pcDNA3.1-fl MV H	Expression vector for flag-tagged MV H protein	MV H ORF, SnaBI (vor flag), XhoI
22	pcDNA3.1-fl MV M	Expression vector for flag-tagged MV M protein	MV M ORF, SnaBI (vor flag), XhoI
23	pCR3-MV F	Expression vector for MV F	by Kerstin Schuhmann
24	pCR3-MV H	Expression vector for MV H	by Kerstin Schuhmann
25	fl-IRF35D	Expression vector for flag-tagged IRF3 with 5 D mutations: constitutive active	by J. Hiscott
26	pCR3- MV M	Expression vector for MV M	by Kerstin Schuhmann
27	pCR3- MV N	Expression vector for MV N	by Kerstin Schuhmann
28	pCR3-MV Cwt44AA	Expression vector for MV Cwt, Mutation 44AA	Mutagenesis: Cwt ORF, EcoRI - XhoI 44AA
29	pCR3-MV Cs44AA	Expression vector for MV Cs, Mutation 44AA	Mutagenesis: Cs ORF, EcoRI - XhoI 44AA, S39T
30	pCR3-fl-MV Cwt44AA	Expression vector for flag-tagged MV Cwt, Mutation 44AA	Mutagenesis: Cwt ORF, EcoRI - XhoI 44AA
31	pCR3-fl-MV Cs44AA	Expression vector for flag-tagged MV Cs, Mutation 44AA	Mutagenesis: Cs ORF, EcoRI - XhoI 44AA, S39T, I103L
32	pcDNA3.1-fl-MV N	Expression vector for flag-tagged MV N	flag-SnaBI-N-XhoI based on pCDNA3.1-flag-IRF7 vector

## Materials

33	pCR3-MV L	Expression vector for MV L		by Kerstin Schuhmann
34	pEF-Bos dRIG-I (1-284)	Expression vector for the CARD domains of RIG-I (constitutive active)		by T. Fujita
35	pBS-HHRz-MVvac2-ATU-HdRz(sc)	Measles virus antigenomic cDNA flanked by Ribozymes with an additional transcription unit between the P and the M gene (gene border duplication of P)		by Christian Pfaller
36	pBS-HHRz-MVvac2-ATU-PdV-HdRz(sc)	Measles virus antigenomic cDNA flanked by Ribozymes with an additional transcription unit between the P and the M gene (gene border duplication of P) and additionally a mutation to abolish V expression		by Christian Pfaller
37	pCR3-fl-MV P	Expression vector for flag-tagged MV P		by Christian Pfaller
38	pBS-HHRz-MVvac2-ATU-PdC-HdRz(sc)	Measles virus antigenomic cDNA flanked by Ribozymes with an additional transcription unit between the P and the M gene (gene border duplication of P) and additionally mutations to abolish C expression	Mutagenesis for Cko	based on MV vac2-ATU
39	fl-IPS-1	Expression vector for flag-tagged IPS-1		by Kerstin Schuhmann
40	pCR3-MV fl-V	Expression vector for flag-tagged MV V		by Kerstin Schuhmann
41	pCR3-fl-dRIG-I	Expression vector for flag-tagged CARD domains of RIG-I 1-284		by Kerstin Schuhmann
42	pCR3-fl-RIG-I	Expression vector for flag-tagged RIG-I		by Martina Rieder
43	IRF3-GFP	Expression vector for GFP tagged IRF3		
44	pCR3-MV P	Expression vector for MV P		by Christian Pfaller
45	pCR3-MV CswtNLS	Expression vector for MV C with wt NLS sequence	Mutagenesis: G44R	based on plasmid pCR3-Cs
46	pCR3-fl-MV CswtNLS	Expression vector for flag tagged MV C with wt NLS sequence	Mutagenesis: G44R	based on plasmid pCR3-fl-Cs
47	pCR3-Ha-Cs	Expression vector for HA-tagged MV Cs	BamHI-Ha-Cs-NotI	
48	pCR3-HA-MV	Expression vector for HA-tagged MV	BamHI-HA-	

## Materials

	CswtNLS	Cs with wildtype NLS	CswtNLS-NotI	
49	pBS-HHRz-MVvac2-Cko-GFP-HdRz(Sc)	Measles virus antigenomic cDNA flanked by Ribozymes with an additional transcription unit between the P and the M gene (gene border duplication of P) encoding for GFP and additionally mutations in the P gene to abolish C expression	SnaBI-GFP-NotI	based on MV vac2 Cko-ATU
50	pCR3-Cwt	Expression vector for MV Cwt	BamHI-Cwt-NotI	
51	pBS-HHRz-MVvac2-Cko-CswtNLS-HdRZ(SC)	Measles virus antigenomic cDNA flanked by Ribozymes with an additional transcription unit between the P and the M gene (gene border duplication of P) encoding for CswtNLS and additionally mutations in the P gene to abolish C expression	SnaBI-CswtNLS-NotI	based on MV vac2 Cko
52	TagRFP-profilin	TagRFP expression vector, tags profilin		ordered from Evrogen
53	pBS-HHRz-MVvac2-wtNLS	Measles virus antigenomic cDNA flanked by Ribozymes with a point mutation in the P gene altering C G44R	Mutagenesis: C G44R	based on MV vac2
54	pBS-HHRz-MVvac2-Cko-Cs-HdRZ(SC)	Measles virus antigenomic cDNA flanked by Ribozymes with an additional transcription unit between the P and the M gene (gene border duplication of P) encoding for Cs and additionally mutations in the P gene to abolish C expression	SnaBI-Cs-NotI	based on MV vac2 Cko-ATU
55	pBS-HHRz-MVvac2-Cko-Cwt-HdRZ(SC)	Measles virus antigenomic cDNA flanked by Ribozymes with an additional transcription unit between the P and the M gene (gene border duplication of P) encoding for Cwt and additionally mutations in the P gene to abolish C expression	SnaBI-Cwt-NotI	based on MV vac2 Cko-ATU
56	pBS-HHRz-MVvac2-Cko-CwtmNLS-HdRZ(SC)	Measles virus antigenomic cDNA flanked by Ribozymes with an additional transcription unit between the P and the M gene (gene border	SnaBI-CwtmNLS-NotI	based on MV vac2 Cko-ATU

## Materials

		duplication of P) encoding for CwtmNLS and additionally mutations in the P gene to abolish C expression		
57	pCR3-SV40NLS-CwtmNLS	Expression vector for CwtmNLS with an additional SV40 NLS at the N terminus	BamHI-SV40NLS-CwtmNLS-NotI	
58	pCR3-HA-Cwt	Expression vector for HA tagged MV Cwt	BamHI-HA-Cwt-NotI	
59	pCR3-HA-CwtmNLS	Expression vector for HA tagged MV CwtmNLS	BamHI-HA-CwtmNLS-NotI	
60	pBS-HHRZ-MVvac2-GFP-HdRZ(SC)	Measles virus antigenomic cDNA flanked by Ribozymes with an additional transcription unit between the P and the M gene (gene border duplication of P) encoding for GFP		by Christian Pfaller
61	pCR3-TagRFP	Expression vector for TagRFP	BamHI-TagRFP-NotI	
62	peGFP-C3	Expression vector for eGFP		by Clontech
63	pCR3-TagRFP-Cwt	Expression vector for a fusion protein between TagRFP and Cwt	BamHI-TagRFP-AscI-Cwt-NotI	
64	pCR3-TagRFP-Cs	Expression vector for a fusion protein between TagRFP and Cs	BamHI-TagRFP-AscI-Cs-NotI	
65	pCR3-TagRFP-CwtmNLS	Expression vector for a fusion protein between TagRFP and CwtmNLS	BamHI-TagRFP-AscI-CwtmNLS-NotI	
66	pCR3-TagRFP-CswtNLS	Expression vector for a fusion protein between TagRFP and CswtNLS	BamHI-TagRFP-AscI-CswtNLS-NotI	
67	pBS-HHRz-MVvac2-Cko-TagRFP-Cwt-HdRZ(SC)	Measles virus antigenomic cDNA flanked by Ribozymes with an additional transcription unit between the P and the M gene (gene border duplication of P) encoding for TagRFP-Cwt and additionally mutations in the P gene to abolish C expression	SnaBI-TagRFP-AscI-Cwt-NotI	based on full length vector MV vac2 Cko-ATU
68	pBS-HHRz-MVvac2-Cko-TagRFP-Cs-HdRZ(SC)	Measles virus antigenomic cDNA flanked by Ribozymes with an additional transcription unit between the	SnaBI-TagRFP-AscI-Cs-NotI	based on full length vector MV vac2 Cko-ATU

## Materials

		P and the M gene (gene border duplication of P) encoding for TagRFP-Cs and additionally mutations in the P gene to abolish C expression		
69	pBS-HHRz-MVvac2-Cko-TagRFP-HdRZ(SC)	Measles virus antigenomic cDNA flanked by Ribozymes with an additional transcription unit between the P and the M gene (gene border duplication of P) encoding for TagRFP and additionally mutations in the P gene to abolish C expression	SnaBI-TagRFP-NotI	based on full length vector MV vac2 Cko-ATU
70	pBS-HHRz-MVvac2-TagRFP-HdRZ(SC)	Measles virus antigenomic cDNA flanked by Ribozymes with an additional transcription unit between the P and the M gene (gene border duplication of P) encoding for TagRFP	SnaBI-TagRFP-NotI	based on full length vector MV vac2 ATU
71	pBS-HHRz-MVvac2-Cko-TagRFP-CwtmNLS-HdRZ(SC)	Measles virus antigenomic cDNA flanked by Ribozymes with an additional transcription unit between the P and the M gene (gene border duplication of P) encoding for TagRFP-CwtmNLS and additionally mutations in the P gene to abolish C expression	SnaBI-TagRFP-AscI-CwtmNLS-NotI	based on full length vector MV vac2 Cko-ATU
72	pBS-HHRz-MVvac2-Cko-TagRFP-CswtNLS-HdRZ(SC)	Measles virus antigenomic cDNA flanked by Ribozymes with an additional transcription unit between the P and the M gene (gene border duplication of P) encoding for TagRFP-CswtNLS and additionally mutations in the P gene to abolish C expression	SnaBI-TagRFP-AscI-CswtNLS-NotI	based on full length vector MV vac2 Cko-ATU
73	PPM1b-GFP	Expression vector for a fusion between protein phosphatase, Mg <sup>2+</sup> /Mn <sup>2+</sup> dependent, 1B (PPM1B), transcript variant 2 and GFP		ordered from Origene
74	pcDNA3-FLAG-DDB1	Expression vector for flag-tagged DNA damage binding protein 1 (DDB1)		ordered from addgene
75	pCR3-HA-IPO8	Expression vector for HA-tagged importin 8 (IPO8)	BamHI-HA-IPO8-NotI	IPO8 mit BamHI-NotI in pCR3
76	pBS-HHRz-MVvac2-VCKo-ATU-	Measles virus antigenomic cDNA flanked by Ribozymes with an		cloned by Kerstin Schuhmann

## Materials

	HdRZ(SC)	additional transcription unit between the P and the M gene (gene border duplication of P) and additionally mutations in the P gene to abolish V & C expression		
77	pBS-HHRz-MVvac2-Cko-fl-Cs-HdRZ(SC)	Measles virus antigenomic cDNA flanked by Ribozymes with an additional transcription unit between the P and the M gene (gene border duplication of P) encoding for flag-tagged Cs and additionally mutations in the P gene to abolish C expression	SnaBI-flag-Cs-NotI	based on full length vector MVvac2 Cko
78	pBS-HHRz-MVvac2-Cko-fl-Cwt-HdRZ(SC)	Measles virus antigenomic cDNA flanked by Ribozymes with an additional transcription unit between the P and the M gene (gene border duplication of P) encoding for flag-tagged Cwt and additionally mutations in the P gene to abolish C expression	SnaBI-flag-Cwt-NotI	based on full length vector MVvac2 Cko
79	pCR3-fl-MAP1B	Expression vector for flag-tagged Microtubule associated protein 1 B	NotI-flag-MAP1B-ApaI	
80	pCR3-fl-MAP1B-fl	Expression vector for flag-tagged Microtubule associated protein 1 B	NotI-flag-MAP1B-flag-ApaI	
81	pCR3-MAP1B-fl	Expression vector for flag-tagged Microtubule associated protein 1 B	NotI-MAP1B-flag-ApaI	
82	pCR3-MAP1B	Expression vector for Microtubule associated protein 1 B	NotI-MAP1B-ApaI	
83	flag-Stat1	Expression vector for flag-tagged Stat1		cloned by Vanessa Hoffmann
84	pCR3-MV F-fl	Expression vector for flag-tagged MV F (C-terminal)	NotI-MV F-flag-XhoI	
85	pCR3-fl-MV H	Expression vector for flag-tagged MV H	NotI-flag-MV H-XhoI	
86	pBS-HHRz-MVvac2-VCKo-Cwt-HdRZ(SC)	Measles virus antigenomic cDNA flanked by Ribozymes with an additional transcription unit between the P and the M gene (gene border duplication of P) coding for Cwt and	SnaBI-Cwt-NotI	based on full length vector MVvac2 VCKo-ATU

**Materials**

		additionally mutations in the P gene to abolish V & C expression		
87	pBS-HHRz-MVvac2-VCko-CwtmNLS-HdRZ(SC)	Measles virus antigenomic cDNA flanked by Ribozymes with an additional transcription unit between the P and the M gene (gene border duplication of P) coding for CwtmNLS and additionally mutations in the P gene to abolish V & C expression	SnaBI-CwtmNLS-NotI	based on full length vector MV vac2 VCko-ATU
88	pBS-HHRz-MVvac2-VCko-CswtNLS-HdRZ(SC)	Measles virus antigenomic cDNA flanked by Ribozymes with an additional transcription unit between the P and the M gene (gene border duplication of P) coding for CswtNLS and additionally mutations in the P gene to abolish V & C expression	SnaBI-CswtNLS-NotI	based on full length vector MV vac2 VCko-ATU
89	pCR3-fl-MV N	Expression vector for flag-tagged MV N (N-terminal)	NotI -flag-MV N-XhoI	
90	pCR3-fl-MV M	Expression vector for flag-tagged MV M	NotI-flag-MV M-XhoI	
91	pCR3-fl-IRGM	Expression vector for flag-tagged IRGM	BamHI-flag-IRGM-NotI	
92	HA-CBP	Expression vector for HA tagged Creb binding protein (CBP)		ordered from addgene
93	HA-p300	Expression vector for HA tagged p300		ordered from addgene

If not stated otherwise, these plasmids were generated during this phd thesis.

**1.9. Viruses**

<b>Name</b>	<b>Description:</b>
rMV vac2	Recombinant MV with the exact vac2 sequence
rMV vac2-Cko	Recombinant MV with the exact vac2 sequence, except for mutations in the P gene, abolishing the expression of the C protein. The C ATG was knocked out as well as two stop codons introduced downstream. No amino acid change in P and V is induced.
rMV vac2-GFP	Recombinant MV with the vac2 sequence and the additional transcription unit between the P and the M gene, duplicating the P gene borders. In this case the transcription unit encodes the GFP protein.

rMV vac2CwtNLS	Recombinant MV with the exact vac2 sequence, except for a point mutation in the P gene, which changes the G44 residue in C to an arginine. In the P and V N-terminus a lysine is changed to an arginine.
rMV vac2- TagRFP	Recombinant MV with the vac2 sequence and the additional transcription unit between the P and the M gene, duplicating the P gene borders. In this case the transcription unit encodes the TagRFP protein.
rMV vac2Cko- TagRFP-Cwt	Recombinant MV with the vac2 sequence and the additional transcription unit between the P and the M gene, duplicating the P gene borders. Expression of the C protein is knocked out as described previously. In this case the transcription unit encodes the TagRFP-MV Cwt fusion protein.
rMV vac2Cko-TagRFP-Cs	Recombinant MV with the vac2 sequence and the additional transcription unit between the P and the M gene, duplicating the P gene borders. Expression of the C protein is knocked out as described previously. In this case the transcription unit encodes the TagRFP-MV Cs fusion protein.
rMV vac2Cko-TagRFP-CwtmNLS	Recombinant MV with the vac2 sequence and the additional transcription unit between the P and the M gene, duplicating the P gene borders. Expression of the C protein is knocked out as described previously. In this case the transcription unit encodes the TagRFP-MV CwtmNLS fusion protein.
rMV vac2Cko-TagRFP-CswtNLS	Recombinant MV with the vac2 sequence and the additional transcription unit between the P and the M gene, duplicating the P gene borders. Expression of the C protein is knocked out as described previously. In this case the transcription unit encodes the TagRFP-MV CswtNLS fusion protein.

### 1.10. Buffers and solutions

If not stated otherwise, the solvent is desalted water.

#### **1x PBS (pH 7.4)**

1 M NaCl, 27 mM KCl, 12 mM KH<sub>2</sub>PO<sub>4</sub>, 65 mN Na<sub>2</sub>HPO<sub>4</sub>·2H<sub>2</sub>O.

#### **70 % EtOH**

H<sub>2</sub>O<sub>dd</sub>, 70 % (v/v) Ethanol abs.

#### **20 % SDS**

H<sub>2</sub>O<sub>dd</sub>, 20 % (w/v) SDS.

**Transformation:**

**LB-Medium**

85 mM NaCl, 0.5 % (w/v) Bacto Yeast-extract, 1 % (w/v) Bactotrypton, 1 mM MgSO<sub>4</sub>, pH 7.5.

**LB++**

LB-Medium, 20 mM MgSO<sub>4</sub>, 10 mM KCl.

**DNA purification (Mini):**

**Flexi I**

100 mM Tris (pH 7.5), 10 mM EDTA, 200 µg/mL RNase.

**Flexi II**

200 mM NaOH, 1 % (v/v) SDS.

**Flexi III**

3 M KOAc, 2 M HOAc (pH 5.75).

**Agarose-Gels:**

**1 % agarose gels**

1 % (w/v) agarose in 1x TAE.

**10x TAE**

400 mM Tris (pH 7.8), 50 mM NaOAc·3H<sub>2</sub>O, 10 mM EDTA.

**Running buffer**

1x TAE, 40 µg/L ethidium bromide.

**Loading buffer (Orange G)**

5x TAE, 0.125 % Orange G, 15 % Ficoll 400.

**1kb marker**

380 µl 10x TE, 100 µl Blue Juice, 20 µl NEB 1kb DNA ladder

**Blue Juice**

50 % 10xTAE, 15% Ficoll 400, 0.125% Bromphenol blue, 0.125% Xylenecyanol, 0.125% Orange G

**Jagow-Proteingels:**

**10x Anode buffer**

2 M Tris (pH 8.9).

**10x Cathode buffer**

Materials

1 M Tris (pH 8.25), 1 M Tricin, 1 % (v/v) SDS.

**Gel buffer**

3 M Tris (pH 8.45), 0.3 % (v/v) SDS.

**Proteingel-lysisbuffer**

Tris (pH 6.8), 10 % glycerol (v/v), 6 M urea 2 % SDS (v/v), 0.01 % (w/v) bromphenol blue, 0.01 % (w/v) phenol red, 5 % (v/v)  $\beta$ -mercapto ethanol.

**10 % APS**

H<sub>2</sub>O<sub>dd</sub>, 10 % (w/v) Ammonium persulfate.

**Native Gels:**

**2x Native sample buffer**

125 mM Tris-Cl, pH 6.8, 30% glycerol, Bromphenolblue

**Lysis buffer**

50mM Tris-Cl, pH 8.0, 1% NP-40, 150 mM NaCl, 5 mM orthovanadate, 100  $\mu$ g/ml leupeptin, 1mM PMSF

**Gel Buffer**

1,5 M Tris, pH 8,8

**Lower Chamber Buffer**

25 mM Tris-Cl, pH 8.4, 192 mM Glycin

**Upper Chamber Buffer**

25 mM Tris-Cl, pH 8.4, 192 mM Glycin, 1% DOC

**Western-Blots:**

**10x Semidry-Buffer**

480 mM Tris (pH 8.6), 390 mM glycine, 0.05 % SDS.

**1x Semidry-Buffer**

10 % 10x Semidry-Buffer, 18 % methanol abs.

**PBS-Tween**

1x PBS, 0.05 % (v/v) Tween20.

**Co-IP:**

**PBS-EDTA**

1x PBS, 5 mM EDTA

**Co-IP Buffer**

50mM Tris (pH 7.5), 150 mM NaCl, 2mM EDTA, 1mM Na<sub>3</sub>VO<sub>4</sub>, NP40 0.5%.

**Co-IP Buffer Wash Buffer II**

50mM Tris (pH 7.5), 150 mM NaCl, 2mM EDTA

**Transfection:**

**PEI**

Sterile solution of PEI in H<sub>2</sub>O (1 mg/mL).

**Silver staining:**

**Fixative solution**

40% ethanol, 10% acetic acid

All other solutions provided by the Silverquest Kit (Invitrogen)

**Northern Blotting**

**50x Phosphate Buffer**

250 mM Na<sub>2</sub>HPO<sub>4</sub> x 2 H<sub>2</sub>O, 250 mM NaH<sub>2</sub>PO<sub>4</sub> x H<sub>2</sub>O

**RNA agarose gel**

2g Agarose, 4mL 50x phosphate buffer, 26.7 mL Formaldehyde 37%, 167.3 mL H<sub>2</sub>O

**Glyoxal solution**

8.8 M Glyoxal

**10x SSC**

1.5 M NaCl, 150 mM Na-citrate x 2 H<sub>2</sub>O, pH = 7.0

**Zeta hybridizing buffer**

250 mM Na<sub>2</sub>HPO<sub>4</sub> x 2 H<sub>2</sub>O, 250 mM NaH<sub>2</sub>PO<sub>4</sub> x H<sub>2</sub>O, 1mM EDTA, 7% SDS, pH = 7.2

**Zeta 5% wash buffer**

8% 50x phosphate buffer, 1mM EDTA, 5% SDS

**Zeta 1% wash buffer**

8% 50x phosphate buffer, 1mM EDTA, 1% SDS

## 2. Methods

### 2.1. Working with DNA

#### 2.1.1. *Mini preparation*

1 mL LB-medium including antibiotic was inoculated with a single bacteria colony from LB-agar plates and shaken over night at 37°C. The grown bacteria were pelleted for 60s at room temperature and 14,000 rpm and the pellet was resuspended in 200 µL FLEXI I buffer. 200 µL of FLEXI II buffer were added and the mixture was incubated at room temperature for 5 minutes to lyse the cells. Upon the addition of 200 µL of FLEXI III buffer to the mixture it was stored on ice for 5 minutes. The protein precipitate was removed by centrifugation (7 min, rt, 14,000 rpm). The supernatant was added onto 400 µl isopropanol abs. and centrifuged again (7 min, rt, 14,000 rpm). After removal of the supernatant the DNA pellet was dried at room temperature and finally dissolved in 50 µL H<sub>2</sub>O<sub>dd</sub>.

Restriction control digestions were carried out to identify clones for sequencing and re-transformation.

#### 2.1.2. *Midi preparation*

*(Nucleobond Plasmid DNA Purification Kit, Macherey&Nagel)*

50mL of an overnight culture of transformed bacteria in LB (+antibiotic) were pelleted at 3,500rpm, 4°C for 20 minutes. The supernatant was discarded and the pellet resuspended in 8 mL of buffer RES. 8 mL of buffer LYS (lysis buffer) were added to the suspension and the mixture was incubated at room temperature. 8 mL of buffer NEU (neutralizing buffer) were added after complete lysis of the bacteria, mixed, resulting in precipitation of proteins, lipids and genomic DNA. One AX 100 (including filter) column was equilibrated with 12 mL buffer EQU (equilibration buffer) and the suspension was loaded. The filter was washed afterwards with 5mL Buffer EQU and after the buffer passed the column removed and 8mL Buffer WASH added to wash the column. Plasmid DNA bound to the column was eluated with 5 mL of buffer ELU (elution buffer). The eluate was mixed with 3.5 mL isopropanol abs. and centrifuged for 20 minutes at 14,000 rpm and 4°C. The supernatant was removed and the DNA pellet washed with 2 mL of ice-cold 70% ethanol and centrifuged for 10 minutes at 14,000 rpm and 4°C. The purified pellet was dried at room temperature and resuspended in 400µl sterile desalted Water

(H<sub>2</sub>O<sub>dd</sub>). DNA concentration was determined photometrically (Nanodrop) and the preparation was finally stored at -20°C.

### **2.1.3. Agarose gel electrophoresis**

A heated 1% agarose solution in TEA buffer was used to cast gels of the required sizes. 12 µL of the preparation were mixed with 3 µL Orange G and loaded into the pockets. Separation was carried out at 120 V and 400mA for 45 minutes in 1x running buffer. The nucleic acids were detected via exciting the ethidium bromide with UV-radiation.

### **2.1.4. PCR**

#### ***Cloning PCR***

The reaction was prepared according to the following scheme:

<b>Enzyme/Buffer</b>	<b>amount</b>
Template	1µl (1pg – 10ng)
Primer 1 (10µM)	5µl
Primer 2 (10µM)	5µl
5xBuffer HF	20µl
DMSO	3µl
dNTPs	0.8µl
Phusion Polymerase	1µl
H <sub>2</sub> O <sub>dd</sub>	64.2µl

A PCR Cycler machine was used to carry out the reaction using the following program:

<b>#</b>	<b>Temperature</b>	<b>Duration</b>
1	98°C	30s
2	98°C	10s
3	50°C (dependent on primer)	30s
4	72°C	15s per kbp -> 30x back to step 2
5	72°C	10 min
6	4°C	pause

To analyse the resulting PCR product by gel electrophoresis, 5 µL of the PCR product was mixed with 1 µL Orange G loading buffer and loaded on an 1% agarose gel. The Electrophoresis was performed at 120 V for 45 min.

**Mutagenesis PCR**

This PCR reaction can be used to introduce site-directed mutations into vectors. Methylated vectors are used as a template and the whole vector is amplified during the PCR resulting in non-methylated mutated vectors. The methylated template is afterwards digested by DpnI.

The PCR reaction was prepared according to the following scheme:

<b>Enzyme/Buffer</b>	<b>amount</b>
Template	1µl (1pg – 10ng)
Primer 1 (10µM)	2.5µl
Primer 2 (10µM)	2.5µl
10xBuffer	10µl
dNTPs	1µl
Pfu Polymerase	1µl
H <sub>2</sub> O <sub>dd</sub>	82µl

A PCR Cycler machine was used to carry out the reaction using the following program:

<b>#</b>	<b>Temperature</b>	<b>Duration</b>
1	95°C	30s
2	95°C	10s
3	50°C (dependent on primer)	30s
4	72°C	120s per kbp -> 18x back to step 2
5	72°C	10 min
6	4°C	pause

To remove the methylated template DNA, DpnI (2.5 U) was added to the reaction mixture and incubated at 37°C for 2h.

**2.1.5. PCR purification**

*(QIAquick PCR Purification Kit)*

500 µL of buffer PBI were added to the PCR reaction, mixed and loaded on a QIAquick column, followed by centrifugation for 1 min at room temperature and 14,000 rpm. The flow-through was discarded, 750 µL PE washing buffer were loaded on the column and centrifuged at room temperature and 14,000 rpm. After removal of the flow-through, the column was centrifuged again to remove remaining residual PE buffer. Bound nucleic acids were eluted with 30 µL H<sub>2</sub>O<sub>dd</sub> by centrifugation for 1 min at 14,000 rpm.

**2.1.6. Preparative restriction**

Blunt-ended PCR products or circular plasmids were digested with suitable restriction enzymes to create specific overhangs for ligation. The PCR product DNA preparations were incubated with the restriction enzymes with restriction sites close to the 3' and 5' ends. The vector for the PCR fragment is digested in the same way to create a linear vector-fragment, which can be religated to a new plasmid with the insert from the PCR.

Plasmid DNA or PCR products were incubated with restriction enzymes as recommended by the supplier (New England Biolabs).

**2.1.7. Gel purification of DNA fragments**

*(QIAquick Gel Purification Kit, QIAEx II Kit)*

Restriction reactions for cloning were separated by electrophoresis as described above. Bands of the predicted size were cut out from the gel. The gel fragment was mixed with thrice its volume buffer QG and incubated at 50°C for 10 min. After dissolving of the gel, the resulting solution was loaded on a QIAquick column and centrifuged at 14,000 rpm for 1 minute at room temperature. The column was washed with 750 µL buffer PE and centrifuged again (same conditions as before). After removal of the flow-through, the column was centrifuged again to remove residual PE buffer. Bound nucleic acids were eluted with 30 µL H<sub>2</sub>O<sub>dd</sub> by centrifugation for 1 min at 14,000 rpm.

For plasmids or inserts longer than 10000nt (e.g. viral cDNA backbones), the QIAExII Kit was used according to the manufacturers protocol.

**2.1.8. Ligation**

Linearised vectors and processed PCR products were ligated using T4 DNA ligase in a reaction as follows:

<b>Enzyme/Buffer</b>	<b>amount</b>
Vector	0.5µl
Insert	10µl
T4 DNA Ligase	1µl
10xBuffer T4 Buffer	2µl
H <sub>2</sub> O <sub>dd</sub>	6.5µl

As a negative control the vector was ligated without the insert. The preparation was incubated for 2 hours at room temperature.

**2.1.9. Transformation**

50  $\mu$ L of a chemically competent *E. coli* XL-1 suspension were thawed on ice and 1  $\mu$ L of plasmid DNA was added. The bacteria were incubated for 20 minutes on ice, followed by a heat-shock for 2 minutes at 42°C and cooling on ice for 2 minutes. After addition of 200  $\mu$ L LB++ medium, the resulting suspension was shaken at 37°C for 30-90 minutes. For midi preparations 75 $\mu$ l of the bacteria suspension were added to 50 mL of LB medium + antibiotic (Ampicillin or Kanamycin, depending on the used plasmids) and shaken for 16 hours at 37°C (180 rpm). For cloning, the whole suspension was plated on LB-agar (+antibiotic) plates and incubated o/n at 37°C.

**2.1.10. Control restriction**

Control restriction reactions were carried out as follows:

DNA (Mini Preparation)	1 $\mu$ L
Restriction enzyme 1/2	0.1 $\mu$ L
100xBSA (if required)	0.1 $\mu$ L
Buffer	1 $\mu$ L
H <sub>2</sub> O <sub>dd</sub>	ad 10 $\mu$ L

The buffers and additional BSA were used as recommended by the supplier of the restriction enzymes (New England Biolabs). The mixture was incubated for 2 h at 37°C.

**2.1.11. Sequencing**

For plasmids or PCR inserts 30-100ng/ $\mu$ l DNA in 20 $\mu$ l water were sent to GATC. Either the provided standard primers were used or custom ordered primers (metabion, Martinsried) were diluted to 10ng/ $\mu$ l and sent as 20 $\mu$ l aliquots separate from the plasmid/PCR DNA to GATC.

Sequencing was carried out by GATC (Konstanz).

**2.2. Working with proteins****2.2.1. Polyacrylamide gel electrophoresis**

For western blots a 10%,12% or 15% denaturing separating gel and a 4% stacking gel were used, prepared in the following way:

	H <sub>2</sub> O <sub>dd</sub>	Gel buffer	Glycerol	Acrylamide	APS	TEMED
<b>separating-gel</b> <b>(15%)</b>	8.4 mL	12.0 mL	2.0 mL	13.5 mL	175 $\mu$ L	17 $\mu$ L

## Methods

<b>separating-gel</b> (12%)	11.1 mL	12.0 mL	2.0 mL	10.8 mL	175 $\mu$ L	17 $\mu$ L
<b>separating-gel</b> (10%)	12.9 mL	12.0 mL	2.0 mL	9.0 mL	175 $\mu$ L	17 $\mu$ L
<b>stacking-gel</b> (4%)	9.0 mL	3.5 mL	-	1.4 mL	116 $\mu$ L	18 $\mu$ L

The polymerization time was about 2h and the acrylamide was provided as a premixed solution.

Gelelectrophoresis:

The cells were treated 24 h p.Tr. with an equal amount of proteingel-lysisbuffer (for 100 $\mu$ L cells-suspension 100 $\mu$ L buffer) then boiled at 95°C for 5 minutes. As a protein marker Precision Plus Protein Standard (BIORAD) was used. Each pocket of the gel was loaded with 5 $\mu$ L of the marker or 50 $\mu$ L-80 $\mu$ L of the cell lysates. The separation was carried out at 37V for ca. 16 h.

### 2.2.2. *Native gels*

Native Gels (7.5%) were cast according to the following procedure without a stacking gel:

<b>Separating Gel:</b>	
water	11.3 mL
acrylamide	3.5 mL
Tris (1.5M)	5 mL
TEMED	20 $\mu$ l
APS	200 $\mu$ l

The gels were prerun 30 minutes at 40mA at 4°C. After loading of the samples the gels ran for approximately 1h at 25mA at 4°C. Blotting and immunodetection were carried out as described before.

### 2.2.3. *Gradient gels*

Gradient Gels (4-20%) were cast according to the following procedure using a gradient mixer. The two solutions were prepared separately:

	H <sub>2</sub> O <sub>dd</sub>	Gel buffer	Glycerol	Acrylamide	APS	TEMED
<b>separating-gel</b> (20%)	1.2 mL	4.0 mL	0.67 mL	6 mL	58.3 $\mu$ L	5.6 $\mu$ L
<b>separating-gel</b> (4%)	6 mL	4.0 mL	0.67 mL	1.2 mL	58.3 $\mu$ L	5.6 $\mu$ L

A stacking gel was added afterwards according to the usual 4% stacking gel.

#### **2.2.4. Western blotting**

After removal of the stacking gel, the separating gel washed for 15 minutes in 1x Semi Dry buffer. Three in 1x Semi Dry buffer soaked Gel-Blotting-Papers were placed on the blotting device and an also in 1x Semi Dry soaked, previously in methanol activated, PVDF membrane (Millipore) laid on top of it. Then the gel and another 3 layers of soaked blotting papers topped the membrane and the blotting chamber was closed. All work was carried out bubble free. The Blotting itself was carried out for 2h at 400mA.

When the transfer was finished, the PVDF membrane was washed with 2.5% milk powder in PBS to block unspecific binding sites 1-2 h at r.t..

#### **2.2.5. Immunodetection**

The blot membrane was washed three times with 20 mL PBS-TWEEN for 10 minutes each time. The primary antibodies were used in required dilution (see Materials) in PBS-TWEEN and incubated with the membrane over night at 4°C. Subsequently the membrane was washed again three times with 20 ml PBS-TWEEN for 10 minutes each time. The secondary antibody was incubated with the membrane for 2h at room temperature diluted in PBS-TWEEN. Afterwards the membrane was washed again three times with 20 mL of PBS-TWEEN.

The Western Lightning Chemiluminescence Reagent Plus (Perkin-Elmer) was mixed immediately before applying it to the membrane (the amount as required for the size of the membrane, about 500 µL per membrane). The Fusion (Vilber-Lourmat) device including the Fusion Cap Software was used to capture images of the blots.

#### **2.2.6. Silver Staining**

*(SilverQuest™ Silver Staining Kit, Life Technologies)*

After fixation of the polyacrylamide gel in the fixative solution for 1h, it was washed with 30% ethanol in water for 10 minutes. Afterwards the sensitizing solution was added onto the gel and incubated while shaking for 10 minutes. Following another two washing steps - first with 30% ethanol, then with water - the gel was incubated for 15 minutes with the staining solution. The staining solution was decanted and the gel quickly washed for 10-30 s with water and then incubated with the developing solution. The reaction was

stopped with the stopping solution after clear bands started to appear (usually around 8-10 minutes after addition of the developer). The gel was then washed with water again and imaged using the Fusion device and the white background light.

## 2.3. Working with cells

### 2.3.1. Cell culture

Cells were cultured in Dulbecco's modified Eagle Medium (DMEM) supplemented with 10% Fetal Calf Serum (FCS), 0.4% Penicillin/Streptomycin and 1% (-)-L-Glutamate and incubated at 37°C and 5% CO<sub>2</sub>. = DMEM+3

Or:

RPMI1640 supplied with 10% Fetal Calf Serum (FCS), 0.4% Penicillin/Streptomycin and incubated at 37°C and 5% CO<sub>2</sub>. = RPMI +2

Stably transfected cell lines were selected using antibiotics as indicated in the list below.

Cell Lines:

HEK-293T	Human embryonic kidney cells, expressing the T antigen of SV40	DMEM+3	
Vero	African green monkey cells	DMEM+3	
Vero-hSLAM	Vero cells stably expressing the human SLAM receptor	DMEM+3	+1:1000 G418 every 2 passages
293-3-46	HEK293 cells stably expressing MV N and P & T7 polymerase	DMEM+3	+1:1000 G418 every 2 passages
Hep2	human larynx carcinoma cell line	DMEM+3	
HeLa	human cervix carcinoma cell line	DMEM+3	
293T-STAT <sup>-/-</sup>	human embryonic kidney cell line 293T with a knockout of the STAT1 gene	DMEM+3	
A549	human lung epithelial cell line	DMEM+3	
DG75 wt	human B cell line	RPMI+2	

### 2.3.2. Transfection methods

#### *Lipofectamin*

This protocol is for 24-well plates and can be scaled up for other plates/dishes:

The plasmids for transfection were mixed in reaction tubes and the total DNA amount was adjusted with stuffer DNA to be equal in each tube.

The required amount of transfection reagent (2.5x the mass of DNA in  $\mu\text{g}$ ) was diluted in D-MEM (50  $\mu\text{L}$ /transfected well) and incubated for 5 min at r.t.. Plasmids were diluted additionally with 50  $\mu\text{L}$  D-MEM. The solutions were combined, mixed carefully and incubated for 20 minutes at r.t.. The transfection mixtures were added drop wise on seeded cells in 24-well plates and mixed carefully. The cells were again incubated at 37°C in an incubator. To determine transfection efficiency, pEGFP was transfected into one well under the same conditions and eGFP expression was determined using UV microscopy 24h p.Tr..

### ***PEI***

This protocol was used for 6cm-dishes and can be adjusted for different dishes/plates:

Plasmids for transfection were mixed in reaction tubes and total DNA amount was adjusted with stuffer DNA to be equal in each tube.

PEI was used as a transfection agent (2.5x the mass of DNA in  $\mu\text{g}$ ), diluted in 200  $\mu\text{L}$  D-MEM and incubated for 5 minutes at room temperature. The DNA was diluted in 200  $\mu\text{L}$  D-MEM. The combined solutions were carefully mixed and further incubated for 20 minutes at room temperature. The seeded cells were treated with the mix, and carefully mixed. The cells were again incubated at 37°C in an incubator. To determine transfection efficiency, pEGFP was transfected into one well under the same conditions and eGFP expression was determined using UV microscopy 24h p.Tr..

### ***Calciumphosphate***

This protocol was used for 6-well-plates and can be adjusted for different dishes/plates:

Plasmids for transfection were mixed in reaction tubes and total DNA amount was adjusted with stuffer DNA to be equal in each tube.

The Calciumphosphate Kit was warmed to room temperature before using. The DNA sample was mixed with 25 $\mu\text{l}$  of the  $\text{CaCl}_2$  solution and filled with nuclease-free water to 200 $\mu\text{l}$ . The mixture was added dropwise to vortexing 200 $\mu\text{l}$  of HEPES-Saline and finally incubated at room temperature for 30 minutes. The seeded cells were treated with the preparation, and carefully mixed. The cells were again incubated at 37°C in

an incubator. 6h p.Tr. the growth medium was changed. To determine transfection efficiency, pEGFP was transfected into one well under the same conditions and eGFP expression was determined using UV microscopy 24h p.Tr..

### **2.3.3. Luciferase assay**

*(Promega Dual Luciferase Reporter Gene Kit)*

24h p.Tr. 293T cells were lysed with 200 $\mu$ l/24-well 1xPassive Lysis Buffer (PLB) at room temperature. Of these lysates 20 $\mu$ l were transferred to 96-well non-transparent plates and the automatic measurement carried out using the Berthold LB-960 Luminometer and the MikroWin 2000 software. The activity of the firefly luciferase was measured by injecting 40 $\mu$ l firefly substrate into one well and detection of light for 5 seconds afterwards. The quantification of the renilla luciferase was performed in a similar manner, using 40 $\mu$ l of Stop&Glo Buffer, which was additionally injected into the well. The analysis of the data was carried out using standard spread sheet programs.

### **2.3.4. Immunofluorescence**

24h p.Tr. Vero/HeLa/A549/Hep2 cells in 24-well plates grown on glass plates (for immunofluorescence) were stimulated with 100 $\mu$ l of Sendai virus defective interfering particles (SeV DI). After 7h the medium was removed and the cells washed with 1xPBS (Phosphate Buffered Saline). If the cells were not stimulated they were washed 24 p.Tr.. After washing the cells were fixed onto the glass plates with 3% PFA for 20 minutes at room temperature, then washed with 1xPBS again before NH<sub>4</sub>Cl-solution in PBS was added for another 10 minutes at room temperature. After removal of the ammonium chloride solution the cells were washed again with 1xPBS, then incubated with 0.5% Triton X-100 in PBS for 10 minutes at room temperature. The free protein binding sites were blocked with 2.5% milk powder in PBS for 15 minutes, after the cells were washed 3 times with 1xPBS. After another washing with 1xPBS 80 $\mu$ l of the primary antibody dilution in PBS was put onto the glass plates and incubated for 1h at 37°C. Three washing steps with 1xPBS followed and the secondary antibody dilution (with ToPro3 for nuclei staining) was added to the cells and incubated at 37°C for additional 60 minutes. The cells were washed with 1xPBS 3 times afterwards and finally 1 time with water. To mount the glass slides on object plates a drop of Vectashield Hard Set(Vector Laboratories) solution was used and the plates were fixed with nail varnish.

For acquiring confocal images a Zeiss LSM 510 was used. The images were afterwards edited with Zeiss LSMBrowser and a standard image processing / vector graphic programs (ImageJ).

### **2.3.5. Co-Immunoprecipitation**

24h p.Tr. of 293T cells grown in 60mm dishes were harvested from the surface using 1mL PBS. The cells were pelleted at 2800rpm, 4°C for 5 minutes and the supernatant removed. The cells were lysed in 300µl Co-IP Buffer. The mixture was incubated at 4°C for 2h and then centrifuged at 14,000 rpm, 4°C for 2 minutes to remove the cell debris. To check the input, 30µL of the cleared lysate were removed and mixed with protein gel loading buffer. The remaining supernatant was added onto 100µl Flag-Beads (α-flag antibody coupled to agarose beads) and incubated o/n at 4°C. To wash the IP, the beads were pelleted (14,000 rpm, 4°C, 2 minutes), the supernatant removed and 500µl Co-IP Buffer added. The washing step was repeat three times, the last time instead of Co-IP Buffer 250µl Protein Gel lysis Buffer were added onto the beads. The protein content of the IP and the input cells were analysed using polyacrylamide gels.

### **2.3.6. IRF3 dimerisation assay**

293T cells were harvested 24h p.Tr. and 18h p. Stimulation with Sendai Virus DI (25µl) in 1 mL PBS and pelleted at 2000 rpm for 10 minutes at 4°C. The pellet was lysed in 100µl Native Lysis Buffer and centrifuged again at 14000 rpm for 10 minutes at 4°C to remove cell debris. The supernatant was stored at -80°C and analysed on native gels.

### **2.3.7. Mass Spectrometry**

The pull-down of the proteins was carried out according to the protocol of co-immunoprecipitations, with the following differences:

Cells from 3 100mm dishes were harvested and after lysis for 2h at 4°C using Co-IP buffer the lysates were cleared by centrifugation and put on 400µL flag-beads. The washing step was repeated 6 times, the buffer for the last 3 washing steps lacked both protease inhibitors as well as the Nonidet P40 detergent.

Elution was carried out using a flag peptide (Sigma) diluted in the washing buffer to a concentration of 300ng/µL. The beads were incubated with the mixture for 30 min at 4°C and the supernatant removed after centrifugation as elution.

The elutions were then subjected to PAGE and subsequently a silver staining.

The elutions were then either subjected to gel electrophoresis and the gel slices used for analysis or the whole elutes. The samples were sent to the Adolf-Butenand Institut of the LMU Munich to Prof. Axel Imhofs Lab. The experiments itself were carried out by Dr. Lars Israel in the lab.

### **2.3.8. Quantitative Realtime PCR**

The cDNA of purified total cellular RNA was analyzed by real-time PCR with the Quantitect SYBR Green PCR Kit (Qiagen) on a LightCycler 2.0 & LightCycler 480 (Roche). Values for relative quantification of single probes were calculated from a standard curve of serial dilutions of one of the samples. The other samples were diluted 1:10 for further analysis. The obtained results in arbitrary units were recalculated setting the mean value for the induction control to 100.

### **2.3.9. Microarray analysis**

*(Affymetrix GeneChip Human Gene 1.0 ST Arrays)*

cDNA from total cellular RNA was amplified using Ambion T7 transcription kits. The preparation of the amplified cDNA as well as the fluorescent labeling was carried out in the microarray facility of Professor Patrick Cramer's lab under the supervision of Kerstin Maier. Following these steps, the probes were hybridized to the microarrays and the fluorescence read out.

Analysis of the resulting data was done using R and Microsoft Excel.

## **2.4. Working with RNA**

### **2.4.1. RNA purification**

*(QIAGEN RNAeasy Kit)*

293T/A549 cells grown in 24-wells were harvested in 350 µl RLT buffer and the complete RNA was extracted using Qiagen RNAeasy Kit according to the manufacturer's protocol. The protocol can be scaled up for usage in 6-wells as well. The protocol was carried out at RT using only RNase-free water.

Cells lysed in RLT were supplemented with the same volume of 70% ethanol in RNase-free water and mixed by pipetting up and down. A new column was loaded with the mixture and centrifuged at 10,000 rpm for 15s to bind the RNA. The column was then washed with 350µl buffer RW1 (10,000 rpm , 15s). Remaining DNA was digested on column using QIAGEN RNase-free DNase I for 15 min at RT. Another 350µl of RW1

was used to wash the column before the final washing step with 500 $\mu$ l buffer RE (2min, 10,000 rpm). The collection tube was removed and replaced with a new one and residual buffers removed by centrifugation for 1 minute at full speed. The RNA was eventually eluted using 30 $\mu$ L RNase-free water.

#### **2.4.2. Reverse transcription**

*(Roche Transcriptor Transcriptase)*

Whole cell isolated RNA was reverse transcribed at 55°C for 30 min using Roche Transcriptor Transcriptase Kit after ligation of oligodT Primer (Invitrogen) at 65°C for 10 min.

#### **2.4.3. RNA Agarose gels**

4-5 $\mu$ g of whole cellular RNA in a total volume of 7.2  $\mu$ l were added to 1.8 $\mu$ l glyoxal and 3 $\mu$ l 5x phosphate buffer. The mix was incubated for 45 min at 56°C and before loading it onto the gel 3 $\mu$ l blue juice was added.

The gel was cast according to the following scheme:

<b>Ingredient:</b>	<b>Amount:</b>
Agarose	2 g
ddH <sub>2</sub> O (ultrapure)	167.3 mL
50x phosphate buffer	4 mL
37% formaldehyde	26.7 mL

The agarose was dissolved in water and phosphate buffer by stirring and heating, while the volume was kept constant. The formaldehyde was added when the cleared solution cooled down to be lukewarm.

A 240 x 200 mm gel was cast from the mixture and the probes loaded. Electrophoresis was performed in 1x phosphate buffer at 25V overnight. Afterwards the RNA was stained using acridin orange and 1x phosphate buffer for washing. Prominent bands (Ribosomal RNA for whole cell extracts) were visualized using UV light to check the integrity of the RNA on the gel.

**2.4.4. Northern Blotting**

*(Vacu-Blot System, Biometra)*

The RNA was transferred on Nylon membranes (Stratagene, GE Healthcare) using the Vacu-Blot system for 2h at 100 mBar. After the membrane is air-dried the RNA is crosslinked on the membrane using 0.125 J UV light.

**2.4.5. Radioactive labelling of probes**

*(Ready Prime II Kit, GE Healthcare)*

The probes were generated from DNA PCR fragments (25ng), radioactively labelled with <sup>32</sup>P-alpha-CTP using the ready prime II Kit (GE Healthcare) according to the manual, followed by purification with the QIAquick Nucleotide removal Kit (QIAGEN) and a denaturing step at 95°C.

**2.4.6. Detection of RNA on Northern Blots**

The nylon membranes were incubated with zeta hybridizing buffer for 10 minutes at 68°C in an orbital shaker. The preincubation buffer was subsequently replaced with 8 mL zeta hybridising buffer including the labelled probe, and incubated overnight at 68°C. The membranes were afterwards washed once with zeta wash buffer 5% and twice with zeta wash buffer 1% for 20 minutes at 68°C each. After air drying the membrane a phosphoscreen was exposed to the labelled blot from 3 days up to 14 days depending on the amount of radioactivity on the blot. Signals on the screen were the read by the Storm scanner (Molecular dynamics, GE Healthcare).

**2.5. Working in silico****2.5.1. Alignments**

*(Clustal Omega, EMBL; Jalview, Barton Lab, University of Dundee)*

The alignments of the primary structure of proteins and nucleic acids were done using ClustalOmega (Sievers et al., 2011). The alignments were afterwards displayed using JALView (Clamp et al., 2004; Waterhouse et al., 2009).

**2.5.2. Conservation scoring**

(ConSurf, Bio-sof LLC)

The conservation scoring was done using ConSurf (Ashkenazy et al., 2010) using its standard parameters. The conservation score was added as a B-value to the ab initio calculated structure to depict the conservation as a colour change.

**2.5.3. Secondary structure prediction**

(Quick 2D)

For secondary structure predictions different programs were used to compare the results. The collection was done using Quick2D which uses the prediction algorithms by PSIPRED (Jones, 1999), JNET (Barton, 1999), Prof (Ouali and King, 2000; Rost, 2001), Coils (Lupas et al., 1991), HMMTOP (Tusnady and Simon, 1998), Phobius (Kall et al., 2004) and IUPRED (Dosztanyi et al., 2005).

**2.5.4. Tertiary ab-initio structure prediction**

(I-Tasser, Zhang Lab, University of Michigan, Pymol )

The ab-initio tertiary structure calculation was done using the freely available I-TASSER (Roy et al., 2010; Zhang, 2008). Images of the structures were taken using pymol.

**2.5.5. Phylogenetic analysis**

(Clustal Omega, EMBL; Jalview, Barton Lab, University of Dundee)

Phylogenetic trees were generated from alignments using Clustal Omega. The trees were subsequently edited and displayed using JalView.

**2.5.6. Mass spectrometry analysis**

(Scaffold, Proteome Software, MASCOT)

The massspectrometry, MASCOT identification of peptides and library search was done in the lab of Professor Axel Imhof by Dr. Lars Israel. Analysis and comparison of the resulting datasets was done using Scaffold 4.0 and Microsoft Excel.

**2.5.7. Protein networks analysis**

(Cytoscape)

Networks of proteins were created using Cytoscape. The data for the interaction maps in those networks was based of the protein-protein interaction databases Biogrid and InnateDB.

## **2.6. Working with viruses**

### **2.6.1. *Measles virus rescue***

293-3-46 cells grown in 6-wells were transfected with calcium phosphate (Promega). The cells were washed twice with DMEM+3 6h p.Tr. and incubated o/n at 37°C and 5% CO<sub>2</sub>. 24h p.Tr. the cells were heat shocked at 42°C for 3h. 48h hours after the heat shock the cells were detached from the surface and added onto Vero-hSLAM cells including the medium. In the following days the cells were examined for syncytia formation, the syncytia then were picked from the cell culture plates and added to Vero cells in T25 flasks. Fully infected flasks were frozen at -20°C o/n and then thawed on ice. The suspension was centrifuged at 2,800 rpm and 4°C for 5 min to remove cell debris, the supernatant was frozen in 1ml aliquots at -80°C and titrated.

### **2.6.2. *Measles virus stock production***

Pelleted Vero cells from 3 confluent T75 flasks were infected with an MOI of 0.005 from a rescue and incubated at 37°C for 1h. After addition of DMEM+3 medium the cell suspension was divided into 6 T75 flasks and incubated at 32°C and 5% CO<sub>2</sub>. Once the desired growth is reached (after 80h for vaccine virus) the media was completely removed and the cells scratched in 2mL Optimem per flask. The combined Optimem and cells from 6 flasks was then frozen to -20°C and thawed on ice for 7-8 h. The cell debris were removed by centrifugation at 4°C, 1,600 rpm for 10 minutes and frozen to -80°C in 1mL aliquots.

### **2.6.3. *Measles virus titration***

Vero-hSLAM or Vero cells growing in 96-well plates were infected with each 100µl of up to 7 times 1:10 diluted viral stocks solutions. After 48h incubation at 37°C and 5% CO<sub>2</sub>, the medium was removed, the cells washed with 1xPBS and fixed with cold 80% acetone for 20 minutes at 4°C. After the acetone was removed the cells were dried and afterwards incubated with 50µl of a 1:2000 dilution of α-MV N-FITC antibody in PBS over night at 4°C. The antibody dilution was removed, the cells washed with 1xPBS and the nucleoprotein of measles virus visualized using a fluorescence microscope. The foci were counted and the infectious titre (foci forming units) was calculated according to the used dilutions.

**2.6.4. Growth curves**

For growth curves,  $5 \times 10^5$  cells per timepoint (6h, 24h, 48h, 72h) were infected with virus in as little volume as possible (around 1 mL). After incubating the mixture for 1h at 37°C each timepoint was seeded in one 6 well including 2 mL of medium. 5h post seeding the cells were washed twice with DMEM+3 and the first timepoint frozen to -20°C including the medium. The other timepoints were frozen to -20°C subsequently. For analysis, the 6-well plates were thawed on ice for 2h, and then the cell lysate and the medium transferred to eppendorf vials. The cell debris was removed by centrifugation (1800 rpm, 4°C, 10 min) and the supernatant titrated.

**2.6.5. Purification of measles virus**

To purify the measles virus, 12 mL of freshly made, already cleared stocks were carefully overlaid on top of 30% sucrose solutions in Beckman Coulter centrifugation tubes. 6 preparations were used for one centrifuge run at 27,000 rpm at 4°C for 2h. After centrifugation the supernatant was completely removed and the pelleted virus resuspended in 500µL Optimem. The fractions were then combined, then aliquots made and frozen to -80°C for subsequent titration and usage.

## RESULTS

### 1. Interferon inhibition of MV C depends on its intracellular localisation

To compare the capacities of the P, V, and C proteins from wildtype MV and vaccine strains, P gene cDNA was cloned into expression vectors from mRNAs of Vero-hSLAM cells (Ono et al., 2001) infected with a clinical MV isolate of the D5 genotype (MVi/Berlin.DEU/04.08), provided by A. Mankertz (RKI Berlin). The sequences for the vaccine strain proteins were subcloned from the full length cDNA of the MV vac2 strain (del Valle et al., 2007), the C protein sequence is the same as the Schwarz vaccine strain C sequence (Devaux et al., 2008; Schwarz, 1964). All of these clones were sequence verified and subcloned for expression studies in pCR3 vectors.

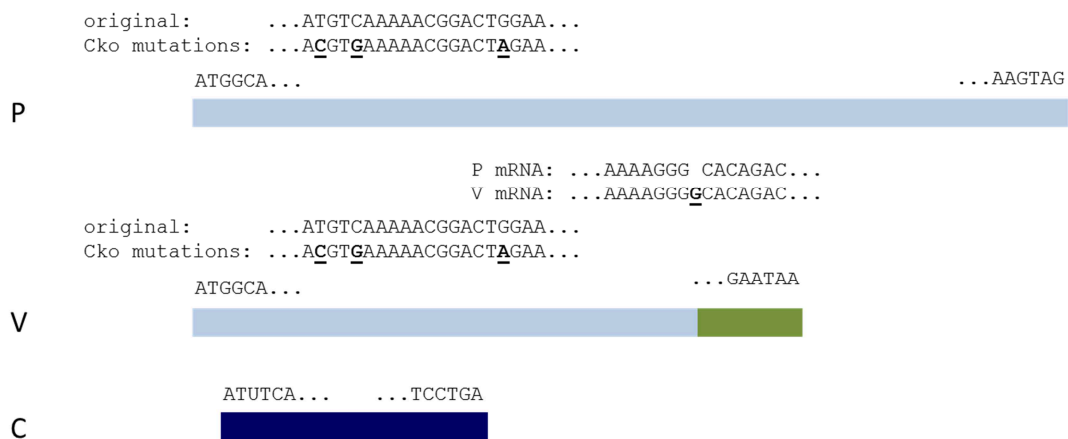


**Figure 6: Scheme of the P, V and C expression vector open reading frames.**

The open reading frames of MV P, V and C are depicted in light blue, green and dark blue respectively. The N-terminal domain shared by P and V is depicted in light blue for both ORFs. The first and the last six nucleotides of the ORFs are indicated above the schemes. Additionally, the mutations introduced in P and V to suppress C expression are highlighted above the respective ORFs and the responsible nucleotides are underlined. The ATG of C was mutated to ACG, and two stop codons were introduced downstream of the mutated ATG to suppress any revertants and prevent translation from alternative start codons. These mutations do not change the P and V amino acid sequence. For V expression from a plasmid, the editing site was mutated mimicking the RNA editing by the viral polymerase, the additional G residue inserted for the frameshift are indicated.

Individual vectors expressing only MV P and V proteins were constructed by introduction of silent mutations disrupting the C translation initiation codon and introducing two nearby stop codons, in order to suppress revertants, which is important especially for the generation of recombinant viruses later on. V expression was directed by inserting the additional G residue in the editing site of the P mRNA. This G residue is inserted into the P mRNA during infection by the viral polymerase complex. The cloning strategy was previously described for the respective MV Schwarz constructs (Pfaller and Conzelmann, 2008).

### 1.1. Measles virus C protein is able to inhibit interferon induction

To determine the ability of each of these proteins to individually interfere with the interferon induction system, dual luciferase reporter gene assays were performed. Expression of firefly luciferase (FL) controlled by the full-length IFN- $\beta$  promoter (p125-Luc plasmid) was transfected in 293T cells, together with plasmids encoding the MV P gene products P, V and C and CMV promoter controlled *Renilla* luciferase for normalisation. These cells then were stimulated with a preparation of Sendai virus (SeV) defective interfering particles (DI-H4), which were kindly provided by Dominique Garcin (Strahle et al., 2007). Stimulation in mock-transfected cells resulted in the induction of firefly luciferase expression, which could be quantitatively measured. Rabies virus P protein (RV P), which counteracts activation of IRF3 by TBK-1 (Brzozka et al., 2005; Rieder et al., 2011) was used as a positive control in these assays and also showed the strongest inhibitory effect observed.

While expression of P of the MV wt isolate (Pwt) had only a marginal effect on the activation of the IFN- $\beta$  promoter, expression of V and C proteins (Vwt and Cwt; respectively) substantially and dose-dependently diminished induction (Fig. 7 A). Since DI-H4 infection is able to activate both MDA-5 and RIG-I (Yount et al., 2008), and MV V is known to prevent MDA-5 activation (Andrejeva et al., 2004; Motz et al., 2013) and NF- $\kappa$ B activity (Schuhmann et al., 2011), an inhibitory effect of Vwt was not unexpected. Notably, however, Cwt protein revealed a similar strong inhibitory effect, suggesting that this protein can individually interfere with RLR-mediated IFN- $\beta$  induction. To assay whether stimulation of the interferon system by factors downstream of the initial recognition of foreign PAMPs by RLR still could be blocked by Cwt, the kinase TBK-1 was overexpressed. Notably both Vwt and Cwt were able to inhibit expression of the reporter gene in a dose-dependent manner (Fig. 7 B). The presence of the proteins was confirmed by western blotting.

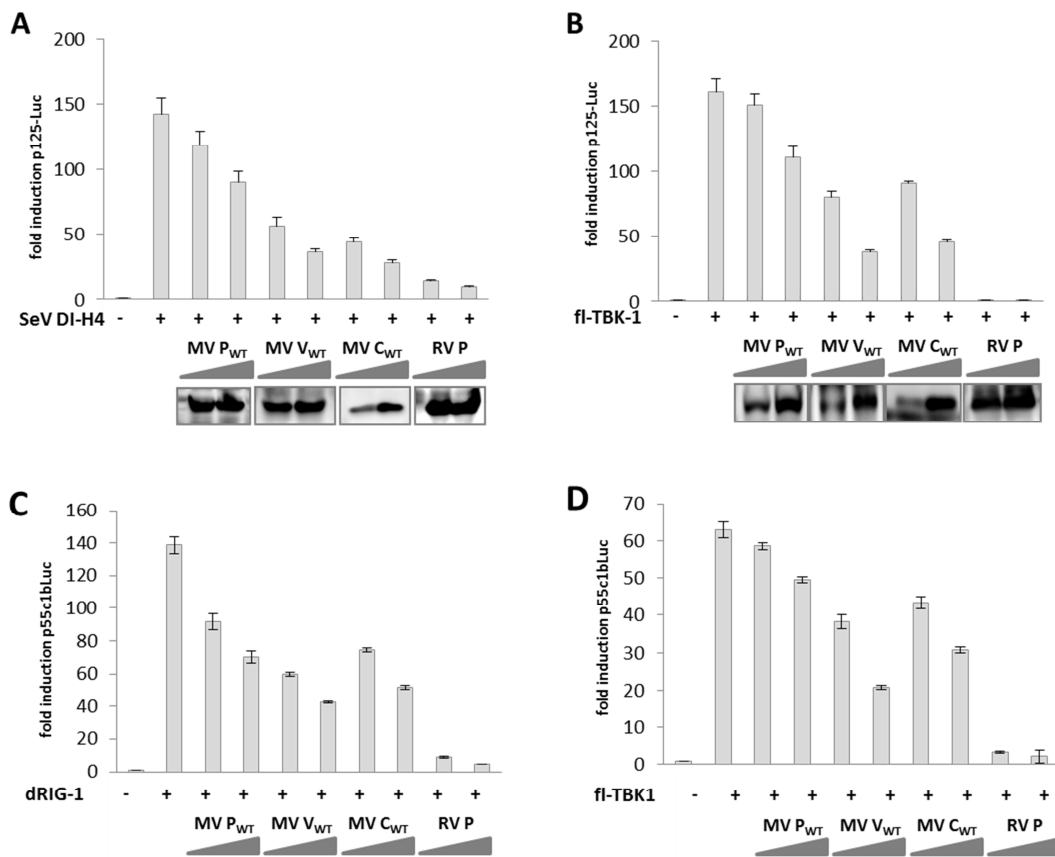


**Figure 7: Inhibition of IFN- $\beta$  promoter and IRF3 binding element promoter activity by wildtype MV P gene products.**

(A) and (B) inhibition of IFN- $\beta$  promoter activity by P gene products from the wildtype MV isolate MV<sub>i</sub>/Berlin.DEU/04.08. Dual luciferase assays from 293T cells transfected with different amounts (300ng, 600ng) of plasmids encoding either P<sub>wt</sub>, V<sub>wt</sub>, or C<sub>wt</sub> protein, or rabies virus phosphoprotein (RV P) as a positive control, and 6 h later infected with Sendai virus (SeV) DI-H4 (A) or overexpression of fl-TBK1 (200ng) (B). Lysates were harvested 18 h post infection or 24h post transfection for luciferase assays and Western blot with specific antisera (lower panel). (C) and (D) Inhibition of IRF3 binding element promoter activity by P gene products from the wildtype MV isolate MV<sub>i</sub>/Berlin.DEU/04.08. Stimulation and transfection occurred with fl-dRIG-I (C) and fl-TBK1 (D) overexpression analogous to A and B. Firefly luciferase (FL) was normalized with renilla luciferase (RL) co-expressed from transfected pRL-CMV and values from mock-infected cells were set to 1. Standard deviations of triplicates are displayed.

The major pathway required for to the induction of interferon beta involves the activation of the transcription factor IRF3. A reporter construct harbouring 6 repeats of the IRF3 DNA binding site controlling expression of firefly luciferase (p55c1b-Luc) was used to determine

the interference with IRF3-dependent promoter stimulation, as the full length interferon beta also harbours binding sites for other transcription factors. 293T cells were stimulated by co-expression of dRIG-I, which is a constitutive active, truncated version of RIG-I consisting only of its CARD domains. Alternatively fl-TBK1 overexpression was used as the stimulus (Fig. 7 C, D). The results obtained were similar to the assays with the full-length interferon beta promoter reporter construct. In both cases Vwt and Cwt were able to inhibit reporter gene expression in a dose dependent manner, whereas the Pwt protein failed to do so. RV P was used again as a positive control in both assays. Interestingly, while the Cwt protein was superior in inhibition of the full length interferon promoter stimulated by SeV DIs, in the case of the IRF3 binding site reporter, the Vwt protein shows the stronger effect after stimulation by plasmid transfection.

To exclude the possibility that one of these MV proteins induces a general shutdown of cellular transcription, a constitutive expressing *Renilla* luciferase plasmid was co-transfected. All luciferase reporter assays were normalized to the amount of renilla luciferase present in the lysates.

Taken together, these results identify the C protein of wildtype MV as an additional inhibitor of the IFN- $\beta$  induction pathway encoded by measles virus.

## 1.2. MV C proteins of vaccine strains show a decreased inhibition

To reveal whether the C protein of the widely used MV Schwarz vaccine strain (C<sub>S</sub>) has retained the ability to inhibit IFN- $\beta$  induction, Cwt and C<sub>S</sub> encoding plasmids were transfected in parallel into 293T cells in addition to the reporter plasmids. Indeed, expression of C<sub>S</sub> reduced IFN- $\beta$  promoter activity after stimulation with DI-H4 or fl-TBK-1 (Fig. 8 A and B). Notably, however, inhibition by C<sub>S</sub> was considerably less pronounced compared to Cwt. While after infection with DI-H4 only marginal differences were detectable (Fig. 8 A), the dissimilarity became more apparent after more downstream stimulation by overexpression of fl-TBK-1 (Fig. 8 B). As confirmed by Western blot experiments of the lysates used in the reporter gene assays, the weaker performance of C<sub>S</sub> was not due to generally lower expression levels.

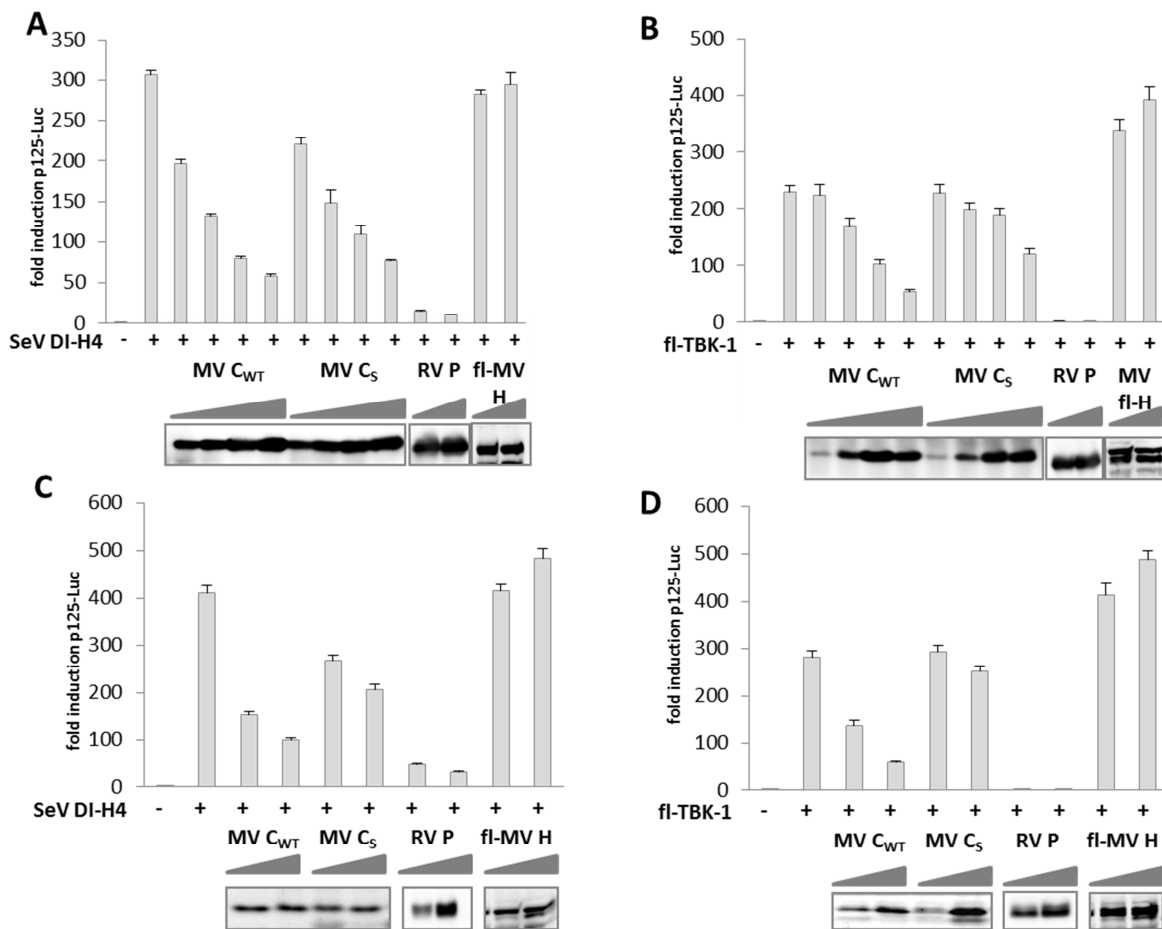


**Figure 8: Inhibition of IFN- $\beta$  promoter activity by different C proteins in 293T and 293T Stat  $-/-$  cells.**

(A) and (B) Inhibition of IFN- $\beta$  promoter activity by different C proteins in 293T cells. Cwt from the wildtype MV isolate MVi/Berlin.DEU/04.08, Cs from the vaccine strain Schwarz. Dual luciferase assays from 293T cells transfected with increasing amounts of plasmids (125ng, 250ng, 500ng and 750ng) encoding either Cwt or Cs protein, rabies virus phosphoprotein (RV P, 500ng and 750ng) as a positive control or MV flag-H as a negative control (500ng and 750ng). (C) and (D) Inhibition of IFN- $\beta$  promoter activity by different C proteins in 293T STAT1  $-/-$  cells. Stimulation and transfection occurred analogous to A and B with 300ng and 600ng transfected for all viral protein encoding plasmids into a STAT1 knockout 293T cell line. Firefly luciferase (FL) values were normalized with *Renilla* luciferase (RL) values co-expressed from transfected pRL-CMV and values from mock-infected cells were set to 1, the other data calculated relatively. Standard deviations of triplicates are displayed. The cells were stimulated 6 h later by infection with Sendai virus (SeV) DI-H4 (A) or overexpression of fl-TBK1 (200ng) (B). Lysates were harvested 18 h post infection or 24h post transfection for luciferase assays and Western blot with specific antisera (lower panels).

MV C protein was also reported to interfere with JAK/STAT signalling (Nakatsu et al., 2008; Shaffer et al., 2003), which could differentially affect the induction of proteins involved in the IFN induction pathways. Experiments were therefore also performed in 293T cells lacking the STAT1 gene, which is necessary for feedback loops induced by interferon from the supernatant. These cells were again stimulated using SeV DI H4 or overexpression of fl-TBK1 and transcription from the interferon beta promoter was measured by expression of firefly luciferase. In these assays however, the superior inhibition by Cwt became even more evident (Fig. 8 C and D), with similar levels of Cwt and Cs expressed and confirmed by western blotting of the lysates.

Again the positive control for these luciferase reporter gene assays was RV P, the negative control was MV fl-H, which showed no reduction of IFN- $\beta$  promoter controlled luciferase induction in all experiments.

In summary, the C proteins of the wildtype MV isolate MVi/Berlin.DEU/04.08 and the Schwarz vaccine strain differ in their ability to prevent interferon induction.

### **1.3. In silico characterisation of MV C**

The C protein is a 186 amino acid short protein, which has a molecular weight of around 21 kDa. The expression by leaky scanning from the P and the V mRNA during infection is quite efficient, and high amounts of the C protein can be detected in lysates of infected cells. The C protein of MV wildtype strains was reported to possess both a nuclear localization signal (NLS) and a nuclear export signal (NES) (Nishie et al., 2007). The NLS is located in the N-terminal part of the protein from amino acid 41-48 comprising a classical basic cluster motif. The NES is located in the middle part of C from amino acid 76-85, representing a classical leucine-rich NES (Figure 9 A). The nuclear export is CRM1 dependent (Nishie et al., 2007).

Alignment of the primary amino acid sequence of C proteins taken from wildtype strains and vaccine strains revealed a prominent difference between vaccine and wildtype strains, namely a mutation in the nuclear localization sequence of the C protein. Another mutation is conserved among the 4 different vaccine strains, which were generated from 4 different isolates (Bankamp et al., 2011): L25P. This mutation however, is also present in one of the wildtype strains in the alignment, MVi/Wincrage. Interestingly, very few mutations were introduced into MV C during generation of the vaccine strains by passaging compared to wildtype isolates (Figure 9 B).

Interferon inhibition of MV C depends on its intracellular localisation

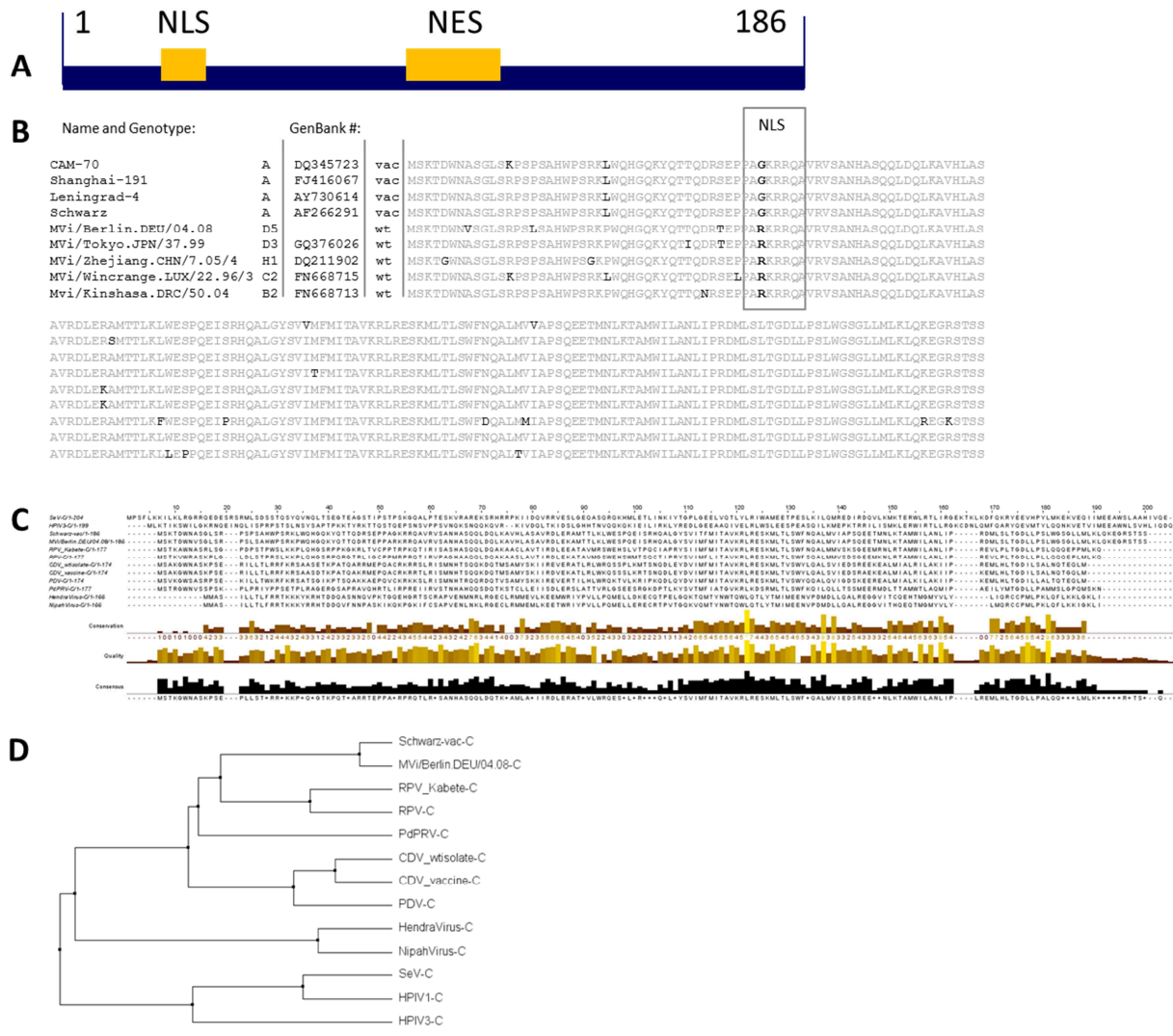


**Figure 9: Alignment analysis of the MV Cwt primary amino acid sequence.**

(A) Scheme of the MV C open reading frame, the reported (Nishie et al., 2007) nuclear localisation signal and the nuclear export signal are highlighted as yellow boxes. (B) Alignment of the sequences of C proteins from MV wt isolates and vaccine strains of different origin. Genotype and GenBank accession numbers are indicated. Deviations from a consensus sequence are shown in black. A canonical nuclear localization signal (NLS; boxed) is only present in the proteins of wildtype isolates. Vaccine strains possess a common R44G exchange. (C) Alignment of the C proteins of different paramyxoviruses as indicated before the sequences. The degree of conservation is indicated below the alignment as well as a consensus sequence when possible. (D) Phylogenetic tree analysis of the paramyxovirus C proteins aligned in C.

All Morbilliviruses encode a C protein as do some other members of the paramyxoviridae family, e.g. Nipah Virus, Hendra virus or human parainfluenza virus 1 and 3. Comparing the primary sequences of C proteins from a selection of paramyxoviruses no apparent conserved region can be identified. Notably, the exact NLS sequence is not conserved (Figure 9 C). Especially the N- and C- termini of the proteins differ considerably and Sendai virus encodes for four different C proteins, the longest C protein is depicted in the figure. Moreover, measles virus C also has a distinct C-terminal sequence, consisting of a cluster of serines.

Phylogenetic analysis of the C proteins showed a clear clustering of the morbilliviruses, whereas all the other paramyxoviruses were more distantly related. The closest relative of MV C is RPV C. Interestingly CDV C clusters with PDV C, being more distinct from MV C than PdPRV C. C proteins of Henipaviruses are even closer related to MV C than those of Sendai or parainfluenza viruses (Figure 9 D). Taken together however, the phylogenetic tree of the C proteins clearly resembles the tree of the N proteins, which is used for the classification of the viruses to certain families and subfamilies. This indicates that C and N proteins evolved to a same degree to form the different virus species.

To analyse the secondary structure of MV C in more detail, the Quick2D assembly (Bioinformatics toolkit of the GeneCenter, LMU Munich) of bioinformatics programs was used to predict helices or beta sheets (Fig 10 A). In addition, unstructured regions were annotated. The four different secondary structure prediction algorithms used (PSIPRED (Jones, 1999), JNET (Barton, 1999), Prof (Ouali and King, 2000; Rost, 2001)) yielded almost similar results. In accordance with results of IUPRED (Dosztanyi et al., 2005), the N-terminal region is supposed to be unstructured. The remainder of the protein can be divided into approximately 4 different alpha helices, intercepted by non-structured regions. There are some hints in the prediction programs that beta sheets may also exist, however they were not predicted with all algorithms and are very short. No coiled-coil structures (PCOILS (Lupas et al., 1991)) could be predicted. The analysis of the primary sequence for transmembrane structures by PHOBIUS (Kall et al., 2004) and HMMTOP (Tusnady and Simon, 1998) was also negative, indicating that the C protein possesses no membrane anchors, as it was expected.

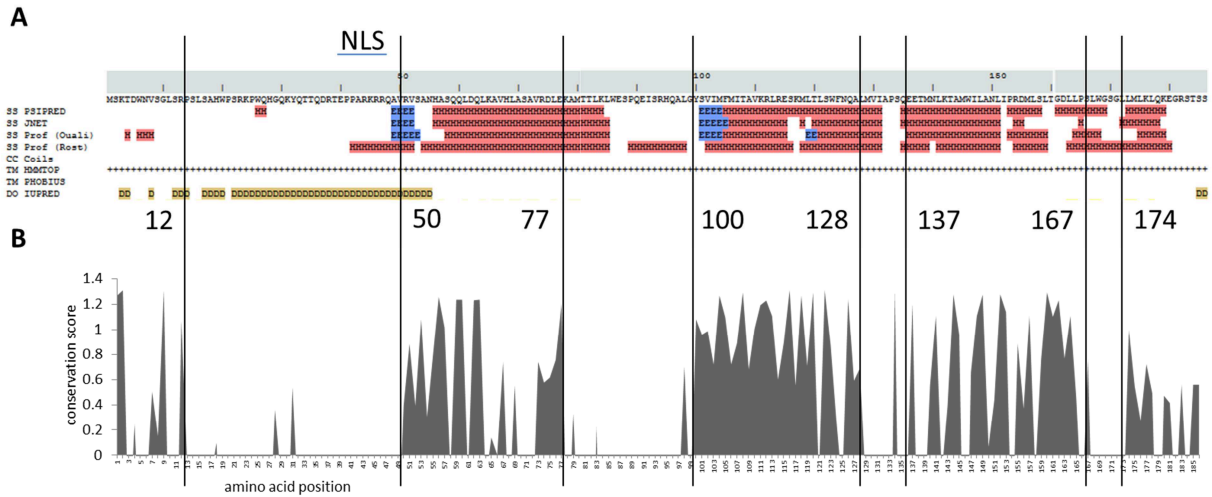


**Figure 10: Secondary structure prediction and conservation scoring of MV Cwt.**

(A) Secondary structure prediction of MV Cwt. Above the predictions the NLS is indicated in the schematic representation of the C ORF, beneath it is the amino acid sequence of MV Cwt. Different algorithms were used as indicated in the figure to predict secondary structure features including alpha and beta sheets, coiled-coil structures, transmembrane regions (PHOBIUS, MMTOP) and disordered regions (IUPRED). The colour red and the letter M indicate an alpha sheet, the colour blue and the letter E a beta sheet. Disordered regions are indicated in yellow using the letter D. There were no coiled-coils regions detected. (B) Conservation scoring of the amino acids according to Consurf. The conservation score is indicated on the y-axis, while the x-axis represents the amino acid position. Black lines were used to highlight the separation of conserved regions and the numbers indicate their respective amino acid positions. The parameters for Consurf and the secondary structure predictions are in the appendix.

For further insight into conserved regions, which might correspond to functional domains, the algorithm of Consurf (Ashkenazy et al., 2010) was used. Consurf accumulates similar protein sequences by BLAST (Altschul et al., 1990) searching. Afterwards these sequences are aligned and the dimension-less conservation score calculated, which represents the degree of conservation of each amino acids. In the case of MV C the conserved regions nicely fit to the predicted secondary structure elements, confirming both prediction programs. Interestingly, the nuclear localisation signal is located at the N-terminal unstructured domain, which represents the longest non-conserved region of the protein. This again confirms the data from previous alignments, that the exact sequence of the NLS is not conserved within the searched cluster of Morbilliviruses. The predicted disordered parts linking the four major helices also seem to be little conserved (Fig. 10 B).

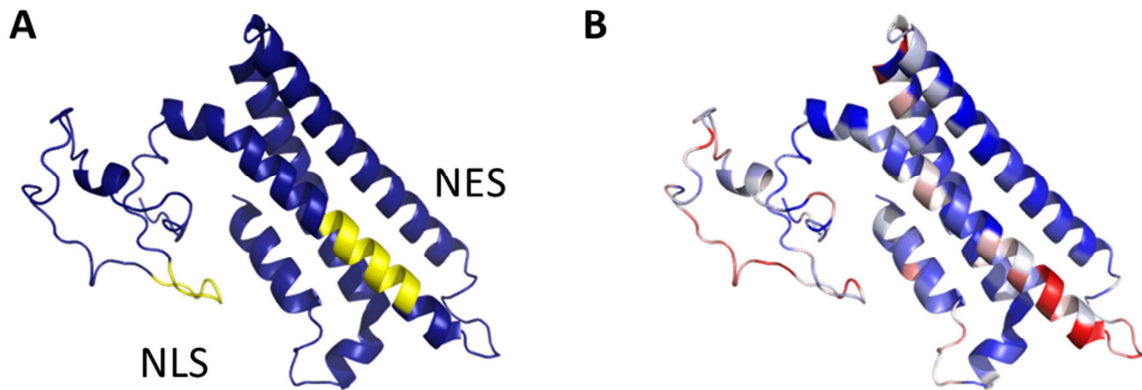


**Figure 11: Ab initio tertiary structure predictions for MV Cwt.**

The predictions were done using I-Tasser, the model represented here has the highest confidence score (C-score=-2.60). The estimated accuracy of the model is:  $0.41 \pm 0.14$  (TM-score)  $11.1 \pm 4.6 \text{ \AA}$  (RMSD). (A) A ribbon model rendered in pymol to highlight the NLS and NES in yellow. Only the backbone of the peptide chain is displayed and the alpha helices are depicted as broader bands, while unstructured regions are represented as a line. (B) Conservation scores colours according to Consurf for the model in (A) blue = high conservation, red = low conservation score.

Structural prediction of the tertiary structure of MV Cwt were done using the ab initio calculation algorithm I-Tasser (Roy et al., 2010), as no structural models of closely related proteins are available. In overall agreement with the prediction of the secondary structure, MV C forms a 4 helix bundle with an unstructured N-terminal domain. The unstructured regions include the NLS, while the NES is located within helix 1 (Fig. 11 A). Conservation colouring (by Consurf conservation scores) revealed that the helices were mostly conserved except for the more C-terminal part of helix 1 (Fig. 11 B), largely confirming the combination of the previous secondary structure predictions with the ConSurf results.

Taken together these results indicated that a major difference between vaccine strains and wildtype strains is a functional nuclear localisation signal. Being located in a predicted unstructured part of the protein, the overall structure of a 4 helix bundle is supposedly not influenced by mutations in this region.

#### 1.4. Nuclear localization of MV C correlates with interferon inhibition

To study the significance of the nuclear localisation signal of C several mutants were generated (Fig. 12).

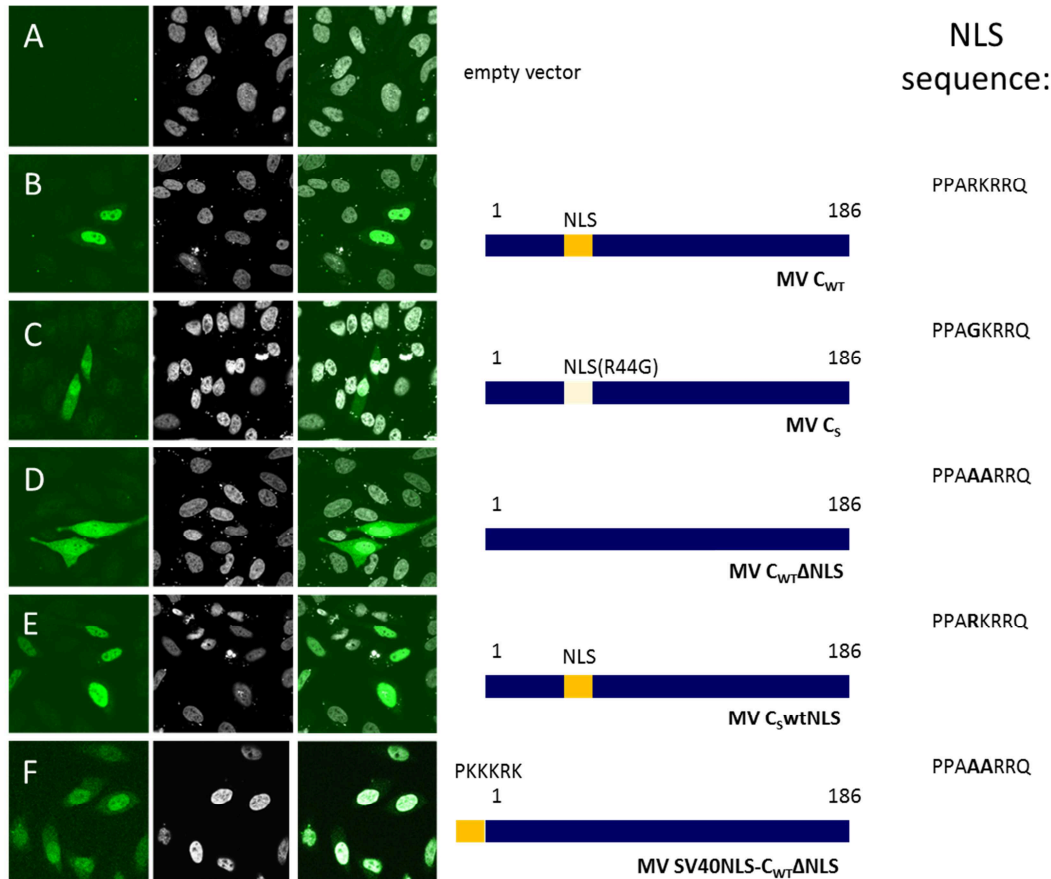


**Figure 12: A functional NLS is a prerequisite for nuclear accumulation of MV C.**

The intracellular localization of the MV C<sub>WT</sub> and C<sub>S</sub> proteins and of the indicated mutants was analyzed by confocal laser scan microscopy in HeLa cells 24 h p.t. transfected with the indicated plasmids. C proteins were stained with the C-specific peptide/rabbit antiserum C1242 and visualized with anti-rabbit-Alexa488 secondary antibody (green). Nuclei were stained with ToPro3 iodine (white). The sequences of the NLS are displayed next to the scheme of the respective mutants.

The functional MV C<sub>WT</sub> NLS was destroyed by site-specific mutation of the basic cluster motif (44RK to 44AA) exchanging arginine and lysine to alanine. Additionally, the defective NLS of MV C<sub>S</sub> was repaired to the wildtype NLS situation by exchanging the G44 residue to an R. Finally a heterologous NLS (SV40 large T antigen NLS) was added to the N-terminus of a MV C<sub>WT</sub> mutation with destroyed NLS (44AA). The subcellular localisation of these mutants was assayed by immunofluorescence and detection of the overexpressed C protein

was done by using specific antibodies. As expected from the predictions, MV Cwt was located exclusively in the nucleus (Fig. 12 B). MV Cs, although possessing a NES signal, was distributed over cytoplasm and nucleus. It still can shuttle to the nucleus, being small enough to fit through the nuclear pores (Fig. 12 C). Mutations in the nuclear localisation signal of Cwt (MV CwtmNLS) abrogate its dominant nuclear accumulation, yielding a localisation phenotype similar to MV Cs (Fig. 12 D). Repairing the basic cluster of the NLS sequence of MV Cs back to the wildtype situation promotes the accumulation of MV CswtNLS in the nucleus (Fig. 12 E). This mutant exhibits the same localisation as MV Cwt. Upon fusing the SV40 large T antigen NLS to the N terminus of CwtmNLS, the localisation of this protein to the nucleus is restored (Fig. 12 F). For all these localisations it has to be considered, that the C protein possesses both an NLS (mutated or not mutated) as well as an unchanged NES. This means that it still shuttles to some degree, whereas the confocal images portrait the localisation of C at an exact timepoint picturing C in its preferential location. Therefore in the case of Cwt the balance between nuclear and cytoplasmic protein is definitely on the side of the nucleus, however it does not mean that the same C molecule is not present at some timepoint in the cytoplasm, as well.

The functional consequences of these mutations and different intracellular localisations were assayed using luciferase reporter gene assays (Fig. 13). The P protein of rabies virus was used again as the positive control, whereas the MV fl-H protein served as the negative control. For normalization purposes the CMV promoter controlled *Renilla* luciferase encoding plasmid was always co-transfected. The expression levels were equal as checked by Western blot analysis (below the luciferase assays).

The p125-luciferase plasmid (Fig. 13 A-B) was co-transfected with plasmids encoding for the different C mutants as well as the stimulus fl-TBK1. MV Cwt was able to inhibit induction of the interferon beta promoter more efficiently than MV Cs, as seen in previous experiments. The wildtype C NLS mutant (CwtmNLS), however, clearly showed a loss of function compared to Cwt, whereas the repaired NLS Cs (CswtNLS) gained function. The inhibitory effect of CwtmNLS was comparable to Cs and the effect of CswtNLS is comparable to Cwt. This indicates that the decreased efficiency of Cs is only due to its cytoplasmic localisation. The protein still can decrease induction of interferon beta, upon its relocation to the nucleus by repairing the NLS.

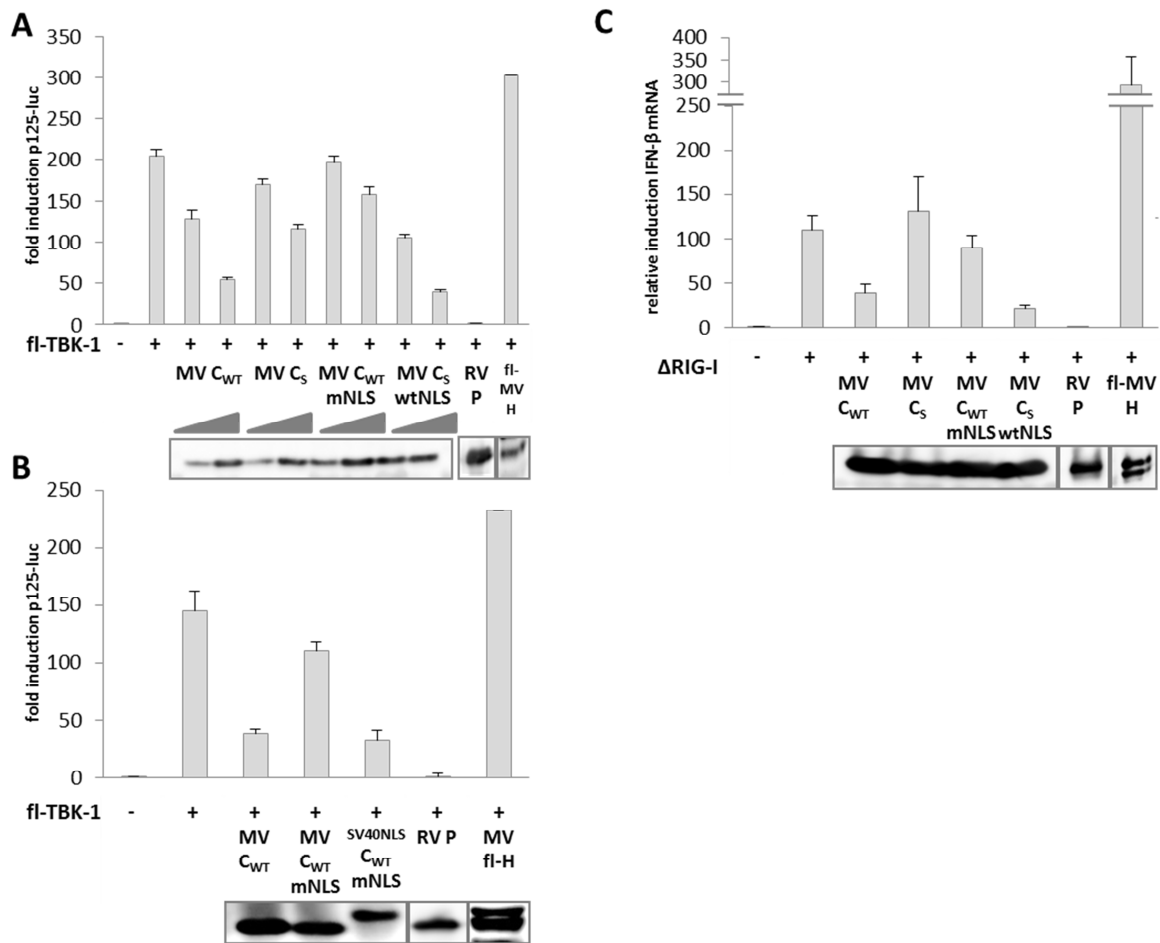


**Figure 13: Nuclear localization of MV C is required for efficient inhibition of IFN- $\beta$  promoter activity.**

(A, B) Dual luciferase assays were used to determine activation of the IFN- $\beta$  promoter. Plasmids encoding the indicated protein constructs (300 and 600 ng of C, 200 ng fl-TBK-1, 600 ng RV P or fl-MV H) were transfected into 293T cells and induction of p125-luc-directed FL activity was determined 24 h p.t.. All assays were normalized with co-expressed RL, mock values set to 1 and relative induction is shown. Standard deviations of triplicates are displayed. (A) The inhibitory activity of C<sub>WT</sub> is completely lost by after disruption of the NLS and C<sub>S</sub> gains full activity after repair of the NLS R44G mutation. (B) An ectopic heterologous SV40 large T antigen NLS can substitute for the authentic internal C protein NLS in SV40NLS-C<sub>WT</sub>mNLS. (C) Quantitative RT-PCR from 293T cells stimulated by expression of  $\Delta$ RIG-I (100ng) in the presence of the indicated viral protein constructs (400ng). IFN- $\beta$  mRNA normalized with GAPDH mRNA. Columns show average values from two experiments, error bars represent standard deviation. Lysates were harvested 24h post transfection for luciferase assays and the protein content analysed by western blotting and immunodetection with specific antisera (lower panels).

Adding an exogenous NLS (SV40 large T antigen NLS) to the N-terminus of CwtmNLS also restored the function of CwtmNLS (Fig. 13 B), reflecting the Cwt situation. This indicates that the exact sequence of the NLS is not important but only the spatial distribution of C inside the cell.

Quantitative realtime PCR of interferon beta messenger RNA showed the same results as the luciferase assays (Fig. 13 C). Cwt and CswtNLS were more efficiently inhibiting the transcription of interferon beta messenger RNA than Cs and CwtmNLS. This time a plasmid coding for a constitutive active mutant of RIG-I, comprising only the CARD domains was used as a transfectable stimulus. The normalisation was done using GAPDH mRNA levels, again indicating that MV C does not induce a general shutdown of transcription as the GAPDH mRNA values of mock and the C transfected cells were similar.

In summary the NLS sequence drives the preferential accumulation of C in the nucleus and the mutation in the vaccine C abrogates the function of the NLS, resulting in a different intracellular distribution of the protein. The inhibition of IFN- $\beta$  induction clearly correlates with the accumulation of C in the nucleus and occurs at a transcriptional level downstream of TBK1.

### **1.5. MV C does not interfere with activation of IRF3**

For effective induction of IFN- $\beta$ , a crucial transcription factor, IRF3, has to be fully activated. The classical activation steps include its phosphorylation at C-terminal serine residues; especially phosphorylation at serine 386 and 396 was shown to be obligatory. The phosphorylated transcription factor then dimerizes and is imported actively into the nucleus. Within the nucleus activated IRF3 binds to the DNA at its recognition sites and is responsible for the recruitment of cofactors required for efficient transcription initiation such as e.g. p300 and CBP (Panne et al., 2007a; Yoneyama et al., 1998).

An IRF3 binding site reporter plasmid (p55c1b-Luciferase) was co-transfected with plasmids coding for Cwt and Cs. Induction was done using overexpression of the transcription factor IRF3 and the luciferase activity was measured afterwards. Only the Cwt protein was able to inhibit reporter gene induction in a dose dependent manner, whereas Cs mostly failed to do so. This indicates an inhibition downstream of IRF3 and upstream of interferon beta translation (Fig. 13 D).

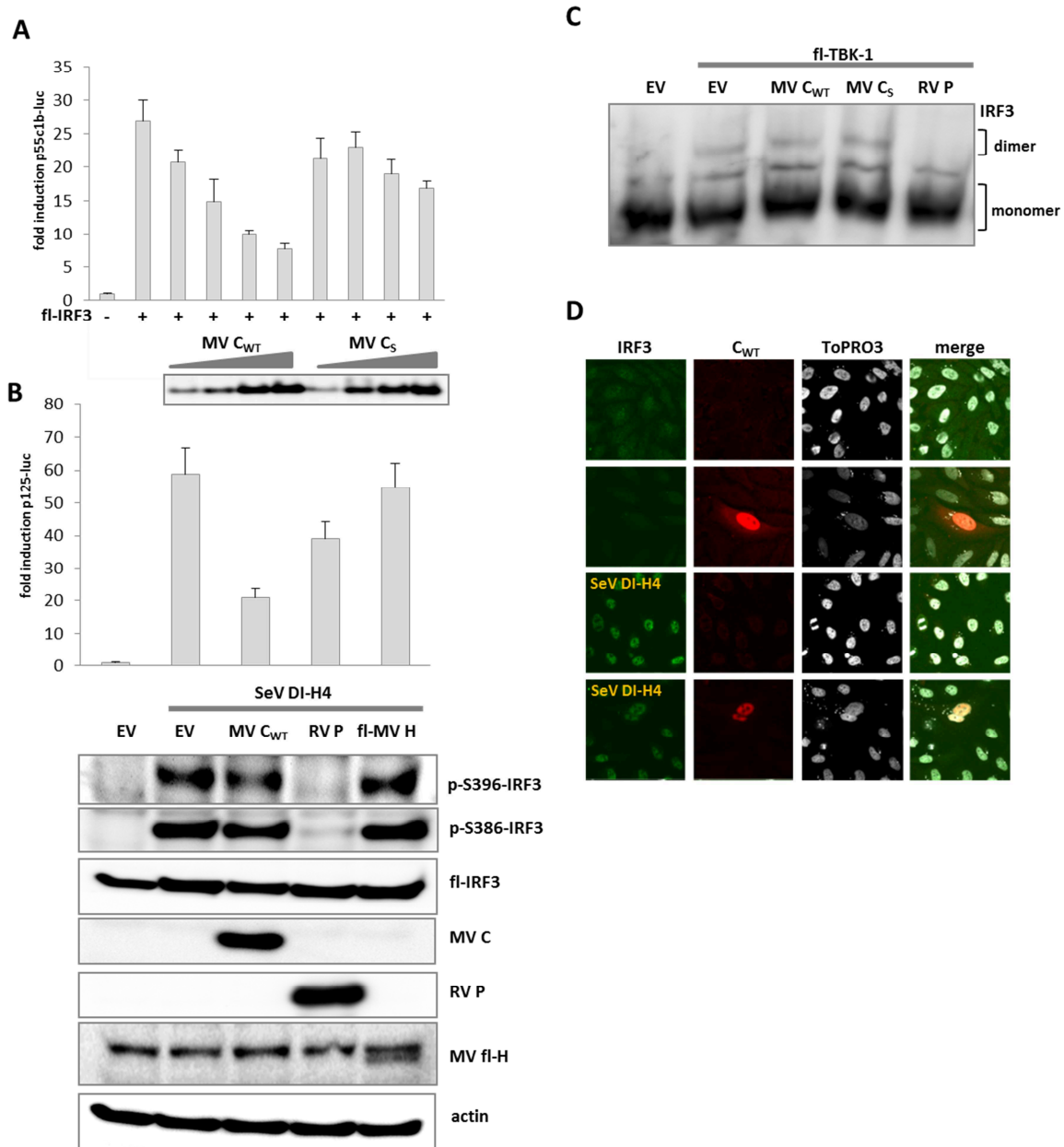


**Figure 14: MV C inhibits IRF3 stimulated interferon induction (A) but does not interfere with IRF3 activation by phosphorylation (B), dimerization (C) or nuclear accumulation (D).**

(A) Dual luciferase assays were used to determine activation of the IRF3 response element (p55c1b) promoter. Plasmids encoding the indicated protein constructs (250 to 750 ng of C, 200 ng fl-IRF3) were transfected into 293T cells and induction of p55c1b-luc-directed FL activity was determined 24 h p.t.. All assays were normalized with co-expressed RL, mock values set to 1 and relative induction is shown. Standard deviations of triplicates are displayed. (B) 293T cells expressing MV C, RV P as a positive control, fl-MV H as a negative control, and flag-tagged IRF3 (fl-IRF3) from transfected plasmids as indicated, were stimulated by SeV DI H4 to activate IRF3. Induction of p125-luc-directed FL activity was determined 12 h p.t.. All assays were normalized with co-expressed RL, mock values set to 1 and relative induction is shown. Standard

deviations of triplicates are displayed (top panel). Phosphorylation of IRF3 S386 and S396 was analyzed by Western blotting following SDS-PAGE of whole cell lysates harvested 12 h post transfection using specific antibodies. The expression level of the overexpressed proteins MV C, RV P, fl-IRF3 and MV fl-H was additionally monitored in the same western blot experiment, as well as the cellular control protein actin (lower panel). (B) Native PAGE of whole lysates collected from 293T cells 24 h post transfection. IRF3 dimerization was stimulated by overexpression of fl-TBK-1. IRF3 was stained with anti-IRF3 antibodies. The sizes of the IRF3 dimer and the monomer are indicated next to the blot. (C) HeLa cells were mock-infected or infected with SeV DI-H4. At 18 h p.i. endogenous IRF3 was visualized by staining with anti-IRF3 antibody and Alexa 488 (green) and fl-Cwt expressed from transfected plasmids by anti-flag and Alexa-555 (red). The nuclei were stained with ToPRO3 (white). The figure shows a representative example of multiple experiments.

To assay the phosphorylation status of overexpressed flag-IRF3, cells stimulated with SeV defective interfering particles H4 were lysed after 12h. A luciferase reporter gene assay of the same lysates showed, that even the initial low level induction of interferon beta by SeV DI H4 is blocked by MV Cwt, whereas RV P is less effective in blocking these initial steps (Fig. 14 A). RV P, however, is able to completely prevent phosphorylation of IRF3 at position 386 and 396 as indicated by phosphorylation-specific antibody western blots (Fig. 14 B). MV Cwt instead does not block visibly any phosphorylation of IRF3 compared to the mock stimulated cells or the negative control (MV fl-H). All inhibitory proteins were confirmed as expressed in this assay by Western blot analysis and subsequent detection of the proteins by specific antibodies.

To assess the dimerization of IRF3, native gel electrophoresis experiments were conducted. RV P co-expression induced a complete loss of IRF3 dimerization after stimulation with fl-TBK1 overexpression. Both MV Cwt and Cs could obviously not inhibit this dimerization step compared to the empty vector control (Fig. 14 C).

The nuclear import is thought to be a final step in activation of IRF3. In non-stimulated cells IRF3 was distributed in the cytoplasm and co-expression of MV Cwt does not alter this localisation. Upon stimulation - with SeV Dis - IRF3 accumulated visibly in the nucleus. Co-expression of MV Cwt again did not alter this behaviour, resulting in both Cwt and IRF3 residing inside the nucleus of activated cells (Fig. 14 D).

Taken together, these results indicate that the mechanism of Cwt does not involve inhibition of phosphorylation, dimerization or nuclear import of IRF3.

## 2. Identification of cellular interaction partners of MV C

Most mechanisms employed by viral proteins to disturb cellular signalling pathways use protein-protein interaction as an interface to manipulate the host. In the case of MV for example, V binds strongly to the cellular helicase MDA-5, thereby inhibiting its ATPase activity and subsequent signalling (Andrejeva et al., 2004). It is therefore likely, that the C protein also interacts with cellular proteins to modify their functions.

Binding assays were mainly done using co-immunoprecipitation experiments in 293T cells, where both putative binding partners were overexpressed. One of the tagged interaction partners was then bound to a matrix either coated with HA or with flag antibodies. The lysates of these pulldowns were then subjected to Western blot analysis followed by immunodetection to show whether the precipitation worked. Possible co-purified protein interaction partners were detected by Western blotting as well. Whole cell lysates were also analysed in a similar fashion to show the presence of the proteins in the input of the pulldown. Alternatively these pulldowns were analysed by mass spectrometry instead of Western blotting to identify endogenous proteins bound to the tagged protein.

Another method employed to identify binding partners of C was overexpression of putative binding partners together with C in Hep2 cells. These cells were stained with fluorescent antibodies and then subjected to confocal microscopy analysis. A co-localisation of two proteins would then indicate an interaction.

### 2.1. Interaction partners in the interferon pathway

The first obvious choices for interaction partners to screen for were proteins involved in major steps in the interferon induction cascade. Among these were the PAMP recognizing helicase RIG-I, the scaffolding protein IPS-1, the kinase TBK1 and the transcription factor IRF3. Additionally, the co-factors needed for efficient transcription of interferon beta mRNA in the nucleus, CBP and p300, were tested. As described above, a nuclear binding partner for Cwt was suggested since the inhibitory strength of MV C correlated with its nuclear

accumulation. Furthermore the inhibition was still visible, although weaker, downstream of stimulation by overexpression of TBK1 or IRF3.

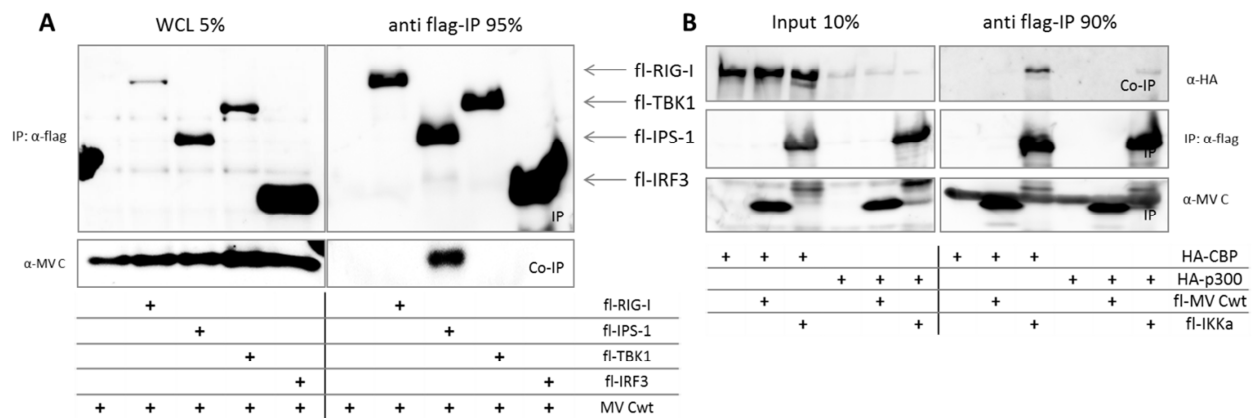


**Figure 15: Co-immunoprecipitation of MV Cwt with various proteins in the interferon pathway.**

The pulldowns of flag-tagged overexpressed proteins in 293T cells together with C were done using a flag-antibody coated matrix. The whole cell lysates before the immunoprecipitation experiments were analysed by Western blots as well as the IP and the Co-IP as indicated in the figure. The percentage indicates the relative amounts of WCL and the IP loaded on the gel. (A) Flag-tagged RIG-I, IPS-1, TBK1 and IRF3 were analysed for binding to MV Cwt. Plasmids coding these proteins were transfected as indicated below the blots. As a negative control for background binding, MV Cwt was overexpressed alone. For detection of the flag-tagged proteins the flag antibody was used (upper panels of the Western blots), for detection of MV Cwt, the anti MV C serum was used (lower Western blot panels). (B) Flag-tagged MV Cwt and IKK $\alpha$  (as a positive control) were analysed for binding to HA-tagged CBP or p300. Plasmids coding these proteins were transfected as indicated below the blots. As a negative control for background binding, the HA constructs were overexpressed alone. For detection of the flag-tagged proteins the flag antibody was used (middle panels of the western blots), for detection of MV Cwt, the anti MV C serum was used (lower western blot panels) and for detection of the HA-tagged proteins anti-HA antibodies were used (upper western blot panels).

Surprisingly, MV Cwt showed a strong interaction with flag-tagged IPS-1 in co-immunoprecipitation experiments (Fig. 15 A). None of the other proteins of the pathway mentioned above were able to co-purify Cwt, although they were all precipitated almost equally efficient or even stronger (fl-IRF3). The transcriptional co-activators -CBP and p300- also show no association with flag-Cwt at all (Fig. 15 B). The positive control flag-IKK $\alpha$

(Yamamoto et al., 2003), however, was able to co-purify both p300 and CBP, proving that the assay worked in principle.

Taken together, MV C is only able to interact with IPS-1, considering the so far assayed possible interaction partners in the interferon induction pathway. All nuclear interaction targets evaluated in these assays did not interact with C.

## **2.2. Known binding partners of MV C**

Two binding partners of MV C were described previously. Weak binding to phosphorylated STAT1 after interferon gamma stimulation was described (Yokota et al., 2011b) and Immunity-related GTPase family M protein (IRGM) (Gregoire et al., 2011). Both proteins were therefore analysed for a co-purification in co-immunoprecipitation experiments to verify the binding partners proposed in the literature. The following experiments were done using Cwt protein as the binding partner, although different variants of vaccine C proteins were used in the literature.

Using co-immunoprecipitation experiments, the interaction of Cwt with phosphorylated Stat1 could not be confirmed (Fig. 16 A). Not even weak binding was visible in the flag matrix pulldown experiments using overexpressed flag-tagged STAT1. Phosphorylation of flag-STAT1 was induced by stimulation of the living cells with recombinant type I interferon for 45 minutes.

To study interaction with mitochondrial proteins IRGM and IPS-1 in comparison, the flag-tagged proteins were co-expressed with HA-tagged Cwt in 293T cells. The pulldown was carried out using a HA-antibody coated matrix. Fl-IRGM was able to co-purify HA-Cwt, thus reproducing the reported interaction (Fig. 16 B). The interaction seems to be comparable to the interaction of HA-Cwt with fl-IPS-1, identified in Figure 15. This experiment additionally confirms the binding of HA-Cwt to fl-IPS-1 using a pulldown with another antibody and matrix.

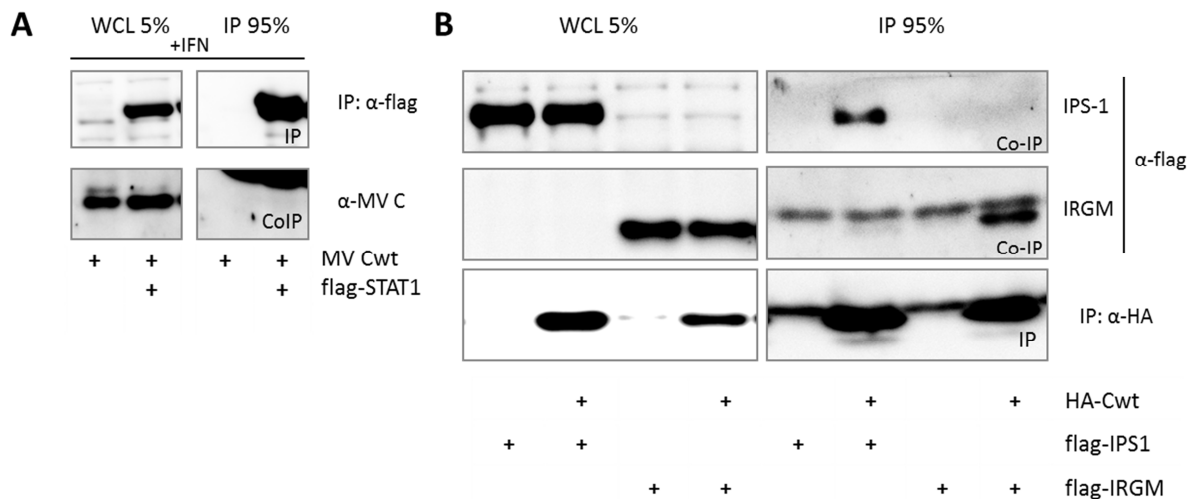


**Figure 16: Co-immunoprecipitation experiments of MV Cwt with known binding partners (pSTAT1 and IRGM).**

The pulldowns were done using a flag-antibody coated matrix (A) or a HA-antibody coated matrix (B) and lysates from 293T cells transfected with plasmids encoding the protein as indicated below the blots. The whole cell lysates before the immunoprecipitation experiments were analysed by Western blots along with the IP and the Co-IP as indicated in the figure. The percentage indicates the relative amounts of WCL and the IP loaded on the gel. (A) Pulldown of flag-STAT1 to co-purify Cwt. All cells were stimulated 45min prior to the harvest with 1000 Units/ml interferon Type I to induce STAT1 phosphorylation. (B) Comparison of the binding of HA-Cwt to either flag-IRGM or flag-IPS-1.

### 2.3. Screening for cellular interaction partners of MV C

Another method to identify co-purified proteins with MV C in the pulldown lysates besides Western blotting and immunodetection is mass spectrometry. The advantage of this technique is, that all proteins present in the pulldown can be detected at once, providing an unbiased screening approach, taking cellular endogenous protein content and expression levels into account. This technique was employed to analyse the endogenous proteins of 293T cells that were pulled down as interaction partners of MV Cwt.

#### 2.3.1. Mass spectrometry driven analysis of Cwt pulldown eluates

Flag tagged Cwt or CwtmNLS was overexpressed in 293T cells and the whole cell lysates incubated with beads coated with flag antibodies. After thoroughly washing away unbound proteins, the bound flag-tagged proteins and their interaction partners were specifically eluted from the beads using flag peptides.

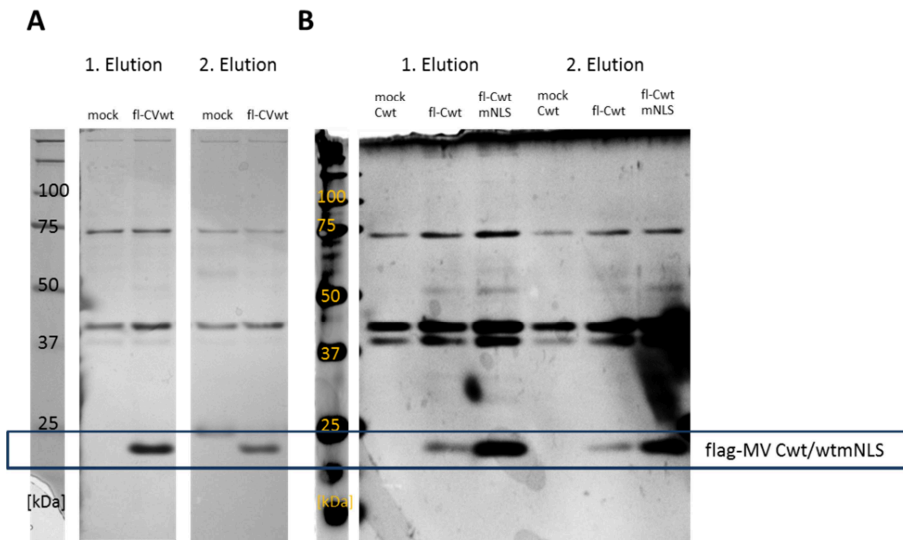


**Figure 17: Silver stained gels of purified proteins.**

For these experiments a flag-antibody coated agarose bead matrix was used to pull down flag-tagged C variants. Elution was done using 300ng/ml flag peptide and the eluted flag-C is highlighted in the figure with a blue box. For both pulldowns the flag-tagged proteins were overexpressed in 293T cells. Two elutions are depicted. A In the first experiment pCAGGS-fl-Cwt was used for the transfection, the mock control were empty vector transfected cells. B In the second experiment pCAGGS constructs of Cwt, fl-Cwt, fl-CwtmNLS were transfected, the mock control was overexpressed untagged Cwt.

To verify that the pulldown itself worked, these elutes were subjected to gel electrophoresis followed by silver staining of the proteins on the gel (Figure 17). Two experiments were done using flag-Cwt (Fig. 17 A, B) and flag-CwtmNLS (Fig. 17 B) as a bait. The first experiment used empty vector transfected cells as a mock control, while in the second experiment Cwt without a tag was overexpressed. In both trials the pulldown itself worked fine, at the correct size (ca. 23 kDa for flag-tagged C constructs) a band appeared only in the fractions which should contain flag-tagged C (Fig. 17 blue box). No untagged C protein was purified (Fig. 17 B, first lane), suggesting that C does not bind unspecifically to the matrix. Unfortunately the flag matrix itself seems to bind strongly to a few cellular proteins around 40 and 64 kDa also visible in the silver stained gel. In both cases, the second elution step worked less well, yielding less pulled down protein, but also less background. Comparing the two pulldowns in Fig. 17 B, it can be said that the elution of MV flag-CwtmNLS from the beads seemed to be more efficient. However, this can also be due to a

higher level of MV fl-CwtmNLS in the input lysates, which were not subjected to silver stain analysis.

In both experiments, no prominent additional binding partners visible on the gel except for a few faint protein bands between 50 and 75 kDa and larger than 150 kDa. These bands, however, indicated that some proteins were specifically co-purified with the flag tagged C proteins compared to the mock controls. There were no obvious differences between Cwt and CwtmNLS visible on the silver stained gel.

The protein content of the eluates in Fig. 17 was then analysed by mass spectrometry followed by peptide identification. These peptides then were attributed to proteins using different protein libraries for the viral protein and for the cellular human proteins (NCBI library). In the first experiment, the lysates were subjected to a short gel electrophoresis and three slices made of the gel, that were subsequently subjected to three different mass spectrometry analysis runs. The runs were later combined to one experiment using the Scaffold software. For the second experiment the lysates were directly analysed in the instrument without a preceding gel separation.

In all elutes, in which flag tagged measles virus C was overexpressed, the protein could be identified (Fig. 18 A). This confirms the bands seen on the silver stained gel were indeed the precipitated flag-tagged C. The quantitative value for the first experiment was higher due to the three runs combined which results in an increased sensitivity of the assay. This quantitative value represents normalized unweighted spectrum counts, which is a relative number for general abundance of the detected protein in the eluate.

In the second run, the pulldown of fl-Cwt was less efficient than that of fl-CwtmNLS again confirming the observations made on the silver-gels.

To identify the cellular proteins in the eluates, the peptides identified by the mass spectrometry were blasted against the NCBI protein database. The resulting proteins that were identified with a probability of at least 80% to be present in the eluates are depicted in Fig. 18 B. The list comprises only proteins which could not be detected in the mock or Cwt controls and present in both experiments. The full dataset is displayed in the appendix. Again it can be seen that the quantitative values in the first experiment are higher, due to the combination of three runs. The table is sorted by the quantitative value of the first mass spectrometry experiment. The most abundant protein in all elutes except the fl-CwtmNLS pulldown was the microtubule associated protein 1B (MAP1B). MAP proteins are involved in development of

the neuronal system, as well as microtubule assembly (Halpain and Dehmelt, 2006). MAP1B is cleaved in the cell to form a heavy chain and a light chain (LC1). The heavy chain can also bind light chain expressed from another gene, namely LC3B, which is an important protein during autophagy (Barth et al., 2010). Fragments of both the heavy chain and the light chain of MAP1B were found in the eluate. Notably, the protein was only co-purified with fl-Cwt, not with fl-CwtmNLS.

Interestingly, a cluster of proteins belonging to the 19S subunit of the proteasome was found specifically binding to fl-Cwt and also to fl-CwtmNLS, although less spectra were found in this pulldown, indicating a weaker binding. These include PSMD1, PSMD2, PSMD3, PSMC1, PSMC2, PSMC3, PSMC5 and PSMD13. PSMD2 was the most abundant interaction partner in both experiments. Insulin receptor substrate 4 (IRS4), which was also detected only in the fl-Cwt elutes, can act as a scaffolding protein for tyrosine kinases and associates with cytoplasmic signalling proteins containing a SH2 domain. It is phosphorylated by the insulin receptor. The phosphoglycerate dehydrogenase (PHGDH) is involved in early steps of L-serine synthesis in animal cells. SLC25A3 (Solute Carrier Family 25) and SLC1A5 (Solute Carrier Family 1 (Neutral Amino Acid Transporter), Member 5) are both soluble molecule carriers. The former one carries phosphates over the mitochondrial membrane, whereas the latter is able to carry neutral amino acids. SLC1A5 was also described as a receptor for the RD114 retrovirus. Both transporters were only co-purified with fl-Cwt.

Ring-finger containing protein 219 (RNF219) is a probable E3 ubiquitin ligase, due to its RING-finder domain; no studies describing its function are so far available. The only annotation is that it acts as an ubiquitin ligase for MyD88, an important adaptor in Toll-like-receptor signalling (Wang et al., 2005). RNF219 was only found in fl-Cwt containing elutes.

Apoptosis-Inducing Factor, Mitochondrion-Associated, 1 (AIFM1) is a protein which is essential for nuclear breakdown during apoptosis. Additionally it can cause mitochondria to release cytochrome c and caspase-9 (Cregan et al., 2004). AIFM1 was found to be associated to both fl-Cwt and fl-CwtmNLS in the pulldown experiments.

Coordinator Of PRMT5, Differentiation Stimulator (COPRS) is a histone-binding protein and required for H4 'Arg-3' methylation mediated by PRMT5 modulating transcription (Lacroix et al., 2008). In the interferon signalling cascades PRMT5 was previously identified as JAK2 binding protein 1 (Pollack et al., 1999).

Identification of cellular interaction partners of MV C

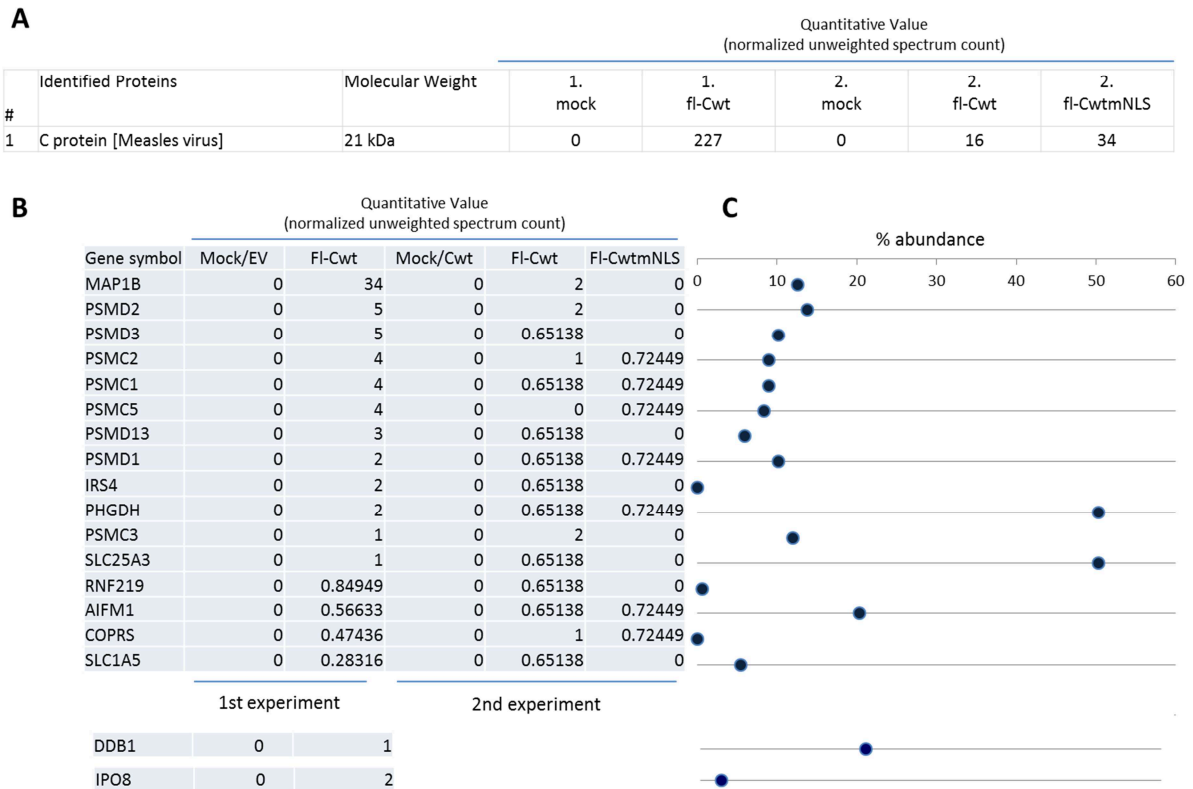


**Figure 18: Identification of protein binding partners of MV Cwt by mass spectrometry.**

The values for the protein detection in the tables are quantitative values for normalized unweighted spectrum counts. (A) The content of the MV Cwt proteins (flag-Cwt, fl-CwtmNLS) in both mass spectrometry experiments (1. and 2.) is indicated in the figure. The counts for the flag-peptide also used for elution were removed. (B) Proteins detected specifically in both experiments are co-purified with either flag-Cwt or flag-CwtmNLS. Proteins also pulled down in the mock control were removed as well as proteins present in only one of the mass spectrometry experiments. The official gene symbols were used to annotate the proteins. Additionally the quantitative values for co-purified of DDB1 and IPO8 is depicted from the first mass spectrometry experiment, both proteins were not detected in the second experiment. (C) Abundance of the proteins in human mass spectrometry pulldown experiments. The database used for the calculations was the PepTracker database.

Two additional proteins are displayed, which were only identified in the first mass spectrometry experiment: DNA-damage-binding protein 1 (DDB1) and importin 8 (IPO8). DDB1 was chosen for further analysis due to its reported interference with the interferon induction pathway, as well as its binding to the PIV5 V protein (Precious et al., 2005). IPO8

was chosen as a putative importin candidate, which could be responsible for the nuclear import of Cwt.

Unfortunately, none of the previously reported interaction partners of C, IPS-1, IRGM and STAT1 could be identified in the mass spectrometry pulldowns. Also the only recently described MV C and P interactor SHCBP1 was not present in the preparations (Ito et al., 2013).

The general abundance in mass spectrometry analysis of these putative binding partners of C was analysed using the PepTracker website, which assembles mass spectrometry data. A higher abundance of the proteins means a higher likelihood of an unspecific association with the protein to any other protein ('sticky proteins'). These proteins are not necessarily unspecific binding partners. They, however, have to be treated carefully in further analysis. Only two proteins of the list have a higher abundance than 50%: SLC25A3 and PHGH. The abundance of all other detected proteins was lower than 30% or they were not even detected before in the experiments listed in the database (Fig. 18 C).

To analyse the putative interaction partners of Cwt in more detail, protein-protein interaction network analysis were conducted. The interactions were gathered from the BIOGRID database. The individual interaction details were merged using Cytoscape, the interaction partners of Cwt coloured in blue (proteasomal components) and yellow (all other interaction partners). The resulting protein-protein interaction network is displayed in Fig. 19 A and surprisingly highly interconnected with an average number of neighbours of 4. The clustering coefficient of the resulting network was 0.2 and the network heterogeneity was 3.13. For further more detailed visualization, all proteins which interact with only one of the putative Cwt interaction partners were eliminated (Fig. 19, B). The proteins identified from the proteasome are all part of a subunit of the 26S proteasome particle, the 19S regulatory subunit. No proteins from the core subunits were found in the mass spectrometry experiments. In both networks, this 19S subunit forms a cluster, centred on the putative interaction partners coloured in blue, whereas the other proteins cluster around it and upon removing the secondary interaction partners (Fig. 19 B) no proteasomal components which belong to the core are still present. This indicates that the C protein might bind individually to the 19S subunit only, without the core subunits present, suggesting that it is an interaction independent of the process of proteasomal degradation. The protein network in Fig. 19 C

varies the size of the nodes according to the connectivity of the proteins, the ubiquitin chains (UBC) were deleted from this view, due to its high interconnectivity. The bigger the nodes are, the more edges connect these nodes to one another, the more interaction partners on of those proteins has. A total of eight proteins are highly connected in this network, besides the putative Cwt interaction partners. F-box only protein 25 (FBXO25) a part of the SCF complex, the Cullin Ring finger ubiquitin E3 ligase CUL3, Ubiquitin D (UBD) an ubiquitin-like protein, the proto oncogene MYC, the Histone deacetylases HDAC5 and SIRT7, the small molecular modifier SUMO2 and the cyclin dependent kinase 2 (CDK2). Interestingly with regard to the interferon system, STAT1 is also found as a secondary interaction partner linking PSMC3 and PHGDH.

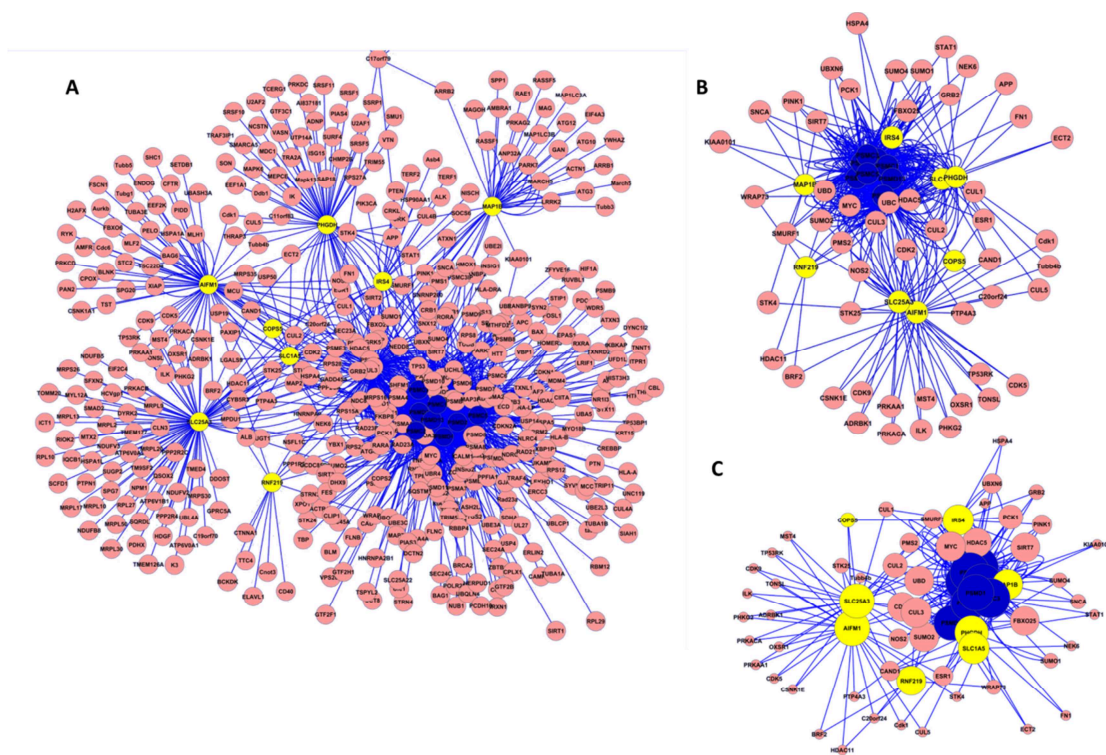


**Figure 19: Protein-protein interaction networks of MVCwt binding partners.**

The binding partners of MV Cwt identified by mass spectrometry are depicted in yellow, the proteasome components detected are depicted in blue. All other proteins are coloured in light red. The networks were generated using Cytoscape and spring-embedded layouts. The interaction data was taken from the BIOGRID database. The blue lines represent interactions, the circles proteins, annotated with their gene symbol. (A) Complete BIOGRID interactions of the proteins specifically interacting with Cwt. (B) Proteins which do at least interact with 2 proteins that were present in the pull-downs. (C) Spring-embedded network layout of the data in (B) with the node size scaling with its connectivity.

In summary, a few endogenous proteins specifically co-purified with Cwt or CwtmNLS and could be identified using mass spectrometry. Cwt seems to preferentially associate with the 19S proteasomal subunits as well as a small number of other proteins as indicated by two independent assays. Already known binding partners like IPS-1, phosphorylated STAT1 and IRGM could not be detected in the pulldown eluates.

### ***2.3.2. Validation of putative interaction partners***

The putative interaction partners identified in the mass spectrometry screens were analysed for binding to Cwt in a different assay: Co-immunoprecipitation followed by immunodetection of the proteins on Western blots (Fig. 20).

Four candidates were chosen to be tested in the initial verification assays: IPO8 (Fig. 20 A) as a potential importin for Cwt, DDB1 (Fig. 20 B) due to its implication in interferon inhibition by PIV5 V , MAP1B (Fig. 20 C) as the protein with the highest abundance that was detected in the mass spectrometry experiments and PSMC3, as a component of the 19S subunit of the proteasome (Fig. 20 D), which was already mentioned as an interactor of Cin a yeast-two-hybrid screening previously (Ito et al., 2013). The interaction between Cwt and DDB1, however could be verified as very weak, as judged from the difference between the exposure of the Co-IP blot and the input blot. In addition, association between the proteasomal component PSMC3 and Cwt could be proven in this assay as well, being moderate strong and comparable to the Cwt – IPS-1 binding as seen in parallel assays (data not shown). The interaction between Cwt and importin 8 could not be verified using this method. The same holds unfortunately true for the interaction between Cwt and MAP1B, which was the most abundant interaction partner in the mass spectrometry pulldowns (Fig. 20).

Taken together, two (DDB1 and PSMC3) of four proteins identified as interaction partners of Cwt by mass spectrometry analysis, could be immediately verified using co-immunoprecipitation experiments with flag-tagged C or HA tagged Cwt and the respective putative interaction partners.

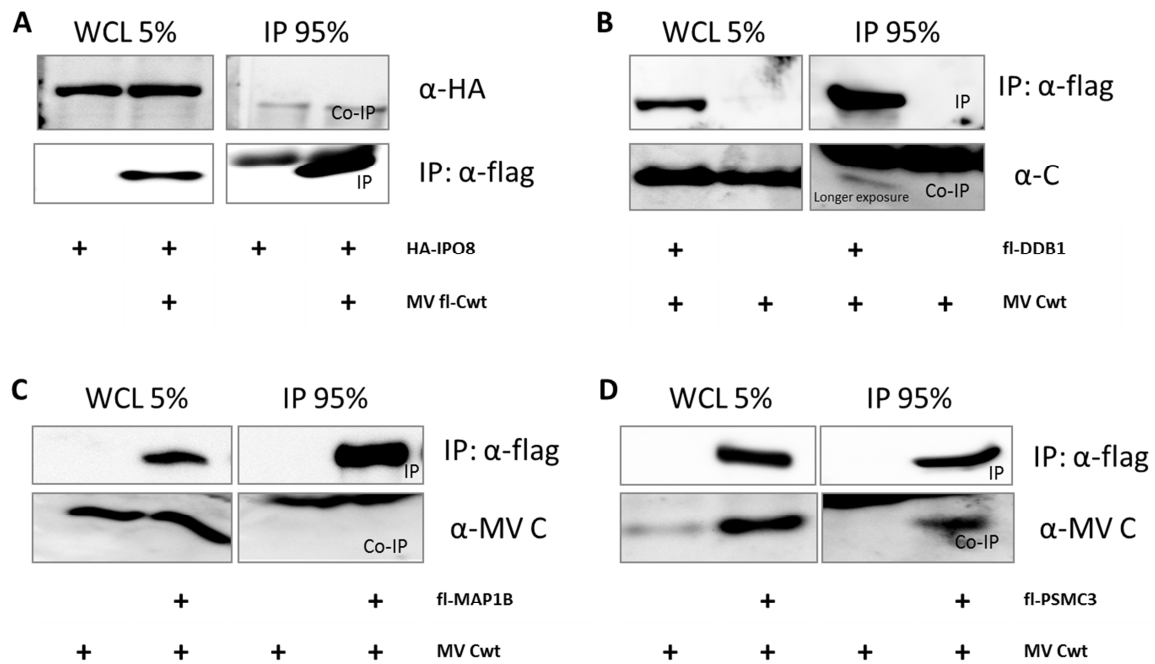


**Figure 20: Co-immunoprecipitation experiments of MV Cwt with putative interaction partners identified by mass spectrometry: IPO8(A), DDB1(B), MAP1B(C) and PSMC3(D).**

The pulldowns were done using HA-antibody (A) or flag-antibody (B,C,D) coated matrix and lysates from 293T cells. The whole cell lysates before the immunoprecipitation experiments were analysed by Western blots as well as the IP and the Co-IP blots as indicated in the figure. The percentage indicates the relative amounts of WCL and the IP loaded on the gel. (A) Co-purification of MV flag-Cwt with importin-8 (IPO8). anti-HA antibodies were used to detect HA-tagged IPO8 (upper panels). anti-flag antibodies were used to detect the flag-tagged Cwt protein (lower panels) (B) Co-purification of MV Cwt with flag-DDB1. anti-flag antibodies were used to detect the flag-tagged DDB1 protein (upper panels) and the C-antibody was used to detect the Cwt protein (lower panels). (C) Co-purification of MV Cwt with flag-MAP1B. anti-flag antibodies were used to detect the flag-tagged MAP1B protein (upper panels) and the C-antibody was used to detect the Cwt protein (lower panels). (D) Co-purification of MV Cwt with flag-PSMC3. anti-flag antibodies were used to detect the flag-tagged PSMC3 protein (upper panels) and the C-antibody was used to detect the Cwt protein (lower panels).

Yet another assay to support the interaction between two proteins in living cells is co-localisation in immunofluorescence. To this end, the Cwt was tagged with TagRFP, depicted as red fluorescence in the figure, to be able to detect it easier, without having to rely on antibodies. TagRFP overexpressed in Hep2 cells is a cytoplasmic protein (Fig. 21 A). If the

Cwt protein is fused N-terminally to TagRFP, the prominent nuclear localisation of the resulting fusion protein is comparable to the localisation of the Cwt protein without the fluorescent tag (Fig. 21 B). The flag tagged proteins were stained using a flag antibody and an Alexa-488 conjugated secondary antibody, appearing as green in the figure. The nuclei were stained with ToPro3 and coloured in blue. Co-localisation of the two overexpressed proteins would result in a yellow colour appearing in the merge images at the respective sites of co-localisation.

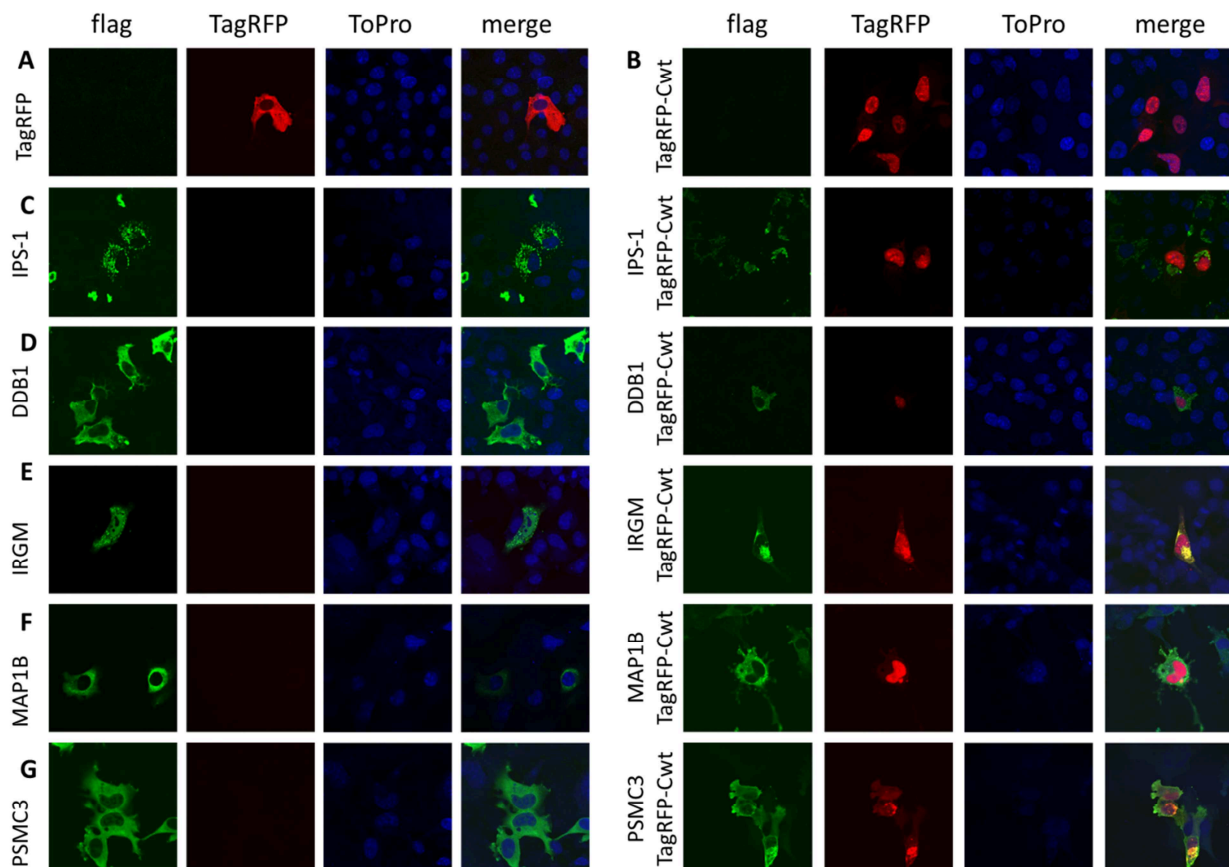


**Figure 21: Immunofluorescent images to detect co-localisation between C and various proposed binding partners.**

All proteins indicated were overexpressed in Hep2 cells and stained using their tags (flag, green fluorescence) or were fluorescently tagged (TagRFP-Cwt, red fluorescence). The flag tagged proteins were stained using anti-flag antibodies and anti-mouse Alexa 488 as a secondary antibody. The nuclei were stained using ToPro3. (A) Overexpression of Tag-RFP alone and (B) overexpression of TagRFP-Cwt. The following proteins were overexpressed with or without TagRFP co-expression as indicated in the figure: IPS-1 (A), DDB1 (B), IRGM (C), MAP1B (D) or PSMC3 (G). A co-localisation is indicated by a yellow colour in the merge images.

Overexpressed flag-IPS-1 was detected in Hep-2 cells clearly as a typical mitochondrial distribution in the cytoplasm. In some cases also the aggregations formed by activated IPS-1 were visible in the staining, hinting that the overexpressed IPS-1 still has the endogenous localisation and function. TagRFP-Cwt showed no clear co-localisation with flag-IPS-1 (Fig. 21 C). Upon overexpression, flag-DDB1 was found to be evenly distributed in the cytoplasm of the cells. As it is the case with IPS-1, no clear co-localisation with TagRFP-Cwt was visible after co-expression of both proteins in the same cells (Fig. 21 D). Flag-IRGM localised to the cytoplasm of the transfected cells as well as partially to the nucleus. However, when TagRFP-Cwt and fl-IRGM were co-expressed in the same cell both altered their intracellular localisation. They co-localised in a peri-nuclear space, the TagRFP-Cwt protein was recruited from the nucleus to the cytoplasm, whereas fl-IRGM accumulated at the exact same spot. Overexpressed fl-MAP1b was distributed in the cytoplasm like DDB1, only the outer nuclear rim seemed to be stained more intensively. Upon co-expression of Tag-RFP-Cwt and fl-MAP1b, both proteins retained their localisation and did co-localise only in a few small cytoplasmic dots. The 19S proteasomal component PSMC3 was detected upon overexpression only in the cytoplasm of the cells, although the 19S subunit was reported to reside in the nucleus of cells (von, 2006). Co-expression of TagRFP-Cwt and flag-PSMC3 led to a recruitment of TagRFP-Cwt out of the nucleus into the cytoplasm to co-localise partially with PSMC3.

In summary the interaction of Cwt with IRGM and PSMC3 could be shown as a co-localisation and change in localisation of the individual proteins in confocal images of living cells expressing both proteins. For MAP1B a co-localisation can be found in a few specific cytoplasmic dots, but the overall localisation of C and MAP1b differed. IPS-1 and DDB1 did not co-localize in the experiments shown here.

### 3. Analysis of MV C in the viral context

MV C has an important role during the course of infection, most probably by regulation of replication and transcription (Devaux and Cattaneo, 2004; Ito et al., 2013; Toth et al., 2009). However, it has to be concluded now, that in addition to the modulation of viral polymerase activity, C is also able to bind to cellular proteins and to modulate host cell behaviour and response. Several approaches were used to elucidate the role of the C protein in MV infected cells focusing on the alteration of cellular pathways during infection as well as viral protein-protein relations.

To this end, MV virus cDNA were cloned and recombinant virus rescued from this cDNA (Fig. 22). The basis for all engineered cDNAs was the full-length genomic cDNA of a vaccine measles virus with a sequence identical to the Schwarz vaccine strain: vac2 (del Valle et al., 2007). C expression from the virus can be abrogated by introducing mutations into the P gene to mutate the C translation start codon, as well as introducing two stop codons downstream. The introduction of more than one single nucleotide change is necessary to avoid a reverting of the virus back to C expression, due to evolutionary pressure. The mutations were the same as introduced into the plasmids to abrogate C expression; details are depicted in Fig. 1R. To express mutants of C from the viral genome, the C coding sequence has to be isolated from the P gene otherwise the alterations made or tags added in the P gene would affect all three encoded proteins: C, V and P. Therefore an additional transcription unit (ATU) was inserted in the backbone of the vac2 strain cDNA by duplicating the P gene borders (pMV vac2-ATU) (Fig. 22 C). The MV gene border transcription start signal (CTTAGG) is placed after the P gene polyA signal, to ensure polyadenylation of the P gene encoded mRNAs and a proper transcription start for the ATU. The very same polyadenylation signal was then introduced after a multiple cloning site. Consequently rMV vac2-ATU expresses a small non-coding RNA from the ATU. The multiple cloning site can be used to introduce new open reading frames by standard cloning techniques. This vector can be combined with mutation in the P gene abrogating C expression. In addition to a knockout of C in the original P gene, the C protein and its mutants can now be inserted in the ATU and are expressed from the additional transcription unit after virus rescue. In the following fluorescence studies, ORFs of TagRFP tagged C constructs as depicted in the figure were inserted into the MV vac2-ATU (Fig. 22 C). It was also possible to revert the Cs defect NLS to the wildtype NLS by inserting a point mutation into the P gene, which induces a G44 to R

transition in C but only a conservative R50K mutation in the P and V N-terminus, which is also present in the wildtype isolate D5 (Fig. 22 D). This virus is called rMV vac2CwtNLS.

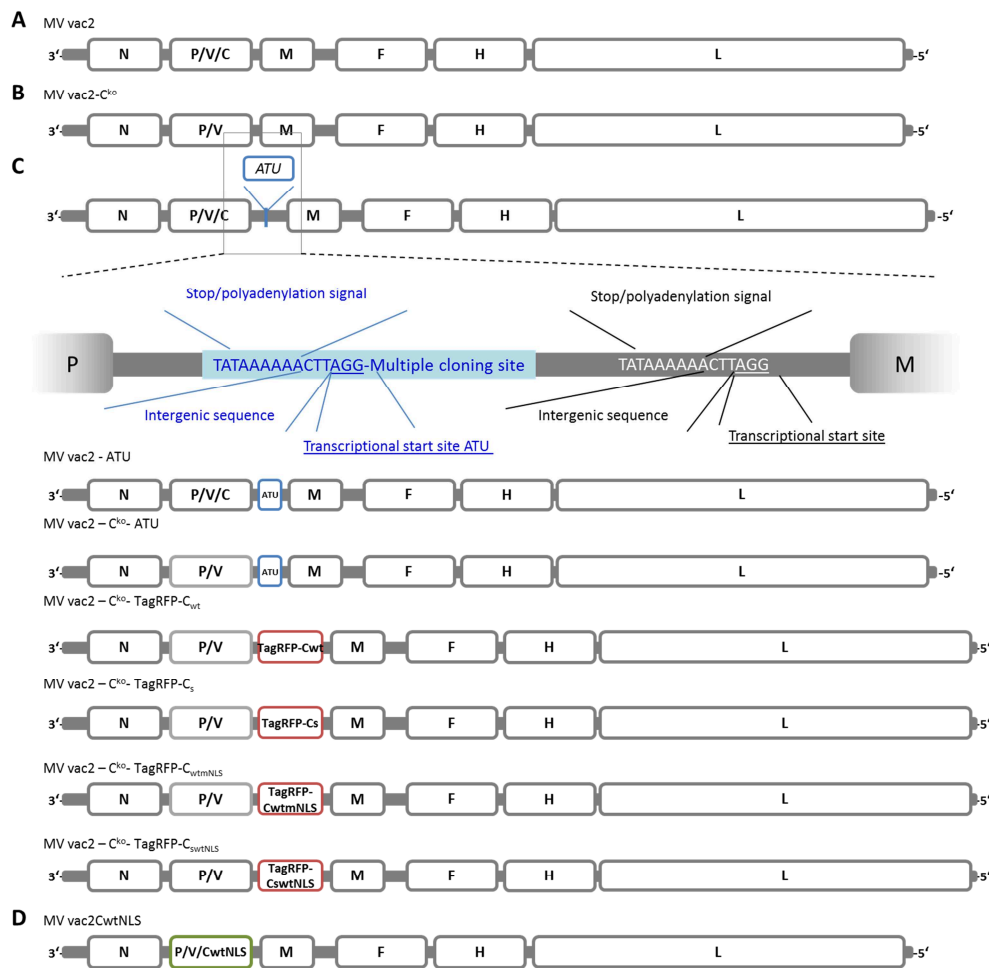


**Figure 22: Scheme representing the genomes of recombinant MVs generated during this thesis.**

The genome is depicted in 3'-5' orientation (leader-trailer) and the open reading frames within the genome highlighted as boxes. The respective encoded protein names are indicated in these boxes. (A) MV vac2: rMV retaining the unchanged vac2 sequence. (B) MV vac2C<sup>ko</sup>: rMV with the vac2 sequence and silent mutations in the P gene to abrogate C expression (deletion of the start codon and introducing two stop codons). These mutations are detailed in Fig.6. (C) The additional transcription unit (ATU) is generated by a duplication of the P gene border between the P and the M gene. The important nucleotides are highlighted in the figure. For cloning purposes a multiple cloning site was inserted into the ATU. MV vac2 - ATU: rMV vac2 with an additional transcription unit between the P and the M gene. The gene borders of the P gene are duplicated and a non-protein coding multiple cloning sites for cloning purposes inserted. MV vac2 - C<sup>ko</sup> - ATU: rMV vac2- ATU with additional mutations in the P gene similar to rMV vac2-C<sup>ko</sup> to abolish C expression. MV vac2-C<sup>ko</sup>-TagRFP-C<sub>wt</sub>/s/wtmNLS/swtNLS: rMV on the

basis of rMV-Cko-ATU with an open reading frame inserted in the additional transcription unit. Here it encodes for the different TagRFP tagged C proteins. (D) MV vac2CwtNLS: rMV having the sequence of the MV Schwarz strain, except for one conservative mutation (R50K) in the P gene, introducing a G44R exchange into C to restore the wildtype nuclear localisation signal. P and V are also affected by a R50K in their common N-terminal domain.

The rescue was done by transfecting full length cDNA and MV L-encoding plasmids into 293-3-46 cells, co-culturing them with Vero-hSLAM cells until syncytia formation from individually rescue events was visible as described in the introduction. These syncytia were picked and isolated and grown on Vero cells. The titration of all the viruses were done on Vero cells (see introduction Fig. I3). The rescue of recombinant virus from all the cDNA constructs depicted in Fig. 22 was successful.

### 3.1. Host transcription regulation induced by rMV vac2 infection

To get an overview how the host cell reacts on an RNA level to an infection by MV, microarray experiments were conducted using rMV vac2 infected B-cells. The viruses used for these experiments were purified by pelletation to remove any cytokines from the supernatant of the stock-producing cells, which could alter the behaviour of infected cells. A B-cell line (DG75) was chosen to represent a cell type which is naturally infected in its host by wildtype measles virus as well as the vaccine strains. The changes in the total mRNA content compared to mock infected cells were subsequently analysed (Fig. 23). They are represented as fold changes of the viral infected cells compared to the mock infected cell population harvested at the same timepoint. Two distinct timepoints were analysed: 24h and 48h post infection with rMV vac2 using an MOI of 1. The total cellular RNA content then was hybridized on Affymetrix Human GeneChip 1.0 arrays and these arrays then analysed for binding of cellular RNAs in the microarray facility of the Cramer group (Genecenter, Munich).

The RNAs detected were 81 fold upregulated or 6 fold downregulated at most compared to mock infected cells after 48h of infection. The differentially regulated cellular RNAs (regulation  $> 2$ ,  $p < 0.5$ ) could be clustered into three basic clusters according to their regulation in infected cells over time: Genes which were downregulated (Fig. 23 A), genes which were upregulated (Fig. 23 B) and genes which were strongly upregulated temporarily after 24h, but then declined after 48h (Fig. 23 C).

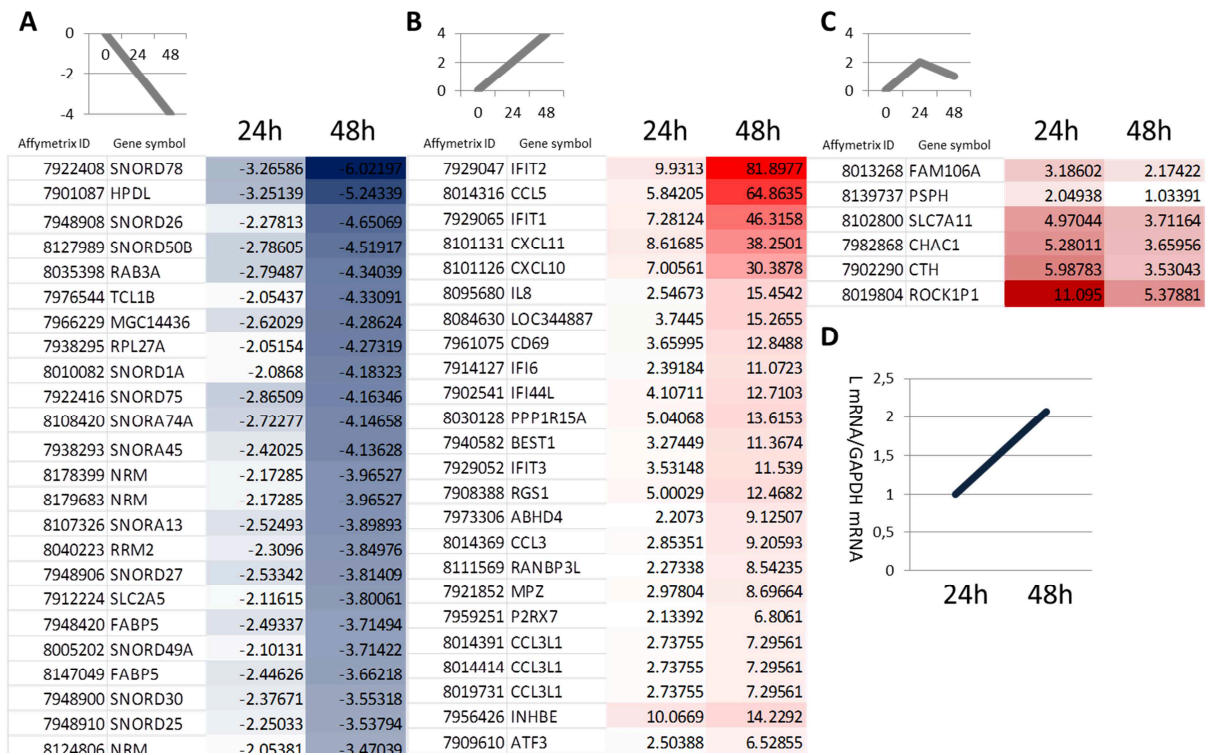


**Figure 23: RNAs regulated by infection with MV vac2 at different timepoints in human B-cells.**

DG75 cells were infected with MV vac2 at an MOI of 1 and the total RNA harvested after 24h and 48h subjected to microarray analysis. (A, B, C) Clusters of regulated RNAs according to the scheme above the lists. The official gene symbol and the affymetrix ID of the probes on the microarray are displayed in the first two columns of the table. The last two columns indicate the fold changes of the RNA detected in comparison to mock infected cells after 24h or 48h. Negative values mean a downregulation, positive values an upregulation. The colour coding was done according to the blue-white-red scheme, blue meaning downregulation, red meaning upregulation. The RNAs displayed showed at least 2 fold regulation and have a p value smaller than 0.5. Only parts of the regulated genes are displayed here, representing the highest changes compared to mock. The complete list of significantly regulated RNAs clustered and unclustered is in the appendix. This experiment represents duplicates. (D) Detection of the L mRNA of measles virus in the samples and relative quantification by qRT-PCR. At 24h the amount of L mRNA was to 1, the value for 48h p.i. calculated relatively. The values represent the mean of the duplicates. The mock infected control was negative for L mRNAs and is therefore not displayed here.

The infection was monitored by quantitative realtime PCR using primers specific for the MV L mRNA (Fig. 23 D) and the 24h value was set to 1, as L mRNA could not be detected in mock infected cells. After 48h, the intracellular content of MV L mRNA doubled, indicating that viral multiplication indeed took place.

To characterize these clusters in further detail, pathway analysis was performed using the web based DAVID bioinformatics server. The first cluster could not be annotated automatically (Fig. 24 A). However, it is obvious that most of these are small nucleolar RNAs (SNORDs). Some of these SNORDs play an important role in the 2'-O-methylation pathway, especially the mainly downregulated SNORDs: 78, 26 and 50B. 4-Hydroxyphenylpyruvate Dioxygenase-Like (HPDL), the second most downregulated RNA is largely uncharacterized in literature. RAB3A mRNA encodes a Ras-related protein involved in exocytosis probably by regulating a late step in synaptic vesicle fusion (Zahraoui et al., 1989).

The upregulated genes (Fig. 23 B) can easily be characterized as interferon and infection stimulated genes (Fig. 24 B), their products representing chemotactic signals for immune cells. Most of these genes encode proteins that are classical interferon stimulated genes (ISGs): e.g. IFIT1, IFIT2 or chemokines (CCL5, CXCL11 & 10). These are part of the typical inflammatory and anti-viral response of a cell and are used to attract the adaptive immune system or as an alert signal to neighbouring cells. IFIT1 binds triphosphorylated RNA and inhibits expression of 2' O-methylation defective RNAs along with IFIT2. They both exhibit direct antiviral activity (Zhou et al., 2013). Secreted CCL5 attracts blood monocytes, memory T helper cells and eosinophils, whereas CXCL11 and 10 are chemotactics for T cells mainly. Notably, the upregulation of the interferon beta mRNA is significant only after 48h to a value of 6-fold, which is fairly low, compared to a 81-fold induction of IFIT2.

Interestingly, the third cluster of genes (Fig. 23 C) contains genes responsible for amino acid metabolism and biosynthesis (Fig. 24 C). Unfortunately there is no annotation for FAM106A (Family With Sequence Similarity 106, Member A), and its function remains unknown. Phosphoserine Phosphatase (PSPH) plays an important role in the biosynthesis of serine, catalysing the last step of L-serine formation. Solute Carrier Family 7 (Anionic Amino Acid Transporter Light Chain, Xc-System), Member 11 (SLC7A11) is an amino acid carrier specific for glutamate and cysteine. Cation Transport Regulator Homolog 1 (CHAC1) is a negative regulator of the notch signalling pathway. The Cystathionase (CTH) protein catalyses the conversion of cystathione into cysteine and therefore is also involved in amino

acid metabolism. For ROCK1P1 (Rho-Associated, Coiled-Coil Containing Protein Kinase 1 Pseudogene 1) no detailed annotation or description could be found.

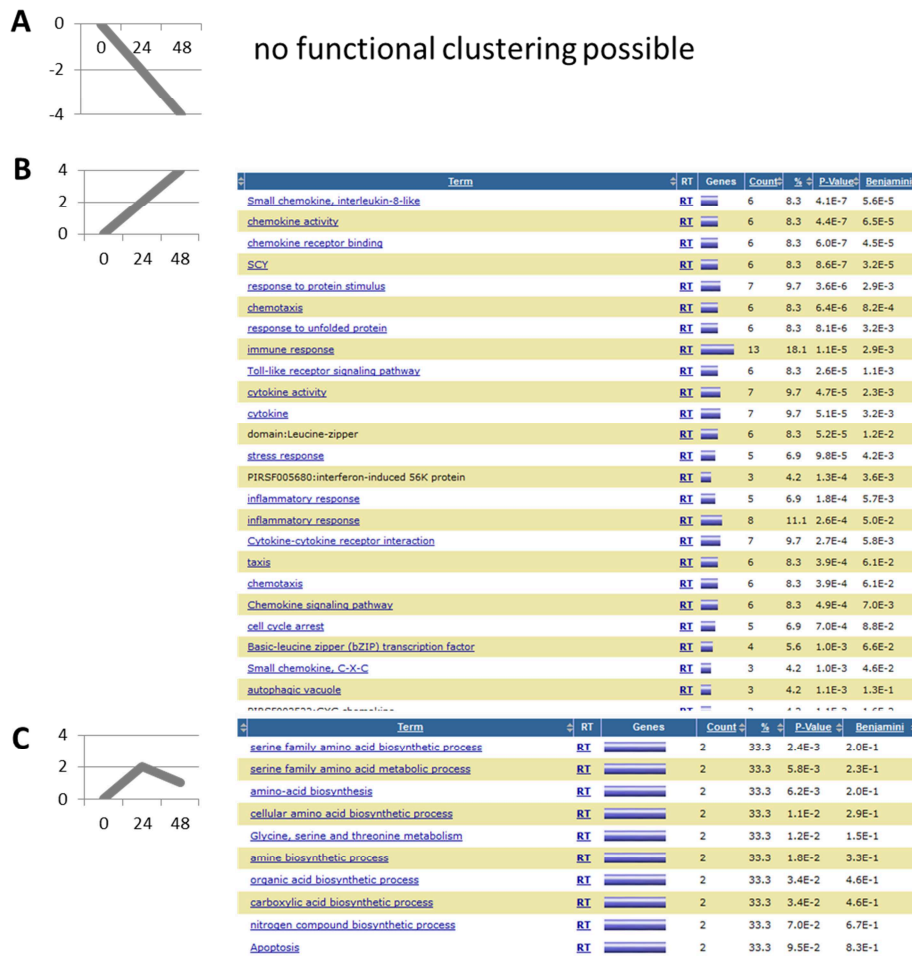


**Figure 24: Functional annotation and clustering of the RNAs found to be regulated more than 2-fold in microarray experiments.**

Three different clusters were made according to the regulation of the RNAs over time (24h and 48h post infection) and the list of genes submitted for functional annotation and clustering using the DAVID website. The full profiles are in the appendix. The pathways are indicated next to the different clusters (A, B and C as in Fig. 23), Count displays the number of genes matching to the pathway which represents the percentage fraction in the next column. Both the p-value and benjamini are indicators of the significance of the overrepresentation of the pathway in the subset of genes submitted for analysis.

In summary, MV infection of B cells induced the expected innate immunity responses apparently, lacking however a robust induction of interferon beta. Notably, the transcription of genes coding for small nucleolar RNAs was severely downregulated.

### 3.2. MV C<sup>ko</sup> viruses are heavily attenuated

The first step approaching the function of the C protein in a viral context is the knock-out of the C ORF from the P and V mRNA. This was done in a similar fashion to the generation of the plasmids coding only for the P and the V protein (see Figure 6). The P gene was mutated within the full-length viral cDNA vector. This mutated cDNA vector was then used for rescuing rMV vac2C<sup>ko</sup>. MV lacking the expression of the C protein are heavily attenuated albeit viable and were reported to induce more interferon than their parenteral viruses (Devaux and Cattaneo, 2004; Devaux et al., 2008; Nakatsu et al., 2008).

A comparative growth curve in Vero cells of rMV vac2 and rMV vac2C<sup>ko</sup> revealed that the C<sup>ko</sup> virus indeed grows to titres approximately 1-1.5 logs lower than the parental strain (Fig. 25 A). Interestingly the cytotoxic phenotype observed after 72h in Vero cells was notably more pronounced in cells infected with MV vac2C<sup>ko</sup>, although the infectious viral titres were lower at that timepoint. At the last timepoint, rMV vac2C<sup>ko</sup> seems to catch up to rMV vac2. Comparing interferon competent (A549) and interferon incompetent (Vero) cell lines (Fig. 25 A and B), it can be concluded that rMV vac2C<sup>ko</sup> is greater attenuated (approximately 2 logs) in a cell line which still has a functional innate immune system. In addition to that, A549 cells survived the infection with the rMVs, whereas the Vero cells were completely dead 96h post infection. Syncytia formation was observed only to a low degree in A549 cells, whereas the Vero cells showed a high syncytia formation ratio. The overall titres of infectious rMV particles in Vero cells were at all timepoints generally higher compared to A549 cells (around 1 log), again underlining the difference between those two cell lines. Notably, a decrease of infectious virus titres in cells is earlier visible in A549 cells (after 48h) than in Vero cells (after 72h), although the Vero cells die earlier.

A lack of expression of the C protein during infection was also confirmed on the western blot of lysates of Vero cells infected with rMV vac2, rMV vac2C<sup>ko</sup> and mock. 48h after infection P and V as well as N are normally expressed and can be detected in the lysates of both virus infected Vero cells. However, only rMV vac2C<sup>ko</sup> failed to produce the C protein, confirming that the knockdown was successful. Importantly, only the C protein is affected and not the other two proteins encoded by the P gene, P and V (Fig. 25 C).

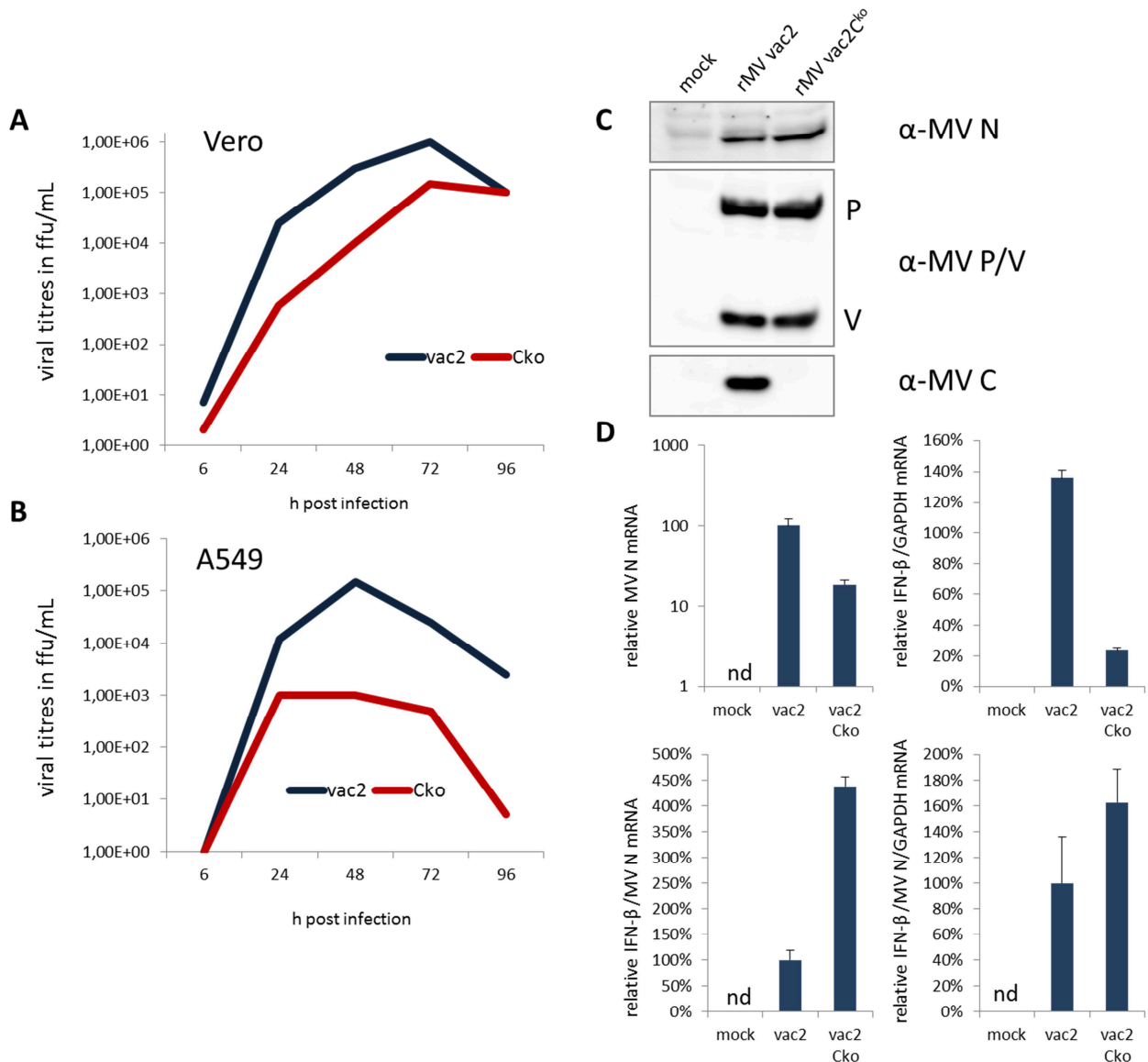


**Figure 25: Characterisation of C knockout MV vac2.**

Growth curves of MV vac2 and MV vac2<sup>ko</sup> in interferon negative Vero cells (A) and interferon competent A549 (B) cells. Viral titres were measured at the indicated timepoints. (C) Western blot analysis showing the lack of MV C expression by rMV vac2<sup>ko</sup>. Vero cells were infected with the indicated viruses and the cells harvested 48h p.i.. Specific antibodies were used to detect the viral proteins. (D) qRT-PCR of infected A549 cells 72h post infection with an MOI of 0.01 comparing rMV vac2 and rMV vac2<sup>ko</sup>. Three RNAs were quantified: the cellular IFN-β and GAPDH mRNAs and the viral N mRNA. 4 different normalisations were done, using the ratios indicated on the y-axis of the charts, effectively showing the higher induction of interferon β in Cko viruses. The mean values of three replicates are shown, with the mock value set to 1 if possible or the value for rMV vac2 set to 100 (%) and the remaining values calculated accordingly.

To further characterize the differences of rMV vac2 and rMVC<sup>ko</sup> focusing on the innate immune system, quantitative realtime RT-PCR was performed to compare the induction of interferon caused by the two rMVs during infection. Overall, rMV vac2 infection with the same MOI induced more interferon  $\beta$  mRNA after 72h. However, rMV vac2C<sup>ko</sup> also shows a reduced transcription of N mRNA, indicating a slower growth, which has to be taken into account. Normalisation of the interferon  $\beta$  mRNA levels with the MV N mRNA levels revealed, that the induction of IFN- $\beta$  mRNA per viral N mRNA is 4.5 times higher for rMV vac2C<sup>ko</sup>. MV vac2 seemed to cause a growth arrest in A549 cells as more cellular RNA could be purified from rMV vac2C<sup>ko</sup> and mock infected cells than rMV vac2 infected cells. Normalisation using GAPDH mRNA was therefore also carried out, still showing that rMV vac2C<sup>ko</sup> induces relatively more interferon  $\beta$  mRNA than rMV vac2 (Fig. 25 D), albeit the effect is less pronounced. These qRT-PCR experiments are in accordance to results published by other groups (McAllister et al., 2010; Toth et al., 2009).

Aberrant RNA production induced by the lack of a C protein could lead to various effects, ranging from increased read-throughs of different genes or the generation of dsRNA. To analyse the viral RNAs produced by the rMV vac2 and rMV vac2C<sup>ko</sup> in comparison, Northern blots were done. 4 $\mu$ g of the total RNA of infected Vero cells was separated on agarose gels according to their size. Within the total cellular RNA the MV mRNAs and transcriptional products were detected on nylon membranes by hybridisation of MV specific radioactively labelled oligonucleotides.

Four different probes were used to detect MV specific RNAs (N, P, H and F sequences) and one cell-specific probe (actin) to visualize the amount of cellular RNA present in the preparations (Fig. 26 A). The calculated sizes of the expected mRNAs and readthrough RNA products are listed in the right panel, next to the northern blot (Fig. 26 A). These calculations do not include the polyA sequence, which elongates the mRNAs by approximately 200 A nucleotides. Identification of the mRNAs and other RNAs was done according to their length and strength of the signal. If not stated otherwise, the bands described for the viral RNAs were visible in both the lanes for rMV vac2 and rMV vac2C<sup>ko</sup> infected cells, and specifically not in the mock control lane.

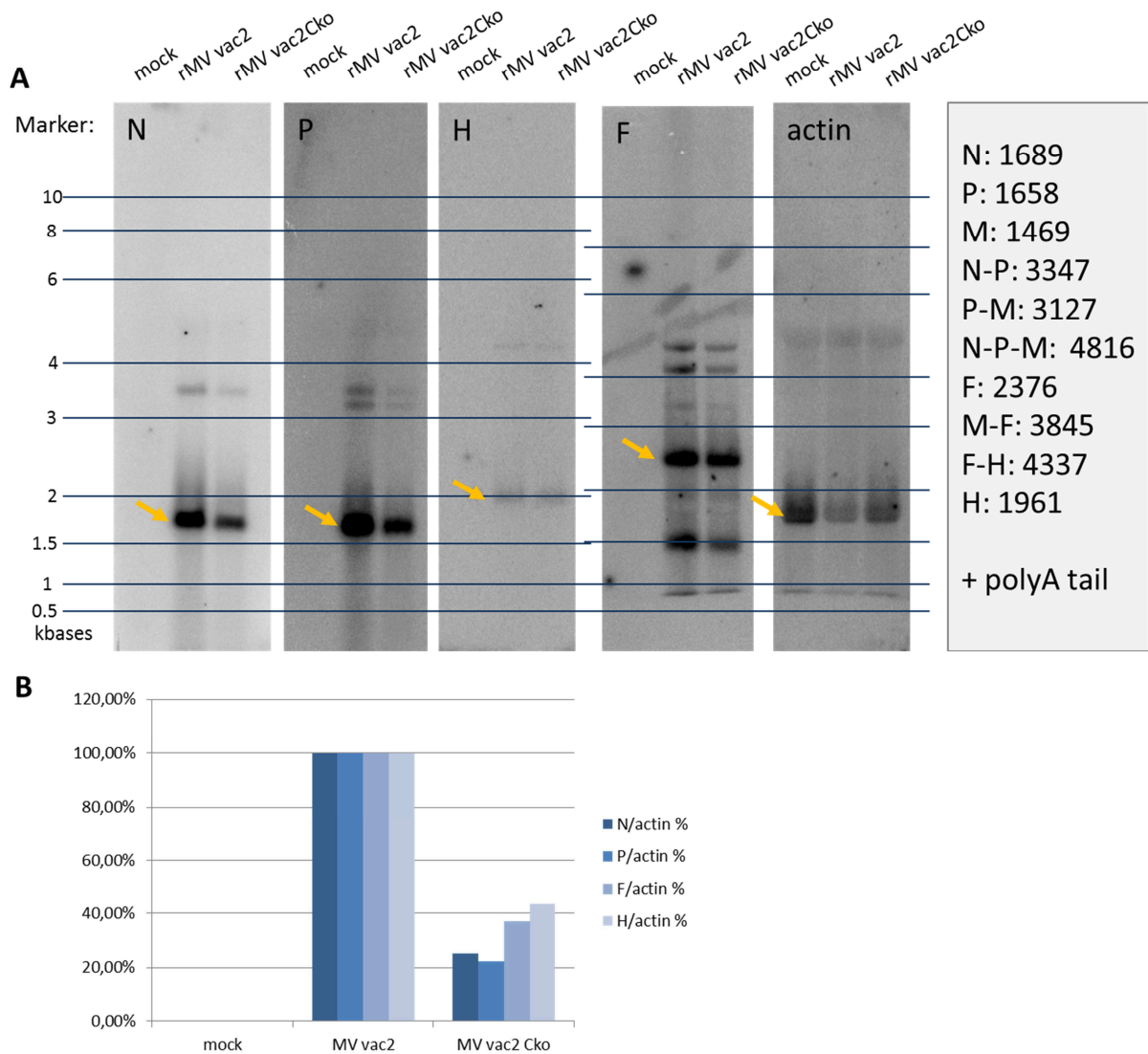


**Figure 26: Northern blot and detection of viral RNAs from rMV vac2 and rMV vac2Cko infected cells.**

(A) Radioactively labelled probes for different mRNAs (MV N, P, H, F and the cellular mRNA actin) were used to detect viral RNA in total RNA extracts from infected and mock infected Vero cells as indicated above the respective blots. The infections were done with an MOI of 0.5 and the cells harvested 36h post infection. The viral mRNAs are indicated with small yellow arrows. In the left panel the sizes of the marker are displayed in kilobases. The blue lines represent a continuation of the marker on the original gel to indicate the sizes of the detected mRNAs. In the right panel the calculated sizes of the expected RNAs are indicated in bases. E.g. F-H indicates the readthrough of the MV F and H mRNA. These calculated sizes do not include the polyA tail, which additionally elongates these RNAs by ca. 200 bases. (B) Quantification of the indicated bands from the northern blot in A. The bands for the mRNAs (yellow arrows) were quantified using ImageJ and normalized to the actin control. The values for vac2 mRNA is always set to 100% and the mRNA amount for rMV vac2C<sup>ko</sup> calculated accordingly.

On the N probe blot, the N mRNA could be detected as the most prominent band with a size of approximately 1.7kb. A second band at 3.5 kb corresponds to the size of N-P readthrough mRNA, a third at ca. 5kb to the N-P-M readthrough mRNAs. The longer the readthrough is the fainter the bands are and the less abundant the RNAs are. In the case of the MV P specific probe, the P mRNA was most prominently detected. As for the N blot, both N-P and N-P-M readthrough transcripts were visible as well at the exact same height. Additionally, at 3.2 kB the P-M readthrough transcript could be detected. The MV H specific probe worked less well, however the H mRNA was still detected. A faint band of an H-F readthrough transcript can be seen at 4.5 kB. In the case of the F specific probe, a multitude of bands was detected, the most abundant transcript being the F mRNA at 2.5 kB. A potential F-H readthrough RNA of 4.5kB was also visible; no F-L transcript could be detected. The other bands at 1.5, 2 and 4 kB however could not be attributed to an RNA species expected. Especially the bands appearing at a lower height than the F mRNA indicate truncated or degraded F transcripts in the preparation. A general degradation of the RNA however, was not visible in the other blots. These additional bands, seen in the F blot are specific for the infected cells, as they do not appear in the mock infected cellular RNA.

The actin mRNA blot revealed that in the mock control cells the most cellular RNA was present, whereas in the case of the rMV vac2 infection the cells already have decreased actin mRNA content. This correlates with the expected beginning of cell death after 36h of infection. To a lesser extend the effects of infection caused cell death were also seen in the rMV vac2C<sup>ko</sup> infected RNA preparation.

Unfortunately, in neither of these blots the genomic or antigenomic RNA was visible, which would appear at a size of approximately 16kB.

Quantification of the bands using ImageJ (Fig. 26 B) further confirmed the visual impression that rMV vac2C<sup>ko</sup> compared to rMV vac2 produces less mRNAs. The amount of mRNAs (N, P, F and H) normalized to the actin control is generally around 80% lower in cells infected with rMV vac2C<sup>ko</sup>. Interestingly, the differences of the mRNA content of the more 3' genes (N, P) between rMV vac2 and rMV vac2C<sup>ko</sup> seems to be greater than that of the more 5' genes (F, H). This could possibly indicate a change in the mRNA transcription gradient.

Judging from the overall mRNA levels in the preparation, the result of the growth curves could be confirmed. rMV vac2C<sup>ko</sup> grows slower and consequently produces less

mRNAs than the rMV vac2. However, no alterations like a different mRNA readthrough transcript composition were visible other than a lower general abundance of viral RNAs. The ratio between genome and mRNA production could not be calculated, as the genome could not be detected.

### **3.3. The localisation of C during infection**

The localisation of MV C during infection was reported to be either in the nucleus or in the cytoplasm (Bellini et al., 1985; Nishie et al., 2007).

To assess the localisation of the C protein during the actual infection, several confocal approaches were used. 48h after infecting Vero cells with rMV vac2, the C and N protein were stained using fluorescent antibodies (Fig. 27 A). Clearly, the C protein (depicted in green) co-localized with the N protein (depicted in red) during these late stages of infection (48h p.i.). An obvious nuclear accumulation is not visible (nuclei in white). This was expected in the case of the C protein of the vaccine strain of measles virus. However, compared to the observed localisation of C during overexpression a notable change are the inclusion bodies or stress granules formed by C and N. Clearly visible however, is the syncytia formation caused by MV infection (bottom images). The nuclei of the fused cells are still intact and cluster in the middle of these giant cells. Infection of Vero cells with wildtype virus failed, and cells that could be infected with wildtype virus proved to be difficult, if not impossible, to stain with antibodies.

Timepoints earlier than 48h p.i. could not be imaged. Later timepoints have to be done using lower MOIs in order to avoid a complete destruction of the cell monolayer. Therefore, plasmids encoding TagRFP-tagged Cwt protein were transfected into cells and afterwards infected with GFP expressing rMV vac2 (rMV vac2-GFP) (Fig. 27 B). The GFP expression was used to monitor the infection while localisation changes in TagRFP-Cwt were visible without having to rely on antibody staining. In non-infected, plasmid expressing cells, TagRFP-Cwt localises exclusively to the nucleus. In infected cells, two different situations could be seen: In some GFP and TagRFP positive cells, TagRFP-Cwt still resided in the nucleus, whereas in some cases TagRFP-Cwt was recruited to the cytoplasm where it formed inclusion bodies. These inclusion bodies are also visible in the GFP staining, as GFP seems to be recruited to these sites as well. They represent probably the same inclusion bodies seen with N antibodies previously. Notably, a recruitment of C to the cytoplasm only occurred in cells, where the GFP inclusion bodies were already visible.

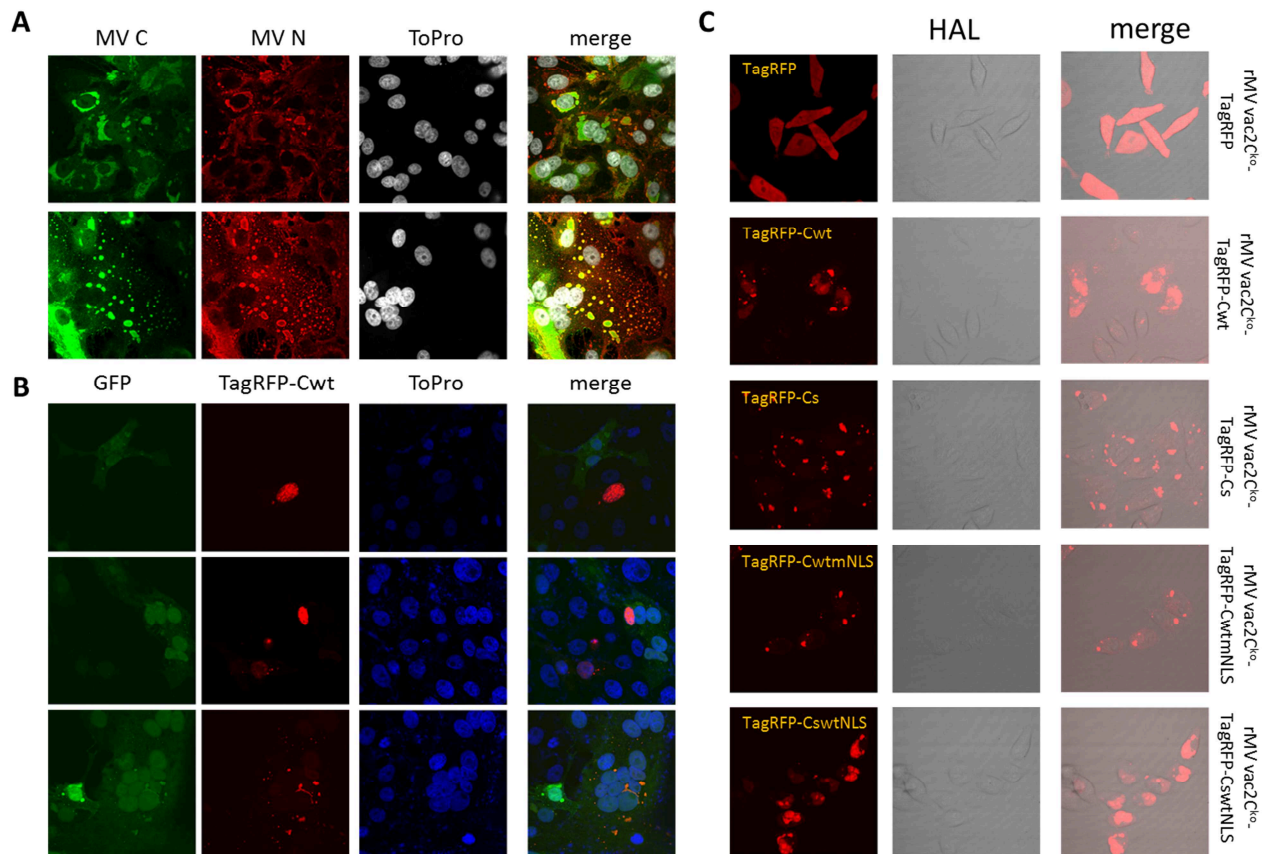


**Figure 27: Intracellular localisation of C and mutants in the viral context.**

(A) Immunofluorescent staining of MV C and N in Vero cells infected with MV vac2 48 p.i.. C protein was stained with anti-1442 C antibodies and anti-rabbit Alexa-488 secondary antibodies (green). MV N was stained using anti-MV N (mouse) and anti-mouse Tetramethylrhodamine as a secondary antibodies (red). The nuclei were stained with ToPro3 (white). The respective proteins detected are indicated above the images. Merge represents the overlay of all three channels, a yellow colour indicating colocalisation. (B) Hep2 cells transfected with a plasmid encoding TagRFP-tagged Cwt and infected with rMV vac2-GFP. 24 p.i. the cells were fixed and the images taken. The nuclei were counterstained using ToPro3 (blue). Green indicates the fluorescence of GFP, whereas red indicates the presence of TagRFP-Cwt. (C) Intracellular localisation of TagRFP-C variants expressed from the recombinant measles viruses indicated next to the images. HeLa cells were infected with the indicated viruses using an MOI of 1 and confocal images takes 24h p.i.. A red fluorescence indicates the presence of the TagRFP-tagged proteins. HAL annotated images depict the cells using normal phase contrast light microscopy. Merge represents the overlay of the two images.

To visualise the intracellular localisation of C expressed by the virus, recombinant viruses were generated as described before (Fig. 22 C). These rMVs harbour TagRFP-tagged C variants in the additional transcription unit, while expression of the original C from the P gene is knocked out (see above). All of these constructs could be rescued and showed bright red fluorescence, indicating the localisation of C during infection. For control purposes, rMV encoding only TagRFP in the additional transcription unit was used to infect HeLa cells. 24h after infection TagRFP fluorescence was visible in the whole cytoplasm and the nucleus, showing no distinct localisations (Fig. 28 C). Fluorescence of rMV  $\text{vac}2\text{C}^{\text{ko}}$ -TagRFP-Cwt, however, could be detected in both the nucleus and cytoplasmic inclusion bodies, whereas the TagRFP-Cs expressed by rMV  $\text{vac}2\text{C}^{\text{ko}}$ -TagRFP-Cs was only found in the inclusion bodies in the cytoplasm. TagRFP-CwtmNLS encoded by rMV  $\text{vac}2\text{C}^{\text{ko}}$ -TagRFP-CwtmNLS was also located exclusively to the cytoplasmic inclusion bodies and completely removed from the cell nucleus. TagRFP-CswtNLS instead was present in the nucleus as well as in the cytoplasmic inclusion bodies, in a similar fashion to TagRFP-Cwt. Interestingly, the nuclear C protein fraction seemed to additionally accumulate in the nucleoli of infected cells.

These localisation studies indicate that the different C proteins behave, even when expressed from a recombinant virus, in accordance with the data observed for protein overexpression. One major difference however, was the occurrence of cytoplasmic inclusion bodies in all viruses, which do not show up during overexpression of the C proteins alone.

The re-localisation of MV Cwt which is observed upon infection suggests that a viral protein or RNA is responsible for that. Alternatively any cellular protein induced during infection could be responsible for the alteration in MV C localisation. It is known from previous studies that co-expression of MV N and P results in the formation of cytoplasmic inclusion bodies containing both P and N, similar to those observed during infection.

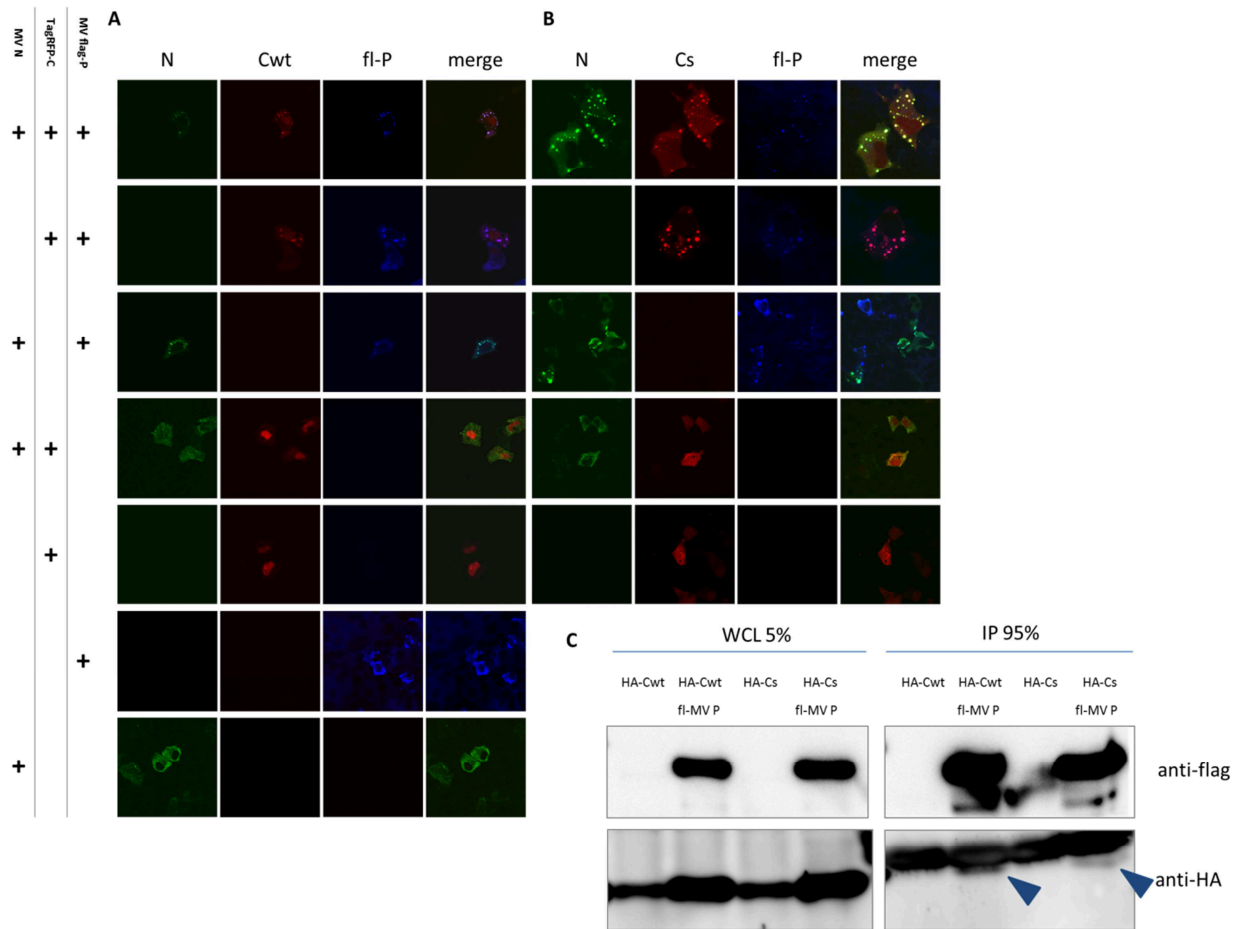


**Figure 28: Immunofluorescent images of MV N, C and P co-expression.**

Hep2 cells were co-transfected with plasmids encoding the MV proteins indicated in the table left of the images. The vac2 N protein was detected using anti-N-FITC antibodies (green). The C proteins (wildtype D5 (A) or schwarz (B)) were tagged with TagRFP at the N-terminus (red). The flag-tagged vac2 P protein was detected using flag antibodies and anti-mouse Alexa 633 as secondary antibodies (blue). The respective proteins detected are indicated above the images. Merge represents the overlay of all three channels, a yellow or purple colour indicating co-localisation. (C) **Co-immunoprecipitation experiments of MV Cwt and Cs with MV flag-P.** The pulldown experiments were done using a flag-antibody coated matrix and lysates from 293T cells and were transfected with plasmids encoding for the proteins indicated above the Western blots. The whole cell lysates before the immunoprecipitation experiments were analysed by western blots as well as the IP and the Co-IP blots as indicated in the figure. The percentage indicates the relative amounts of WCL and the IP loaded on the gel. The blue arrows highlight the faint band for HA-MV C in the co-immunoprecipitation Western blot, the stronger band above is unspecifically detected by the antibody. HA-antibodies and flag-antibodies were used for the detection of the tagged proteins as indicated next to the blots.

To test, whether co-transfection of MV N or P also induces a localisation change for Cwt, immunofluorescence experiments were conducted. Indeed, a triple overexpression of MV C, N and P showed a clear co localisation of those three proteins in dots, which look like cytoplasmic inclusion bodies in the cells (Fig. 28). This is the case for both Cwt (Fig. 28 A) and Cs (Fig. 28 B). Overexpression of N and P results in the expected co-localisation and inclusion body formation. Interestingly, both P and N showed a cytoplasmic distributed localisation upon individual overexpression, while Cwt retained its nuclear localisation and Cs the cytoplasmic-nuclear distribution. Co-expression of MV C and N did not result in any localisation change of both proteins. Surprisingly, however, MV P and C co-expression clearly showed the inclusion body formation with C and P co localising in the cytoplasmic aggregations. Thus, P alone is sufficient to recruit Cwt or Cs completely to the cytoplasm and together they are able to induce dots or cytoplasmic aggregates during infection even in the absence of MV N. These dots resembled the inclusion body formation observed during infection, but were much smaller.

Consequently the binding of Cwt to MV P was checked by co-immunoprecipitation. And indeed C was able to bind to P in these experiments; however the interaction seemed to be very weak, suggesting an indirect binding (Fig. 28 C, blue arrows).

In summary, expression of MV P is sufficient to recruit C to the cytoplasm where they both form granules, regardless whether C is derived from the vaccine strain or the wildtype strain. MV P and Cs/wt can interact, as seen in co-immunoprecipitations, although very weak.

### **3.4. Characterisation of C and its NLS in the viral context**

The rMV vac2C<sup>ko</sup> virus has many defects regarding replication to be useful as an immediate tool to study the details of the influence of the C protein on the host cells. These defects could lead to unwanted variables regarding the interferon induction, like aberrant production of stimulating RNAs. Therefore, it is necessary to try different mutants of C (e.g. NLS mutants) to assess the effects of the differently regulated C localisation in a viral context during infection.

To this end, two recombinant viruses were used: rMV vac2, the authentic recombinant vaccine strain and rMV vac2CwtNLS a recombinant virus which has only one point mutation compared to rMV vac2 in the P gene (Fig. 22 D). This point mutation causes the expression of a C with a restored wildtype NLS similar to CswtNLS mentioned above (G44R).

Comparing rMV vac2 with rMV vac2CwtNLS no differences in growth were observed in interferon gene negative Vero cells. In the interferon competent A549 cells these viruses also grew almost similar, diverging however at later timepoints for up to 0.5 logs. Interestingly, the rMV vac2 seems to grow slower than rMV vac2CwtNLS (Fig. 29 A). The experiments were done in parallel using the same virus stocks for infection, to ensure comparability.

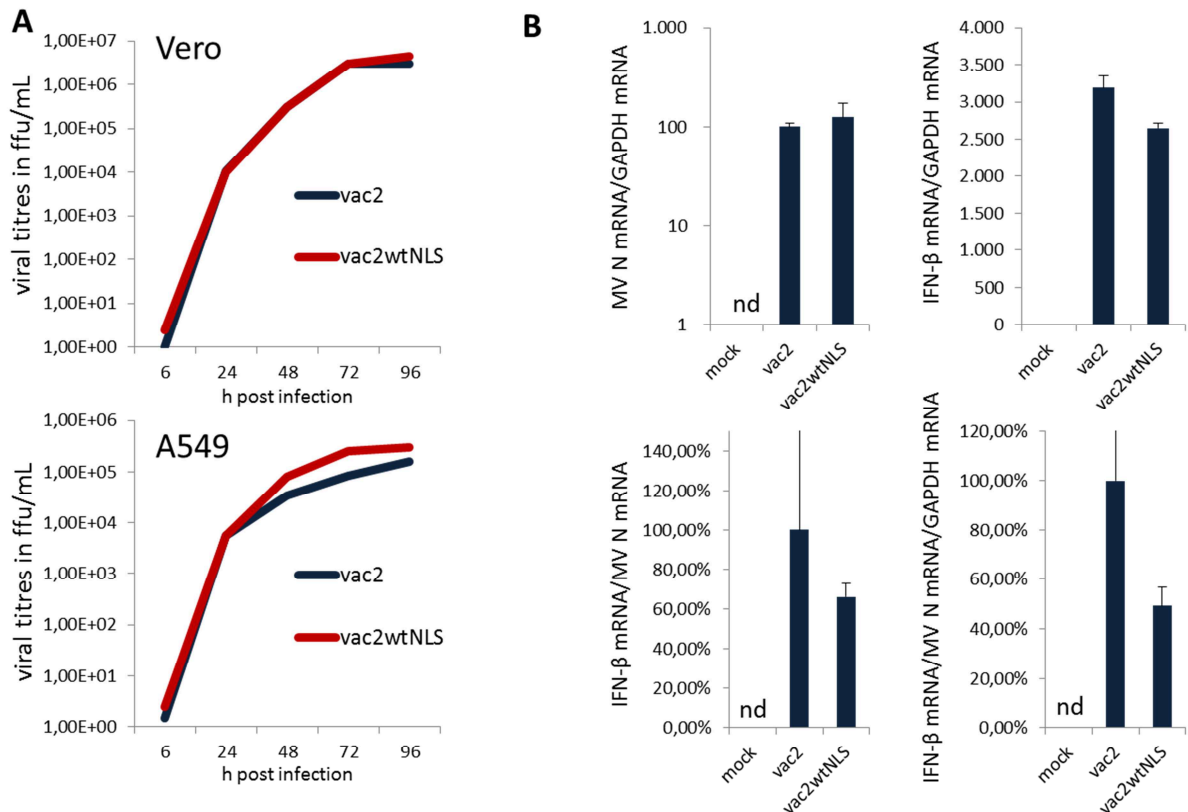


**Figure 29: Comparison of rMV vac2CwtNLS and rMV vac2.**

(A) Growth curves of rMV vac2CwtNLS in comparison to rMV vac2. Two different cell lines were used for growth comparisons: interferon negative Vero cells (top panel) and interferon competent A549 cells (bottom panel). Viral titres were measured after the indicated timepoints. (B) qRT-PCR of rMV vac2, rMV vac2CwtNLS and mock infected A549 cells 12h post infection with an MOI of 10 comparing rMV vac2 and rMV vac2C<sup>ko</sup>. Three RNAs were quantified: the cellular IFN-β and GAPDH mRNAs and the viral N mRNA. 4 different normalisations were done, using the ratios indicated on the y-axis of the charts. The mean values of two replicates are shown, with the mock value set to 1 if possible or the value for rMV vac2 set to 100 (%) and the remaining values calculated accordingly.

Quantitative realtime PCR experiments were performed to compare the IFN- $\beta$  mRNA induced upon infection of A549 cells with rMV vac2 or rMV vac2CwtNLS. The cells were infected with an MOI of 10 and harvested after 12h. The mRNA levels of interferon  $\beta$ , GAPDH as a normalisation control and measles virus N as the infection control were quantified. The amount of interferon  $\beta$  mRNA normalised to GAPDH mRNA induced by rMV vac2 was higher than in the case of rMV vac2CwtNLS (Fig. 29, B). The infection however was equal or even slightly higher in the case of rMV vac2CwtNLS as indicated by the MV N mRNA content normalised to GAPDH mRNA. A higher MV N mRNA content is thought to correspond to a higher PAMP generation by intracellular measles virus replication as well as a higher growth rate. Therefore a normalisation was done for interferon  $\beta$  mRNAs on GAPDH mRNAs and the MV N mRNA. In this analysis the difference between both strains is even more obvious; the induction caused by rMV vac2 was up to 50% higher.

Taken together, these experiments indicate behaviour of these two different viruses (rMV vac2 and rMV vac2CwtNLS) according to what was observed in the protein overexpression assays. rMV vac2CwtNLS seems to grow better in interferon competent cells, while the induction of interferon  $\beta$  mRNA was lower after 12h of infection.

# DISCUSSION

## 1. The impact of MV infection on host transcription

Analysis of the whole RNA content of cells after infection with rMV vac2 and a harvest after 24h and 48h revealed that several cellular genes are regulated in different ways. This regulation can be either a response of the cell to eliminate the invading pathogen, or an active regulation induced by the virus. Both possibilities however, cannot be fully separated in the data presented here.

As commonly observed in infections, the upregulation of ISGs, namely cytokines and IFITs is a response of the cell to the infection. Due to the infection with an MOI of 1, not all cells are infected after 24h or even 48h of infection. Therefore, the little interferon and cytokines released by the infected cells, could elicit a huge response in the non-infected cells. In the infected cells however, the whole extent of the response would be limited by the presence of V and P. The cytokine response as well as the interferon response was expected.

Interestingly, small nucleolar RNAs seemed to be measles virus infection specifically downregulated, up to 6 fold after 48h. Notably, C seems to accumulate in nucleoli during infection, prompting the suggesting, that it can possibly modulate or degrade snoRNAs there. The lot of these snRNAs found to be downregulated are involved in the 2' O' methylation guidance (Maden and Hughes, 1997). 2'-O methylation of the mRNA cap is an important marker to discriminate cellular RNAs from viral RNAs, which supposedly lack these modifications. This methylation could be an important mechanism discriminating self and non-self mRNAs, and mRNAs lacking this methylation were proposed to be MDA-5 inducers (Zust et al., 2011). For measles virus it was reported that the cap structure of the RNA is identical to the cellular mRNAs, though 2'-O methylation was not tested (Yoshikawa et al., 1986). A putative 2'-O methyltransferase domain however, was identified within the viral polymerase L (Ferron et al., 2002). In contrast to the prediction, a closely related virus, RSV was reported to produce mRNAs that lack 2'-O methylation (Barik, 1993). Regarding the microarrays, a downregulation of 2'-O methylating guidance enzymes could either result in a general lower abundance of correctly modified RNAs or a lower specificity of the methylation machinery in general. The former possibility would supposedly induce the innate immune system, especially MDA-5. In the case of a MV infection, the involvement of the snoRNA

guidance in 2'-O methylation seems highly unlikely. The replication and viral RNA production occurs in the cytoplasm of infected cells, whereas the 2'-O methylation machinery is located in the nucleoli. Therefore, the role of the downregulation of snoRNAs during MV infection remains speculative. Unfortunately only one other study regarding microarrays and measles infection is available up to date (Bolt et al., 2002). In this paper, human PBMCs were infected with wildtype and Edmonston MV, and the response of the cell differed in respect to the innate immunity response. The vaccine MV was able to upregulate the host genes stronger than the wildtype variant. Specifically, innate immunity related proteins, chaperones, transcription factors and other proteins of the endoplasmic reticulum stress response were found to be upregulated. This supports the data obtained in the results presented here, with the exception of the snoRNAs, which were supposedly not detected by the microarray they used.

## 2. MV C is a nuclear inhibitor of innate immunity – alone and during infection

The C protein of measles virus was initially characterised as a modulator of viral replication and transcription. In addition to these functions, C influences cellular signalling cascades as well. Recombinant viruses lacking C expression were reported to induce more interferon than their parenteral strains (Devaux and Cattaneo, 2004; Nakatsu et al., 2006; Nakatsu et al., 2008) *in vitro*. In addition to that, it was reported that C is able to prevent the phosphorylation and activation of the PKR induction cascade during infection (McAllister et al., 2010; Toth et al., 2009). Due to the work presented here, it can be concluded that C is able to inhibit the induction of interferon  $\beta$  independently of a viral infection. This inhibition is dependent on its nuclear accumulation. Consequently, as production of one of the major cytokine is diminished, a proper response of the innate immune system as a whole can be weakened by MV C. Previously it was reported that C is also able to inhibit the interferon signalling pathway (Shaffer et al., 2003). As a mechanism it was proposed that C binds phosphorylated STAT1 and thus sequester it in the cytoplasm (Yokota et al., 2011a). The interferon induction inhibition is still visible in STAT1 knockout cells, proving, that the blockage of interferon signalling is not responsible for the inhibitory effect on interferon induction observed here, via feedback pathways. Therefore it can be concluded that MV C, like the V protein (Caignard et al., 2009; Caignard et al., 2007; Lu et al., 2008; Pfaller and

Conzelmann, 2008; Schuhmann et al., 2011) is an inhibitor of both interferon signalling and interferon induction.

Nuclear localisation of MV C was found to be critical for optimal interferon  $\beta$  inhibitory function. The nuclear localisation signal therefore defines whether a MV C protein is a potent inhibitor of IFN- $\beta$  or not. Subcellular localisation of the C protein according to its NLS is observed after individual expression and in the viral context in infected cell culture.

### **2.1. Nuclear localisation of C as a hallmark of wildtype strains**

Previously it was reported that wildtype strains tend to induce less interferon than laboratory passaged strains or vaccine strains in cell culture (Kessler et al., 2011; Shingai et al., 2007). Consequently, the differences regarding the NLS sequence between vaccine and wildtype C proteins can be speculated to be a result of the attenuation and adaption process during vaccine generation by passaging on interferon negative cells (Bankamp et al., 2011; Schwarz, 1964). Unfortunately, the sequences of the wildtype predecessors of all vaccine strains are not available (Rota et al., 1994), so this hypothesis cannot be proven by comparing the sequences. By passaging the virus on interferon negative cells it could be possible that a mutation in the NLS can be artificially induced. However, introduction of mutation occurs randomly, and only afterwards the strains are selected according to their fitness. Therefore it is possible, that another mutation in the NLS sequence or elsewhere in the C ORF, compromising its function is sufficient to induce a vaccine-like phenotype. The very same conditions in which the adaptation happened for the established vaccine strains therefore cannot be reproduced. The significance, however, that in 4 supposedly independently generated vaccine strains (Edmonston/Schwarz (ENDERS et al., 1962; Schwarz, 1964), Cam-70 (Athman and Philpott, 2004), Leningrad-4 (Smorodintsev et al., 1960), Shanghai-191(Xiang and Chen, 1983)) this very mutation is found, is striking. If these strains do not share a common origin it would therefore be possible to conduct in vivo attenuation experiments resulting in the appearance of a compromised NLS. This would indicate that the NLS mutation is a more general feature of attenuation in IFN competent cells, which does not result in a growth, or otherwise influences the fitness of the virus in cell culture. Thus, with the current vaccine strains and wildtype strains in comparison it can be concluded that the NLS of C is able to serve as a marker discriminating the established vaccine strains from the wildtype strains in addition to CD46 usage as a receptor.

## **2.2. Comparison of overexpression experiments and infection**

### ***MV C intracellular localisation***

As pointed out before, the C proteins of vaccine viruses do not possess a proper nuclear localisation signal. In overexpression experiments it could be shown that its intracellular localisation is indeed more in the cytoplasm than in the nucleus. Consequently Cwt and the NLS mutations localise according to their NLS, with Cwt being present exclusively in the nucleus. During viral infection, the nuclear content of MV C correlated with the localisation pattern observed in overexpression experiments. In addition, fractions of MV C localised to cytoplasmic inclusion bodies during infection, regardless of its NLS. This phenotype however, could be explained by the presence of another viral protein MV P, which apparently recruits C to the viral replication factories (Nakatsu et al., 2009; Nakatsu et al., 2008). As shown here, expression of MV P was sufficient to recruit C to cytoplasmic granules. Weak interaction of P and C in co-immunoprecipitation could also be shown here, probably indirect via endogenous SHCBP1 (Ito et al., 2013). Additional expression of MV N resulted in a co-localisation of N, P and C in cytoplasmic inclusion bodies similar to those observed during C and P co-expression. The viral perinuclear replication factories, however, looked slightly different during infection, being broader and less dot-like. It can be speculated that the viral RNA and the assembly of RNPs during the progress of the infection additionally is able to influence the shape and provide a compartmentalisation for efficient viral replication. Additionally, in polarised cells, the RNPs were observed to be transported along the microtubule network, this mechanism was totally dispensable in non-polarised cells (Jones, 1999).

### ***Interferon induction***

The induction of interferon  $\beta$  caused by infection with recombinant MV viruses harbouring intact or compromised NLS sequences was found to be in agreement with the results obtained using overexpression systems. The difference between a virus expressing C with an intact NLS and the rMV vac2, however, was not as pronounced as in the experiments with transfected plasmids. This can be partially attributed to the contribution of other MV encoded proteins, which are additionally able to inhibit the interferon response. V was found to inhibit interferon induction as well, by blocking NF- $\kappa$ B signalling and MDA-5 binding (Caignard et al., 2009), and it could be speculated that V expressed from the virus can compensate the lack of a robust C inhibition in cell culture during infection. In addition to that it was suggested, that MV N can additionally block activation of IRF3. During plasmid

transfection experiments, defined stimuli were used such as SeV DIs or overexpression of stimulatory proteins such as TBK1. These stimuli always represent only a subset of pathways the cell uses to induce interferon  $\beta$  after pathogen infection. The difference between CwtNLS and Cs therefore could be more visible using the specific stimuli assayed in this thesis than induction caused by MV, which triggers a variety of cellular signalling pathways upon infection. Generally, the IFN- $\beta$  induction caused by MV infection is relatively weak, thus the innate immune response impact on the growth of MV in cell culture can also be regarded as low. This would explain the relatively small differences in growth between rMV vac2CwtNLS and rMV vac2. Whether the lower interferon  $\beta$  induction caused by MV strains with wildtype C NLS can modulate the viral growth *in vivo* more drastically can only be speculated to date.

### 2.3. Infections in vivo vs cell culture

In vivo studies using measles virus are unfortunately very difficult to do, as no established animal model exists apart from macaques (Auwaerter et al., 1999; de Swart, 2009). These animals, however, also react differently to a measles challenge than the human organism. Therefore, in vivo studies can either relate on insights gained by inadequate animal models or observations made with patients infected with wildtype measles.

In general, during all animal and human infections, the impact of a fully functional immune system *in vivo* on the growth and clearance of the virus is higher than in cell culture models *in vitro*. Both innate and adaptive immune system stimulate each other, and blockage of the Type I interferon response is thought to greatly modulate the adaptive response induced as well (Le Bon and Tough, 2002). Cell culture experiments are very limited in this respect, providing no adaptive immune system and no interplay between different cell types within an organism. In many cultured cell lines even the innate immune system and other important cellular pathways are compromised as a result of the immortalization and transformation of the cells.

The few studies done in macaques suggest that MV is influenced greatly by the immune system, and the reaction induced by mutants. It was seen for MV C<sup>ko</sup> viruses that they are rapidly cleared from the organism (Devaux et al., 2008), although in cell culture the virus is more attenuated than parenteral strains, growing only up to 2 logs lower titres. This leads to the speculation that the higher induction of innate immune system in combination with the

growth defect exhibited by MV C<sup>ko</sup> causes immediate activation of protective immune responses and subsequent clearance of the virus from the organism.

Regarding the NLS defect of vaccine strains, it can be speculated that these strains might still exhibit a high interferon induction within an animal. In contrast to C<sup>ko</sup> strains however, they lack the growth defect caused by the complete lack of C. Thus, the strains with a compromised NLS might lead to an immune reaction within the organism, which facilitates the easy clearance of this attenuated virus. The infection however, would last long enough to induce a robust innate and adaptive immune response resulting in the establishment of memory B-cells and lifelong immunity. Thus it can be speculated that NLS compromised MV virus can serve as a vaccine, being attenuated enough to be rapidly and complication-free cleared from a healthy organism, but on the other hand are replicative enough to induce life-long immunity.

#### **2.4. Comparison to related C proteins**

The C proteins of related viruses are also involved in the regulation of the innate immune system. Notably, Rinderpest virus C protein for example is also located in the nucleus and responsible for interferon inhibition there (Boxer et al., 2009).

A more distantly related paramyxovirus, Sendai virus, possess 4 different C proteins, a nested set with 4 different start codons in the P gene. They were found to be responsible for inhibition of innate immunity pathways as well (Strahle et al., 2007). In addition to that, these C proteins are also able to inhibit the induction of the antiviral state by recombinant interferon (Garcin et al., 1999).

Nipah and Hendra virus C protein was found to inhibit the interferon induction in reporter-gene assays as well, although the targets and mechanisms remain unknown to date (Basler, 2012; Shaw et al., 2005). Additionally, the W protein expressed by Hendra and Nipah virus is also able to inhibit interferon induction and its nuclear localisation of seemed to be of importance. In that respect W acts similar to the C protein of MV.

In summary, the observed interferon inhibition caused by the measles virus C protein fits well, comparing the functions of related proteins. Unfortunately, in most cases little to nothing is known about the mechanism those proteins employ. As shown in the alignments, RPV C is the closest C protein of all paramyxoviruses, suggesting a probable common mechanism. Interestingly, the sequence of the NLS of RPV C, CDV C and MV C, however, is conserved, hinting that the localisation but not the exact sequence is of importance and

conserved. Taken together, previously published results for MV C related proteins clearly support the role of MV C as an innate immune modulator.

## 2.5. The attenuation of C<sup>ko</sup> viruses

As shown many times before, recombinant C knockout MVs are heavily attenuated in cell culture, but viable. C is therefore not essential for viral propagation and growth, although it contributes significantly. Strikingly, the interferon induction caused by rMV vac2C<sup>ko</sup> infection is multiple times higher than that caused by rMV vac2 infection *in vitro* and *in vivo*. This would also explain the severe attenuation found *in vivo* for C<sup>ko</sup> strains (Devaux et al., 2008) which are quickly cleared from the host. There are two options regarding the reason for the high interferon  $\beta$  induction. Either C inhibits the natural stimulation caused by MV infection, or C ensures a proper transcription and replication, and therefore a C<sup>ko</sup> virus just generates more PAMPs. Most probably, both hypotheses could apply and the resulting interferon induction is a combination of higher induction and lower inhibition. Interestingly it is suggested, that C modulates the viral polymerase complex (Ito et al., 2013; Nakatsu et al., 2008). Aberrant RNA produced by a defective viral polymerase complex could lead to an increase in the stimulation of innate immunity pathways. Notably, influenza virus NS1 protein, which is known for its dsRNA binding ability, was reported to complement the growth defect of rMV C<sup>ko</sup> (Nakatsu et al., 2006). Previously it was reported, that C<sup>ko</sup> viruses lead to an activation of PKR, suggesting formation of dsRNA in the cytoplasm (McAllister et al., 2010; Toth et al., 2009). It was also shown for the human parainfluenza virus 1 C protein, that it is able to prevent dsRNA accumulation in the cytoplasm and therefore also prevent activation of PKR (Boonyaratanakornkit et al., 2011). For the Sendai virus C proteins it is known, that they prevent the formation of defective interfering particles as well as dsRNA formation during viral replication (Strahle et al., 2007; Takeuchi et al., 2008). Both, the defective particles and the dsRNA are good stimulants of pattern recognition receptors. A similar defective interfering particle accumulation was reported to be caused by a recombinant PIV5 lacking V protein expression. Notably, the V protein of PIV5 is located in the nucleus. As PIV5 generally lacks the expression of a C protein it can be speculated that the nuclear PIV5 V therefore takes over the functions of a nuclear C protein.

For studies involving recombinant C<sup>ko</sup> the effects of C on the replication and transcription of MV have to be taken into account. However, with state of the art technology employed (Deep Sequencing, Par-CLIPs.) aberrant RNA PAMPs generated by C<sup>ko</sup> MV can be more easily identified and characterised as *in vivo* ligands of RLRs.

## **2.6. Mechanistic proposals**

In this thesis, C was shown to interfere with transcriptional induction of interferon  $\beta$ . In addition to that, the activation of a crucial transcription factor – IRF3 – was found to be unaltered. Several molecular mechanisms explaining the observations can be considered. The most likely case is the interaction of MV C with RNA, DNA or cellular proteins. These interactions then can cause an inhibition of pathways leading to the induction of interferon. However, it has to be considered as well, that the miRNA content of the cell can be altered as a consequence of an interaction as well. Additionally epigenetic regulation might be induced by nuclear C or its interaction partners and cause a decrease in transcription from the interferon  $\beta$  gene. It could also be possible that MV C performs an enzymatic function such as a dephosphorylation, but no putative catalytic domains could be predicted.

### ***RNA interaction***

RNA binding to MV C was speculated to be a possible mechanism of interference (Nakatsu et al., 2006; Nakatsu et al., 2008). These studies suggested that C might be able to bind dsRNA generated by the viral polymerase complex. The sequestration of stimulating RNAs, which could serve as PAMPs, as the proposed mechanism can be excluded in the work presented here, since inhibition of interferon induction by overexpression of more downstream stimulatory proteins was still observed. A sequestration or degradation of interferon  $\beta$  mRNA specifically seems highly unlikely as an RNA binding motif within C was neither predicted nor experimentally identified until now. Therefore it can only be speculated, that C might employ a yet unknown motif, to specifically target the interferon  $\beta$  mRNA, this has to be studied in further detail however.

### ***DNA interaction and modification***

Due to its nuclear localisation it is also possible, that MV C interacts with the cellular DNA. No DNA binding motifs were experimentally found so far or could be predicted. Nevertheless, a disturbance of a proper interferon expression enhanceosome at the promoter level would be an efficient mechanism to inhibit transcription of interferon  $\beta$ . Additionally, epigenetic modifications of the genomic DNA would possibly be induced by C to inhibit interferon induction. DNA binding and modification has to be addressed in further detail in the future.

### ***Protein interaction***

The most likely mechanism is the interaction of C with nuclear cellular protein, thereby modulating its functions. Potential targets include the master regulators of transcription CBP and p300, which were tested in IP experiments. No interaction between C and CBP or p300 could be shown yet.

Previously, a few interaction partners of MV C were also published: IRGM, SHCBP1 and phosphorylated STAT1. Immunity-associated GTPase family M (IRGM) was reported to be a common target of a variety of proteins encoded by negative strand RNA viruses, among them also MV. The binding of MV C to IRGM was shown to increase the rate of autophagy in transfected cells (Gregoire et al., 2011). The reported co-localisation of MV C and IRGM in the cytoplasm could be confirmed in the work presented here. Moreover the association of IRGM and MV C in co-immunoprecipitation experiments could also be reproduced. Yet another protein found to interact with MV C is SHCBP1 (Ito et al., 2013). Interestingly, the interaction of C and SHCBP1 is the strongest in the presence of another viral protein MV P and they both co-localise with SHCBP1 as shown in the literature (Ito et al., 2013). The interaction with SHCBP1 was suggested to modulate the activity of the viral polymerase complex, though the mechanism remains unknown. Notably P is responsible for the re-localisation of C to cytosolic inclusion bodies as shown here. Additionally, the cellular functions of the protein SHCBP1 are not known, except that it contains a putative SHC binding domain and was therefore named SHC binding protein 1. However, all these so far described protein-MV C interactions cannot explain the inhibition of interferon induction. The only reported interaction partner that could be involved in the interferon induction pathways by feedback loops was phosphorylated STAT1 (Yokota et al., 2011a). The inhibition of interferon  $\beta$  mRNA transcription caused by MV C was found to occur still in STAT1 knockout cells, excluding the involvement of STAT1. In addition to that, the interaction of pSTAT1 and MV C could not be reproduced in this study here. Notably, none of the three published interaction partners (IRGM, SHCBP1 and STAT1) could be confirmed using mass spectrometry detection of the protein content of the MV Cwt pulldowns, this can be explained however due to their overall low abundance in 293T cells as well as the need for a stimulus for the induction of pSTAT1. In addition to that it can be speculated, that the detection of all peptides using mass spectrometry is not similar and consequently some proteins will not be identified during the peptide detection.

During this study a few more promising interaction partners could be identified by different methods. The results are summarized in Table 1D.

**Table 1D: Summary of the interaction partners of MV C and their interaction in three different assays** (yes or no). Co-immunoprecipitation (Co-IP), Co-localisation Immunofluorescence (Co-Loc IF) and Massspectrometry analysis of co-purified proteins (MS analysis)

protein	Co-IP	Co-Loc IF	MS analysis
Map1B	no	no	yes
PSMC3	yes	yes	yes
IPS-1	yes	no	no
DDB1	yes	no	yes
IPO8	no	n.d.	yes
IRGM	yes	yes	no

The most likely interaction partners for inhibitors of interferon induction can be found in the signalling pathway itself. Such proteins (RIG-I, IPS-1, TBK1, IRF3) were therefore tested by directed immunoprecipitation experiments using overexpression. In initial experiments only the adaptor protein IPS-1 (interferon promoter stimulated-1) showed a strong binding ability to Cwt. Neither the inducing helicase (retinoic-acid inducible gene 1, RIG-I), a crucial kinase (Tank-binding kinase 1, TBK1) nor the respective transcription factor (interferon regulatory factor 3, IRF3) could bind to MV C in this assay.

Furthermore, to establish a general picture of the mechanism of the Cwt protein, a different method was used to analyse the lysates of the pulldowns performed. This more unbiased approach used the endogenous proteins of a cell line as binding partners, which were subsequently identified by mass spectrometry. In this approach, it could be shown that a few strong cellular MV C association partners are indeed present in those cells.

Among the previously identified interaction partners, IPS-1 could not be detected using this method, although it was found to strongly interact in immunoprecipitation experiments. The method used to perform these assays was the same as for the pulldowns with immunodetection, in the latter case IPS-1 was overexpressed. This artificially increased

expression is expected to lead to activation of the cells and an increased abundance of IPS-1 or its modifications which could explain binding to Cwt, while endogenous IPS-1 is too weakly expressed to be detected as a major binding partner in non activated cells using mass spectrometry. In the confocal images however, no apparent interaction between Cwt and IPS-1 was visible as co-localisation, although both proteins were overexpressed. A difference in intracellular localisation -C in the nucleus, while IPS-1 is in the cytoplasm, anchored to mitochondria - can be neglected during the pulldown, which is performed using whole cell lysates. Moreover, the binding of IPS-1 to Cwt could be still only transient or too weak than needed to induce a drastic change of localisation and recruit C to the cytoplasm. As C is a shuttling protein, a residual cytoplasmic fraction is always present, which might not be visible as a clear co-localisation during static confocal microscopy. Experiments at different timepoints for observation of localisation could solve the problem, as IPS-1 is known to undergo drastic rearrangements regarding its intracellular localisation upon stimulation or overexpression (Onoguchi et al., 2010a). In addition to that fluorescence complementation assays or FRET assays could show that a transient interaction exists in the cytoplasm. Moreover, the already published interaction partner of C, immunity-associated GTPase family M (IRGM), binds to IPS-1 (Gregoire et al., 2011). Whether this interaction is direct, was unfortunately not assayed in this publication, therefore interaction with IRGM can be indirect via IPS-1 or vice versa. IRGM was also not detected during the mass spectrometry experiments. Additionally it is localised to the cytoplasm usually as well. Interestingly, in contrast to IPS-1, overexpressed IRGM was able to recruit Cwt to the cytoplasm, and both proteins co-localised there, whereas the same effect was not observed for IPS-1 and C overexpression. Therefore it is possible that the co-purification of IPS-1 with C is mediated by endogenous IRGM. The major interferon inhibition however, occurs in the nucleus, so this interaction might play a role during a different cytoplasmic pathway. As implicated for IRGM already, autophagy could be the target cellular system in that case.

However, numerous protein-protein interactions not apparently related to the IFN induction system could be detected in the mass spectrometry approach. Amongst them, most importantly, were components of the proteasome (PSMD2, PSMC3 and others) as well as an ATPase (ATP1A1) and a microtubule rearrangement protein MAP1B, linking C to autophagy. Interestingly, MAP1B was found to be required for in the interferon inhibitory functions of RSV non-structural proteins, being essential for STAT2 and TBK1 degradation (Swedan et al., 2011). Additionally, MAP1B is responsible for microtubule rearrangements, which can be

essential for trafficking of viral particles and proteins. Furthermore MAP1B is involved in autophagy being in a complex with ATG proteins and DDB1. The protein itself is processed in the cell into a heavy and a light chain. The heavy chain is able to bind light chains of other MAP1 proteins, like MAPLC3, a protein known to be a marker of autophagosomes (Behrends et al., 2010). The interaction between C and MAP1B could so far not be confirmed in co-immunoprecipitation and immunofluorescence experiments. This, however, might be due to a specific complex formed by MAP1B in the cells, which is recognized by C. This complex however, might not be formed with endogenous proteins or obscured by highly overexpressed MAP1B.

Among the weaker interaction partners was DDB1, which was previously described to bind to PIV5 V (Precious et al., 2007). The PIV5 V/DDB1 complex was found to be responsible for STAT1 degradation. Co-immunoprecipitation of DDB1 with MV C suggested a weak association. However, the association was not strong enough to direct the C protein to the cytoplasm in confocal experiments. Overexpression of DDB1 and Cwt was not enough to induce a probable complex formation, which is then clearly visible in confocal microscopy experiments. Also as mentioned before, the shuttling ability of Cwt can of course obscure possible co-localisation, if only one timepoint is analysed. Moreover, only a transient binding could be sufficient to execute the pathways leading to interferon inhibition.

Judging from protein-protein interaction network analysis however, it is also possible that by recruiting the proteasome components and MAP1B/ATP1A1 C is able to induce degradation of certain proteins. This theory is supported by the fact that published viral interactions with MAP1B and/or DDB1 lead to degradation of certain signalling molecules (Precious et al., 2005; Precious et al., 2007; Swedan et al., 2011). TBK1 degradation as reported for MAP1B and RSV NS (Swedan et al., 2011) proteins could not be seen for MV C in the Western blots of luciferase assays done in this thesis. In addition, it was not observed that C overexpression reduced STAT1 amounts or levels of other proteins of the interferon induction pathway.

To analyse the mass spectrometry data in more detail, the overlap between the interactomes of the C binding partners using two databases Biogrid and InnateDB was calculated. Surprisingly, only a small number of proteins connect the putative binding partners directly. These proteins are usually found in complexes with each other in the cell. They were identified to be mainly histone de-acetylases, acting in the nucleus of the cells to alter transcription levels and histone modifications (Greco et al., 2011). The reason, that these

proteins are missing in the co-purification of C might be, that they are excluded from a complex or degraded via the proteasome. Notably, the fl-CwtmNLS pulldown and subsequent mass spectrometry analysis showed a decreased binding efficiency to both proteasomal components and MAP1B. A possible mechanism of nuclear C protein would therefore be the induced nuclear degradation of HDACs via the nuclear proteasome and adaptor molecules, interconnected by C. Interestingly, HDAC6 was found to be critical for IFN- $\beta$  induction (Chattopadhyay et al., 2013). However, one major issue is the lack of any E3 ligase in the mass spectrometry data associated to HDACs. Classically these ubiquitin ligases are needed to recognize the target and transfer the polyubiquitin chains on the targets to mark them for proteasomal degradation. In the mass spectrometry experiments conducted here, only RNF219 could be co-purified, which was described as an Ubiquitin ligase for MyD88 (Wang et al., 2005), no other annotations exist. In addition to that, the proteasome is responsible for the degradation of I $\kappa$ B, the inhibitor of the NF- $\kappa$ B transcription factor (Alkalay et al., 1995). Any interference with the proteasomal system leading to its attenuation can also be regarded as an inhibitor of NF- $\kappa$ B induction and therefore proper interferon  $\beta$  response. Especially the early response, quickly after RLR activation seems to be crucial for resistance towards RNA virus replication (Wang et al., 2010). In general, the identification of the target of a degradation process is usually a complex issue, due to the fact that it is not present in a protein pulldown.

Notably, one major point to consider is that only parts of the 19S subunit of the proteasome were co-purified with MV C (Fig. 30 B). Classically, the 19S subunit is involved in the regulation of the protein degradation caused by the 20S proteasome core complex (Peters et al., 1994). Together they form the 26S particle (Fig. 30 A). Ubiquitylated proteins are recognized by the ATPase-rich 19S subunit and eventually recruited into the cavity of the 20S subunit (Smith et al., 2005), which then performs the degradation. However, both the 19S and the 20S degradation unit can act independently of each other. It was implied, that in the nucleus of cells, the 19S subunit is more abundant than in the cytoplasm (von, 2006), possibly explaining the interaction differences to Cwt and CwtmNLS. Within the nucleus it is responsible in association with the core subunits for the degradation of important transcription factors or alternatively for transcriptional regulation, independently of degradation processes (Ferdous et al., 2001). Increased degradation of the transcription factor IRF3 by MV C co-expression, however, was not observed in experiments in this thesis (data not shown). Nevertheless, transcriptional regulation by the 19S proteasomal subunit could be

a putative mechanism alternative for the inhibition of interferon  $\beta$  induction. It was reported that the expression of MHC-II mRNA is regulated by the 19S subunit via the co-activator CIITA (Koues et al., 2008). Additionally the 19S subunit influences the activity of the histone acetylation modulator SAGA (Lee et al., 2005), globally influencing Histone 3 acetylation levels.



**Figure 30: Model of the proteasome and the Cwt interacting subunits.**

(A) Schematic model of the 26S complete proteasome, the 19S particle indicated in blue, in grey the 20S core subunit. (B) Protein composition of the 19S regulatory subunit, proteins found in the mass spectrometry experiments are coloured in orange.

### 3. Model of C in the context of infection

As stated above, the localisation of the C protein during infection resembles the localisations found for the different NLS variants in the overexpression system. In addition to that a fraction of all C variants, regardless of their NLS sequence, co-localised with the viral replication centres during infection. 24h post infection, Cwt and CswtNLS are clearly seen in the nucleus supporting the interferon inhibitory role in the nucleus. Although little Cs is in the nucleus as well, the interferon  $\beta$  stimulation during vac2 infection remains fairly low, as seen in the microarray experiments, rising up to 6-fold only 48h post infection. This indicates that another viral protein might compensate for the defect (V or P) or only a little amount of PAMPs are generated during MV infection and the induction of interferon is generally very low. As mentioned above, however slight differences in interferon induction between MV possessing a functional C NLS and MV harbouring a compromised C NLS could be observed.

Recently, it was reported that during paramyxovirus infection the content of defective interfering particles is critical for the induction of interferon and other cytokines (Killip et al., 2011). Defective interfering particles can also be found in MV preparations (Calain and Roux, 1988) and might even contribute to a strong innate immune activation phenotype by vaccine strains. It can therefore be speculated, that the induction of the immune system by a 'perfect' measles replication and propagation is very weak. This might be due to shielding of PAMPs and the tendency of MV to avoid production of PAMPs like dsRNA intermediates. In addition to self-induced interferon, a virus has to cope with IFN induced by co-infecting pathogens and therefore encodes interferon induction antagonists. Strikingly, the main cause of MV induced mortality in developing countries are co-infections with other pathogens.

Taken all results together, the following model of C action during infection can be proposed. This model only regards the immunosuppression caused by measles C, not any implications in replicational or transcriptional processes (Fig. 31).

MV and DIs, as well as other invading pathogens (bacteria, viruses exemplary depicted in Fig. 31) are able to activate the immune system. Whereas signalling by interferon can be efficiently blocked by V and P (and C to some extent) (Caignard et al., 2009; Caignard et al., 2007; Devaux et al., 2007; Ramachandran et al., 2008; Shaffer et al., 2003), the interferon induction can only be blocked partially by V by blocking MDA-5 signalling (Andrejeva et al., 2004; Childs et al., 2007; Motz et al., 2013) and inhibiting IRF3 activation (Lu et al., 2008), Toll-like receptor signalling (Pfaller and Conzelmann, 2008) and sequestration of NF- $\kappa$ B p65 (Schuhmann et al., 2011). MV C protein residing in the nucleus could additionally inhibit the cellular response particularly to these stimuli. As revealed in the localisation studies with recombinant MV encoding different C variants, only Cwt and CswtNLS are able to substantially accumulate in the nucleus during infection. Consequently, a lower capacity of counteracting innate immunity activation of the infected cells with vaccine or C NLS compromised recombinant MV would be expected.

Stimulation in low extend caused by MV replication itself, can also be restricted earlier by a nuclear mechanism than a more cytoplasmic mechanism. Signalling starting from RLRs by incoming virus activation takes an estimated 12h to activate IRF3 and the first transcription of interferon  $\beta$  mRNA. A mechanism in the nucleus would lead to a time-advantage for the virus, as its accessory proteins like V and C have to be synthesized first to inhibit the earlier steps of induction of interferon  $\beta$ . Therefore, the later and the more

downstream the inhibitory step is, the better the virus can defend itself against the first wave of interferon induction. This is supported by data obtained after MV infection of 12h.

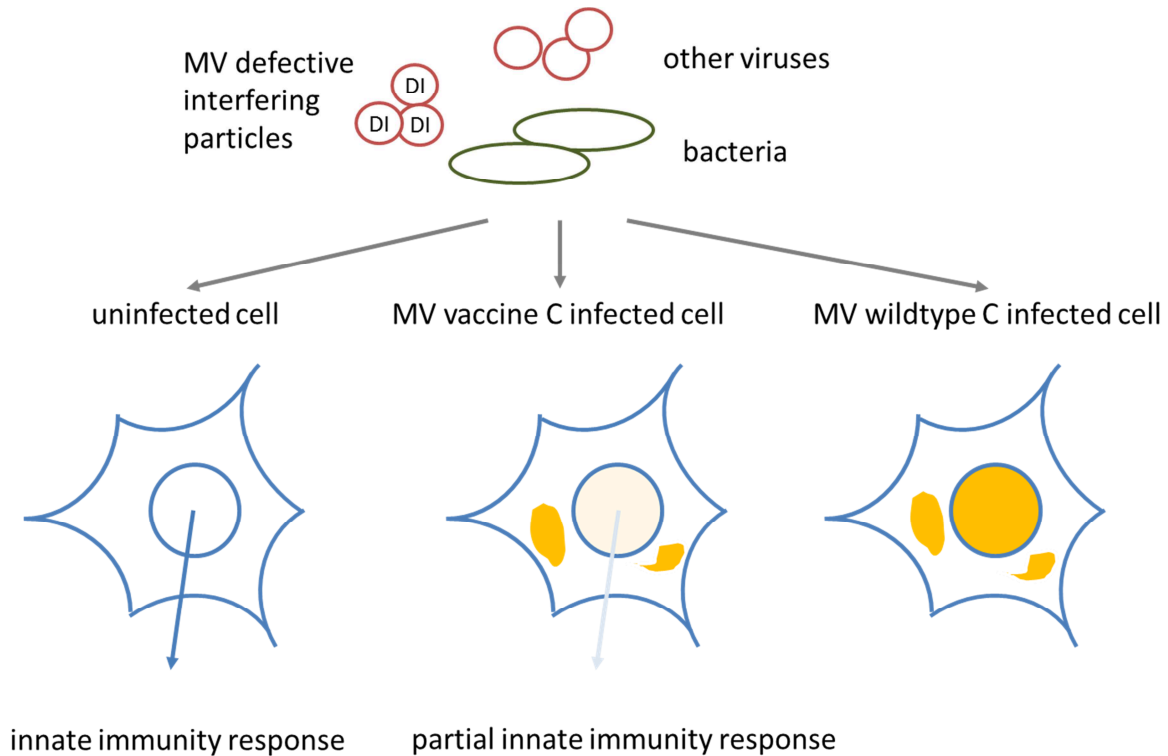


**Figure 31: Model of C during infection with exogenous innate immunity stimuli.**

Viruses are depicted in red, bacteria in green and the human cells in blue. Intracellular expression of the C protein during infection is visualized by a yellow colour. The innate immune response including the production of interferon  $\beta$  is indicated by a blue arrow. Incoming DIs or other pathogens (exemplary bacteria and viruses) are able to activate the innate immune system. MV C expression in the nucleus is able to counteract this induction, causing a lower cellular response.

In summary, the nuclear localisation of MV C is likely to contribute to the strong immunoinhibitory phenotype observed during wildtype MV infections. This striking phenotype seems to be absent during vaccinations the established vaccine strains, lacking the C NLS.

## 4. Outlook and future perspectives

During this study, MV C could be identified as a major inhibitor of interferon  $\beta$  induction encoded by MV. This inhibition is dependent on the nuclear accumulation of C, both during overexpression experiments and during infection with recombinant MV. The localisation of different C variants was determined during infection and resembled the overexpression experiments. Additionally, several protein-protein interaction partners of C could be identified. The molecular mechanism of C to inhibit interferon induction could however not be fully revealed during this thesis. However, a lot of possibilities could be excluded and some are more likely now.

The most probable mechanism involves regulation of the 19S subunit either by alteration of proteasomal degradation pathways or direct transcriptional regulation. Further experiments are needed however, to clarify whether this hypothesis holds true. Assays controlling the already known regulated genes could be done, as well as localisation studies regarding the interaction partners found in their endogenous context, meaning fully assembled 19S particles. To test for an influence on the degradation system by C, functional assays of the proteasome have to be conducted and the degradation of C itself by the proteasome checked.

For future studies it will be definitely be interesting to elucidate the role of C at mitochondria in more detail. Both IRGM and IPS-1 are mitochondrial proteins and C binds strongly to both. The former even causes a re-localisation of C upon co-expression. They implicate a role of C in the autophagy system, which was already reported before, however this system needs to be studied in more detail. Additionally, C interaction with IPS-1 could have multiple other effects on different cellular pathways as well. These pathways could be studied using screening approaches employing microarrays or siRNA knockdown screens.

It has been speculated that binding of C to RNA or DNA can occur (Nakatsu et al., 2008). There was however, no prove provided since and the question still remains to be answered. MV C does not contain any classical RNA or DNA binding motifs, but this does not rule out an actual binding. Interaction of MV C with RNA and DNA definitively has to be studied especially focusing on the possible interaction with the interferon  $\beta$  promoter in further detail using chromatin immunoprecipitation experiments.

If C is responsible for a downregulation of snoRNAs, it can be speculated that this mechanism might influence interferon induction of the virus as well. However this would not explain the interferon inhibitory effect observed in the overexpression system. Nonetheless downregulation of snoRNAs might be an important regulatory mechanism by either the cell or MV to modulate viral growth. This has to be studied further, to reveal any implications.

Additionally it will be of interest to study viruses in more detail which lack both of its interferon induction inhibitory proteins. It is possible that V can at least partially compensate the interferon inhibition in cell culture. As  $V^{ko}$  viruses grow perfectly well in cell culture and do not show an obvious interferon inhibition defect, it would be possible to combine V and C knockout in the P gene, and complement this virus with the different C mutants. It is likely that the effect of the C mutants would become even more pronounced.

## REFERENCES

- Ader, N., M. Brindley, M. Avila, C. Orvell, B. Horvat, G. Hiltensperger, J. Schneider-Schaulies, M. Vandeveld, A. Zurbriggen, R.K. Plemper, and P. Plattet. 2013. Mechanism for active membrane fusion triggering by morbillivirus attachment protein. *Journal of virology*. 87:314-326.
- Alkalay, I., A. Yaron, A. Hatzubai, A. Orian, A. Ciechanover, and Y. Ben-Neriah. 1995. Stimulation-dependent I kappa B alpha phosphorylation marks the NF-kappa B inhibitor for degradation via the ubiquitin-proteasome pathway. *Proceedings of the National Academy of Sciences of the United States of America*. 92:10599-10603.
- Altschul, S.F., W. Gish, W. Miller, E.W. Myers, and D.J. Lipman. 1990. Basic local alignment search tool. *Journal of molecular biology*. 215:403-410.
- Andrejeva, J., K.S. Childs, D.F. Young, T.S. Carlos, N. Stock, S. Goodbourn, and R.E. Randall. 2004. The V proteins of paramyxoviruses bind the IFN-inducible RNA helicase, mda-5, and inhibit its activation of the IFN-beta promoter. *Proc.Natl.Acad.Sci.U.S.A.* 101:17264-17269.
- Arneborn, P., and G. Biberfeld. 1983. T-lymphocyte subpopulations in relation to immunosuppression in measles and varicella. *Infect Immun*. 39:29-37.
- Ashkenazy, H., E. Erez, E. Martz, T. Pupko, and N. Ben-Tal. 2010. ConSurf 2010: calculating evolutionary conservation in sequence and structure of proteins and nucleic acids. *Nucleic acids research*. 38:W529-533.
- Athman, R., and D. Philpott. 2004. Innate immunity via Toll-like receptors and Nod proteins. *Current opinion in microbiology*. 7:25-32.
- Auwaerter, P.G., P.A. Rota, W.R. Elkins, R.J. Adams, T. DeLozier, Y. Shi, W.J. Bellini, B.R. Murphy, and D.E. Griffin. 1999. Measles virus infection in rhesus macaques: altered immune responses and comparison of the virulence of six different virus strains. *J.Infect.Dis*. 180:950-958.
- Bankamp, B., M. Takeda, Y. Zhang, W. Xu, and P.A. Rota. 2011. Genetic characterization of measles vaccine strains. *J.Infect.Dis*. 204 Suppl 1:S533-S548.
- Bankamp, B., J. Wilson, W.J. Bellini, and P.A. Rota. 2005. Identification of naturally occurring amino acid variations that affect the ability of the measles virus C protein to regulate genome replication and transcription. *Virology*. 336:120-129.
- Barik, S. 1993. The structure of the 5' terminal cap of the respiratory syncytial virus mRNA. *The Journal of general virology*. 74 ( Pt 3):485-490.
- Barrett, T., and B. Underwood. 1985. Comparison of messenger RNAs induced in cells infected with each member of the morbillivirus group. *Virology*. 145:195-199.
- Barth, S., D. Glick, and K.F. Macleod. 2010. Autophagy: assays and artifacts. *J.Pathol*. 221:117-124.
- Barton, J.A.C.a.G.J. 1999. Application of enhanced multiple sequence alignment profiles to improve protein secondary structure prediction. *Proteins*. 40:502-511.
- Basler, C.F. 2012. Nipah and hendra virus interactions with the innate immune system. *Current topics in microbiology and immunology*. 359:123-152.
- Behrends, C., M.E. Sowa, S.P. Gygi, and J.W. Harper. 2010. Network organization of the human autophagy system. *Nature*. 466:68-76.
- Bellini, W.J., G. Englund, S. Rozenblatt, H. Arnheiter, and C.D. Richardson. 1985. Measles virus P gene codes for two proteins. *J.Virol*. 53:908-919.
- BLACK, F.L., J.L. MELNICK, and M. REISSIG. 1956. Formation of multinucleated giant cells in measles virus infected cultures deprived of glutamine. *Virology*. 2:836-838.

- Bolt, G., K. Berg, and M. Blixenkrone-Moller. 2002. Measles virus-induced modulation of host-cell gene expression. *The Journal of general virology*. 83:1157-1165.
- Boonyaratanakornkit, J., E. Bartlett, H. Schomacker, S. Surman, S. Akira, Y.S. Bae, P. Collins, B. Murphy, and A. Schmidt. 2011. The C proteins of human parainfluenza virus type 1 limit double-stranded RNA accumulation that would otherwise trigger activation of MDA5 and protein kinase R. *J.Virol.* 85:1495-1506.
- Boxer, E.L., S.K. Nanda, and M.D. Baron. 2009. The rinderpest virus non-structural C protein blocks the induction of type 1 interferon. *Virology*. 385:134-142.
- Brindley, M.A., M. Takeda, P. Plattet, and R.K. Plemper. 2012. Triggering the measles virus membrane fusion machinery. *Proceedings of the National Academy of Sciences of the United States of America*. 109:E3018-3027.
- Brzozka, K., S. Finke, and K.K. Conzelmann. 2005. Identification of the rabies virus alpha/beta interferon antagonist: phosphoprotein P interferes with phosphorylation of interferon regulatory factor 3. *J.Virol.* 79:7673-7681.
- Brzozka, K., S. Finke, and K.K. Conzelmann. 2006. Inhibition of interferon signaling by rabies virus phosphoprotein P: activation-dependent binding of STAT1 and STAT2. *J.Virol.* 80:2675-2683.
- Caignard, G., M. Bourai, Y. Jacob, F. Tangy, and P.O. Vidalain. 2009. Inhibition of IFN-alpha/beta signaling by two discrete peptides within measles virus V protein that specifically bind STAT1 and STAT2. *Virology*. 383:112-120.
- Caignard, G., M. Guerbois, J.L. Labernardiere, Y. Jacob, L.M. Jones, F. Wild, F. Tangy, and P.O. Vidalain. 2007. Measles virus V protein blocks Jak1-mediated phosphorylation of STAT1 to escape IFN-alpha/beta signaling. *Virology*. 368:351-362.
- Calain, P., and L. Roux. 1988. Generation of measles virus defective interfering particles and their presence in a preparation of attenuated live-virus vaccine. *Journal of virology*. 62:2859-2866.
- Calain, P., and L. Roux. 1993. The rule of six, a basic feature for efficient replication of Sendai virus defective interfering RNA. *J Virol.* 67:4822-4830.
- Cattaneo, R., K. Kaelin, K. Baczko, and M.A. Billeter. 1989. Measles virus editing provides an additional cysteine-rich protein. *Cell*. 56:759-764.
- Cattaneo, R., G. Rebmann, A. Schmid, K. Baczko, V. ter Meulen, and M.A. Billeter. 1987. Altered transcription of a defective measles virus genome derived from a diseased human brain. *EMBO J.* 6:681-688.
- Chaplin, D.D. 2006. 1. Overview of the human immune response. *The Journal of allergy and clinical immunology*. 117:S430-435.
- Charles A Janeway, J., Paul Travers, Mark Walport, and Mark J Shlomchik. 2001. Immunobiology.
- Chattopadhyay, S., V. Fensterl, Y. Zhang, M. Velepparambil, J.L. Wetzel, and G.C. Sen. 2013. Inhibition of viral pathogenesis and promotion of the septic shock response to bacterial infection by IRF-3 are regulated by the acetylation and phosphorylation of its coactivators. *mBio*. 4.
- Chattopadhyay, S., J.T. Marques, M. Yamashita, K.L. Peters, K. Smith, A. Desai, B.R. Williams, and G.C. Sen. 2010. Viral apoptosis is induced by IRF-3-mediated activation of Bax. *EMBO J.* 29:1762-1773.
- Childs, K., N. Stock, C. Ross, J. Andrejeva, L. Hilton, M. Skinner, R. Randall, and S. Goodbourn. 2007. mda-5, but not RIG-I, is a common target for paramyxovirus V proteins. *Virology*. 359:190-200.
- Clamp, M., J. Cuff, S.M. Searle, and G.J. Barton. 2004. The Jalview Java alignment editor. *Bioinformatics*. 20:426-427.

- Conzelmann, K.K. 2004. Reverse genetics of mononegavirales. *Curr.Top.Microbiol.Immunol.* 283:1-41.
- Conzelmann, K.K. 2005. Transcriptional activation of alpha/beta interferon genes: interference by nonsegmented negative-strand RNA viruses. *J Virol.* 79:5241-5248.
- Conzelmann, K.K., J.H. Cox, L.G. Schneider, and H.J. Thiel. 1990. Molecular cloning and complete nucleotide sequence of the attenuated rabies virus SAD B19. *Virology.* 175:485-499.
- Cregan, S.P., V.L. Dawson, and R.S. Slack. 2004. Role of AIF in caspase-dependent and caspase-independent cell death. *Oncogene.* 23:2785-2796.
- Cruz, C.D., H. Palosaari, J.P. Parisien, P. Devaux, R. Cattaneo, T. Ouchi, and C.M. Horvath. 2006. Measles virus V protein inhibits p53 family member p73. *J.Virol.* 80:5644-5650.
- Cui, S., K. Eisenacher, A. Kirchhofer, K. Brzozka, A. Lammens, K. Lammens, T. Fujita, K.K. Conzelmann, A. Krug, and K.P. Hopfner. 2008. The C-terminal regulatory domain is the RNA 5'-triphosphate sensor of RIG-I. *Mol.Cell.* 29:169-179.
- de Swart, R.L. 2009. Measles studies in the macaque model. *Curr.Top.Microbiol.Immunol.* 330:55-72.
- de Swart, R.L., M. Ludlow, W.L. de, Y. Yanagi, A.G. van, S. McQuaid, S. Yuksel, T.B. Geijtenbeek, W.P. Duprex, and A.D. Osterhaus. 2007. Predominant infection of CD150+ lymphocytes and dendritic cells during measles virus infection of macaques. *PLoS.Pathog.* 3:e178.
- de Vries, R.D., K. Lemon, M. Ludlow, S. McQuaid, S. Yuksel, G. van Amerongen, L.J. Rennick, B.K. Rima, A.D. Osterhaus, R.L. de Swart, and W.P. Duprex. 2010. In vivo tropism of attenuated and pathogenic measles virus expressing green fluorescent protein in macaques. *Journal of virology.* 84:4714-4724.
- de Weerd, N.A., S.A. Samarajiwa, and P.J. Hertzog. 2007. Type I interferon receptors: biochemistry and biological functions. *The Journal of biological chemistry.* 282:20053-20057.
- del Valle, J.R., P. Devaux, G. Hodge, N.J. Wegner, M.B. McChesney, and R. Cattaneo. 2007. A vectored measles virus induces hepatitis B surface antigen antibodies while protecting macaques against measles virus challenge. *Journal of virology.* 81:10597-10605.
- Devaux, P., and R. Cattaneo. 2004. Measles virus phosphoprotein gene products: conformational flexibility of the P/V protein amino-terminal domain and C protein infectivity factor function. *J.Virol.* 78:11632-11640.
- Devaux, P., G. Hodge, M.B. McChesney, and R. Cattaneo. 2008. Attenuation of V- or C-defective measles viruses: infection control by the inflammatory and interferon responses of rhesus monkeys. *J.Virol.* 82:5359-5367.
- Devaux, P., M. von, V. W. Songsunthong, C. Springfield, and R. Cattaneo. 2007. Tyrosine 110 in the measles virus phosphoprotein is required to block STAT1 phosphorylation. *Virology.* 360:72-83.
- Dorig, R.E., A. Marcil, A. Chopra, and C.D. Richardson. 1993. The human CD46 molecule is a receptor for measles virus (Edmonston strain). *Cell.* 75:295-305.
- Dörig, R.E., A. Marcil, A. Chopra, and C.D. Richardson. 1993. The human CD46 molecule is a receptor for measles virus (Edmonston strain). *Cell.* 75:295-305.
- Dosztanyi, Z., V. Csizmok, P. Tompa, and I. Simon. 2005. The pairwise energy content estimated from amino acid composition discriminates between folded and intrinsically unstructured proteins. *Journal of molecular biology.* 347:827-839.
- Edelson, P.J. 2012. Patterns of measles transmission among airplane travelers. *Travel medicine and infectious disease.* 10:230-235.

- ENDERS, J.F., S.L. KATZ, and A. HOLLOWAY. 1962. Development of attenuated measles-virus vaccines. A summary of recent investigation. *Am.J.Dis.Child.* 103:335-340.
- Escoffier, C., S. Manie, S. Vincent, C.P. Muller, M. Billeter, and D. Gerlier. 1999. Nonstructural C protein is required for efficient measles virus replication in human peripheral blood cells. *J.Virol.* 73:1695-1698.
- Fensterl, V., and G.C. Sen. 2009. Interferons and viral infections. *BioFactors.* 35:14-20.
- Ferdous, A., F. Gonzalez, L. Sun, T. Kodadek, and S.A. Johnston. 2001. The 19S regulatory particle of the proteasome is required for efficient transcription elongation by RNA polymerase II. *Molecular cell.* 7:981-991.
- Ferron, F., S. Longhi, B. Henrissat, and B. Canard. 2002. Viral RNA-polymerases -- a predicted 2'-O-ribose methyltransferase domain shared by all Mononegavirales. *Trends in biochemical sciences.* 27:222-224.
- Fields, B.N., D.M. Knipe, and P.M. Howley. 2007. Fields virology. Wolters Kluwer Health/Lippincott Williams & Wilkins, Philadelphia. 2 v. (xix, 3091, 3086 p.) pp.
- Fine, P.E. 1993. Herd immunity: history, theory, practice. *Epidemiologic reviews.* 15:265-302.
- Fontana, J.M., B. Bankamp, W.J. Bellini, and P.A. Rota. 2008. Regulation of interferon signaling by the C and V proteins from attenuated and wild-type strains of measles virus. *Virology.* 374:71-81.
- Furuse, Y., A. Suzuki, and H. Oshitani. 2010. Origin of measles virus: divergence from rinderpest virus between the 11th and 12th centuries. *Virol.J.* 7:52.
- Garcin, D., P. Latorre, and D. Kolakofsky. 1999. Sendai virus C proteins counteract the interferon-mediated induction of an antiviral state. *Journal of virology.* 73:6559-6565.
- Gerlier, D., H. Valentin, D. Laine, C. Roubourdin-Combe, and C. Servet-Delprat. 2006. Subversion of the immune system by measles virus: a model for the intricate interplay between a virus and the human immune system. *Microbial subversion of host immunity:*225-292.
- Gerlier, D., and H. Valentin. 2009. Measles virus interaction with host cells and impact on innate immunity. *Curr Top Microbiol Immunol.* 329:163-191.
- Ghanem, A., A. Kern, and K.K. Conzelmann. 2012. Significantly improved rescue of rabies virus from cDNA plasmids. *European journal of cell biology.* 91:10-16.
- Goodbourn, S., and R.E. Randall. 2009. The regulation of type I interferon production by paramyxoviruses. *J.Interferon Cytokine Res.* 29:539-547.
- Greco, T.M., F. Yu, A.J. Guise, and I.M. Cristea. 2011. Nuclear import of histone deacetylase 5 by requisite nuclear localization signal phosphorylation. *Molecular & cellular proteomics : MCP.* 10:M110 004317.
- Gregoire, I.P., C. Richetta, L. Meyniel-Schicklin, S. Borel, F. Pradezynski, O. Diaz, A. Deloire, O. Azocar, J. Baguet, B.M. Le, P.E. Mangeot, V. Navratil, P.E. Joubert, M. Flacher, P.O. Vidalain, P. Andre, V. Lotteau, M. Biard-Piechaczyk, C. Roubourdin-Combe, and M. Faure. 2011. IRGM is a common target of RNA viruses that subvert the autophagy network. *PLoS.Pathog.* 7:e1002422.
- Griffin, D.E. 2010. Measles virus-induced suppression of immune responses. *Immunol.Rev.* 236:176-89.:176-189.
- Griffin, D.E., R.T. Johnson, V.G. Tamashiro, T.R. Moench, E. Jauregui, I. Lindo de Soriano, and A. Vaisberg. 1987. In vitro studies of the role of monocytes in the immunosuppression associated with natural measles virus infections. *Clinical immunology and immunopathology.* 45:375-383.
- Griffin, D.E., and M.B. Oldstone. 2009. Measles. History and basic biology. Introduction. *Curr.Top.Microbiol.Immunol.* 329:1.:1.

- Halpain, S., and L. Dehmelt. 2006. The MAP1 family of microtubule-associated proteins. *Genome Biol.* 7:224.
- Haralambieva, I.H., I.G. Ovsyannikova, N. Dhiman, R.A. Vierkant, R.M. Jacobson, and G.A. Poland. 2010. Differential cellular immune responses to wild-type and attenuated edmonston tag measles virus strains are primarily defined by the viral phosphoprotein gene. *J.Med.Virol.* 82:1966-1975.
- Hilleman, M.R., E.B. Buynak, R.E. Weibel, J. Stokes, Jr., J.E. Whitman, Jr., and M.B. Leagus. 1968. Development and evaluation of the Moraten measles virus vaccine. *JAMA : the journal of the American Medical Association.* 206:587-590.
- Hirsch, R.L., D.E. Griffin, R.T. Johnson, S.J. Cooper, I. Lindo de Soriano, S. Roedenbeck, and A. Vaisberg. 1984. Cellular immune responses during complicated and uncomplicated measles virus infections of man. *Clin Immunol Immunopathol.* 31:1-12.
- Horikami, S.M., S. Smallwood, B. Bankamp, and S.A. Moyer. 1994. An amino-proximal domain of the L protein binds to the P protein in the measles virus RNA polymerase complex. *Virology.* 205:540-545.
- Hornung, V., J. Ellegast, S. Kim, K. Brzozka, A. Jung, H. Kato, H. Poeck, S. Akira, K.K. Conzelmann, M. Schlee, S. Endres, and G. Hartmann. 2006. 5'-Triphosphate RNA is the ligand for RIG-I. *Science.* 314:994-997.
- Ikegame, S., M. Takeda, S. Ohno, Y. Nakatsu, Y. Nakanishi, and Y. Yanagi. 2010. Both RIG-I and MDA5 RNA helicases contribute to the induction of alpha/beta interferon in measles virus-infected human cells. *J.Virol.* 84:372-379.
- Ito, M., M. Iwasaki, M. Takeda, T. Nakamura, Y. Yanagi, and S. Ohno. 2013. Measles virus non-structural C protein modulates viral RNA polymerase activity by interacting with a host protein SHCBP1. *J.Virol.*
- Johnson, R.T., D.E. Griffin, R.L. Hirsch, J.S. Wolinsky, S. Roedenbeck, d.S. Lindo, I, and A. Vaisberg. 1984. Measles encephalomyelitis--clinical and immunologic studies. *N.Engl.J.Med.* 310:137-141.
- Jones, D.T. 1999. Protein secondary structure prediction based on position-specific scoring matrices. *Journal of molecular biology.* 292:195-202.
- Kall, L., A. Krogh, and E.L. Sonnhammer. 2004. A combined transmembrane topology and signal peptide prediction method. *Journal of molecular biology.* 338:1027-1036.
- Kawai, T., and S. Akira. 2008. Toll-like receptor and RIG-I-like receptor signaling. *Ann.N.Y.Acad.Sci.* 1143:1-20.
- Kawai, T., and S. Akira. 2011. Toll-like receptors and their crosstalk with other innate receptors in infection and immunity. *Immunity.* 34:637-650.
- Kawai, T., K. Takahashi, S. Sato, C. Coban, H. Kumar, H. Kato, K.J. Ishii, O. Takeuchi, and S. Akira. 2005. IPS-1, an adaptor triggering RIG-I- and Mda5-mediated type I interferon induction. *Nat.Immunol.* 6:981-988.
- Kessler, J.R., J.R. Kremer, and C.P. Muller. 2011. Interplay of measles virus with early induced cytokines reveals different wild type phenotypes. *Virus Res.* 155:195-202.
- Killip, M.J., D.F. Young, C.S. Ross, S. Chen, S. Goodbourn, and R.E. Randall. 2011. Failure to activate the IFN-beta promoter by a paramyxovirus lacking an interferon antagonist. *Virology.* 415:39-46.
- Kingsbury, D.W. 1974. The molecular biology of paramyxoviruses. *Med Microbiol Immunol.* 160:73-83.
- Koues, O.I., R.K. Dudley, A.D. Truax, D. Gerhardt, K.P. Bhat, S. McNeal, and S.F. Greer. 2008. Regulation of acetylation at the major histocompatibility complex class II proximal promoter by the 19S proteasomal ATPase Sug1. *Molecular and cellular biology.* 28:5837-5850.

- Kumar, H., T. Kawai, and S. Akira. 2009. Toll-like receptors and innate immunity. *Biochem.Biophys.Res.Commun.* 388:621-625.
- Kumar, H., T. Kawai, and S. Akira. 2011. Pathogen recognition by the innate immune system. *Int.Rev.Immunol.* 30:16-34.
- Kumar, H., T. Kawai, H. Kato, S. Sato, K. Takahashi, C. Coban, M. Yamamoto, S. Uematsu, K.J. Ishii, O. Takeuchi, and S. Akira. 2006. Essential role of IPS-1 in innate immune responses against RNA viruses. *J Exp Med.* 203:1795-1803.
- Lacroix, M., M.S. El, G. Rodier, C.A. Le, C. Sardet, and E. Fabbriozio. 2008. The histone-binding protein COPR5 is required for nuclear functions of the protein arginine methyltransferase PRMT5. *EMBO Rep.* 9:452-458.
- Lassen, S.G., M. Schuster, M. Stemmler, A. Steinmuller, D. Matysiak-Klose, A. Mankertz, S. Santibanez, O. Wichmann, and G. Falkenhorst. 2013. Measles outbreak spreading from the community to an anthroposophic school, Berlin, 2011. *Epidemiology and infection:*1-8.
- Le Bon, A., and D.F. Tough. 2002. Links between innate and adaptive immunity via type I interferon. *Curr.Opin.Immunol.* 14:432-436.
- Lee, D., E. Ezhkova, B. Li, S.G. Pattenden, W.P. Tansey, and J.L. Workman. 2005. The proteasome regulatory particle alters the SAGA coactivator to enhance its interactions with transcriptional activators. *Cell.* 123:423-436.
- Levy, D.E., I. Marie, E. Smith, and A. Prakash. 2002. Enhancement and diversification of IFN induction by IRF-7-mediated positive feedback. *J Interferon Cytokine Res.* 22:87-93.
- Li, T., X. Chen, K.C. Garbutt, P. Zhou, and N. Zheng. 2006. Structure of DDB1 in complex with a paramyxovirus V protein: viral hijack of a propeller cluster in ubiquitin ligase. *Cell.* 124:105-117.
- Liston, P., and D.J. Briedis. 1994. Measles virus V protein binds zinc. *Virology.* 198:399-404.
- Liston, P., C. DiFlumeri, and D.J. Briedis. 1995. Protein interactions entered into by the measles virus P, V, and C proteins. *Virus Res.* 38:241-259.
- Litman, G.W., J.P. Rast, and S.D. Fugmann. 2010. The origins of vertebrate adaptive immunity. *Nature reviews. Immunology.* 10:543-553.
- Lu, L.L., M. Puri, C.M. Horvath, and G.C. Sen. 2008. Select paramyxoviral V proteins inhibit IRF3 activation by acting as alternative substrates for inhibitor of kappaB kinase epsilon (IKKe)/TBK1. *J.Biol.Chem.* 283:14269-14276.
- Ludlow, M., L.J. Rennick, S. Sarlang, G. Skibinski, S. McQuaid, T. Moore, R.L. de Swart, and W.P. Duprex. 2010. Wild-type measles virus infection of primary epithelial cells occurs via the basolateral surface without syncytium formation or release of infectious virus. *The Journal of general virology.* 91:971-979.
- Lupas, A., M. Van Dyke, and J. Stock. 1991. Predicting coiled coils from protein sequences. *Science.* 252:1162-1164.
- Maden, B.E., and J.M. Hughes. 1997. Eukaryotic ribosomal RNA: the recent excitement in the nucleotide modification problem. *Chromosoma.* 105:391-400.
- McAllister, C.S., and C.E. Samuel. 2009. The RNA-activated protein kinase enhances the induction of interferon-beta and apoptosis mediated by cytoplasmic RNA sensors. *J.Biol.Chem.* 284:1644-1651.
- McAllister, C.S., A.M. Toth, P. Zhang, P. Devaux, R. Cattaneo, and C.E. Samuel. 2010. Mechanisms of protein kinase PKR-mediated amplification of beta interferon induction by C protein-deficient measles virus. *J. Virol.* 84:380-386.
- McChesney, M.B., A. Altman, and M.B. Oldstone. 1988. Suppression of T lymphocyte function by measles virus is due to cell cycle arrest in G1. *J.Immunol.* 140:1269-1273.

- McChesney, M.B., J.H. Kehrl, A. Valsamakis, A.S. Fauci, and M.B. Oldstone. 1987. Measles virus infection of B lymphocytes permits cellular activation but blocks progression through the cell cycle. *J.Virol.* 61:3441-3447.
- Motz, C., K.M. Schuhmann, A. Kirchhofer, M. Moldt, G. Witte, K.K. Conzelmann, and K.P. Hopfner. 2013. Paramyxovirus V proteins disrupt the fold of the RNA sensor MDA5 to inhibit antiviral signaling. *Science.* 339:690-693.
- Mrkic, B., B. Odermatt, M.A. Klein, M.A. Billeter, J. Pavlovic, and R. Cattaneo. 2000. Lymphatic dissemination and comparative pathology of recombinant measles viruses in genetically modified mice. *J.Virol.* 74:1364-1372.
- Muhlebach, M.D., M. Mateo, P.L. Sinn, S. Prufer, K.M. Uhlig, V.H. Leonard, C.K. Navaratnarajah, M. Frenzke, X.X. Wong, B. Sawatsky, S. Ramachandran, P.B. McCray, Jr., K. Cichutek, M. von, V, M. Lopez, and R. Cattaneo. 2011. Adherens junction protein nectin-4 is the epithelial receptor for measles virus. *Nature.* 480:530-533.
- Murch, S.H., A. Anthony, D.H. Casson, M. Malik, M. Berelowitz, A.P. Dhillon, M.A. Thomson, A. Valentine, S.E. Davies, and J.A. Walker-Smith. 2004. Retraction of an interpretation. *Lancet.* 363:750.
- Nakatsu, Y., M. Takeda, M. Iwasaki, and Y. Yanagi. 2009. A highly attenuated measles virus vaccine strain encodes a fully functional C protein. *J.Virol.* 83:11996-12001.
- Nakatsu, Y., M. Takeda, S. Ohno, R. Koga, and Y. Yanagi. 2006. Translational inhibition and increased interferon induction in cells infected with C protein-deficient measles virus. *J.Virol.* 80:11861-11867.
- Nakatsu, Y., M. Takeda, S. Ohno, Y. Shirogane, M. Iwasaki, and Y. Yanagi. 2008. Measles virus circumvents the host interferon response by different actions of the C and V proteins. *J.Virol.* 82:8296-8306.
- Naniche, D., G. Varior-Krishnan, F. Cervoni, T.F. Wild, B. Rossi, C. Roubardin-Combe, and D. Gerlier. 1993. Human membrane cofactor protein (CD46) acts as a cellular receptor for measles virus. *J.Virol.* 67:6025-6032.
- Nielsen, L., M. Blixenkrone-Moller, M. Thylstrup, N.J. Hansen, and G. Bolt. 2001. Adaptation of wild-type measles virus to CD46 receptor usage. *Archives of virology.* 146:197-208.
- Niewiesk, S., I. Eisenhuth, A. Fooks, J.C. Clegg, J.J. Schnorr, S. Schneider-Schaulies, and M. Ter, V. 1997. Measles virus-induced immune suppression in the cotton rat (*Sigmodon hispidus*) model depends on viral glycoproteins. *J.Virol.* 71:7214-7219.
- Nishie, T., K. Nagata, and K. Takeuchi. 2007. The C protein of wild-type measles virus has the ability to shuttle between the nucleus and the cytoplasm. *Microbes.Infect.* 9:344-354.
- Normile, D. 2008. Rinderpest. Driven to extinction. *Science.* 319:1606-1609.
- Noyce, R.S., D.G. Bondre, M.N. Ha, L.T. Lin, G. Sisson, M.S. Tsao, and C.D. Richardson. 2011. Tumor cell marker PVRL4 (nectin 4) is an epithelial cell receptor for measles virus. *PLoS pathogens.* 7:e1002240.
- Nozawa, Y., N. Ono, M. Abe, H. Sakuma, and H. Wakasa. 1994. An immunohistochemical study of Warthin-Finkeldey cells in measles. *Pathology international.* 44:442-447.
- Ohno, S., N. Ono, F. Seki, M. Takeda, S. Kura, T. Tsuzuki, and Y. Yanagi. 2007. Measles virus infection of SLAM (CD150) knockin mice reproduces tropism and immunosuppression in human infection. *Journal of virology.* 81:1650-1659.
- Ohno, S., N. Ono, M. Takeda, K. Takeuchi, and Y. Yanagi. 2004. Dissection of measles virus V protein in relation to its ability to block alpha/beta interferon signal transduction. *J.Gen.Virol.* 85:2991-2999.

- Ohno, S., and T. Taniguchi. 1983. The 5'-flanking sequence of human interferon-beta 1 gene is responsible for viral induction of transcription. *Nucleic Acids Res.* 11:5403-5412.
- Ono, N., H. Tatsuo, Y. Hidaka, T. Aoki, H. Minagawa, and Y. Yanagi. 2001. Measles viruses on throat swabs from measles patients use signaling lymphocytic activation molecule (CDw150) but not CD46 as a cellular receptor. *J. Virol.* 75:4399-4401.
- Onoguchi, K., K. Onomoto, S. Takamatsu, M. Jogi, A. Takemura, S. Morimoto, I. Julkunen, H. Namiki, M. Yoneyama, and T. Fujita. 2010a. Virus-infection or 5'ppp-RNA activates antiviral signal through redistribution of IPS-1 mediated by MFN1. *PLoS.Pathog.* 6:e1001012.
- Onoguchi, K., K. Onomoto, S. Takamatsu, M. Jogi, A. Takemura, S. Morimoto, I. Julkunen, H. Namiki, M. Yoneyama, and T. Fujita. 2010b. Virus-infection or 5'ppp-RNA activates antiviral signal through redistribution of IPS-1 mediated by MFN1. *PLoS pathogens.* 6:e1001012.
- Ouali, M., and R.D. King. 2000. Cascaded multiple classifiers for secondary structure prediction. *Protein science : a publication of the Protein Society.* 9:1162-1176.
- Palosaari, H., J.P. Parisien, J.J. Rodriguez, C.M. Ulane, and C.M. Horvath. 2003. STAT protein interference and suppression of cytokine signal transduction by measles virus V protein. *J.Virol.* 77:7635-7644.
- Pancer, Z., and M.D. Cooper. 2006. The evolution of adaptive immunity. *Annual review of immunology.* 24:497-518.
- Panne, D., T. Maniatis, and S.C. Harrison. 2007a. An atomic model of the interferon-beta enhanceosome. *Cell.* 129:1111-1123.
- Panne, D., S.M. McWhirter, T. Maniatis, and S.C. Harrison. 2007b. Interferon regulatory factor 3 is regulated by a dual phosphorylation-dependent switch. *J Biol Chem.* 282:22816-22822.
- Parks, C.L., R.A. Lerch, P. Walpita, M.S. Sidhu, and S.A. Udem. 1999. Enhanced measles virus cDNA rescue and gene expression after heat shock. *Journal of virology.* 73:3560-3566.
- Patterson, J.B., D. Thomas, H. Lewicki, M.A. Billeter, and M.B. Oldstone. 2000. V and C proteins of measles virus function as virulence factors in vivo. *Virology.* 267:80-89.
- Peters, J.M., W.W. Franke, and J.A. Kleinschmidt. 1994. Distinct 19 S and 20 S subcomplexes of the 26 S proteasome and their distribution in the nucleus and the cytoplasm. *The Journal of biological chemistry.* 269:7709-7718.
- Pfaller, C. 2010. Subversion of Toll-like receptor 7/9 signaling by Measles virus –V holds the key. *phD Thesis.*
- Pfaller, C.K., and K.K. Conzelmann. 2008. Measles virus V protein is a decoy substrate for IkappaB kinase alpha and prevents Toll-like receptor 7/9-mediated interferon induction. *J.Virol.* 82:12365-12373.
- Philpott, D.J., and S.E. Girardin. 2004. The role of Toll-like receptors and Nod proteins in bacterial infection. *Molecular immunology.* 41:1099-1108.
- Pichlmair, A., O. Schulz, C.P. Tan, T.I. Naslund, P. Liljestrom, F. Weber, and R.e. Sousa. 2006. RIG-I-mediated antiviral responses to single-stranded RNA bearing 5'-phosphates. *Science.* 314:997-1001.
- Pichlmair, A., and R.e. Sousa. 2007. Innate recognition of viruses. *Immunity.* 27:370-383.
- Pollack, B.P., S.V. Kotenko, W. He, L.S. Izotova, B.L. Barnoski, and S. Pestka. 1999. The human homologue of the yeast proteins Skb1 and Hsl7p interacts with Jak kinases and contains protein methyltransferase activity. *J.Biol.Chem.* 274:31531-31542.
- Pomeroy, L.W., O.N. Bjornstad, and E.C. Holmes. 2008. The evolutionary and epidemiological dynamics of the paramyxoviridae. *Journal of molecular evolution.* 66:98-106.

- Precious, B., K. Childs, V. Fitzpatrick-Swallow, S. Goodbourn, and R.E. Randall. 2005. Simian virus 5 V protein acts as an adaptor, linking DDB1 to STAT2, to facilitate the ubiquitination of STAT1. *J. Virol.* 79:13434-13441.
- Precious, B.L., T.S. Carlos, S. Goodbourn, and R.E. Randall. 2007. Catalytic turnover of STAT1 allows PIV5 to dismantle the interferon-induced anti-viral state of cells. *Virology.* 368:114-121.
- Radecke, F., and M.A. Billeter. 1996. The nonstructural C protein is not essential for multiplication of Edmonston B strain measles virus in cultured cells. *Virology.* 217:418-421.
- Radecke, F., P. Spielhofer, H. Schneider, K. Kaelin, M. Huber, C. Dotsch, G. Christiansen, and M.A. Billeter. 1995. Rescue of measles viruses from cloned DNA. *EMBO J.* 14:5773-5784.
- Ramachandran, A., and C.M. Horvath. 2010. Dissociation of paramyxovirus interferon evasion activities: universal and virus-specific requirements for conserved V protein amino acids in MDA5 interference. *J. Virol.* 84:11152-11163.
- Ramachandran, A., J.P. Parisien, and C.M. Horvath. 2008. STAT2 is a primary target for measles virus V protein-mediated alpha/beta interferon signaling inhibition. *J. Virol.* 82:8330-8338.
- Randall, R.E., and S. Goodbourn. 2008. Interferons and viruses: an interplay between induction, signalling, antiviral responses and virus countermeasures. *J. Gen. Virol.* 89:1-47.
- Reutter, G.L., C. Cortese-Grogan, J. Wilson, and S.A. Moyer. 2001. Mutations in the measles virus C protein that up regulate viral RNA synthesis. *Virology.* 285:100-109.
- Riddell, M.A., W.J. Moss, D. Hauer, M. Monze, and D.E. Griffin. 2007. Slow clearance of measles virus RNA after acute infection. *J. Clin. Virol.* 39:312-317.
- Rieder, M., K. Brzozka, C.K. Pfaller, J.H. Cox, L. Stitz, and K.K. Conzelmann. 2011. Genetic dissection of interferon-antagonistic functions of rabies virus phosphoprotein: inhibition of interferon regulatory factor 3 activation is important for pathogenicity. *J. Virol.* 85:842-852.
- Rieder, M., and K.K. Conzelmann. 2009. Rhabdovirus evasion of the interferon system. *J. Interferon Cytokine Res.* 29:499-509.
- Rima, B.K., and W.P. Duprex. 2009. The measles virus replication cycle. *Curr Top Microbiol Immunol.* 329:77-102.
- Rost, B. 2001. Review: protein secondary structure prediction continues to rise. *Journal of structural biology.* 134:204-218.
- Rota, J.S., Z.D. Wang, P.A. Rota, and W.J. Bellini. 1994. Comparison of sequences of the H, F, and N coding genes of measles virus vaccine strains. *Virus Res.* 31:317-330.
- Roy, A., A. Kucukural, and Y. Zhang. 2010. I-TASSER: a unified platform for automated protein structure and function prediction. *Nat. Protoc.* 5:725-738.
- Ryon, J.J., W.J. Moss, M. Monze, and D.E. Griffin. 2002. Functional and phenotypic changes in circulating lymphocytes from hospitalized zambian children with measles. *Clin Diagn Lab Immunol.* 9:994-1003.
- Saitoh, T., A. Tun-Kyi, A. Ryo, M. Yamamoto, G. Finn, T. Fujita, S. Akira, N. Yamamoto, K.P. Lu, and S. Yamaoka. 2006. Negative regulation of interferon-regulatory factor 3-dependent innate antiviral response by the prolyl isomerase Pin1. *Nat Immunol.* 7:598-605.
- Santiago, C., E. Bjorling, T. Stehle, and J.M. Casasnovas. 2002. Distinct kinetics for binding of the CD46 and SLAM receptors to overlapping sites in the measles virus hemagglutinin protein. *J Biol Chem.* 277:32294-32301.

- Schlender, J., J.J. Schnorr, P. Spielhoffer, T. Cathomen, R. Cattaneo, M.A. Billeter, M. Ter, V, and S. Schneider-Schaulies. 1996. Interaction of measles virus glycoproteins with the surface of uninfected peripheral blood lymphocytes induces immunosuppression in vitro. *Proc.Natl.Acad.Sci.U.S.A.* 93:13194-13199.
- Schneider, H., K. Kaelin, and M.A. Billeter. 1997. Recombinant measles viruses defective for RNA editing and V protein synthesis are viable in cultured cells. *Virology.* 227:314-322.
- Schnell, M.J., T. Mebatsion, and K.K. Conzelmann. 1994. Infectious rabies viruses from cloned cDNA. *EMBO J.* 13:4195-4203.
- Schuhmann, K.M., C.K. Pfaller, and K.K. Conzelmann. 2011. The Measles Virus V Protein Binds to p65 (RelA) To Suppress NF- $\kappa$ B Activity. *J.Virol.* 85:3162-3171.
- Schwarz, K. 1964. Immunization 1964. *Nurs.Times.* 60:1315-1316.
- Shaffer, J.A., W.J. Bellini, and P.A. Rota. 2003. The C protein of measles virus inhibits the type I interferon response. *Virology.* 315:389-397.
- Shaw, M.L., W.B. Cardenas, D. Zamarin, P. Palese, and C.F. Basler. 2005. Nuclear localization of the Nipah virus W protein allows for inhibition of both virus- and toll-like receptor 3-triggered signaling pathways. *J.Virol.* 79:6078-6088.
- Shingai, M., T. Ebihara, N.A. Begum, A. Kato, T. Honma, K. Matsumoto, H. Saito, H. Ogura, M. Matsumoto, and T. Seya. 2007. Differential type I IFN-inducing abilities of wild-type versus vaccine strains of measles virus. *J.Immunol.* 179:6123-6133.
- Sievers, F., A. Wilm, D. Dineen, T.J. Gibson, K. Karplus, W. Li, R. Lopez, H. McWilliam, M. Remmert, J. Soding, J.D. Thompson, and D.G. Higgins. 2011. Fast, scalable generation of high-quality protein multiple sequence alignments using Clustal Omega. *Molecular systems biology.* 7:539.
- Sleeman, K., B. Bankamp, K.B. Hummel, M.K. Lo, W.J. Bellini, and P.A. Rota. 2008. The C, V and W proteins of Nipah virus inhibit minigenome replication. *The Journal of general virology.* 89:1300-1308.
- Slifka, M.K., D. Homann, A. Tishon, R. Pagarigan, and M.B. Oldstone. 2003. Measles virus infection results in suppression of both innate and adaptive immune responses to secondary bacterial infection. *J.Clin.Invest.* 111:805-810.
- Smith, D.M., G. Kafri, Y. Cheng, D. Ng, T. Walz, and A.L. Goldberg. 2005. ATP binding to PAN or the 26S ATPases causes association with the 20S proteasome, gate opening, and translocation of unfolded proteins. *Molecular cell.* 20:687-698.
- Smith, E.C., A. Popa, A. Chang, C. Masante, and R.E. Dutch. 2009. Viral entry mechanisms: the increasing diversity of paramyxovirus entry. *FEBS J.* 276:7217-7227.
- Smorodintsev, A.A., L.M. Boichuk, E.S. Shikina, T.B. Batanova, L.V. Bystryakova, and T.V. Peradze. 1960. Clinical and immunological response to live tissue culture vaccine against measles. *Acta virologica.* 4:201-204.
- Strahle, L., J.B. Marq, A. Brini, S. Hausmann, D. Kolakofsky, and D. Garcin. 2007. Activation of the beta interferon promoter by unnatural Sendai virus infection requires RIG-I and is inhibited by viral C proteins. *J.Virol.* 81:12227-12237.
- Stram, Y., and L. Kuzntzova. 2006. Inhibition of viruses by RNA interference. *Virus Genes.* 32:299-306.
- Swedan, S., J. Andrews, T. Majumdar, A. Musiyenko, and S. Barik. 2011. Multiple functional domains and complexes of the two nonstructural proteins of human respiratory syncytial virus contribute to interferon suppression and cellular location. *J.Virol.* 85:10090-10100.
- Takamatsu, S., K. Onoguchi, K. Onomoto, R. Narita, K. Takahasi, F. Ishidate, T.K. Fujiwara, M. Yoneyama, H. Kato, and T. Fujita. 2013. Functional characterization of domains of IPS-1 using an inducible oligomerization system. *PloS one.* 8:e53578.

- Takayama, I., H. Sato, A. Watanabe, M. Omi-Furutani, A. Sugai, K. Kanki, M. Yoneda, and C. Kai. 2012. The nucleocapsid protein of measles virus blocks host interferon response. *Virology*. 424:45-55.
- Takeda, M., K. Takeuchi, N. Miyajima, F. Kobune, Y. Ami, N. Nagata, Y. Suzaki, Y. Nagai, and M. Tashiro. 2000. Recovery of pathogenic measles virus from cloned cDNA. *J.Virol.* 74:6643-6647.
- Takeuchi, K., T. Komatsu, Y. Kitagawa, K. Sada, and B. Gotoh. 2008. Sendai virus C protein plays a role in restricting PKR activation by limiting the generation of intracellular double-stranded RNA. *J.Virol.* 82:10102-10110.
- Tatsuo, H., N. Ono, K. Tanaka, and Y. Yanagi. 2000. SLAM (CDw150) is a cellular receptor for measles virus. *Nature*. 406:893-897.
- Tatsuo, H., N. Ono, and Y. Yanagi. 2001. Morbilliviruses use signaling lymphocyte activation molecules (CD150) as cellular receptors. *J Virol.* 75:5842-5850.
- tenOever, B.R., M.J. Servant, N. Grandvaux, R. Lin, and J. Hiscott. 2002. Recognition of the measles virus nucleocapsid as a mechanism of IRF-3 activation. *J.Virol.* 76:3659-3669.
- Thanos, D., W. Du, and T. Maniatis. 1993. The high mobility group protein HMG I(Y) is an essential structural component of a virus-inducible enhancer complex. *Cold Spring Harb Symp Quant Biol.* 58:73-81.
- Toth, A.M., P. Devaux, R. Cattaneo, and C.E. Samuel. 2009. Protein kinase PKR mediates the apoptosis induction and growth restriction phenotypes of C protein-deficient measles virus. *J.Virol.* 83:961-968.
- Tusnady, G.E., and I. Simon. 1998. Principles governing amino acid composition of integral membrane proteins: application to topology prediction. *Journal of molecular biology.* 283:489-506.
- Valsamakis, A., H. Schneider, P.G. Auwaerter, H. Kaneshima, M.A. Billeter, and D.E. Griffin. 1998. Recombinant measles viruses with mutations in the C, V, or F gene have altered growth phenotypes in vivo. *J.Virol.* 72:7754-7761.
- van Binnendijk, R.S., M.C. Poelen, K.C. Kuijpers, A.D. Osterhaus, and F.G. Uytdehaag. 1990. The predominance of CD8+ T cells after infection with measles virus suggests a role for CD8+ class I MHC-restricted cytotoxic T lymphocytes (CTL) in recovery from measles. Clonal analyses of human CD8+ class I MHC-restricted CTL. *J.Immunol.* 144:2394-2399.
- Vo, N., and R.H. Goodman. 2001. CREB-binding protein and p300 in transcriptional regulation. *J Biol Chem.* 276:13505-13508.
- von, M.A. 2006. The nuclear ubiquitin-proteasome system. *J.Cell Sci.* 119:1977-1984.
- Wang, J., S.H. Basagoudanavar, X. Wang, E. Hopewell, R. Albrecht, A. Garcia-Sastre, S. Balachandran, and A.A. Beg. 2010. NF-kappa B RelA subunit is crucial for early IFN-beta expression and resistance to RNA virus replication. *Journal of immunology.* 185:1720-1729.
- Wang, T., S. Gu, T. Ronni, Y.C. Du, and X. Chen. 2005. In vivo dual-tagging proteomic approach in studying signaling pathways in immune response. *J.Proteome.Res.* 4:941-949.
- Ward, B.J., R.T. Johnson, A. Vaisberg, E. Jauregui, and D.E. Griffin. 1991. Cytokine production in vitro and the lymphoproliferative defect of natural measles virus infection. *Clin Immunol Immunopathol.* 61:236-248.
- Waterhouse, A.M., J.B. Procter, D.M. Martin, M. Clamp, and G.J. Barton. 2009. Jalview Version 2--a multiple sequence alignment editor and analysis workbench. *Bioinformatics.* 25:1189-1191.

- WHO. 2001. Nomenclature for describing the genetic characteristics of wild-type measles virus. *Weekly Epidemiology Records*. 76:249-251.
- WHO. 2013a. Fact sheet N°286 February 2013.
- WHO. 2013b. Measles Reports.
- WHO. 2013c. Measles Surveillance Data.
- Wild, T.F., E. Malvoisin, and R. Buckland. 1991. Measles virus: both the haemagglutinin and fusion glycoproteins are required for fusion. *J.Gen.Virol.* 72 ( Pt 2):439-442.
- Wileman, T. 2007. Aggresomes and pericentriolar sites of virus assembly: cellular defense or viral design? *Annu Rev Microbiol.* 61:149-167.
- Wu, B., A. Peisley, C. Richards, H. Yao, X. Zeng, C. Lin, F. Chu, T. Walz, and S. Hur. 2013. Structural basis for dsRNA recognition, filament formation, and antiviral signal activation by MDA5. *Cell.* 152:276-289.
- Xiang, J.Z., and Z.H. Chen. 1983. Measles vaccine in the People's Republic of China. *Reviews of infectious diseases.* 5:506-510.
- Xu, L.G., Y.Y. Wang, K.J. Han, L.Y. Li, Z. Zhai, and H.B. Shu. 2005. VISA is an adapter protein required for virus-triggered IFN-beta signaling. *Mol Cell.* 19:727-740.
- Yamamoto, Y., U.N. Verma, S. Prajapati, Y.T. Kwak, and R.B. Gaynor. 2003. Histone H3 phosphorylation by IKK-alpha is critical for cytokine-induced gene expression. *Nature.* 423:655-659.
- Yanagi, Y., M. Takeda, and S. Ohno. 2006. Measles virus: cellular receptors, tropism and pathogenesis. *The Journal of general virology.* 87:2767-2779.
- Yie, J., M. Merika, N. Munshi, G. Chen, and D. Thanos. 1999. The role of HMG I(Y) in the assembly and function of the IFN-beta enhanceosome. *EMBO J.* 18:3074-3089.
- Yokota, S., T. Okabayashi, and N. Fujii. 2011a. Measles virus C protein suppresses gamma-activated factor formation and virus-induced cell growth arrest. *Virology.* 414:74-82.
- Yokota, S., T. Okabayashi, N. Yokosawa, and N. Fujii. 2008. Measles virus P protein suppresses Toll-like receptor signal through up-regulation of ubiquitin-modifying enzyme A20. *FASEB J.* 22:74-83.
- Yokota, S., H. Saito, T. Kubota, N. Yokosawa, K. Amano, and N. Fujii. 2003. Measles virus suppresses interferon-alpha signaling pathway: suppression of Jak1 phosphorylation and association of viral accessory proteins, C and V, with interferon-alpha receptor complex. *Virology.* 306:135-146.
- Yokota, S.I., T. Okabayashi, and N. Fujii. 2011b. Measles virus C protein suppresses gamma-activated factor formation and virus-induced cell growth arrest. *Virology.*
- Yoneyama, M., W. Suhara, Y. Fukuhara, M. Fukuda, E. Nishida, and T. Fujita. 1998. Direct triggering of the type I interferon system by virus infection: activation of a transcription factor complex containing IRF-3 and CBP/p300. *EMBO J.* 17:1087-1095.
- Yoshikawa, Y., K. Mizumoto, and K. Yamanouchi. 1986. Characterization of messenger RNAs of measles virus. *The Journal of general virology.* 67 ( Pt 12):2807-2812.
- Yount, J.S., L. Gitlin, T.M. Moran, and C.B. Lopez. 2008. MDA5 participates in the detection of paramyxovirus infection and is essential for the early activation of dendritic cells in response to Sendai Virus defective interfering particles. *J.Immunol.* 180:4910-4918.
- Zahraoui, A., N. Touchot, P. Chardin, and A. Tavitian. 1989. The human Rab genes encode a family of GTP-binding proteins related to yeast YPT1 and SEC4 products involved in secretion. *J.Biol.Chem.* 264:12394-12401.
- Zeng, W., L. Sun, X. Jiang, X. Chen, F. Hou, A. Adhikari, M. Xu, and Z.J. Chen. 2010. Reconstitution of the RIG-I pathway reveals a signaling role of unanchored polyubiquitin chains in innate immunity. *Cell.* 141:315-330.

- Zhang, M., Y. Tian, R.P. Wang, D. Gao, Y. Zhang, F.C. Diao, D.Y. Chen, Z.H. Zhai, and H.B. Shu. 2008. Negative feedback regulation of cellular antiviral signaling by RBCK1-mediated degradation of IRF3. *Cell Res.* 18:1096-1104.
- Zhang, Y. 2008. I-TASSER server for protein 3D structure prediction. *BMC bioinformatics.* 9:40.
- Zhou, X., J.J. Michal, L. Zhang, B. Ding, J.K. Lunney, B. Liu, and Z. Jiang. 2013. Interferon induced IFIT family genes in host antiviral defense. *Int.J.Biol.Sci.* 9:200-208.
- Zust, R., L. Cervantes-Barragan, M. Habjan, R. Maier, B.W. Neuman, J. Ziebuhr, K.J. Szretter, S.C. Baker, W. Barchet, M.S. Diamond, S.G. Siddell, B. Ludewig, and V. Thiel. 2011. Ribose 2'-O-methylation provides a molecular signature for the distinction of self and non-self mRNA dependent on the RNA sensor Mda5. *Nature immunology.* 12:137-143.

# APPENDIX

## List of abbreviations

293T	Human embryonic kidney cells 293 T
5'-ppp	5'-triphosphate
A	alanine
aa	amino acid
AP-1	activator protein 1
APS	ammonium persulfate
bp	base pair
CARD	terminal caspase activation and recruitment domain
CBP	CREB-binding protein
cDNA	copy DNA
CDV	Canine distemper virus
CoIP	co-immunoprecipitation
cRNA	copy (antigenomic) RNA
C-terminus	Carboxy-terminus
Cwt	MV C wildtype
Cs	MV C Schwarz
CwtmNLS	MV C wildtype with mutated NLS
CswtNLS	MV C Schwarz with repaired NLS
DAMPs	danger associated molecular patterns
DCs	dendritic cells
DI	defective interfering
DMEM	Dulbecco's Modified Eagle Medium
DNA	deoxyribonucleic acid
ds	double-strand
DTT	1,4-dithiothreitol
E. coli	Escherichia coli
EDTA	ethylene-diamin-tetraacetic acid-disodium salt
EV	empty vector
F	fusion protein
FCS	fetal calf serum

## List of abbreviations

---

ffu	focus forming units
FITC	fluorescein isothiocyanate
Fl	Flag-tag
G	guanosine
GAPDH	Glyceraldehyde 3-phosphate dehydrogenase
GFP	green fluorescent protein
H	hemagglutinin protein
HA	hemagglutinin tag
PO	horseradish peroxidase
IFN	interferon
IFN- $\beta$	interferon $\beta$
IFNR	IFN receptor
IKK	I $\kappa$ B kinase
IL	interleukin
IPS-1	interferon beta promoter stimulator 1
IRAK	interleukin-1 receptor associated kinase
IRF	interferon regulatory factor
ISG	interferon stimulated genes
I $\kappa$ B	inhibitor of $\kappa$ B
JAK	Janus kinase
K	lysine
KO	knock out
L	large protein
Le	leader
LGP2	laboratory of genetics and physiology 2
M	matrix protein
MAPK	mitogen-activated protein kinase
MDA-5	melanoma differentiation-associated gene 5
MOI	multiplicity of infection
MV	measles virus
MyD88	myeloid differentiation factor 88
N	nucleocapsid protein
NEMO	NF- $\kappa$ B essential modifier
NES	nuclear export signal

---

## List of abbreviations

NF- $\kappa$ B	nuclear factor $\kappa$ B
NiV	Nipah virus
NLS	nuclear localization signal
N-terminus	Amino-terminus
OAS	2'5'-oligoadenylate synthetase
P	phosphoprotein
p.i.	post infection
p.tr.	post transfection
PAGE	polyacrylamide gel electrophoresis
PAMP	pathogen-associated molecular pattern
PBMCs	peripheral blood mononuclear cells
PBS	Phosphate buffered saline
PCR	polymerase chain reaction
pDCs	plasmacytoid dendritic cells
PDV	phocine distemper virus
PdPRV	Peste-de-petit ruminants virus
PEI	polyethyleneimine
PFA	paraformaldehyde
PIV 5	Parainfluenza virus type 5
PO	peroxidase
Poly(I:C)	polyriboinosinic:polyribocytidylic acid
PRR	pattern recognition receptor
PVDF	polyvinylidene fluoride
R	Arginine
RD	regulatory domain
RHD	Rel homology domain
RIG-I	retinoic acid-inducible gene I
RL	Renilla luciferase
RLR	RIG-like receptor
RNA	ribonucleic acid
RNP	ribonucleoprotein
RPV	Rinderpest Virus
RT	reverse transcriptase
RV	rabies virus

## List of abbreviations

---

S	serine
SDS	sodium-dodecyl sulfate
SLAM	Signaling lymphocytic activation molecule
ss	single-strand
SSPE	Subacute sclerosing panencephalitis
STAT	signal transducer and activator of transcription
TagRFP	red fluorescent protein variant from the wild-type RFP from sea anemone <i>Entacmaea quadricolor</i>
TANK	TRAF family member-associated activator NF- $\kappa$ B
TBK-1	TANK-binding kinase 1
TEMED	tetramethylenediamine
TIR	Toll/interleukin-1-receptor
TLR	Toll-like receptor
TNF	Tumor necrosis factor
Tr	trailer
TRADD	TNF receptor 1-associated death domain protein
TRAF	TNF-receptor-associated factor
TRIF	TIR domain-containing adapter inducing IFN- $\beta$
vRdRp	viral RNA-dependent RNA polymerase
vRNA	viral (genomic) RNA
WB	Western blot
WHO	world health organization
wt	wild-type

## List of figures

### Introduction:

Figure 1: Measles wildtype genotype distribution worldwide in 2012.....	4
Figure 2: Measles virus morphology, replication and transcription.....	6
Figure 3: Schematic view on the transcription and translation from the MV P gene. ....	8
Figure 4: Schematic depiction of the intracellular signalling pathway leading to interferon beta induction and the interferon signalling pathway. ....	12
Figure 5: Schematic depiction of MV rescue and the plasmids used.....	18

### Results:

Figure 6: Scheme of the P, V and C expression vector open reading frames. ....	57
Figure 7: Inhibition of IFN- $\beta$ promoter and IRF3 binding element promoter activity by wildtype MV P gene products.....	59
Figure 8: Inhibition of IFN- $\beta$ promoter activity by different C proteins in 293T and 293T Stat -/- cells.....	61
Figure 9: Alignment analysis of the MV Cwt primary amino acid sequence.....	63
Figure 10: Secondary structure prediction and conservation scoring of MV Cwt.....	65
Figure 11: Ab initio tertiary structure predictions for MV Cwt.....	66
Figure 12: A functional NLS is a prerequisite for nuclear accumulation of MV C.....	67
Figure 13: Nuclear localization of MV C is required for efficient inhibition of IFN- $\beta$ promoter activity.....	69
Figure 14: MV C inhibits IRF3 stimulated interferon induction (A) but does not interfere with IRF3 activation by phosphorylation (B), dimerization (C) or nuclear accumulation (D).....	71
Figure 15: Co-immunoprecipitation of MV Cwt with various proteins in the interferon pathway. ....	74
Figure 16: Co-immunoprecipitation experiments of MV Cwt with known binding partners (pSTAT1 and IRGM). ....	76
Figure 17: Silver stained gels of purified proteins. ....	77
Figure 18: Identification of protein binding partners of MV Cwt by mass spectrometry.....	80
Figure 19: Protein-protein interaction networks of MVCwt binding partners.....	82
Figure 20: Co-immunoprecipitation experiments of MV Cwt with putative interaction partners identified by mass spectrometry: IPO8(A), DDB1(B), MAP1B(C) and PSMC3(D). ....	84

List of figures

Figure 21: Immunofluorescent images to detect co-localisation between C and various proposed binding partners. .... 85

Figure 22: Scheme representing the genomes of recombinant MVs generated during this thesis..... 88

Figure 23: RNAs regulated by infection with MV vac2 at different timepoints in human B-cells..... 90

Figure 24: Functional annotation and clustering of the RNAs found to be regulated more than 2-fold in microarray experiments. .... 92

Figure 25: Characterisation of C knockout MV vac2. .... 94

Figure 26: Northern blot and detection of viral RNAs from rMV vac2 and rMV vac2Cko infected cells..... 96

Figure 27: Intracellular localisation of C and mutants in the viral context..... 99

Figure 28: Immunofluorescent images of MV N, C and P co-expression. .... 101

Figure 29: Comparison of rMV vac2CwtNLS and rMV vac2..... 103

Discussion:

Figure 30: Model of the proteasome and the Cwt interacting subunits..... 118

Figure 31: Model of C during infection with exogenous innate immunity stimuli..... 120





Supplementary Data:

Rank	TM-score	RMSD <sup>a</sup>	IDEN <sup>b</sup>	Cov.	EC-Score	PDB Hit	EC No.
1	0.7941	3.32	0.13	0.97	0.7323	<a href="#">2v1qH</a>	<a href="#">1.3.99.2</a>
2	0.7943	3.33	0.12	0.97	0.7003	<a href="#">1jq1A</a>	<a href="#">1.3.99.2</a>
3	0.7949	3.13	0.10	0.96	0.6505	<a href="#">3mdda</a>	<a href="#">1.3.99.3</a>
4	0.7909	3.18	0.10	0.97	0.6351	<a href="#">1bucB</a>	<a href="#">1.3.99.2</a>
5	0.7915	3.34	0.09	0.97	0.6168	<a href="#">1bucA</a>	<a href="#">1.3.99.2</a>

- (a) Ranking is based on EC-score, which is a confidence score for the Enzyme Classification (EC) Number prediction.
- (b) RMSD<sup>a</sup> is the RMSD between models and the PDB structure in the structurally aligned regions by TM-align.
- (c) IDEN<sup>b</sup> is percentage sequence identity in the structurally aligned region.
- (d) Cov. represents the coverage of the alignment and is equal to the number of structurally aligned residues divided by length of model.
- (e) EC-Score is defined based on the C-score of the structure prediction and similarity of the model with known enzyme structures, as identified using both global and local structural alignment programs. The global similarity score uses TM-score, IDEN<sup>b</sup>, RMSD<sup>a</sup> and Cov. of the structural alignment by TM-align, while the local match compares the structural and chemical similarity of local spatial motifs in the model with known catalytic site of enzymes. A prediction with a EC-score >1.1 signifies a prediction with high confidence (up to 3 digit numbers of EC) and vice versa (For details, see Inferring protein function by global and local similarity of structural analogs, 2010, submitted).

Rank	TMscore	RMSD <sup>a</sup>	IDEN <sup>b</sup>	Cov.	PDB Hit	Fh-Score	Associated GO Terms
1	0.7941	3.32	0.13	0.97	<a href="#">2v1qH</a>	0.73	<a href="#">GO:0000062</a> <a href="#">GO:0044085</a> <a href="#">GO:0009055</a> <a href="#">GO:0050660</a> <a href="#">GO:0050662</a> <a href="#">GO:0006631</a> <a href="#">GO:0006635</a> <a href="#">GO:0009056</a> <a href="#">GO:0009987</a> <a href="#">GO:0019395</a> <a href="#">GO:0031667</a> <a href="#">GO:0032787</a> <a href="#">GO:0042221</a> <a href="#">GO:0042594</a> <a href="#">GO:0044248</a> <a href="#">GO:0046395</a> <a href="#">GO:0051984</a> <a href="#">GO:0055114</a> <a href="#">GO:0056223</a> <a href="#">GO:0057377</a> <a href="#">GO:0057399</a> <a href="#">GO:0057598</a> <a href="#">GO:0031974</a> <a href="#">GO:0043228</a> <a href="#">GO:0044429</a> <a href="#">GO:0044444</a>
2	0.7942	3.33	0.12	0.97	<a href="#">1jq1B</a>	0.70	<a href="#">GO:0044085</a> <a href="#">GO:0009055</a> <a href="#">GO:0050660</a> <a href="#">GO:0050662</a> <a href="#">GO:0006631</a> <a href="#">GO:0009987</a> <a href="#">GO:0032787</a> <a href="#">GO:0055114</a> <a href="#">GO:0005622</a> <a href="#">GO:0005623</a> <a href="#">GO:0005737</a> <a href="#">GO:0005739</a> <a href="#">GO:0005759</a> <a href="#">GO:0031974</a> <a href="#">GO:0043228</a> <a href="#">GO:0044429</a> <a href="#">GO:0044444</a>
3	0.7994	3.29	0.11	0.97	<a href="#">2a1fD</a>	0.67	<a href="#">GO:0003995</a> <a href="#">GO:0009055</a> <a href="#">GO:0050660</a> <a href="#">GO:0050662</a> <a href="#">GO:0006631</a> <a href="#">GO:0006635</a> <a href="#">GO:0009056</a> <a href="#">GO:0009987</a> <a href="#">GO:0019395</a> <a href="#">GO:0032787</a> <a href="#">GO:0044248</a> <a href="#">GO:0046395</a> <a href="#">GO:0055114</a> <a href="#">GO:0005622</a> <a href="#">GO:0005623</a> <a href="#">GO:0005737</a> <a href="#">GO:0005739</a> <a href="#">GO:0005759</a> <a href="#">GO:0031974</a> <a href="#">GO:0043228</a> <a href="#">GO:0044429</a> <a href="#">GO:0044444</a>
4	0.7955	3.23	0.10	0.96	<a href="#">3mdeB</a>	0.65	<a href="#">GO:0003995</a> <a href="#">GO:0009055</a> <a href="#">GO:0050660</a> <a href="#">GO:0050662</a> <a href="#">GO:0006631</a> <a href="#">GO:0006635</a> <a href="#">GO:0009056</a> <a href="#">GO:0009987</a> <a href="#">GO:0019395</a> <a href="#">GO:0032787</a> <a href="#">GO:0044248</a> <a href="#">GO:0046395</a> <a href="#">GO:0055114</a> <a href="#">GO:0005622</a> <a href="#">GO:0005623</a> <a href="#">GO:0005737</a> <a href="#">GO:0005739</a> <a href="#">GO:0005759</a> <a href="#">GO:0031974</a> <a href="#">GO:0043228</a> <a href="#">GO:0044429</a> <a href="#">GO:0044444</a>
5	0.7932	3.33	0.10	0.97	<a href="#">2dvlB</a>	0.65	<a href="#">GO:0003995</a> <a href="#">GO:0009055</a> <a href="#">GO:0050660</a> <a href="#">GO:0050662</a> <a href="#">GO:0006631</a> <a href="#">GO:0006635</a> <a href="#">GO:0009056</a> <a href="#">GO:0009987</a> <a href="#">GO:0019395</a> <a href="#">GO:0032787</a> <a href="#">GO:0044248</a> <a href="#">GO:0046395</a> <a href="#">GO:0055114</a> <a href="#">GO:0005622</a> <a href="#">GO:0005623</a> <a href="#">GO:0005737</a> <a href="#">GO:0005739</a> <a href="#">GO:0005759</a> <a href="#">GO:0031974</a> <a href="#">GO:0043228</a> <a href="#">GO:0044429</a> <a href="#">GO:0044444</a>
6	0.7886	3.14	0.10	0.96	<a href="#">2aa1D</a>	0.65	<a href="#">GO:0003995</a> <a href="#">GO:0009055</a> <a href="#">GO:0050660</a> <a href="#">GO:0050662</a> <a href="#">GO:0006631</a> <a href="#">GO:0006635</a> <a href="#">GO:0009056</a> <a href="#">GO:0009987</a> <a href="#">GO:0019395</a> <a href="#">GO:0032787</a> <a href="#">GO:0044248</a> <a href="#">GO:0046395</a> <a href="#">GO:0055114</a> <a href="#">GO:0005622</a> <a href="#">GO:0005623</a> <a href="#">GO:0005737</a> <a href="#">GO:0005739</a> <a href="#">GO:0005759</a> <a href="#">GO:0031974</a> <a href="#">GO:0043228</a> <a href="#">GO:0044429</a> <a href="#">GO:0044444</a>
7	0.7822	3.28	0.10	0.97	<a href="#">1rx0D</a>	0.64	<a href="#">GO:0003995</a> <a href="#">GO:0009055</a> <a href="#">GO:0050660</a> <a href="#">GO:0050662</a> <a href="#">GO:0006631</a> <a href="#">GO:0006635</a> <a href="#">GO:0009056</a> <a href="#">GO:0009987</a> <a href="#">GO:0019395</a> <a href="#">GO:0032787</a> <a href="#">GO:0044248</a> <a href="#">GO:0046395</a> <a href="#">GO:0055114</a> <a href="#">GO:0005622</a> <a href="#">GO:0005623</a> <a href="#">GO:0005737</a> <a href="#">GO:0005739</a> <a href="#">GO:0005759</a> <a href="#">GO:0031974</a> <a href="#">GO:0043228</a> <a href="#">GO:0044429</a> <a href="#">GO:0044444</a>
8	0.7909	3.18	0.10	0.97	<a href="#">1bucB</a>	0.64	<a href="#">GO:0003995</a> <a href="#">GO:0009055</a> <a href="#">GO:0050660</a> <a href="#">GO:0050662</a> <a href="#">GO:0006631</a> <a href="#">GO:0006635</a> <a href="#">GO:0009056</a> <a href="#">GO:0009987</a> <a href="#">GO:0019395</a> <a href="#">GO:0032787</a> <a href="#">GO:0044248</a> <a href="#">GO:0046395</a> <a href="#">GO:0055114</a> <a href="#">GO:0005622</a> <a href="#">GO:0005623</a> <a href="#">GO:0005737</a> <a href="#">GO:0005739</a> <a href="#">GO:0005759</a> <a href="#">GO:0031974</a> <a href="#">GO:0043228</a> <a href="#">GO:0044429</a> <a href="#">GO:0044444</a>
9	0.7611	3.39	0.10	0.96	<a href="#">2ifonC</a>	0.63	<a href="#">GO:0003995</a> <a href="#">GO:0009055</a> <a href="#">GO:0050660</a> <a href="#">GO:0050662</a> <a href="#">GO:0006631</a> <a href="#">GO:0006635</a> <a href="#">GO:0009056</a> <a href="#">GO:0009987</a> <a href="#">GO:0019395</a> <a href="#">GO:0032787</a> <a href="#">GO:0044248</a> <a href="#">GO:0046395</a> <a href="#">GO:0055114</a> <a href="#">GO:0005622</a> <a href="#">GO:0005623</a> <a href="#">GO:0005737</a> <a href="#">GO:0005739</a> <a href="#">GO:0005759</a> <a href="#">GO:0031974</a> <a href="#">GO:0043228</a> <a href="#">GO:0044429</a> <a href="#">GO:0044444</a>
10	0.7888	3.17	0.10	0.96	<a href="#">2d29B</a>	0.63	<a href="#">GO:0003995</a> <a href="#">GO:0009055</a> <a href="#">GO:0050660</a> <a href="#">GO:0050662</a> <a href="#">GO:0006631</a> <a href="#">GO:0006635</a> <a href="#">GO:0009056</a> <a href="#">GO:0009987</a> <a href="#">GO:0019395</a> <a href="#">GO:0032787</a> <a href="#">GO:0044248</a> <a href="#">GO:0046395</a> <a href="#">GO:0055114</a> <a href="#">GO:0005622</a> <a href="#">GO:0005623</a> <a href="#">GO:0005737</a> <a href="#">GO:0005739</a> <a href="#">GO:0005759</a> <a href="#">GO:0031974</a> <a href="#">GO:0043228</a> <a href="#">GO:0044429</a> <a href="#">GO:0044444</a>

Consensus Prediction of Gene Ontology terms

Molecular Function		Biological Process		Cellular Location	
GO term	GO-Score	GO term	GO-Score	GO term	GO-Score
<a href="#">GO:0009055</a>	0.659	<a href="#">GO:0008152</a>	0.659	<a href="#">GO:0043229</a>	0.638
<a href="#">GO:0003995</a>	0.659	<a href="#">GO:0044237</a>	0.466	<a href="#">GO:0005737</a>	0.638
<a href="#">GO:0050660</a>	0.594	<a href="#">GO:0009987</a>	0.466	<a href="#">GO:0005623</a>	0.638
<a href="#">GO:0050662</a>	0.594	<a href="#">GO:0006629</a>	0.466	<a href="#">GO:0005622</a>	0.638
<a href="#">GO:004085</a>	0.207	<a href="#">GO:0044238</a>	0.466	<a href="#">GO:0044444</a>	0.638
<a href="#">GO:000062</a>	0.073	<a href="#">GO:0055114</a>	0.403	<a href="#">GO:0005739</a>	0.575
<a href="#">GO:008289</a>	0.073	<a href="#">GO:0044255</a>	0.402	<a href="#">GO:0044429</a>	0.511
<a href="#">GO:0005504</a>	0.073	<a href="#">GO:0032787</a>	0.402	<a href="#">GO:0005759</a>	0.395
<a href="#">GO:0016634</a>	0.063	<a href="#">GO:0006631</a>	0.402	<a href="#">GO:0031974</a>	0.395
<a href="#">GO:0003997</a>	0.063	<a href="#">GO:0019752</a>	0.402	<a href="#">GO:0070013</a>	0.395

- (a) Ranking in the first table is based on a function prediction score (Fh-score), which is calculated based on the C-score of the structure prediction and the TM-score, IDEN<sup>b</sup>, RMSD<sup>a</sup> and Cov. of the structural alignment by TM-align between the predicted model and the PDB structures (For details, see Inferring protein function by global and local similarity of structural analogs, 2010, submitted).
- (b) RMSD<sup>a</sup> is the RMSD between models and the PDB structure in the structurally aligned regions by TM-align.
- (c) IDEN<sup>b</sup> is the percentage sequence identity in the structurally aligned region.
- (d) Cov. represents the coverage of the alignment and is equal to the number of structurally aligned residues divided by length of model.
- (e) A consensus prediction of GO terms is derived from the structural analogs that have an Fh-score of >=1.0. The GO-Score associated with each prediction is defined as the average weight of the GO term, where the weights are assigned based on the Fh-score of the template from which the GO term is derived. A prediction with a GO-score >0.5 signifies a prediction with high confidence and vice versa.

Identified structural analogs with similar binding site:

Rank	PDB Hit	TM-score	RMSD <sup>a</sup>	IDEN <sup>b</sup>	Cov.	BS-score	Lig. Name	Download Complex	Predicted binding site residues in the model
1	 <a href="#">2pq0B</a>	0.7922	3.3200	0.0820	0.9731	1.1581	FAD	<a href="#">Download</a>	90,92,97,100,101,102,158,159,160,161,162,163
2	 <a href="#">3oibA</a>	0.7951	3.0600	0.0440	0.9624	1.1076	FDA	<a href="#">Download</a>	90,92,97,100,102,158,159,160,161,162
3	 <a href="#">2c0uA</a>	0.7911	3.2000	0.1050	0.9624	1.0249	POL	<a href="#">Download</a>	103,158,159,160,161
4	 <a href="#">2r0mA</a>	0.7849	3.2300	0.0710	0.9677	0.8162	4NI	<a href="#">Download</a>	112,113,116,117,121,141,148,149
5	 <a href="#">2c12F</a>	0.7897	3.1100	0.1050	0.9570	1.0196	FAD	<a href="#">Download</a>	74,76,117,142,144,145,146,148
6	 <a href="#">3epnC</a>	0.7713	3.3500	0.0610	0.9516	0.8240	341	<a href="#">Download</a>	79,80,152,156,176,179,180

Spin On/Off

## Supplementary Data:

	7	<a href="#">1gc8</a>	0.7973	3.2900	0.1100	0.9677	0.4348	CO8	<a href="#">Download</a>	3,4,5,8,44,54,55,57,61,64,65,67,68,138,180,181,185
	8	<a href="#">2jfd</a>	0.7908	3.1900	0.0880	0.9677	0.9876	FAD	<a href="#">Download</a>	90,97,100,104,158,159,160,161,164
	9	<a href="#">3d9g</a>	0.7900	3.1200	0.1050	0.9570	1.0250	POL	<a href="#">Download</a>	103,158,159,160,161
	10	<a href="#">3obA</a>	0.7951	3.0600	0.0440	0.9624	0.6506	FDA	<a href="#">Download</a>	76,79,80,81,106,107,108,112,113,114,115,143,147,150,151,153,154,156

Click on the radio buttons to visualize predicted binding sites and residues.

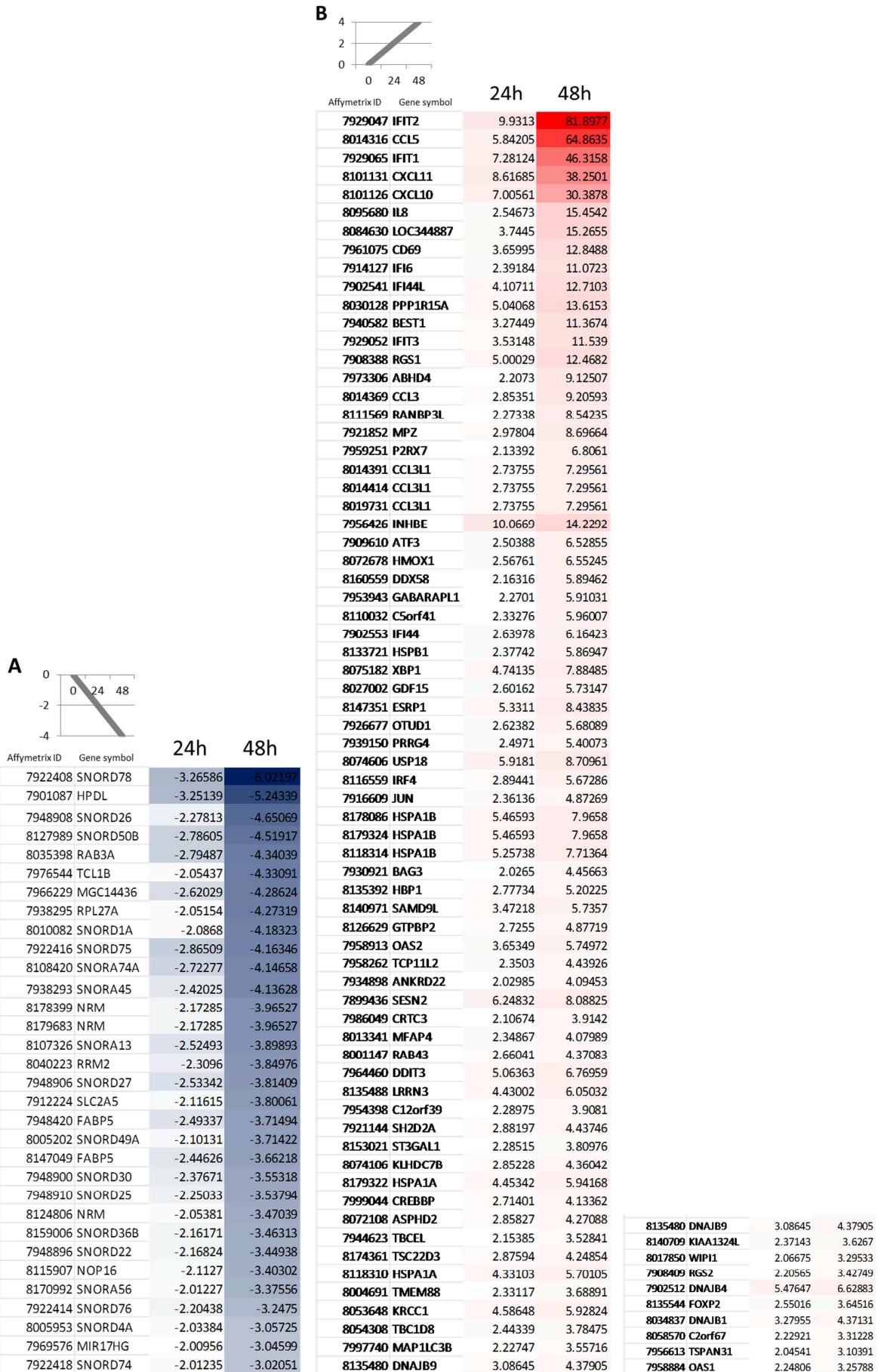
(a) Ranking of the predicted binding sites is based on the size of the clusters formed after local superposition of ligands of the templates onto the query structure.  
(b) BS score is a measure of local sequence & structure similarity between template's binding site and predicted binding site in the query structure. Based on large scale benchmarking analysis, binding site predictions with BS-score>1.1 signify predictions with high confidence.  
(c) RMSD<sup>2</sup> the RMSD between residues that are structurally aligned by TM-align.  
(d) IDEN<sup>2</sup> is the percentage sequence identity in the structurally aligned region.  
(e) Cov. represents the coverage of the alignment by TM-align and is equal to the number of structurally aligned residues divided by length of the model.  
(f) For details, see COFACTOR: protein-ligand binding site predictions by global structure match and local geometry refinement. (In preparation)

Please cite following articles when you use the I-TASSER server:

1. Amrishi Roy, Alper Kucukural, Yang Zhang. I-TASSER: a unified platform for automated protein structure and function prediction. Nature Protocols, vol 5, 725-738 (2010).
2. Yang Zhang. Template-based modeling and free modeling by I-TASSER in CASP7. Proteins, vol 69 (Suppl 8), 108-117 (2007).

**App. 3: Full Clustering:**

Supplementary Data:



**App. 4: Full Annotations:**

The functional annotations were done using the go.david website and the standard pathway settings.

**Genes upregulated after 24h and declining after 48h:**

Category	Term	Count	%	PValue	List Total	Pop Hits	Pop Total	Fold Enrichment	Bonferroni	Benjamini
GOTERM_BP_FAT	GO:0009070-serine family amino acid biosynthetic process	2	33.3333333	0.00162566	3	11	13528	819.878788	0.07662694	0.07662694
GOTERM_BP_FAT	GO:0009069-serine family amino acid metabolic process	2	33.3333333	0.00384033	3	26	13528	346.871795	0.17183121	0.08996221
SP_PIR_KEYWORDS	amino-acid biosynthesis	2	33.3333333	0.00498196	5	24	19235	320.583333	0.10405565	0.10405565
KEGG_PATHWAY	hsa00260:Glycine, serine and threonine metabolism	2	33.3333333	0.00609636	2	31	5085	164.032258	0.02416336	0.02416336
GOTERM_BP_FAT	GO:0008652-cellular amino acid biosynthetic process	2	33.3333333	0.00752598	3	51	13528	176.836601	0.30938158	0.11608049
GOTERM_BP_FAT	GO:0009309-amine biosynthetic process	2	33.3333333	0.01193975	3	81	13528	111.341564	0.44487865	0.13682872
GOTERM_BP_FAT	GO:0016053-organic acid biosynthetic process	2	33.3333333	0.02278499	3	155	13528	58.1849462	0.67676657	0.20218306
GOTERM_BP_FAT	GO:0046394-carboxylic acid biosynthetic process	2	33.3333333	0.02278499	3	155	13528	58.1849462	0.67676657	0.20218306
GOTERM_BP_FAT	GO:0044271-nitrogen compound biosynthetic process	2	33.3333333	0.04747306	3	325	13528	27.7497436	0.90774581	0.32780128

**Genes upregulated after 24h and further upregulated after 48h:**

Category	Term	Count	%	PValue	List Total	Pop Hits	Pop Total	Fold Enrichment	Bonferroni	Benjamini
SP_PIR_KEYWORDS	Antiviral defense	19	4.41860465	3.01E-16	403	62	19235	14.626791	1.07E-13	1.07E-13
GOTERM_BP_FAT	GO:0009615-response to virus	22	5.11627907	6.04E-15	281	109	13528	9.71680434	1.01E-11	1.01E-11
PIR_SUPERFAMILY	PIRSF001934:interferon alpha	11	2.55813953	1.28E-14	142	15	7396	38.1953052	1.89E-12	1.89E-12
INTERPRO	IPR000471:Interferon alpha/beta/delta	11	2.55813953	2.24E-13	347	17	16659	31.0644177	1.38E-10	1.38E-10
INTERPRO	IPR015589:Interferon alpha	10	2.3255814	4.31E-13	347	13	16659	36.9297273	2.66E-10	1.33E-10
KEGG_PATHWAY	hsa04060:Cytokine-cytokine receptor interaction	28	6.51162791	5.05E-13	103	262	5085	5.27606907	4.95E-11	4.95E-11
SMART	SM00076:IFabd	11	2.55813953	1.43E-12	230	17	9079	25.5419437	2.34E-10	2.34E-10
KEGG_PATHWAY	hsa04622:RIG-I-like receptor signaling pathway	15	3.48837209	6.46E-11	103	71	5085	10.4300561	6.33E-09	3.17E-09
SP_PIR_KEYWORDS	antiviral	9	2.09302326	9.14E-11	403	14	19235	30.6832683	2.94E-08	1.47E-08
KEGG_PATHWAY	hsa04630:Jak-STAT signaling pathway	20	4.65116279	1.20E-10	103	155	5085	6.37018478	1.17E-08	3.91E-09
KEGG_PATHWAY	hsa04140:Regulation of autophagy	11	2.55813953	8.17E-10	103	35	5085	15.5159501	8.01E-08	2.00E-08
INTERPRO	IPR012351:Four-helical cytokine, core	12	2.79069767	1.84E-09	347	46	16659	12.5239945	1.14E-06	3.79E-07
GOTERM_BP_FAT	GO:0006952-defense response	38	8.8372093	4.80E-09	281	615	13528	2.97464919	8.13E-06	4.07E-06
KEGG_PATHWAY	hsa04650:Natural killer cell mediated cytotoxicity	17	3.95348837	5.46E-09	103	133	5085	6.31031462	5.35E-07	1.07E-07
KEGG_PATHWAY	hsa04623:Cytosolic DNA-sensing pathway	12	2.79069767	7.05E-09	103	55	5085	10.7714034	6.91E-07	1.15E-07
SP_PIR_KEYWORDS	leukocyte	8	1.86046512	9.21E-09	403	15	19235	25.4557486	2.97E-06	9.88E-07
KEGG_PATHWAY	hsa04620:Toll-like receptor signaling pathway	14	3.25581395	7.44E-08	103	101	5085	6.8432183	7.29E-06	1.04E-06
SP_PIR_KEYWORDS	cytokine	18	4.18604651	2.70E-07	403	181	19235	4.74658295	6.68E-05	2.17E-05
KEGG_PATHWAY	hsa05320:Autoimmune thyroid disease	10	2.3255814	5.57E-07	103	51	5085	9.68018275	5.46E-05	6.83E-06
GOTERM_MF_FAT	GO:0005132-interferon-alpha/beta receptor binding	6	1.39534884	6.29E-07	291	9	12983	29.7434135	2.90E-04	2.90E-04
UP_SEQ_FEATURE	compositionally biased region:Poly-Ser	29	6.74418605	9.91E-07	402	475	19113	2.9027337	0.0011335	0.0011335
GOTERM_MF_FAT	GO:0005125-cytokine activity	18	4.18604651	1.77E-06	291	195	12983	4.11831879	8.14E-04	4.07E-04
KEGG_PATHWAY	hsa04612:Antigen processing and presentation	11	2.55813953	4.87E-06	103	83	5085	6.54287051	4.77E-04	5.30E-05
GOTERM_BP_FAT	GO:0006917-induction of apoptosis	21	4.88372093	1.14E-05	281	320	13528	3.15934164	0.01917395	0.0064326
GOTERM_BP_FAT	GO:0012502-induction of programmed cell death	21	4.88372093	1.20E-05	281	321	13528	3.14949945	0.0200404	0.0050482
GOTERM_BP_FAT	GO:0043067-regulation of programmed cell death	36	8.37209302	2.99E-05	281	812	13528	2.13438985	0.0493232	0.01006523
GOTERM_BP_FAT	GO:0001775-cell activation	19	4.41860465	3.02E-05	281	287	13528	3.18712413	0.04981729	0.00848067
GOTERM_BP_FAT	GO:0010941-regulation of cell death	36	8.37209302	3.22E-05	281	815	13528	2.1265332	0.05302025	0.0077523
GOTERM_BP_FAT	GO:0043068-positive regulation of programmed cell death	24	5.58139535	3.48E-05	281	433	13528	2.66839808	0.05723971	0.00734083
UP_SEQ_FEATURE	compositionally biased region:Ser-rich	24	5.58139535	3.62E-05	402	425	19113	2.68488147	0.0406274	0.02052432
GOTERM_BP_FAT	GO:0010942-positive regulation of cell death	24	5.58139535	3.70E-05	281	435	13528	2.65612959	0.06076683	0.00694152
GOTERM_BP_FAT	GO:0042981-regulation of apoptosis	35	8.13953488	5.71E-05	281	804	13528	2.09574901	0.09220711	0.00962726
GOTERM_BP_FAT	GO:0043065-positive regulation of apoptosis	23	5.34883721	8.98E-05	281	430	13528	2.57505586	0.14107233	0.01372948
GOTERM_CC_FAT	GO:0005615-extracellular space	28	6.51162791	1.40E-04	235	685	12782	2.22330175	0.03625952	0.03625952
GOTERM_BP_FAT	GO:0045321-leukocyte activation	16	3.72093023	1.58E-04	281	242	13528	3.18296521	0.23497433	0.02207323
GOTERM_BP_FAT	GO:0006955-immune response	30	6.97674419	2.30E-04	281	690	13528	2.0931456	0.32289592	0.02954926
GOTERM_BP_FAT	GO:0043122-regulation of I-kappaB kinase/NF-kappaB cascade	10	2.3255814	3.74E-04	281	107	13528	4.49928493	0.46924831	0.04423882
SP_PIR_KEYWORDS	zinc-finger	57	13.255814	5.61E-04	403	171 8 204	19235	1.58357574	0.16529645	0.03549063
UP_SEQ_FEATURE	mutagenesis site	65	15.1162791	7.19E-04	402	5	19113	1.51120315	0.56114082	0.24006743
GOTERM_BP_FAT	GO:0043123-positive regulation of I-kappaB kinase/NF-kappaB cascade	9	2.09302326	8.97E-04	281	97	13528	4.46681586	0.7810111	0.09629197
PIR_SUPERFAMILY	PIRSF038749:interferon lambda	3	0.69767442	0.001069 19	142	3	7396	52.084507	0.14642784	0.07611031
GOTERM_BP_FAT	GO:0030278-regulation of ossification	8	1.86046512	0.001138 5	281	78	13528	4.9376768	0.85464612	0.11355527
GOTERM_MF_FAT	GO:0005072-transforming growth factor beta receptor, cytoplasmic mediator activity	4	0.93023256	0.001593 19	291	11	12983	16.2236801	0.52051726	0.21730782

Interferon induction inhibition by MV C - Appendix

Supplementary Data:

GOTERM_BP_FAT	GO:0007243~protein kinase cascade	18	4.18604651	0.00183802	281	370	13528	2.34206021	0.95560543	0.16741004
BIOCARTA	h_tgfbPathway:TGF beta signaling pathway	5	1.1627907	0.00189621	49	17	1437	8.62545018	0.15702755	0.15702755
GOTERM_BP_FAT	GO:0012501~programmed cell death	25	5.81395349	0.00200148	281	611	13528	1.96981787	0.96635509	0.17174859
GOTERM_BP_FAT	GO:0008219~cell death	28	6.51162791	0.00201702	281	719	13528	1.87480635	0.96723071	0.16465345
GOTERM_BP_FAT	GO:0016265~death	28	6.51162791	0.00219323	281	724	13528	1.86185879	0.97569836	0.16961064
SP_PIR_KEYWORDS	zinc	66	15.3488372	0.00227545	403	2189	19235	1.43908126	0.51978935	0.11507738
GOTERM_BP_FAT	GO:0010740~positive regulation of protein kinase cascade	11	2.55813953	0.00251082	281	167	13528	3.17105291	0.98582345	0.18345607
GOTERM_BP_FAT	GO:0046649~lymphocyte activation	12	2.79069767	0.00287904	281	199	13528	2.90305621	0.99241243	0.19898427
SP_PIR_KEYWORDS	Proto-oncogene	13	3.02325581	0.00340796	403	230	19235	2.69775596	0.66687455	0.14532477
PIR_SUPERFAMILY	PIRSF028804:protein yippee-like	3	0.69767442	0.0034754	142	5	7396	31.2507042	0.40265183	0.15781175
GOTERM_BP_FAT	GO:0006915~apoptosis	24	5.58139535	0.00349101	281	602	13528	1.9192963	0.99731646	0.22695513
INTERPRO	IPR004910:Yippee-like protein	3	0.69767442	0.00412659	347	5	16659	28.8051873	0.92202569	0.47156949
GOTERM_BP_FAT	GO:0045449~regulation of transcription	73	16.9767442	0.00433142	281	1	13528	1.35116934	0.99935677	0.26376723
GOTERM_BP_FAT	GO:0006357~regulation of transcription from RNA polymerase II promoter	27	6.27906977	0.00459627	281	727	13528	1.78795518	0.99959003	0.26800162
GOTERM_CC_FAT	GO:0044421~extracellular region part	30	6.97674419	0.00521178	235	960	12782	1.69973404	0.74829747	0.49830036
GOTERM_BP_FAT	GO:0051252~regulation of RNA metabolic process	54	12.5581395	0.00540288	281	1813	13528	1.43391441	0.99989608	0.29725727
GOTERM_BP_FAT	GO:0006355~regulation of transcription, DNA-dependent	53	12.3255814	0.00550885	281	1773	13528	1.43911138	0.99991323	0.29275656
GOTERM_BP_FAT	GO:0010627~regulation of protein kinase cascade	13	3.02325581	0.00577208	281	249	13528	2.51345596	0.99994457	0.29532326
INTERPRO	IPR000340:Protein-tyrosine phosphatase, dual specificity	5	1.1627907	0.00703622	347	37	16659	6.4876548	0.98717932	0.58160913
PIR_SUPERFAMILY	PIRSF005552:guanine nucleotide-binding protein 1	3	0.69767442	0.00711749	142	7	7396	22.3219316	0.65255742	0.23224835
GOTERM_MF_FAT	GO:0046914~transition metal ion binding	81	18.8372093	0.00731476	291	2785	12983	1.29760314	0.96610527	0.57092515
GOTERM_BP_FAT	GO:0045087~innate immune response	9	2.09302326	0.00798828	281	138	13528	3.1397184	0.99999873	0.37388614
GOTERM_MF_FAT	GO:0008270~zinc ion binding	69	16.0465116	0.00830259	291	2311	12983	1.33208278	0.97858086	0.53638187
INTERPRO	IPR018957:Zinc finger, C3HC4 RING-type	12	2.79069767	0.00831643	347	228	16659	2.52677082	0.99421618	0.57632217
INTERPRO	IPR003191:Guanylate-binding protein, C-terminal	3	0.69767442	0.00843027	347	7	16659	20.5751338	0.99461171	0.52584362
INTERPRO	IPR000340:Dual specificity phosphatase, catalytic domain	5	1.1627907	0.00848377	347	39	16659	6.15495456	0.99478814	0.48164882
INTERPRO	IPR019787:Zinc finger, PHD-finger	7	1.62790698	0.0085032	347	85	16659	3.95365316	0.99485076	0.44313592
GOTERM_BP_FAT	GO:0042742~defense response to bacterium	8	1.86046512	0.00863897	281	112	13528	3.4387392	0.99999958	0.38715557
GOTERM_BP_FAT	GO:0010629~negative regulation of gene expression	20	4.65116279	0.00873534	281	504	13528	1.91041066	0.99999965	0.38069532
SP_PIR_KEYWORDS	metal-binding	81	18.8372093	0.00909267	403	2972	19235	1.30083843	0.94719932	0.30764323
UP_SEQ_FEATURE	domain:Rhodanese	4	0.93023256	0.00920732	402	21	19113	9.05614783	0.99997486	0.92919345
BIOCARTA	h_il7Pathway:IL-7 Signal Transduction	4	0.93023256	0.00983068	49	14	1437	8.37900875	0.58899058	0.35889983
GOTERM_BP_FAT	GO:0006942~regulation of striated muscle contraction	4	0.93023256	0.0100961	281	22	13528	8.75315432	0.99999997	0.41541992
GOTERM_BP_FAT	GO:0045944~positive regulation of transcription from RNA polymerase II promoter	16	3.72093023	0.01039143	281	371	13528	2.07621989	0.99999998	0.41485824
INTERPRO	IPR019542:Enhancer of polycomb-like	3	0.69767442	0.01108693	347	8	16659	18.0032421	0.99897066	0.4973614
GOTERM_BP_FAT	GO:0006350~transcription	59	13.7209302	0.01172954	281	2101	13528	1.35192698	1	0.44429312
GOTERM_BP_FAT	GO:0045667~regulation of osteoblast differentiation	5	1.1627907	0.01176595	281	43	13528	5.59794753	1	0.43589261
SP_PIR_KEYWORDS	alternative splicing	180	41.8604651	0.01185776	403	7488	19235	1.14734444	0.97852826	0.3473927
UP_SEQ_FEATURE	repeat:TNFR-Cys 3	4	0.93023256	0.01188758	402	23	19113	8.26865672	0.99999887	0.93533698
INTERPRO	IPR011029:DEATH-like	6	1.39534884	0.01268068	347	67	16659	4.29928169	0.99961949	0.51120836
INTERPRO	IPR001763:Rhodanese-like	4	0.93023256	0.01301065	347	24	16659	8.00144092	0.99969041	0.49000495
GOTERM_BP_FAT	GO:0001817~regulation of cytokine production	10	2.3255814	0.01311895	281	181	13528	2.65979827	1	0.46261338
GOTERM_BP_FAT	GO:0052173~response to defenses of other organism during symbiotic interaction	3	0.69767442	0.0139605	281	9	13528	16.0474496	1	0.47443837
GOTERM_BP_FAT	GO:0052200~response to host defenses	3	0.69767442	0.0139605	281	9	13528	16.0474496	1	0.47443837
GOTERM_BP_FAT	GO:0075136~response to host	3	0.69767442	0.0139605	281	9	13528	16.0474496	1	0.47443837
GOTERM_CC_FAT	GO:0031410~cytoplasmic vesicle	21	4.88372093	0.01426702	235	642	12782	1.77916087	0.97748602	0.71763071
SP_PIR_KEYWORDS	Apoptosis	16	3.72093023	0.0145941	403	381	19235	2.00438965	0.99120813	0.37711464
GOTERM_BP_FAT	GO:0007623~circadian rhythm	5	1.1627907	0.01482863	281	46	13528	5.232864	1	0.4860358
UP_SEQ_FEATURE	repeat:TNFR-Cys 2	4	0.93023256	0.01497015	402	25	19113	7.60716418	0.99999997	0.9437755

Interferon induction inhibition by MV C - Appendix

Supplementary Data:

UP_SEQ_FEATURE	repeat:TNFR-Cys 1	4	0.93023256	0.014970 15	402	25	19113	7.60716418	0.99999997	0.9437755
GOTERM_BP_FAT	GO:0016481-negative regulation of transcription	18	4.18604651	0.014974 5	281	459	13528	1.88793525	1	0.48053887
UP_SEQ_FEATURE	splice variant	179	41.627907	0.015235 19	402	745 8	19113	1.14112563	0.99999998	0.91883092
GOTERM_CC_FAT	GO:0000323-lytic vacuole	10	2.3255814	0.015731 82	235	211	12782	2.5777957	0.98479631	0.64885438
GOTERM_CC_FAT	GO:0005764-lysosome	10	2.3255814	0.015731 82	235	211	12782	2.5777957	0.98479631	0.64885438
GOTERM_BP_FAT	GO:0042110-T cell activation	8	1.86046512	0.015811 38	281	126	13528	3.05665706	1	0.49062149
GOTERM_MF_FAT	GO:0008138-protein tyrosine/serine/threonine phosphatase activity	5	1.1627907	0.016422 68	291	44	12983	5.06990003	0.99951614	0.71980944
KEGG_PATHWAY	hsa05220:Chronic myeloid leukemia	6	1.39534884	0.016761 52	103	75	5085	3.94951456	0.80920413	0.15266158
KEGG_PATHWAY	hsa04010:MAPK signaling pathway	12	2.79069767	0.017257 93	103	267	5085	2.21882841	0.81841677	0.14366588
INTERPRO	IPR008343:MAP kinase phosphatase	3	0.69767442	0.017336 41	347	10	16659	14.4025937	0.9999794	0.56396306
GOTERM_CC_FAT	GO:0005773-vacuole	11	2.55813953	0.017758 04	235	252	12782	2.37423168	0.99117572	0.6117282
SP_PIR_KEYWORDS	transcription regulation	57	13.255814	0.017829 29	403	202 6	19235	1.34283471	0.99695065	0.4094026
GOTERM_BP_FAT	GO:0007242-intracellular signaling cascade	38	8.8372093	0.017862 53	281	125 6	13528	1.45653603	1	0.52491367
GOTERM_MF_FAT	GO:0046332-SMAD binding	5	1.1627907	0.019072 35	291	46	12983	4.8494696	0.99986048	0.71865755
GOTERM_BP_FAT	GO:0009617-response to bacterium	10	2.3255814	0.019152 88	281	193	13528	2.49442222	1	0.54137975
GOTERM_BP_FAT	GO:0010558-negative regulation of macromolecule biosynthetic process	20	4.65116279	0.019183 19	281	547	13528	1.76023213	1	0.53355753
GOTERM_CC_FAT	GO:0043235-receptor complex	7	1.62790698	0.019772 6	235	116	12782	3.28224505	0.99486802	0.58468189
GOTERM_BP_FAT	GO:0009967-positive regulation of signal transduction	13	3.02325581	0.020105 08	281	295	13528	2.12152723	1	0.54226781
GOTERM_BP_FAT	GO:0045934-negative regulation of nucleobase, nucleoside, nucleotide and nucleic acid metabolic process	19	4.41860465	0.020186 42	281	512	13528	1.78653247	1	0.53570164
UP_SEQ_FEATURE	domain:Bromo	4	0.93023256	0.020362 64	402	28	19113	6.79211087	1	0.9473708
UP_SEQ_FEATURE	DNA-binding region:Basic motif	9	2.09302326	0.020524 5	402	161	19113	2.65778252	1	0.92852026
INTERPRO	IPR010919:SAND-like	3	0.69767442	0.020901 22	347	11	16659	13.093267	0.99999781	0.60580497
INTERPRO	IPR015894:Guanylate-binding protein, N-terminal	3	0.69767442	0.020901 22	347	11	16659	13.093267	0.99999781	0.60580497
GOTERM_BP_FAT	GO:0045893-positive regulation of transcription, DNA-dependent	18	4.18604651	0.020953 28	281	477	13528	1.81669241	1	0.54130319
GOTERM_CC_FAT	GO:0031982-vesicle	21	4.88372093	0.021559 55	235	670	12782	1.70480788	0.99682984	0.56044664
SMART	SM00450:RHOD	4	0.93023256	0.021687 76	230	24	9079	6.57898551	0.97256482	0.83436432
INTERPRO	IPR001315:Caspase Recruitment	4	0.93023256	0.021770 71	347	29	16659	6.62188214	0.99999874	0.59561721
GOTERM_BP_FAT	GO:0051254-positive regulation of RNA metabolic process	18	4.18604651	0.022855 71	281	481	13528	1.80158478	1	0.56518998
GOTERM_BP_FAT	GO:0051172-negative regulation of nitrogen compound metabolic process	19	4.41860465	0.022906 71	281	519	13528	1.76243666	1	0.55838223
GOTERM_BP_FAT	GO:0030500-regulation of bone mineralization	4	0.93023256	0.023584 41	281	30	13528	6.41897983	1	0.56160209
GOTERM_BP_FAT	GO:0043281-regulation of caspase activity	6	1.39534884	0.023855 74	281	79	13528	3.65638092	1	0.55848633
INTERPRO	IPR004827:Basic-leucine zipper (bZIP) transcription factor	5	1.1627907	0.024115 85	347	53	16659	4.5291175	0.99999971	0.60990483
GOTERM_BP_FAT	GO:0031327-negative regulation of cellular biosynthetic process	20	4.65116279	0.024164 31	281	561	13528	1.71630477	1	0.55603579
UP_SEQ_FEATURE	zinc finger region:C3H1-type 2	4	0.93023256	0.024474 6	402	30	19113	6.33930348	1	0.94141082
UP_SEQ_FEATURE	zinc finger region:C3H1-type 1	4	0.93023256	0.024474 6	402	30	19113	6.33930348	1	0.94141082
INTERPRO	IPR016129:Peptidase C14, ICE, catalytic subunit p20, active site	3	0.69767442	0.024741 49	347	12	16659	12.0021614	0.99999981	0.59718017
INTERPRO	IPR006011:Syntaxin, N-terminal	3	0.69767442	0.024741 49	347	12	16659	12.0021614	0.99999981	0.59718017
INTERPRO	IPR002138:Peptidase C14, caspase non-catalytic subunit p10	3	0.69767442	0.024741 49	347	12	16659	12.0021614	0.99999981	0.59718017
SP_PIR_KEYWORDS	coiled coil	56	13.0232558	0.024840 5	403	201 9	19235	1.32385022	0.99969636	0.49082929
INTERPRO	IPR011616:bZIP transcription factor, bZIP-1	4	0.93023256	0.025983 15	347	31	16659	6.19466394	0.99999991	0.59441305
SP_PIR_KEYWORDS	Transcription	57	13.255814	0.026281 39	403	207 1	19235	1.31365675	0.99981138	0.48298171
GOTERM_MF_FAT	GO:0030528-transcription regulator activity	46	10.6976744	0.026889 68	291	151 2	12983	1.35733832	0.99999651	0.79210699
KEGG_PATHWAY	hsa04710:Circadian rhythm	3	0.69767442	0.026911 3	103	13	5085	11.3928305	0.93098586	0.1997147
GOTERM_BP_FAT	GO:0052548-regulation of endopeptidase activity	6	1.39534884	0.027491 26	281	82	13528	3.52261088	1	0.59650255
GOTERM_BP_FAT	GO:0070167-regulation of biomineral formation	4	0.93023256	0.027958 89	281	32	13528	6.01779359	1	0.59579161
UP_SEQ_FEATURE	short sequence motif:SH3-binding	5	1.1627907	0.028124 88	402	55	19113	4.32225237	1	0.94867107
UP_SEQ_FEATURE	domain:Leucine-zipper	7	1.62790698	0.028452 09	402	110	19113	3.02557666	1	0.93633837
GOTERM_CC_FAT	GO:0030054-cell junction	17	3.95348837	0.028528 3	235	518	12782	1.78504888	0.99951965	0.61523543
UP_SEQ_FEATURE	compositionally biased region:Asp-rich	4	0.93023256	0.029000	402	32	19113	5.94309701	1	0.92513141



Interferon induction inhibition by MV C - Appendix

Supplementary Data:

GOTERM_CC_FAT	GO:0005924~cell-substrate adherens junction	6	1.39534884	0.04511645	235	106	12782	3.07876355	0.99999491	0.63783285
INTERPRO	IPR001841:Zinc finger, RING-type	12	2.79069767	0.04583251	347	296	16659	1.94629644	1	0.64435733
GOTERM_BP_FAT	GO:0045941~positive regulation of transcription	19	4.41860465	0.0458876	281	564	13528	1.62181671	1	0.71136829
GOTERM_CC_FAT	GO:0016023~cytoplasmic membrane-bounded vesicle	17	3.95348837	0.04624783	235	550	12782	1.68119149	0.99999628	0.6177185
GOTERM_MF_FAT	GO:0008509~anion transmembrane transporter activity	8	1.86046512	0.046895	291	147	12983	2.42803376	1	0.86639964
GOTERM_BP_FAT	GO:0031328~positive regulation of cellular biosynthetic process	22	5.11627907	0.04704476	281	685	13528	1.54617762	1	0.71495123
SMART	SM00115:CA5c	3	0.69767442	0.04722436	230	14	9079	8.45869565	0.99964152	0.73347109
GOTERM_BP_FAT	GO:0035195~gene silencing by miRNA	3	0.69767442	0.04732248	281	17	13528	8.4957086	1	0.71164272
SP_PIR_KEYWORDS	bromodomain	4	0.93023256	0.0475884	403	39	19235	4.89533626	0.99999985	0.5623429
INTERPRO	IPR006012:Syntaxin/epimorphin, conserved site	3	0.69767442	0.04763707	347	17	16659	8.47211392	1	0.64599898
GOTERM_MF_FAT	GO:0005247~voltage-gated chloride channel activity	3	0.69767442	0.04855701	291	16	12983	8.36533505	1	0.8522464
GOTERM_MF_FAT	GO:0008656~caspase activator activity	3	0.69767442	0.04855701	291	16	12983	8.36533505	1	0.8522464
SMART	SM00208:TNFR	4	0.93023256	0.04960441	230	33	9079	4.78471673	0.99976214	0.69637888
SP_PIR_KEYWORDS	GTPase activation	8	1.86046512	0.04986304	403	159	19235	2.40148571	0.99999993	0.56110761
INTERPRO	IPR001487:Bromodomain	4	0.93023256	0.04988334	347	40	16659	4.80086455	1	0.65090345
INTERPRO	IPR013655:PAS fold-3	3	0.69767442	0.05287307	347	18	16659	8.00144092	1	0.66080705
GOTERM_BP_FAT	GO:0007264~small GTPase mediated signal transduction	12	2.79069767	0.05294172	281	305	13528	1.8941252	1	0.74702878
GOTERM_BP_FAT	GO:0010557~positive regulation of macromolecule biosynthetic process	21	4.88372093	0.05309218	281	654	13528	1.54585524	1	0.74288258
GOTERM_BP_FAT	GO:0009891~positive regulation of biosynthetic process	22	5.11627907	0.05328257	281	695	13528	1.52393046	1	0.73906185
SMART	SM00276:GLECT	3	0.69767442	0.05360386	230	15	9079	7.89478261	0.99988089	0.67678186
UP_SEQ_FEATURE	compositionally biased region:Poly-Pro	15	3.48837209	0.05414333	402	413	19113	1.72680785	1	0.97646224
GOTERM_MF_FAT	GO:0005160~transforming growth factor beta receptor binding	3	0.69767442	0.05423849	291	17	12983	7.87325652	1	0.86158616
GOTERM_BP_FAT	GO:0051241~negative regulation of multicellular organismal process	8	1.86046512	0.05439736	281	164	13528	2.34840726	1	0.74147834
GOTERM_CC_FAT	GO:0030055~cell-substrate junction	6	1.39534884	0.05479877	235	112	12782	2.91382979	0.99999965	0.65449222
GOTERM_BP_FAT	GO:0019221~cytokine-mediated signaling pathway	5	1.1627907	0.05697396	281	70	13528	3.4387392	1	0.75310316
SP_PIR_KEYWORDS	cytoplasm	83	19.3023256	0.05923926	403	333	19235	1.18894084	1	0.60794451
UP_SEQ_FEATURE	domain:PAS 1	3	0.69767442	0.05936651	402	19	19113	7.50706991	1	0.97961811
UP_SEQ_FEATURE	domain:PAS 2	3	0.69767442	0.05936651	402	19	19113	7.50706991	1	0.97961811
GOTERM_CC_FAT	GO:0005911~cell-cell junction	8	1.86046512	0.06064448	235	190	12782	2.29016797	0.99999993	0.66748756
GOTERM_MF_FAT	GO:0046983~protein dimerization activity	19	4.41860465	0.06066844	291	542	12983	1.56399868	1	0.87265977
GOTERM_BP_FAT	GO:0045343~regulation of MHC class I biosynthetic process	2	0.46511628	0.06082151	281	3	13528	32.0948992	1	0.77133339
INTERPRO	IPR012852:Coiled-coil transcriptional coactivator-like	2	0.46511628	0.06102709	347	3	16659	32.0057637	1	0.70302704
INTERPRO	IPR015479:Transcription factor AF4	2	0.46511628	0.06102709	347	3	16659	32.0057637	1	0.70302704
INTERPRO	IPR007651:Lipin, N-terminal conserved region	2	0.46511628	0.06102709	347	3	16659	32.0057637	1	0.70302704
UP_SEQ_FEATURE	region of interest:N-LIP	2	0.46511628	0.0616333	402	3	19113	31.6965174	1	0.97836859
UP_SEQ_FEATURE	region of interest:Intramolecular interaction with C- terminus	2	0.46511628	0.0616333	402	3	19113	31.6965174	1	0.97836859
UP_SEQ_FEATURE	region of interest:Intramolecular interaction with N- terminus	2	0.46511628	0.0616333	402	3	19113	31.6965174	1	0.97836859
UP_SEQ_FEATURE	short sequence motif:DXDXT motif	2	0.46511628	0.0616333	402	3	19113	31.6965174	1	0.97836859
UP_SEQ_FEATURE	region of interest:C-LIP	2	0.46511628	0.0616333	402	3	19113	31.6965174	1	0.97836859
GOTERM_BP_FAT	GO:0006937~regulation of muscle contraction	5	1.1627907	0.06195503	281	72	13528	3.34321866	1	0.77310907
UP_SEQ_FEATURE	active site:Proton acceptor	21	4.88372093	0.06218865	402	658	19113	1.51738647	1	0.97467139
GOTERM_MF_FAT	GO:0004715~non-membrane spanning protein tyrosine kinase activity	4	0.93023256	0.06312491	291	41	12983	4.35269466	1	0.86520183
GOTERM_BP_FAT	GO:0051607~defense response to virus	3	0.69767442	0.0635045	281	20	13528	7.22135231	1	0.77710698
INTERPRO	IPR002398:Peptidase C14, caspase precursor p45	3	0.69767442	0.063915	347	20	16659	7.20129683	1	0.70914082
GOTERM_CC_FAT	GO:0005768~endosome	11	2.55813953	0.06417745	235	315	12782	1.89938534	0.99999998	0.66527138
GOTERM_BP_FAT	GO:0031349~positive regulation of defense response	5	1.1627907	0.06452912	281	73	13528	3.29742115	1	0.77815142
SP_PIR_KEYWORDS	biological rhythms	3	0.69767442	0.06463196	403	20	19235	7.15942928	1	0.62391179
UP_SEQ_FEATURE	zinc finger region:C3H1-type 3	3	0.69767442	0.06507224	402	20	19113	7.13171642	1	0.97449013
GOTERM_MF_FAT	GO:0015297~antiporter activity	5	1.1627907	0.06539294	291	68	12983	3.28052355	1	0.85752138

Interferon induction inhibition by MV C - Appendix

Supplementary Data:

GOTERM_CC_FAT	GO:0005912~adherens junction	7	1.62790698	0.065463	235	155	12782	2.45638984	0.99999998	0.65055332
GOTERM_CC_FAT	GO:0005637~nuclear inner membrane	3	0.69767442	0.065637	235	23	12782	7.09454209	0.99999998	0.63054937
GOTERM_BP_FAT	GO:0051240~positive regulation of multicellular organismal process	10	2.3255814	0.066794	281	244	13528	1.97304708	1	0.78561011
GOTERM_BP_FAT	GO:0045892~negative regulation of transcription, DNA-dependent	13	3.02325581	0.067152	281	356	13528	1.75800712	1	0.78311477
KEGG_PATHWAY	hsa04520:Adherens junction	5	1.1627907	0.067957	103	77	5085	3.20577481	0.99898911	0.41170837
GOTERM_MF_FAT	GO:0003700~transcription factor activity	30	6.97674419	0.069156	291	975	12983	1.37277293	1	0.85677927
GOTERM_BP_FAT	GO:0042752~regulation of circadian rhythm	3	0.69767442	0.069257	281	21	13528	6.87747839	1	0.78940734
GOTERM_BP_FAT	GO:0030101~natural killer cell activation	3	0.69767442	0.069257	281	21	13528	6.87747839	1	0.78940734
GOTERM_BP_FAT	GO:0016441~posttranscriptional gene silencing	3	0.69767442	0.069257	281	21	13528	6.87747839	1	0.78940734
GOTERM_BP_FAT	GO:0035194~posttranscriptional gene silencing by RNA	3	0.69767442	0.069257	281	21	13528	6.87747839	1	0.78940734
SP_PIR_KEYWORDS	chromosomal rearrangement	11	2.55813953	0.069302	403	279	19235	1.88180937	1	0.63413611
GOTERM_BP_FAT	GO:0002274~myeloid leukocyte activation	4	0.93023256	0.069458	281	46	13528	4.1862912	1	0.78620466
SP_PIR_KEYWORDS	Aminotransferase	3	0.69767442	0.070476	403	21	19235	6.81850408	1	0.62488758
UP_SEQ_FEATURE	domain:Protein kinase	16	3.72093023	0.070591	402	469	19113	1.62199663	1	0.97785395
SP_PIR_KEYWORDS	chloride	5	1.1627907	0.071982	403	75	19235	3.18196857	1	0.61794526
SP_PIR_KEYWORDS	isopeptide bond	12	2.79069767	0.072808	403	319	19235	1.79546816	1	0.6078928
GOTERM_MF_FAT	GO:0008047~enzyme activator activity	13	3.02325581	0.073237	291	335	12983	1.73133303	1	0.85743005
GOTERM_BP_FAT	GO:0051253~negative regulation of RNA metabolic process	13	3.02325581	0.073967	281	362	13528	1.72886888	1	0.80333658
PIR_SUPERFAMILY	PIRSF023976:PIRSF023976	2	0.46511628	0.074118	142	4	7396	26.0422535	0.99998878	0.85036663
INTERPRO	IPRO13320:Concanavalin A-like lectin/glucanase, subgroup	5	1.1627907	0.076227	347	77	16659	3.11744452	1	0.76280496
SMART	SM00249:PHD	6	1.39534884	0.076769	230	90	9079	2.6315942	0.99999795	0.76672153
GOTERM_BP_FAT	GO:0032582~negative regulation of gene-specific transcription	4	0.93023256	0.076838	281	48	13528	4.0118624	1	0.81195534
GOTERM_BP_FAT	GO:0042108~positive regulation of cytokine biosynthetic process	4	0.93023256	0.076838	281	48	13528	4.0118624	1	0.81195534
UP_SEQ_FEATURE	domain:t-SNARE coiled-coil homology	3	0.69767442	0.076998	402	22	19113	6.48337856	1	0.98147788
GOTERM_BP_FAT	GO:0051173~positive regulation of nitrogen compound metabolic process	20	4.65116279	0.077053	281	644	13528	1.495104	1	0.80900051
GOTERM_MF_FAT	GO:0005254~chloride channel activity	5	1.1627907	0.077221	291	72	12983	3.09827224	1	0.85771779
GOTERM_CC_FAT	GO:0005794~Golgi apparatus	23	5.34883721	0.078327	235	872	12782	1.43463791	1	0.67803979
GOTERM_MF_FAT	GO:0008483~transaminase activity	3	0.69767442	0.079050	291	21	12983	6.37358861	1	0.85015697
GOTERM_MF_FAT	GO:0005484~SNAP receptor activity	3	0.69767442	0.079050	291	21	12983	6.37358861	1	0.85015697
SMART	SM00297:BROMO	4	0.93023256	0.079163	230	40	9079	3.9473913	0.99999866	0.74142113
GOTERM_BP_FAT	GO:0045776~negative regulation of blood pressure	3	0.69767442	0.081243	281	23	13528	6.27943679	1	0.82242761
GOTERM_BP_FAT	GO:0010604~positive regulation of macromolecule metabolic process	25	5.81395349	0.081296	281	857	13528	1.4043859	1	0.81894626
UP_SEQ_FEATURE	short sequence motif:LXXIL motif	2	0.46511628	0.081323	402	4	19113	23.7723881	1	0.98251994
UP_SEQ_FEATURE	short sequence motif:Nuclear localization signal	12	2.79069767	0.082159	402	325	19113	1.75549943	1	0.98028785
GOTERM_CC_FAT	GO:0005770~late endosome	4	0.93023256	0.082873	235	56	12782	3.88510638	1	0.68079805
GOTERM_CC_FAT	GO:0005635~nuclear envelope	8	1.86046512	0.082993	235	205	12782	2.12259471	1	0.66351144
SP_PIR_KEYWORDS	glycosidase	5	1.1627907	0.083542	403	79	19235	3.02085624	1	0.6466907
GOTERM_MF_FAT	GO:0008308~voltage-gated anion channel activity	3	0.69767442	0.085715	291	22	12983	6.08388004	1	0.86015471
KEGG_PATHWAY	hsa05210:Colorectal cancer	5	1.1627907	0.087333	103	84	5085	2.93862691	0.999871	0.4725468
GOTERM_BP_FAT	GO:0051223~regulation of protein transport	6	1.39534884	0.087912	281	114	13528	2.53380783	1	0.84003559
GOTERM_BP_FAT	GO:0001503~ossification	6	1.39534884	0.090442	281	115	13528	2.51177472	1	0.84528604
PIR_SUPERFAMILY	PIRSF016017:PIRSF016017	2	0.46511628	0.091779	142	5	7396	20.8338028	0.99999935	0.86937041
GOTERM_CC_FAT	GO:0009897~external side of plasma membrane	7	1.62790698	0.092359	235	170	12782	2.23964956	1	0.68741608
GOTERM_MF_FAT	GO:0016504~peptidase activator activity	3	0.69767442	0.092541	291	23	12983	5.81936351	1	0.86930015
INTERPRO	IPRO00571:Zinc finger, CCCH-type	4	0.93023256	0.093372	347	52	16659	3.69297273	1	0.82236305
GOTERM_MF_FAT	GO:0031404~chloride ion binding	5	1.1627907	0.093400	291	77	12983	2.89708573	1	0.85989314
INTERPRO	IPRO17441:Protein kinase, ATP binding site	15	3.48837209	0.093586	347	455	16659	1.5827026	1	0.81438017
GOTERM_BP_FAT	GO:0045669~positive regulation of osteoblast differentiation	3	0.69767442	0.093811	281	25	13528	5.77708185	1	0.85294408
UP_SEQ_FEATURE	zinc finger region:PHD-type	4	0.93023256	0.095577	402	52	19113	3.65729047	1	0.98801444
GOTERM_CC_FAT	GO:0070161~anchoring junction	7	1.62790698	0.096360	235	172	12782	2.21360713	1	0.68746288

Supplementary Data:

				48						
KEGG_PATHWAY	hsa04350:TGF-beta signaling pathway	5	1.1627907	0.0963786	103	87	5085	2.83729494	0.9999514	0.48424295
GOTERM_MF_FAT	GO:0005253--anion channel activity	5	1.1627907	0.09681501	291	78	12983	2.85994361	1	0.85856908
GOTERM_BP_FAT	GO:0045935--positive regulation of nucleobase, nucleoside, nucleotide and nucleic acid metabolic process	19	4.41860465	0.09746835	281	624	13528	1.4658728	1	0.86095413
SP_PIR_KEYWORDS	immune response	9	2.09302326	0.09871792	403	224	19235	1.91770427	1	0.69737942
UP_SEQ_FEATURE	compositionally biased region:Poly-Gln	7	1.62790698	0.09880019	402	151	19113	2.20406247	1	0.98786389
GOTERM_BP_FAT	GO:0007167--enzyme linked receptor protein signaling pathway	12	2.79069767	0.09910167	281	342	13528	1.68920522	1	0.86265232
GOTERM_BP_FAT	GO:0052555--positive regulation by organism of immune response of other organism during symbiotic interaction	2	0.46511628	0.0993069	281	5	13528	19.2569395	1	0.86018948
GOTERM_BP_FAT	GO:0052556--positive regulation by symbiont of host immune response	2	0.46511628	0.0993069	281	5	13528	19.2569395	1	0.86018948
GOTERM_BP_FAT	GO:0052305--positive regulation by organism of innate immunity in other organism during symbiotic interaction	2	0.46511628	0.0993069	281	5	13528	19.2569395	1	0.86018948
GOTERM_BP_FAT	GO:0052166--positive regulation by symbiont of host innate immunity	2	0.46511628	0.0993069	281	5	13528	19.2569395	1	0.86018948
GOTERM_BP_FAT	GO:0002282--microglial cell activation during immune response	2	0.46511628	0.0993069	281	5	13528	19.2569395	1	0.86018948
GOTERM_BP_FAT	GO:0052306--modulation by organism of innate immunity in other organism during symbiotic interaction	2	0.46511628	0.0993069	281	5	13528	19.2569395	1	0.86018948
GOTERM_BP_FAT	GO:0052552--modulation by organism of immune response of other organism during symbiotic interaction	2	0.46511628	0.0993069	281	5	13528	19.2569395	1	0.86018948
GOTERM_BP_FAT	GO:0052553--modulation by symbiont of host immune response	2	0.46511628	0.0993069	281	5	13528	19.2569395	1	0.86018948
GOTERM_BP_FAT	GO:0052167--modulation by symbiont of host innate immunity	2	0.46511628	0.0993069	281	5	13528	19.2569395	1	0.86018948
GOTERM_BP_FAT	GO:0045988--negative regulation of striated muscle contraction	2	0.46511628	0.0993069	281	5	13528	19.2569395	1	0.86018948
INTERPRO	IPR005814:Aminotransferase class-III	2	0.46511628	0.09963416	347	5	16659	19.2034582	1	0.82625745
INTERPRO	IPR007797:AF-4 proto-oncoprotein	2	0.46511628	0.09963416	347	5	16659	19.2034582	1	0.82625745
INTERPRO	IPR004865:Sp100	2	0.46511628	0.09963416	347	5	16659	19.2034582	1	0.82625745

App. 5: Individual Massspectrometry data:

All data is presented as 80% protein identification probability:

Experiment I:

#	Bio View:Identified Proteins (290)	Accession Number	Molecular Weight	Protein Grouping Ambiguity	Mock	MVCwt
49	26S proteasome subunit p97 [Homo sapiens]	gi 1060888 (+3)	100 kDa		0	11
55	solute carrier family 25 (mitochondrial carrier; adenine nucleotide translocator), member 5, isoform CRA_b [Homo sapiens]	gi 119610275 (+3)	28 kDa		0	9
56	filamin-A isoform 1 [Homo sapiens]	gi 116063573 (+3)	280 kDa		0	14
59	unnamed protein product [Homo sapiens]	gi 189054540 (+1)	113 kDa		0	8
66	Chain B, Structural Basis Of The Interaction Of Rbap46RBAP48 WITH Histone H4	gi 190016327 (+6)	47 kDa	true	0	3
71	proteasome 26S ATPase subunit 2 [Homo sapiens]	gi 4506209 (+1)	49 kDa		0	8
79	Proteasome (prosome, macropain) 26S subunit, non-ATPase, 3 [Homo sapiens]	gi 15126760 (+8)	61 kDa		0	9
80	26S proteasome non-ATPase regulatory subunit 6 [Homo sapiens]	gi 7661914	46 kDa		0	8
85	26S proteasome non-ATPase regulatory subunit 12 isoform 2 [Homo sapiens]	gi 28872765 (+3)	51 kDa		0	7
86	proteasome (prosome, macropain) 26S subunit, ATPase, 1, isoform CRA_b [Homo sapiens]	gi 119601826 (+5)	45 kDa		0	7
88	microtubule-associated protein 1B [Homo sapiens]	gi 153945728 (+1)	271 kDa		0	26
93	26S protease regulatory subunit 6B isoform 1 [Homo sapiens]	gi 5729991 (+1)	47 kDa		0	7
98	PREDICTED: proteasome binding 26S non-ATPase subunit 13 isoform 3 [Pan troglodytes]	gi 114635315 (+7)	43 kDa		0	5
101	thyroid receptor interactor [Homo sapiens]	gi 695370 (+3)	46 kDa		0	7
103	lactotransferrin [Homo sapiens]	gi 119585171 (+19)	78 kDa		0	5
112	ATPase, Ca++ transporting, cardiac muscle, slow twitch 2, isoform CRA_a [Homo sapiens]	gi 119618308 (+5)	101 kDa		0	4
113	proteasome subunit p112 [Homo sapiens]	gi 1808578 (+2)	106 kDa		0	5
126	proteasome subunit p42 [Homo sapiens]	gi 1526426 (+2)	44 kDa		0	5
133	insulin receptor substrate 4 [Homo sapiens]	gi 4504733	134 kDa		0	4
139	unnamed protein product [Homo sapiens]	gi 21754583 (+1)	48 kDa	true	0	41
140	unnamed protein product [Homo sapiens]	gi 193787479 (+4)	53 kDa		0	3
143	unnamed protein product [Homo sapiens]	gi 189067539 (+4)	37 kDa		0	4
145	unnamed protein product [Homo sapiens]	gi 158257224 (+6)	47 kDa		0	3
154	ribosomal protein S4, X-linked, isoform CRA_a [Homo sapiens]	gi 119592221 (+5)	43 kDa		0	3
155	RANBP8 [Homo sapiens]	gi 2337918 (+1)	120 kDa		0	4
175	proteasome 26S non-ATPase subunit 8 [Homo sapiens]	gi 156631005 (+2)	40 kDa		0	3
179	damage-specific DNA binding protein 1, 127kDa, isoform CRA_a [Homo sapiens]	gi 119594339 (+4)	121 kDa		0	3
182	myosin VI, isoform CRA_b [Homo sapiens]	gi 119569114 (+6)	147 kDa		0	2
183	Unknown (protein for IMAGE:2901253) [Homo sapiens]	gi 13111809 (+4)	35 kDa		0	4
195	t-complex polypeptide 1 [Homo sapiens]	gi 36796 (+1)	60 kDa		0	3
196	unnamed protein product [Homo sapiens]	gi 194390656 (+3)	35 kDa		0	1

Interferon induction inhibition by MV C - Appendix

Supplementary Data:

203	unnamed protein product [Homo sapiens]	gi 194383294 (+1)	52 kDa	true	0	4
205	Phosphoglycerate mutase family member 5 [Homo sapiens]	gi 14198272 (+1)	28 kDa		0	3
210	RecName: Full=OTU domain-containing protein 4; AltName: Full=HIV-1-induced protein HIN-1	gi 118572680	124 kDa		0	2
211	Chain A, Crystal Structure Of The Heterodimeric Complex Of Human Rgs10 And Activated Gi Alpha 3	gi 119390147 (+2)	37 kDa		0	3
214	unnamed protein product [Homo sapiens]	gi 34527290	53 kDa	true	0	2
215	lipocalin-1 precursor [Homo sapiens]	gi 4504963 (+1)	19 kDa		0	2
216	PREDICTED: similar to protein kinase, DNA-activated, catalytic polypeptide [Homo sapiens]	gi 113430845 (+5)	465 kDa		0	8
217	angiomotin isoform 1 [Homo sapiens]	gi 166064029	118 kDa		0	2
218	unnamed protein product [Homo sapiens]	gi 158259511 (+4)	36 kDa		0	3
219	hCG2027326 [Homo sapiens]	gi 119611832 (+2)	10 kDa		0	3
220	ribosomal protein S20 isoform 1 [Homo sapiens]	gi 226246671 (+1)	16 kDa		0	3
221	solute carrier family 16, member 1 [Homo sapiens]	gi 115583685 (+2)	54 kDa	true	0	3
224	proteasome (prosome, macropain) 26S subunit, non-ATPase, 4 [Homo sapiens]	gi 150439371 (+4)	22 kDa		0	2
233	solute carrier family 25 (mitochondrial carrier; phosphate carrier), member 3, isoform CRA_c [Homo sapiens]	gi 119618006 (+6)	26 kDa		0	2
235	emerin [Homo sapiens]	gi 4557553 (+1)	29 kDa		0	2
241	chromosome 13 open reading frame 7, isoform CRA_b [Homo sapiens]	gi 119600993 (+1)	81 kDa		0	2
242	clathrin, heavy polypeptide (Hc), isoform CRA_c [Homo sapiens]	gi 119614803 (+5)	192 kDa		0	2
245	unnamed protein product [Homo sapiens]	gi 158260761 (+1)	28 kDa		0	3
251	Chain A, Structural Changes Of The Active Site Cleft And Different Saccharide Binding Modes In Human Lysozyme Co-Crystallized With Hexa-N-Acetyl-Chitohexaose At Ph 4.0	gi 1065033 (+130)	15 kDa		0	1
256	PREDICTED: similar to cleavage and polyadenylation specific factor 6, 68 kD subunit [Macaca mulatta]	gi 109097742 (+6)	63 kDa		0	1
257	Chain A, Crystal Structure Of Human Cleavage And Polyadenylation Specificity Factor 5 (Cpsf5)	gi 109157347 (+6)	27 kDa		0	2
262	transmembrane protein [Homo sapiens]	gi 1160963 (+10)	84 kDa		0	1
263	desmoglein-2 preproprotein [Homo sapiens]	gi 116534898 (+1)	122 kDa		0	1
265	ribosomal protein L18, isoform CRA_b [Homo sapiens]	gi 119572744 (+4)	19 kDa		0	2
271	coatomer protein complex, subunit beta 2 (beta prime), isoform CRA_b [Homo sapiens]	gi 119599446 (+1)	99 kDa		0	1
272	chromosome 13 open reading frame 10, isoform CRA_c [Homo sapiens]	gi 119600999 (+5)	112 kDa		0	1
275	chromosome 1 open reading frame 27, isoform CRA_b [Homo sapiens]	gi 119611614 (+3)	40 kDa		0	1
276	importin 9, isoform CRA_a [Homo sapiens]	gi 119611781 (+5)	112 kDa		0	1
277	leucine zipper protein 1, isoform CRA_a [Homo sapiens]	gi 119615440 (+5)	120 kDa		0	1
279	Chaperonin containing TCP1, subunit 3 (gamma) [Homo sapiens]	gi 14124984 (+9)	60 kDa		0	1
281	Chain A, Phosphorylation Independent Interactions Between 14-3-3 And Exoenzyme S: From Structure To Pathogenesis	gi 161172138 (+5)	26 kDa		0	2
282	apoptosis-inducing factor 1, mitochondrial isoform 5 [Homo sapiens]	gi 195927006 (+4)	35 kDa		0	1
283	glyceraldehyde-3-phosphate dehydrogenase [Homo sapiens]	gi 31645 (+7)	36 kDa		0	2
285	filaggrin family member 2 [Homo sapiens]	gi 62122917	248 kDa		0	2
288	protein phosphatase 1, regulatory (inhibitor) subunit 12A, isoform CRA_a [Homo sapiens]	gi 119617757 (+11)	102 kDa		0	1
73	Chain A, Crystal Structure Of The 9-10 8 Glycine Insertion Mutant Of Ubiquitin.	gi 109157803 (+26)	9 kDa		1	10
97	beta-tubulin [Homo sapiens]	gi 338695 (+1)	50 kDa	true	3	28
32	unnamed protein product [Homo sapiens]	gi 158259731 (+3)	50 kDa		3	18
90	MYL6 protein [Homo sapiens]	gi 113812151 (+4)	16 kDa		1	6
105	heat shock 60kDa protein 1 (chaperonin), isoform CRA_c [Homo sapiens]	gi 119590557 (+5)	41 kDa		1	5
118	capping protein (actin filament) muscle Z-line, beta, isoform CRA_b [Homo sapiens]	gi 119615295 (+6)	30 kDa		1	5
19	tubulin, beta 2C, isoform CRA_b [Homo sapiens]	gi 119608775 (+4)	49 kDa	true	7	26
31	heat shock 70 kDa protein 1A/1B [Homo sapiens]	gi 167466173 (+4)	70 kDa	true	6	22
4	WD repeat domain 77 [Homo sapiens]	gi 13129110 (+2)	37 kDa		50	183
84	spindlin-1 [Homo sapiens]	gi 112293285 (+3)	30 kDa		2	7
77	BTB/POZ domain-containing protein KCTD5 [Homo sapiens]	gi 9506651	26 kDa		2	6
116	RecName: Full=Elongation factor Tu, mitochondrial; Short=EF-Tu; AltName: Full=P43; Flags: Precursor	gi 1706611 (+3)	50 kDa		1	3
134	PSMA4 protein [Homo sapiens]	gi 34783332 (+1)	29 kDa		1	3
136	ribosomal protein S16 [Homo sapiens]	gi 4506691 (+2)	16 kDa		1	3
157	DNA-binding protein B [Homo sapiens]	gi 181486 (+1)	40 kDa		1	3
159	chloride channel, nucleotide-sensitive, 1A [Homo sapiens]	gi 4502891 (+1)	26 kDa		1	3
161	guanine nucleotide-binding protein G(I)/G(S)/G(T) subunit beta-2 [Mus musculus]	gi 13937391 (+1)	37 kDa		1	3
193	ribosomal protein S14 [Homo sapiens]	gi 5032051	16 kDa		1	3
1	actin, beta [Homo sapiens]	gi 14250401	41 kDa	true	214	570
69	tropomyosin alpha-3 chain isoform 4 [Homo sapiens]	gi 114155144 (+2)	29 kDa	true	3	7
67	albumin, isoform CRA_h [Homo sapiens]	gi 119626071 (+17)	69 kDa		4	9
2	protein arginine N-methyltransferase 5 isoform a [Homo sapiens]	gi 20070220	73 kDa		76	156
76	myosin regulatory light chain 12B [Homo sapiens]	gi 15809016 (+3)	20 kDa		3	6
96	poly(A) binding protein, cytoplasmic 1, isoform CRA_c [Homo sapiens]	gi 119612222 (+6)	47 kDa	true	2	4
121	ribosomal protein L13 [Homo sapiens]	gi 15431295 (+1)	24 kDa		2	4
129	PREDICTED: similar to ribosomal protein isoform 2 [Pan troglodytes]	gi 114606879 (+2)	15 kDa		2	4
162	nucleolar protein family A member 1 [Homo sapiens]	gi 56566042 (+1)	21 kDa		1	2
60	Unknown (protein for IMAGE:3544292) [Homo sapiens]	gi 13097759 (+3)	27 kDa		4	7
23	vimentin [Homo sapiens]	gi 340219 (+3)	54 kDa	true	11	19
74	peroxiredoxin 1, isoform CRA_b [Homo sapiens]	gi 119627382 (+3)	21 kDa	true	3	5
102	myosin-14 isoform 2 [Homo sapiens]	gi 116284394 (+6)	228 kDa	true	5	8
72	type I keratin 16 [Homo sapiens]	gi 1195531 (+1)	51 kDa	true	43	68
115	Heat shock 70kDa protein 9 (mortalin) [Homo sapiens]	gi 12653415 (+5)	74 kDa		2	3
119	ribosomal protein L3, isoform CRA_d [Homo sapiens]	gi 119580717 (+5)	49 kDa		2	3
142	ribosomal protein S8, isoform CRA_a [Homo sapiens]	gi 119627428 (+2)	27 kDa		2	3
165	peroxiredoxin-6 [Homo sapiens]	gi 4758638	25 kDa		2	3
209	unnamed protein product [Homo sapiens]	gi 189053201 (+4)	13 kDa		2	3
120	small nuclear ribonucleoprotein Sm D2 isoform 1 [Homo sapiens]	gi 4759158 (+1)	14 kDa		3	4
26	PREDICTED: keratin 6A [Pan troglodytes]	gi 114644568 (+5)	60 kDa	true	42	55
14	unnamed protein product [Homo sapiens]	gi 193786319 (+1)	53 kDa	false	19	24
70	6-phosphofructo-2-kinase/fructose-2,6-biphosphatase 3, isoform CRA_a [Homo sapiens]	gi 119606803 (+8)	58 kDa	true	4	5
7	Myosin, heavy chain 10, non-muscle [Homo sapiens]	gi 109734611 (+2)	229 kDa	true	82	101
12	hCG15164, isoform CRA_b [Homo sapiens]	gi 119605719 (+2)	16 kDa		34	41
39	78 kDa glucose-regulated protein precursor [Mus musculus]	gi 254540166	72 kDa	true	11	13
5	myosin-9 [Homo sapiens]	gi 12667788	227 kDa	true	114	132
10	heat shock cognate 71 kDa protein isoform 1 [Homo sapiens]	gi 5729877	71 kDa	true	31	35
17	Keratin 14 [Homo sapiens]	gi 12803709 (+1)	52 kDa	true	62	66

Interferon induction inhibition by MV C - Appendix

Supplementary Data:

24	HNRPH1 [Homo sapiens]	gi 48145673 (+2)	49 kDa	true	17	17
28	kinesin-related protein [Homo sapiens]	gi 1155084 (+2)	119 kDa		11	11
75	unnamed protein product [Homo sapiens]	gi 194374523 (+8)	66 kDa		4	4
125	ribosomal protein S13 [Homo sapiens]	gi 4506685	17 kDa		3	3
141	tyrosine-protein kinase JAK1 [Homo sapiens]	gi 102469034 (+1)	133 kDa		2	2
158	RuvB-like 1 [Homo sapiens]	gi 197692395 (+3)	50 kDa		2	2
167	ribosomal protein L30 [Homo sapiens]	gi 4506631	13 kDa		2	2
188	ribosomal protein S9, isoform CRA_c [Homo sapiens]	gi 119592618 (+4)	17 kDa		2	2
190	ribosomal protein L6 [Homo sapiens]	gi 16753227 (+5)	33 kDa		2	2
191	hCG26523, isoform CRA_a [Homo sapiens]	gi 119617765 (+3)	17 kDa		2	2
207	serine/arginine repetitive matrix protein 2 [Homo sapiens]	gi 118572613 (+5)	300 kDa		2	2
6	keratin 10 (epidermolytic hyperkeratosis; keratosis palmaris et plantaris), isoform CRA_b [Homo sapiens]	gi 119581085 (+3)	63 kDa	true	153	150
3	keratin 1 [Homo sapiens]	gi 11935049 (+1)	66 kDa	true	252	234
16	unnamed protein product [Homo sapiens]	gi 16549132 (+2)	61 kDa		20	18
47	Chain L, Crystal Structure Of Fab Fragment Complexed With Gibberellin A4	gi 24158782	24 kDa	true	10	9
8	epidermal cytokeatin 2 [Homo sapiens]	gi 181402 (+1)	66 kDa	true	130	112
25	keratin, type II cytoskeletal 5 [Homo sapiens]	gi 119395754 (+1)	62 kDa	true	59	50
27	RNA binding motif protein 10, isoform CRA_d [Homo sapiens]	gi 119579690 (+1)	110 kDa		13	11
9	cytokeatin 9 [Homo sapiens]	gi 435476 (+2)	62 kDa	true	93	71
30	serine/threonine kinase 38 [Homo sapiens]	gi 6005814	54 kDa	true	12	9
45	U4/U6 snRNP-associated 61 kDa protein [Homo sapiens]	gi 18249847 (+1)	55 kDa		8	6
104	thymopoietin zeta isoform [Homo sapiens]	gi 119214988 (+7)	27 kDa		4	3
35	histone H2A type 2-C [Homo sapiens]	gi 24638446 (+1)	14 kDa	true	14	10
53	unnamed protein product [Homo sapiens]	gi 31092 (+10)	50 kDa		7	5
108	insulin-like growth factor 2 mRNA-binding protein 1 isoform 1 [Homo sapiens]	gi 56237027	63 kDa		3	2
109	drebrin 1, isoform CRA_a [Homo sapiens]	gi 119605395 (+8)	76 kDa		3	2
114	ribosomal protein, large, P0, isoform CRA_a [Homo sapiens]	gi 119618576 (+6)	31 kDa		3	2
123	unnamed protein product [Homo sapiens]	gi 194378142 (+4)	82 kDa	true	3	2
135	snRNP polypeptide B [Homo sapiens]	gi 190247 (+9)	30 kDa		3	2
137	unnamed protein product [Homo sapiens]	gi 158260331 (+2)	33 kDa		3	2
144	ribosomal protein L7 [Homo sapiens]	gi 307388	29 kDa		3	2
83	histone 1, H4c [Homo sapiens]	gi 119575932 (+5)	14 kDa		5	3
91	mitogen-activated protein kinase kinase kinase 7-interacting protein 1 isoform beta [Homo sapiens]	gi 41281798 (+2)	50 kDa		5	3
20	PREDICTED: heterogeneous nuclear ribonucleoprotein K isoform 8 [Callithrix jacchus]	gi 296189587	?		24	12
99	influenza virus NS1A-binding protein [Homo sapiens]	gi 24475847 (+5)	72 kDa		4	2
106	small nuclear ribonucleoprotein Sm D1 [Homo sapiens]	gi 5902102	13 kDa		4	2
168	hCG1994130, isoform CRA_b [Homo sapiens]	gi 119570641 (+5)	29 kDa		2	1
176	60S ribosomal protein L15 [Homo sapiens]	gi 12006350 (+3)	24 kDa		2	1
186	Similar to ribophorin I [Homo sapiens]	gi 14124942 (+3)	65 kDa		2	1
194	sub2.3 [Homo sapiens]	gi 444021 (+2)	32 kDa	true	2	1
222	hCG1640785, isoform CRA_a [Homo sapiens]	gi 119569329 (+3)	14 kDa		2	1
223	hCG2028724 [Homo sapiens]	gi 119601423 (+7)	30 kDa		2	1
232	PREDICTED: RuvB-like 2 isoform 2 [Pan troglodytes]	gi 114678325 (+2)	47 kDa		2	1
234	Mitogen-activated protein kinase kinase kinase 7 interacting protein 3 [Homo sapiens]	gi 21619770 (+1)	79 kDa		2	1
92	KIAA0965 protein [Homo sapiens]	gi 20521714 (+1)	57 kDa	true	7	3
68	heterogeneous nuclear ribonucleoprotein A1 isoform b [Homo sapiens]	gi 14043070 (+4)	39 kDa		11	4
54	RNA binding motif protein, X-linked, isoform CRA_b [Homo sapiens]	gi 119608862 (+3)	24 kDa		9	3
89	nucleolin, isoform CRA_c [Homo sapiens]	gi 119591368 (+5)	59 kDa		6	2
160	ribosomal protein L23a, isoform CRA_a [Homo sapiens]	gi 119571516 (+3)	22 kDa		3	1
185	hCG33299, isoform CRA_a [Homo sapiens]	gi 119597983 (+7)	30 kDa		3	1
192	ribosomal protein L22, isoform CRA_c [Homo sapiens]	gi 119591926 (+3)	12 kDa		3	1
201	BAT1 protein [Homo sapiens]	gi 114306812 (+5)	51 kDa		3	1
202	calcium homeostasis endoplasmic reticulum protein [Homo sapiens]	gi 119226260 (+3)	104 kDa		3	1
204	fus-like protein [Homo sapiens]	gi 1040970 (+7)	53 kDa		3	1
206	ribosomal protein L4, isoform CRA_b [Homo sapiens]	gi 119598180 (+5)	53 kDa		3	1
11	mitochondrial import inner membrane translocase subunit TIM14 [Homo sapiens]	gi 21687102 (+1)	12 kDa		90	28
18	anti-colorectal carcinoma heavy chain [Homo sapiens]	gi 425518	51 kDa		64	19
29	growth regulated nuclear 68 protein	gi 226021 (+1)	67 kDa	true	19	5
107	myotubularin-related protein 14 isoform 2 [Homo sapiens]	gi 117938270 (+3)	72 kDa		4	1
117	interleukin enhancer binding factor 3, 90kDa, isoform CRA_c [Homo sapiens]	gi 119604539 (+13)	92 kDa		4	1
138	ribosomal protein L12 [Homo sapiens]	gi 4506597	18 kDa		4	1
166	ribosomal protein [Homo sapiens]	gi 337518 (+1)	22 kDa		4	1
174	ribosomal protein L10A [Rattus norvegicus]	gi 13592009 (+3)	25 kDa		4	1
64	heterogeneous nuclear ribonucleoprotein H2 [Homo sapiens]	gi 9624998	49 kDa	true	23	5
37	heterogeneous nuclear ribonucleoprotein L [Homo sapiens]	gi 11527777 (+4)	64 kDa		15	3
62	splicing factor, arginine/serine-rich 1 isoform 2 [Homo sapiens]	gi 118582269 (+4)	22 kDa		10	2
78	spliceosomal protein SAP 155 [Homo sapiens]	gi 4033735 (+1)	146 kDa		5	1
95	pre-mRNA-processing factor 19 [Homo sapiens]	gi 7657381	55 kDa		5	1
111	mitogen-activated protein kinase kinase kinase 7 isoform B [Homo sapiens]	gi 21735562 (+3)	67 kDa		5	1
122	unnamed protein product [Homo sapiens]	gi 158255716 (+2)	54 kDa		5	1
153	karyopherin (importin) beta 1, isoform CRA_b [Homo sapiens]	gi 119615215 (+3)	94 kDa		5	1
52	dermcidin preproprotein [Homo sapiens]	gi 16751921	11 kDa		24	4
15	unnamed protein product [Homo sapiens]	gi 189053924 (+1)	22 kDa	true	41	6
40	ATP-dependent RNA helicase A [Homo sapiens]	gi 100913206 (+2)	141 kDa		17	2
33	heterogeneous nuclear ribonucleoprotein M, isoform CRA_c [Homo sapiens]	gi 119589327 (+4)	78 kDa		20	2
61	Lamin B1 [Homo sapiens]	gi 15126742 (+1)	66 kDa		10	1
63	histone H2B type 1-D [Homo sapiens]	gi 10800138 (+11)	14 kDa		10	1
130	probable ATP-dependent RNA helicase DDX17 isoform 3 [Homo sapiens]	gi 148613856 (+6)	80 kDa	true	10	1
21	heterogeneous nuclear ribonucleoprotein U isoform b [Homo sapiens]	gi 141411161 (+5)	89 kDa		32	3
42	histone H3 [Homo sapiens]	gi 1568559 (+11)	15 kDa		14	1
51	heterogeneous nuclear ribonucleoproteins C1/C2 isoform b [Homo sapiens]	gi 117190174 (+5)	32 kDa		16	1
36	unnamed protein product [Homo sapiens]	gi 158256968 (+3)	136 kDa		22	1
13	heterogeneous nuclear ribonucleoproteins A2/B1 isoform B1 [Homo sapiens]	gi 14043072	37 kDa		47	1
22	heterogeneous nuclear ribonucleoprotein A3, isoform CRA_a [Homo sapiens]	gi 119631468 (+1)	37 kDa		35	0
34	lamin A/C, isoform CRA_c [Homo sapiens]	gi 119573383 (+2)	87 kDa		23	0
38	unnamed protein product [Homo sapiens]	gi 194387670 (+1)	19 kDa		21	0
41	rRNA 2'-O-methyltransferase fibrillar [Homo sapiens]	gi 12056465 (+2)	34 kDa		19	0

Interferon induction inhibition by MV C - Appendix

Supplementary Data:

43	nucleophosmin isoform 1 [Homo sapiens]	gi 10835063 (+7)	33 kDa		20	0
44	PRP8 pre-mRNA processing factor 8 homolog (yeast), isoform CRA_b [Homo sapiens]	gi 119610995 (+2)	274 kDa		17	0
46	KIAA0788 protein [Homo sapiens]	gi 20521660 (+2)	232 kDa		17	0
48	NOP58 protein [Homo sapiens]	gi 33872137 (+1)	59 kDa		17	0
50	PREDICTED: U5 snRNP-specific protein, 116 kD isoform 1 [Pan troglodytes]	gi 114666744 (+7)	108 kDa		15	0
57	splicing factor proline/glutamine-rich (polypyrimidine tract binding protein associated), isoform CRA_e [Homo sapiens]	gi 119627830 (+3)	66 kDa		13	0
58	NOP56 protein [Homo sapiens]	gi 118142846 (+8)	50 kDa		13	0
65	unnamed protein product [Homo sapiens]	gi 10435335 (+6)	40 kDa		11	0
81	Chain A, Crystal Structure Of Human Apo-Eif4a11	gi 114794619 (+7)	45 kDa		10	0
82	matrin-3 [Homo sapiens]	gi 21626466 (+1)	95 kDa		10	0
87	HNRPF protein [Homo sapiens]	gi 16876910 (+2)	46 kDa	true	15	0
94	heterogeneous nuclear ribonucleoprotein U-like 2 [Homo sapiens]	gi 118601081 (+2)	85 kDa		9	0
100	Chain A, Solution Structure Of The Rrm Domain Of Sr Rich Factor 9g8	gi 119389969 (+5)	11 kDa	true	8	0
110	hCG39912, isoform CRA_b [Homo sapiens]	gi 119576757 (+5)	21 kDa		5	0
124	unnamed protein product [Homo sapiens]	gi 194387362 (+3)	35 kDa		6	0
127	splicing factor, arginine/serine-rich 10 (transformer 2 homolog, Drosophila), isoform CRA_c [Homo sapiens]	gi 119598613 (+6)	34 kDa		6	0
128	PREDICTED: hypothetical protein isoform 2 [Pan troglodytes]	gi 114638645 (+7)	90 kDa		9	0
131	histone H2A type 1-B/E [Homo sapiens]	gi 10645195 (+3)	14 kDa	true	18	0
132	HNRPR protein [Homo sapiens]	gi 111494085 (+6)	68 kDa	true	5	0
146	ATP synthase, H+ transporting, mitochondrial F1 complex, alpha subunit 1, cardiac muscle [Homo sapiens]	gi 127798841 (+3)	60 kDa		5	0
147	DEAH (Asp-Glu-Ala-His) box polypeptide 15, isoform CRA_g [Homo sapiens]	gi 119613226 (+4)	81 kDa		5	0
148	heterogeneous nuclear ribonucleoprotein D (AU-rich element RNA binding protein 1, 37kDa), isoform CRA_a [Homo sapiens]	gi 119626277 (+11)	41 kDa		4	0
149	splicing factor, arginine/serine-rich 3, isoform CRA_c [Homo sapiens]	gi 119624305 (+2)	15 kDa	true	6	0
150	interleukin enhancer binding factor 2 [Mus musculus]	gi 13385872 (+4)	43 kDa		5	0
151	unnamed protein product [Homo sapiens]	gi 194386598 (+4)	123 kDa		5	0
152	histone H2A.Z [Homo sapiens]	gi 4504255 (+2)	14 kDa	true	7	0
156	Dyskeratosis congenita 1, dyskerin [Homo sapiens]	gi 14602859 (+4)	58 kDa		5	0
163	PREDICTED: similar to 40S ribosomal protein S2 isoform 1 [Macaca mulatta]	gi 109108085 (+11)	20 kDa		4	0
164	DNA topoisomerase 1 [Homo sapiens]	gi 11225260 (+15)	91 kDa		4	0
169	splicing factor, arginine/serine-rich 13A isoform 2 [Homo sapiens]	gi 16905517 (+8)	31 kDa		4	0
170	polypyrimidine tract binding protein 1, isoform CRA_b [Homo sapiens]	gi 119581557 (+5)	57 kDa	true	4	0
171	WD40 repeat-containing protein SMU1 [Bos taurus]	gi 84370185	58 kDa		4	0
172	SYNCRIP protein [Homo sapiens]	gi 116283697 (+10)	51 kDa	true	4	0
173	splicing factor, arginine/serine-rich 2, isoform CRA_d [Homo sapiens]	gi 119609849 (+5)	24 kDa		4	0
177	thyroid hormone receptor-associated protein 3 [Homo sapiens]	gi 167234419 (+2)	109 kDa		4	0
178	Chain A, Structure Of A Human Prp31-15.5k-U4 Snrna Complex	gi 145580328 (+3)	14 kDa		5	0
180	small nuclear ribonucleoprotein 70kDa polypeptide (RNP antigen), isoform CRA_g [Homo sapiens]	gi 119572837 (+3)	45 kDa		5	0
181	unnamed protein product [Homo sapiens]	gi 158261255 (+5)	73 kDa		5	0
184	hCG2002711, isoform CRA_b [Homo sapiens]	gi 119574041 (+5)	30 kDa		5	0
187	putative RNA-binding protein Luc7-like 2 [Homo sapiens]	gi 116812577 (+3)	47 kDa		4	0
189	Chain A, Solution Structure Of Rrm Domain In Splicing Factor 3b	gi 159163578 (+3)	11 kDa		4	0
197	ribosomal protein SA, isoform CRA_c [Homo sapiens]	gi 119584991 (+8)	20 kDa		4	0
198	hCG27481, isoform CRA_b [Homo sapiens]	gi 119599362 (+4)	115 kDa		4	0
199	ribosomal protein L9, isoform CRA_a [Homo sapiens]	gi 119613332 (+3)	15 kDa		4	0
200	proline rich 6, isoform CRA_b [Homo sapiens]	gi 119624905 (+3)	30 kDa		4	0
208	chromobox protein homolog 3 [Homo sapiens]	gi 15082258 (+1)	21 kDa		3	0
212	PREDICTED: hypothetical protein isoform 1 [Pan troglodytes]	gi 114578550 (+4)	54 kDa		4	0
213	unnamed protein product [Homo sapiens]	gi 194380928 (+2)	117 kDa		4	0
225	U5 small nuclear ribonucleoprotein 40 kDa protein [Homo sapiens]	gi 115298668 (+4)	39 kDa		3	0
226	PRP4 pre-mRNA processing factor 4 homolog (yeast) [Homo sapiens]	gi 13938549 (+5)	58 kDa		3	0
227	Chain A, Solution Structure Of The Oxidized Microsomal Human Cytochrome B5	gi 158428699 (+7)	12 kDa		3	0
228	unnamed protein product [Homo sapiens]	gi 189067487 (+4)	60 kDa		3	0
229	unnamed protein product [Homo sapiens]	gi 194386160 (+3)	151 kDa		3	0
230	chromosome 1 open reading frame 77, isoform CRA_e [Homo sapiens]	gi 119573679 (+6)	24 kDa		3	0
231	karyopherin alpha 3 (importin alpha 4), isoform CRA_b [Homo sapiens]	gi 119629243 (+5)	56 kDa		3	0
236	SRp55-3 [Homo sapiens]	gi 1049086 (+5)	38 kDa	true	3	0
237	PREDICTED: HP1-BP74 isoform 3 [Pan troglodytes]	gi 114554472 (+6)	44 kDa		3	0
238	DEAD (Asp-Glu-Ala-Asp) box polypeptide 46, isoform CRA_a [Homo sapiens]	gi 119582642 (+6)	100 kDa		3	0
239	TAR DNA binding protein, isoform CRA_a [Homo sapiens]	gi 119592075 (+3)	39 kDa		3	0
240	chromosome 20 open reading frame 14, isoform CRA_c [Homo sapiens]	gi 119595582 (+6)	102 kDa		3	0
243	RNA-binding protein with serine-rich domain 1 isoform 2 [Mus musculus]	gi 121674799 (+5)	32 kDa		3	0
244	Similar to ribosomal protein L23 [Homo sapiens]	gi 13097600 (+2)	14 kDa		3	0
246	Chain A, Crystal Structure Of First Two Rrm Domains Of Fir Bound To Ssdna From A Portion Of Fuse	gi 169404577 (+8)	23 kDa		3	0
247	ATP synthase beta subunit [Homo sapiens]	gi 179279 (+4)	57 kDa		3	0
248	60S acidic ribosomal protein P2 [Homo sapiens]	gi 4506671	12 kDa		3	0
249	splicing factor 3 subunit 1 isoform 1 [Homo sapiens]	gi 5032087 (+1)	89 kDa		3	0
250	aldolase A, fructose-bisphosphate, isoform CRA_b [Homo sapiens]	gi 119600342 (+5)	40 kDa		3	0
252	ribosomal protein S19, isoform CRA_b [Homo sapiens]	gi 119577478 (+2)	17 kDa		2	0
253	zinc finger protein 326, isoform CRA_b [Homo sapiens]	gi 119593532 (+3)	68 kDa		2	0
254	splicing factor 3B subunit 5 [Homo sapiens]	gi 13775200	10 kDa		2	0
255	pinin [Homo sapiens]	gi 11320891 (+8)	82 kDa		3	0
258	nuclear pore complex-associated protein TPR [Homo sapiens]	gi 114155142 (+4)	267 kDa		2	0
259	PREDICTED: hypothetical protein LOC466117 isoform 6 [Pan troglodytes]	gi 114631381 (+13)	15 kDa		2	0
260	PREDICTED: similar to MGC107852 protein isoform 3 [Pan troglodytes]	gi 114660748 (+10)	52 kDa		2	0
261	Chain A, Crystal Structure Of Human Carboxylesterase In Complex With Cholate And Palmitate	gi 114793717 (+17)	60 kDa		2	0
264	RBM25 protein [Homo sapiens]	gi 118196855 (+6)	100 kDa		2	0
266	heterogeneous nuclear ribonucleoprotein U-like 1, isoform CRA_c [Homo sapiens]	gi 119577432 (+9)	85 kDa		2	0
267	ELAV (embryonic lethal, abnormal vision, Drosophila)-like 1 (Hu antigen R), isoform CRA_b [Homo sapiens]	gi 119589356 (+2)	50 kDa		2	0
268	U2 (RNU2) small nuclear RNA auxiliary factor 2, isoform CRA_a [Homo sapiens]	gi 119592808 (+5)	42 kDa		2	0
269	ribosomal protein L5, isoform CRA_b [Homo sapiens]	gi 119593494 (+5)	28 kDa		2	0
270	ARS2 protein, isoform CRA_b [Homo sapiens]	gi 119596872 (+12)	102 kDa		2	0
273	SWI/SNF related, matrix associated, actin dependent regulator of chromatin, subfamily a,	gi 119604569 (+20)	144 kDa		2	0

Interferon induction inhibition by MV C - Appendix

Supplementary Data:

	member 4, isoform CRA_b [Homo sapiens]					
274	THO complex 4 [Homo sapiens]	gi 119610105 (+1)	25 kDa		2	0
278	splicing factor 3a, subunit 3, 60kDa, isoform CRA_b [Homo sapiens]	gi 119627711 (+7)	59 kDa		2	0
280	unnamed protein product [Homo sapiens]	gi 158254512 (+2)	51 kDa		2	0
284	ribosomal protein L38 [Homo sapiens]	gi 4506645	8 kDa		2	0
286	SF3A2 protein [Homo sapiens]	gi 116283242 (+5)	51 kDa		2	0
287	procollagen-proline, 2-oxoglutarate 4-dioxygenase (proline 4-hydroxylase), beta polypeptide, isoform CRA_d [Homo sapiens]	gi 119610102 (+8)	41 kDa		2	0
289	regulator of chromosome condensation 1 isoform a [Homo sapiens]	gi 114796644 (+8)	48 kDa		2	0
290	nucleoporin 210kDa, isoform CRA_a [Homo sapiens]	gi 119584554 (+5)	106 kDa		1	0

Experiment 2 (Protein identification probability 50%):

#	Identified Proteins (65/121)	Accession Number	Molecular Weight	Protein Grouping Ambiguity	mock	MV fl-Cwt	MV fl-CwtNLS
1	Chain A, Crystal Structure Of Apo Human Ptp1b (C215s) Mutant	gi 15825777 (+5)	36 kDa		108	68	71
2	putative [Homo sapiens]	gi 553734	2 kDa		52	28	26
3	heat shock cognate 71 kDa protein isoform 2 [Homo sapiens]	gi 24234686 (+2)	54 kDa	true	1	13	13
4	tubulin, alpha 1c [Homo sapiens]	gi 14389309 (+12)	50 kDa		0	7	3
5	Chain A, Crystal Structure Of The Human Hsp70 ATPase Domain In The Apo Form	gi 166007012 (+10)	43 kDa	true	0	5	9
6	Tubulin, beta 2C [Homo sapiens]	gi 20809886 (+3)	50 kDa	true	0	14	8
7	small nuclear ribonucleoprotein Sm D1 [Homo sapiens]	gi 5902102	13 kDa		0	5	4
8	heterogeneous nuclear ribonucleoprotein U isoform b [Homo sapiens]	gi 14141161 (+4)	89 kDa		0	4	4
9	tropomyosin alpha-3 chain isoform 4 [Homo sapiens]	gi 114155144 (+4)	29 kDa		0	0	6
10	78 kDa glucose-regulated protein [Homo sapiens]	gi 16507237 (+3)	72 kDa	true	0	4	3
11	heat shock 60kDa protein 1 (chaperonin), isoform CRA_c [Homo sapiens]	gi 119590557 (+5)	41 kDa		0	2	3
12	PREDICTED: hypothetical protein isoform 19 [Pan troglodytes]	gi 114625192 (+11)	51 kDa		0	1	4
13	heterogeneous nuclear ribonucleoprotein A1, isoform CRA_g [Homo sapiens]	gi 119617173 (+9)	33 kDa		0	2	2
14	Na <sup>+</sup> /K <sup>+</sup> ATPase [Homo sapiens]	gi 1359715 (+11)	112 kDa		0	2	2
15	hCG19195 [Homo sapiens]	gi 119597218 (+6)	9 kDa		0	2	1
16	proteasome (prosome, macropain) 26S subunit, ATPase, 2, isoform CRA_a [Homo sapiens]	gi 119603737 (+2)	32 kDa		0	2	1
17	OTUD4 protein [Homo sapiens]	gi 118142854 (+8)	36 kDa		0	2	1
18	chromosome 17 open reading frame 79, isoform CRA_a [Homo sapiens]	gi 119600666 (+2)	19 kDa		0	2	1
19	PREDICTED: similar to P26s4 isoform 1 [Pan troglodytes]	gi 114654363 (+6)	41 kDa		0	1	1
20	nucleophosmin isoform 1 [Homo sapiens]	gi 10835063 (+12)	33 kDa		0	1	0
21	small nuclear ribonucleoprotein Sm D2 isoform 2 [Homo sapiens]	gi 237649049 (+1)	12 kDa		0	1	2
22	26S proteasome subunit p97 [Homo sapiens]	gi 1060888 (+7)	100 kDa		0	3	0
23	PSMD1 protein [Homo sapiens]	gi 116283467 (+9)	95 kDa		0	1	1
24	Chain A, Structure Of Tab1	gi 116668415 (+5)	44 kDa		0	1	1
25	thymopoietin zeta isoform [Homo sapiens]	gi 119214988 (+10)	27 kDa		0	1	1
26	DnaJ (Hsp40) homolog, subfamily A, member 1, isoform CRA_d [Homo sapiens]	gi 119578931 (+4)	42 kDa		0	1	1
27	tropomodulin 1, isoform CRA_a [Homo sapiens]	gi 119579249 (+4)	44 kDa		0	1	1
28	Unknown (protein for IMAGE:3544292) [Homo sapiens]	gi 13097759 (+5)	27 kDa		0	1	1
29	mitogen-activated protein kinase kinase kinase 7-interacting protein 2 [Homo sapiens]	gi 14149669 (+4)	76 kDa		0	1	1
30	unnamed protein product [Homo sapiens]	gi 193787479 (+4)	53 kDa		0	1	1
31	myosin VI [Homo sapiens]	gi 56204015	145 kDa		0	1	1
32	actin-like protein [Homo sapiens]	gi 62421170	12 kDa	true	0	4	7
33	apoptosis-inducing factor 1, mitochondrial isoform 5 [Homo sapiens]	gi 195927006 (+3)	35 kDa		0	1	1
34	RecName: Full=Monocarboxylate transporter 1; Short=MCT 1; AltName: Full=Solute carrier family 16 member 1	gi 13432183 (+1)	54 kDa		0	1	0
35	Plasminogen [Homo sapiens]	gi 38051823	91 kDa		0	1	0
36	unnamed protein product [Homo sapiens]	gi 158257224 (+6)	47 kDa		0	3	0
37	proteasome (prosome, macropain) 26S subunit, non-ATPase, 4 [Homo sapiens]	gi 150439371 (+5)	22 kDa		0	0	1
38	hCG23783, isoform CRA_a [Homo sapiens]	gi 119621875 (+5)	23 kDa		0	2	0
39	microtubule-associated protein 1B, isoform CRA_a [Homo sapiens]	gi 119616102 (+2)	257 kDa		0	3	0
40	DOK6 protein [Homo sapiens]	gi 114325404 (+6)	29 kDa		0	0	1
41	PREDICTED: similar to mSUG1 protein isoform 7 [Pan troglodytes]	gi 114669878 (+5)	43 kDa		0	0	1
42	PREDICTED: heterogeneous nuclear ribonucleoprotein M isoform 7 [Pan troglodytes]	gi 114675132 (+11)	61 kDa		0	0	1
43	hCG1640785, isoform CRA_a [Homo sapiens]	gi 119569329 (+3)	14 kDa		0	0	1
44	chromosome 1 open reading frame 77, isoform CRA_d [Homo sapiens]	gi 119573678 (+7)	17 kDa		0	0	1
45	6-phosphofructo-2-kinase/fructose-2,6-biphosphatase 3, isoform CRA_a [Homo sapiens]	gi 119606803 (+10)	58 kDa		0	0	1
46	Chain A, Macrophage Migration Inhibitory Factor (Mif) Complexed With Inhibitor.	gi 13399777 (+5)	13 kDa		0	0	1
47	Unknown (protein for IMAGE:3897044) [Homo sapiens]	gi 14789595 (+3)	30 kDa		0	0	1
48	U4/U6 snRNP-associated 61 kDa protein [Homo sapiens]	gi 18249847 (+3)	55 kDa		0	0	1
49	unnamed protein product [Homo sapiens]	gi 189066512 (+5)	48 kDa		0	0	1
50	actin beta related pseudogene	gi 223597	42 kDa	true	0	0	3
51	Rig homolog [human, brain, Peptide Partial], 135 aa	gi 262391 (+1)	16 kDa		0	0	1
52	hCG2028078 [Homo sapiens]	gi 119569445 (+4)	7 kDa		0	0	1
53	tat-associated protein	gi 1096067 (+7)	31 kDa		0	1	0
54	myc-associated zinc finger protein isoform 2 [Homo sapiens]	gi 110347459 (+11)	51 kDa		0	1	0
55	GLS2 protein [Homo sapiens]	gi 111185682 (+6)	28 kDa		0	1	0
56	PREDICTED: proteasome 26S non-ATPase subunit 13 isoform 3 [Pan troglodytes]	gi 114635315 (+9)	43 kDa		0	1	0
57	chromosome 13 open reading frame 7, isoform CRA_b [Homo sapiens]	gi 119600993 (+2)	81 kDa		0	1	0
58	solute carrier family 25 (mitochondrial carrier; phosphate carrier), member 3, isoform CRA_c [Homo sapiens]	gi 119618006 (+6)	26 kDa		0	1	0
59	TAK1-binding protein 3, isoform CRA_b [Homo sapiens]	gi 119619464 (+6)	80 kDa		0	1	0
60	Solute carrier family 1 (neutral amino acid transporter), member 5 [Homo sapiens]	gi 12652633 (+9)	57 kDa		0	1	0
61	Proteasome (prosome, macropain) 26S subunit, non-ATPase, 3 [Homo sapiens]	gi 15126760 (+9)	61 kDa		0	1	0
62	RecName: Full=Phosphotyrosine phosphatase PTPRQ; AltName: Full=Receptor-type tyrosine-protein phosphatase Q; Short=R-PTP-Q; Short=PTP-RQ; Flags: Precursor	gi 158563998	261 kDa		0	1	0
63	insulin receptor substrate 4 [Homo sapiens]	gi 4504733	134 kDa		0	1	0
64	hCG2044124 [Homo sapiens]	gi 119582767 (+11)	185 kDa		0	1	0
65	unnamed protein product [Homo sapiens]	gi 158260761 (+1)	28 kDa		0	1	0

## Publications and Presentations

### Vorträge/Präsentationen:

**2013:** Vortrag: Measles Virus Mini Symposium, Annecy, Frankreich

**2013:** Vortrag: Negative Strand RNA Virus Meeting, Granada, Spanien

**2013:** Vortrag: Interferon Workshop, Braunschweig, Deutschland

**2013:** Vortrag: Tagung der deutschen Gesellschaft für Virologie, Kiel, Deutschland

**2012:** Posterpräsentation: Awaji International Forum on Infection and Immunity, Awaji, Osaka, Japan

**2012:** Vortrag: Retreat des DFG Graduiertenkolleg 1202

**2012:** Posterpräsentation: Retreat des Genzentrums

**2011:** Vortrag: Interferon Workshop in St. Andrews, Schottland

**2011:** Posterpräsentation: Tagung der deutschen Gesellschaft für Virologie in Freiburg

**2010:** Posterpräsentation: Abschluss Symposium des SFB 455

### Publikationen:

Click-modified anandamide siRNA enables delivery and gene silencing in neuronal and immune cells.

Willibald J, Harder J, **Sparrner K**, Conzelmann KK, Carell T.

J Am Chem Soc. 2012 Aug 1;134(30):12330-3. doi: 10.1021/ja303251f. Epub 2012 Jul 23.

Measles virus C protein interferes with Beta interferon transcription in the nucleus.

**Sparrner KM**, Pfaller CK, Conzelmann KK.

J Virol. 2012 Jan;86(2):796-805. doi: 10.1128/JVI.05899-11. Epub 2011 Nov 9.